Evaluation of Tomographic 3D Ultrasound in Vascular Disease

A thesis submitted to The University of Manchester for the degree of

Doctor of Philosophy

in the Faculty of Biology, Medicine and Health.

2019

Steven K. Rogers

School of Medical Sciences

Division of Cardiovascular Science

Table of Contents

List of tables, figures and diagrams

Chapter 1

Chapter 2

Figure 14.
2D duplex ultrasound of a calcified posterior tibial artery. Poor colour filling [red colour] is due to calcification which is highlighted by yellow arrows

Figure 15.
tUS angio image of the posterior tibial artery in a healthy subject showing muscular branches

Figure 16.
tUS vein map of a long saphenous vein with branches and perforators

Figure 17.
A pre-operative radial artery and cephalic vein map showing anatomical orientation and proximity with the venae comitantes

Chapter 4

Figure 18.
Tomographic ultrasound image of the four sections of artery (IMA, Renal, Carotid, Aorta) suspended on surgical silk set within an Agar gel

Figure 19.
Visual representation of tomographic ultrasound scan within the PIUR imaging software of the Aortic arterial segment. The images demonstrate a 3D reconstruction and multi-planar reconstructions. The coloured lines allow angle correction within the axial, sagittal or coronal planes. The yellow line with cross-hairs demonstrates line measurements

Figure 20.
Flow diagram for the volume calculation of the tomographic ultrasound scan within the PIUR imaging software. Top left shows the manual annotation of the vessel lumen and outer wall. Bottom left demonstrates the 3mm slice thickness in the coronal plane. Bottom right and top right show the volume calculation from the manual planimetry and the 3D reconstruction

Figure 21.
Visual representation of the CT scan of the whole phantom demonstrating the coloured lines for angle correction within the axial [top left panel], sagittal [top right panel] or coronal planes [bottom left panel] and the 3D image reconstruction [bottom right panel] with the line measurements within the Imfusion software

Figure 22.
Flow diagram for the volume calculation of the CT or MR scans within the Imfusion software. Top left shows the manual annotation of the vessel lumen and outer wall. Top middle and top right demonstrate the 3mm slice thickness in the coronal and sagittal planes. Bottom right, middle and left show the volume calculation from the manual planimetry and the 3D reconstructed volume

Figure 23.
Intra-observer agreement for each type of measure for the aorta by modality

Chapter 5

Chapter 6

Chapter 7

Chapter 8

Chapter 9

Chapter 10

Chapter 12

Figure 58.
Left; A sound pulse with a large bandwidth and long spatial pulse length due to poor damping, Right; A sound pulse with a small bandwidth and short spatial pulse length due to good damping

Figure 59.
Left; Emission of pulse from each PZT crystal forming Huygens wavelets that interact to form a single wave-front. Right; The PZT crystals at the edges of the transducer are given a time delay for pulse emission converging the wavelets on a specific location electronically focusing the sound

Figure 60.
Electronic beam steering as a result of individual PZT crystal time delays and wavelet interaction

Figure 61.
Ultrasound crystals emitting Huygens wavelets interacting to form a focused wave-front with the ultrasound beam profile demonstrating the near field, focal zone and far field

Figure 62.
Top; If both pulses are true inversions of one another the summed signal will cancel out. Bottom; Pulses undergo non-linear propagation non-uniformly and therefore generate a harmonic signal

Figure 63.
Left, Microbubble undergoing equal stable cavitation. Right, Peak negative pressure is sufficient to cause harmonic cavitation

Table 20.
Different tissue types and their associated speeds of sound. Red starred tissues make up the majority of ultrasound tissue types. Yellow star is the assumed average speed of sound within soft tissue

List of Abbreviations

95% Confidence Intervals (95%CI)

Abdominal Aortic Aneurysm (AAA)

Ankle-Brachial Pressure Indices (ABPI)

Anterior Tibial Artery (ATA)

Anterior-Posterior (AP)

Arterio-Venous Fistulae (AVF)

Artificial Intelligence (AI)

As Low As Reasonably Achievable (ALARA)

Asymptomatic Carotid Atherosclerosis Study (ACAS)

Asymptomatic Carotid Surgery Trial (ACST)

Asymptomatic Carotid Surgery Trial 2 (ACST2)

Best Medical Therapy (BMT)

B-Mode (Brightness Mode)

Body Mass Index (BMI)

Cardiovascular Disease (CVD)

Carotid Endarterectomy (CEA)

Carotid IMT (CIMT)

Carotid Plaque Volume (CPV)

Cerebral Vascular Accident (CVA)

Chronic Kidney Disease (CKD)

Computed Tomography (CT)

Contrast Enhanced Tomographic Ultrasound (CEtUS)

Contrast enhanced Ultrasound (CEUS)

Coronary Artery Bypass Grafts (CABG)

CT angiography (CTa)

Cycles Per Second (CPS)

Deep Inferior Epigastric Perforator (DIEP)

Deep Vein Thrombosis (DVT)

Diabetes Mellitus (DM)

Digital Subtraction Angiography (DSA)

Dorsalis Pedis (DP)

DSA using CO_2 (DSA-CO_2)

Duplex Ultrasound (DUS)

Electro-Cardio-Gram (ECG)

Endovascular Aneurysm Repair (EVAR)

European Carotid Surgery Trial (ECST)

European Society of Vascular Surgery (ESVS)

Fast Fourier Transformation (FFT)

Fenestrated EVAR (FEVAR)

Four dimensional (4D)

Four dimensional US (4D US)

Grey Scale Median (GSM)

Haemodialysis (HD)

Hertz (Hz)

Inferior Mammary Artery (IMA)

Inferior Vena Cava (IVC)

Inner wall to Inner wall (ITI)

Internal Carotid Artery (ICA)

Internal Mammary Artery (IMA)

Intima-Media boundary (IMB)

Intima-Media Thickness (IMT)

Intra-Class Correlation (ICC)

Intra-operative CEUS (iCEUS)

Intra-Vascular Ultrasound (IVUS)

Intra-Venous (IV)

Kilohertz (kHz)

Lead Zirconate Titonate (PZT)

Limit Of Agreement (LOA)

Long Saphenous Vein (LSV)

Magnetic Resonance (MR)

Magnetic Resonance angiography (MRa)

Magnetic Resonance Imaging (MRI)

Maximal Orthogonal (MO)

Mean Difference (MD)

Mechanical Index (MI)

Media-intimal boundary (MIB)

Megahertz (MHz)

MR angiography (MRa)

Multi-Planar Reconstruction MPR)

National AAA Screening Programme (NAAASP)

National Health Service (NHS)

National Institute of Clinical Excellence (NICE)

North American Symptomatic Carotid Endarterectomy Trial (NASCET)

Outer wall to Outer wall (OTO)

Peripheral Arterial Disease (PAD)

Peripheral Bypass Grafts (BPG)

Peritoneal Dialysis (PD)

Peroneal Artery (PeR A)

Picture Archive and Communication System (PACS)

Popliteal Artery (PoP A)

Posterior Tibial Artery (PTA)

Pulse Repetition Frequency (PRF)

Renal Cell Carcinoma (RCC)

Repetitive Strain Injury (RSI)

Research Ethics Committee (REC)

Reversible Ischemic Neurological Deficit (RIND)

Society of Vascular Surgery (SVS)

Society of Vascular Technology (SVT)

Spatial Pulse Length (SPL)

Standard Deviation (SD)

Surgical Care Practitioner (SCP)

Thermal Index (TI)

Three dimensional (3D)

Three dimensional US (3D US)

Tibio-Peroneal Trunk (TPT)

Toe-Brachial Pressure Indices (TBPI)

Tomographic Ultrasound (tUS)

Total Wall Volume (TWV)

Trans-catheter Aortic Valve Insertion (TAVI)

Transient Ischemic Attach (TIA)

Two dimensional (2D)

Two dimensional US (2D US)

Ultrasound (US)

USA Food and Drug Administration (FDA)

Vascular Surgical Society (VS)

Thesis Abstract

Steven K. Rogers
The University of Manchester
Degree Title: Doctor of Philosophy
Thesis Title: Evaluation of Tomographic 3D Ultrasound in Vascular Disease
May 2019

Objectives

The emerging use of Tomographic 3D Ultrasound (tUS) for vascular disease imaging is novel. This thesis aimed to establish whether tUS is the most accurate investigation for each indication, while demonstrating the potential value of tUS in vascular surgery.

Methods

The validity of tUS for measurement accuracy was first established using a phantom model. Subsequently six studies were designed on different vascular disease modalities to determine diagnostic accuracy, utility, reproducibility and intra-/inter-observer agreement of tUS. The clinical areas investigated were, Abdominal Aortic Aneurysm, Endo-Vascular Aneurysm Repair (EVAR) completion imaging to detect renal patency and endoleak, Carotid Plaque Volume as a measure of vulnerability, Peripheral Artery Disease (PAD) angiography, potential autologous bypass mapping and Arterio-Venous Fistula surveillance. To establish measurement precision tUS was compared to current gold standard index tests.

Results

Two broad tUS utilities emerged. tUS can be used with and without microbubble contrast and the implications of each are crucially important to implementation into daily use. tUS can readily be utilised to accurately measure artery geometry; namely, length, diameter and volume. When compared to CTa, there is greater variability in diameter measurements for patients who have had EVAR than AAA's pre-treatment. Anterior-Posterior diameters remain the most accurate method of measurement. Contrast-enhanced tUS (CEtUS) and CEUS were non-inferior to rotational angiography at detecting endoleak, particularly type II. The patient safety benefits and capacity of CEtUS may mean it is superior to rotational angiography in certain circumstances but 33% of renal vessels were not identified. This thesis reports the first investigation on the accuracy of CEtUS at the detection of clinically significant stenoses and occlusions of run-off vessels which proved highly reproducible with a significant degree of precision, but discrepancies between both CEtUS and angiography were found. tUS is also highly reproducible for measuring CPV with minimal bias and a high degree of precision with narrow confidence intervals. The relatively less skill and shorter time required to assess artery geometry, potential conduits or AVF by tUS, in comparison to the standard DUS, has added benefits for both the patient and the workforce representing a potential increased scanning capacity and decreased RSI risk. Due to capacity and availability, tUS could be the imaging modality of choice with the benefit of drastically reduce radiation and nephrotoxic contrast exposure possibly.

Conclusion

We have shown that tUS is an accurate, reproducible and precise imaging modality for various disease modalities. This thesis has added evidence to the published literature while addressing it's aims, laying the foundations for future work with tUS for vascular disease. Based on the evidence available tUS can readily be utilised for arterial geometry assessment and vessel mapping/surveillance. Contrast-Enhanced tUS should be used as part of a careful imaging strategy on EVAR completion as well as for targeted angiographic imaging for PAD or careful CPV measurement.

Declaration

No portion of the work referred to in the thesis has been submitted in support of an application for another degree or qualification of this or any other University or other institute of learning.

Copyright Statement

I. The author of this thesis (including any appendices and/or schedules to this thesis) owns certain copyright or related rights in it (the "Copyright") and s/he has given The University of Manchester certain rights to use such Copyright, including for administrative purposes.

II. Copies of this thesis, either in full or in extracts and whether in hard or electronic copy, may be made **only** in accordance with the Copyright, Designs and Patents Act 1988 (as amended) and regulations issued under it or, where appropriate, in accordance with licensing agreements which the University has from time to time. This page must form part of any such copies made.

III. The ownership of certain Copyright, patents, designs, trademarks and other intellectual property (the "Intellectual Property") and any reproductions of copyright works in the thesis, for example graphs and tables ("Reproductions"), which may be described in this thesis, may not be owned by the author and may be owned by third parties. Such Intellectual Property and Reproductions cannot and must not be made available for use without the prior written permission of the owner(s) of the relevant Intellectual Property and/or Reproductions.

IV. Further information on the conditions under which disclosure, publication and commercialisation of this thesis, the Copyright and any Intellectual Property and/or Reproductions described in it may take place is available in the University IP Policy (see http://documents.manchester.ac.uk/DocuInfo.aspx?DocID=24420), in any relevant Thesis restriction declarations deposited in the University Library, The University Library's regulations (see http://www.library.manchester.ac.uk/about/regulations/) and in The University's policy on Presentation of Theses.

Rationale for submitting the thesis in alternative format

Tomographic 3D ultrasound is a novel and emerging technology. My thesis was designed around multiple differing studies from Peripheral Arterial Disease to Abdominal Aortic Aneurysms and Carotid disease. This work therefore lent itself to individual research manuscripts and I have the intention to publish these in high ranking journals relevant to my field. Following discussion with the Supervisorial team it was decided that a thesis written in the alternative format would be applicable and most relevant to my thesis. To date two papers are under journal review and the remaining five will be submitted subsequently.

The research included in this thesis by its very nature, is multi-disciplinary and collaborative. The skills necessary to complete this body of work are not possessed by a single person. Collaborations were multinational and included clinical vascular scientists, vascular surgeons, radiologists, medical imaging specialists, computer scientists and research assistants/nurses.

Acknowledgment

I would like to thank the unwavering support of both Professor C. McCollum and Mr J. Ghosh whom continue to be enthusiastic about this research. I would also like to thank the staff and managers of IVS Ltd, particularly the Vascular Studies Unit, Wythenshawe Hospital. None of this research would be possible if it were not for their support and enthusiasm for the potential this research could make to their daily work. Particular thanks must be paid to Ms. Denise Nixon for her attention to detail and Mr Joao Carreira for his long hours second reporting. I would also like to thank the staff of Piur imaging and Imfusion for their dedication to providing the equipment and resources to complete this research. Final thanks must be paid to my family for their wholehearted support.

Section 1 – Introduction

Chapter 1 - Vascular Imaging

History of Ultrasound

Ultrasound (US) owes its origins to Sonar, first developed during World War II to help detect credible U-boat forces. It wasn't until 1942 that the first published successful application of diagnostic ultrasound transmission was reported [1]. The first successful use of ultrasound in medicine, reported in the UK, was in 1958, by Ian Donald, who reported the use of pulsed sound in the imaging of abdominal masses [2]. US was adopted initially by very few hospitals due to expense and limited diagnostic capability, but did make a significant contribution to the early development of modern diagnostic radiology. Homes and Howry made the next significant advance in US with the commercialisation of B-Mode (Brightness Mode) imaging in 1963 [3]. The Doppler effect has since been added to grey scale, "B-Mode" imaging, to detect blood flow and in 1974 was refined by Barber *et. al.* who reported the first commercial duplex scanner [4].

US has subsequently become established for routine vascular investigation in hospitals across industrialised nations and is fundamental to tertiary vascular centres. The use of B-Mode, colour Doppler and spectral Doppler analysis simultaneously, triplex imaging, also referred to as duplex ultrasound (DUS), are now considered basic vascular ultrasound pre-requisites. Recent advances in DUS instruments, such as contrast and B-Flow imaging, have revolutionised vascular US surveillance. A new development of US technology through the advent of three-dimensional (3D) reconstructions, could yield a new era, that could enhance vascular surgical follow up. Little work however, has been done on 3D US accuracy, variability, reproducibility and utility.

Basic Physics of Ultrasound

A basic introduction to the fundamental physical principles of US and US instruments is available in Appendix 1.

Vascular Ultrasound

DUS is ideal for vascular patients due to the advent of multi-element compound transducers with electronic beam steering and focusing [5], with high frame rates as well as their relatively small size and low cost when compared to Computed Tomography (CT) and Magnetic Resonance (MR) scanners. DUS is safe and suited for long-term patient surveillance with no ionising radiation or nephrotoxic contrast as it is not invasive. The mainstay of DUS use within vascular surgery is Doppler. The ability to assess velocity shifts across diseased segments allows the estimation of disease severity; ideal for Surgeons trying to decide whether to treat or not. This means disease can be measured in terms of functional severity giving additional flow information as well as diameter reduction calculations like angiography.

The small size of modern DUS transducers means multiple scanning angles are possible allowing insonation around artefacts. The reporting of vascular DUS imaging is usually completed by the persons acquiring the images; there is little time between scan and report, unlike other radiology-based assessments. The key advantage of DUS is its portability; it can be used in the community, outpatients, at the bedside, in theatre, or even intensive care.

DUS has become adopted for a wide range of vascular diseases and is the gold standard imaging modality for deep vein thrombosis (DVT) [6-8] and varicose vein assessment [9-11]. DUS has also become the first-line modality for Carotid [12-14] and peripheral arterial disease (PAD) investigation [15, 16] and has an established role in abdominal aortic aneurysm (AAA) disease [17-20], endovascular aneurysm repair (EVAR) [21-23], and arterio-venous fistula (AVF) [24, 25] surveillance.

Limitations of Vascular Duplex Ultrasound

DUS for vascular surgery is highly operator-dependent and is performed in the UK by Vascular Scientists or Sonographers with a high level of skill, and less commonly by Vascular Radiologists [26]. Skilled operators build a 3D mental image of the vascular pathology [27] and related anatomy from standard DUS images throughout the length of the relevant vessel. Untrained practitioners have difficulty interpreting these images meaning they may be uncomfortable about making clinical decisions and therefore prefer to arrange expensive and possibly unnecessary alternative imaging techniques such as CT angiography (CTa), MR angiography (MRa) and catheter angiography, where they can see the vascular anatomy and pathology themselves.

Although safer for patients, DUS surveillance is prone to error, as it is a representation of a small slice of 3D anatomy and therefore, anterior, medial and posterior transducer positions/scanning planes mean the exact same location cannot be guaranteed during follow-up [27]. By far the largest limitation remains artefact that produce acoustic shadowing, such as bowel gas and calcification (Fig. 1) that obscure the view of pathology, which can be hampered further by vessel depth. For carotid or aortic disease assessment this is a particular hindrance that significantly decreases sensitivity where alternative scan planes can avoid total obscurity and shorten depth. Other artefacts such as reverberation and mirror image, can falsify DUS images, creating the challenge of determining what is real for the operator.

Measurements are also challenging when using 2D DUS images. Volumetric assessment with DUS, such as for AAA or tumour size, calculated from circumferential and length measurements is traditionally inaccurate and with conventional technology it is not possible for complex structures like carotid plaque. A highly tortuous, kinked or coiled vessel can additionally cause flow to centrifugate and become turbulent, which falsely elevates Doppler velocities, meaning grading criteria based on blood velocities become redundant. Heart failure, sepsis or changes in vascular bed resistance, such as infection or temperature, can also change the pressure gradient caused through vaso-dilation, that can falsify Doppler velocities making measurement of stenosis severity complex. These challenges contribute to the continued role of CTa and MRa imaging for surgical clarification.

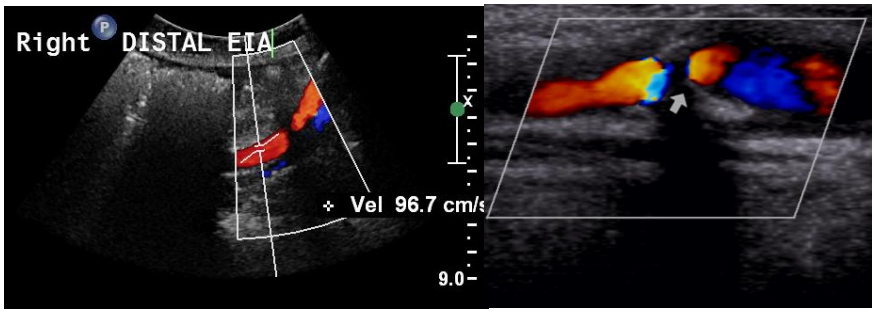

(Figure 1. Left, extensive bowel gas obscuring the view of the proximal and mid external iliac artery. Right, acoustic shadowing covering the view of the carotid plaque and proximal internal carotid artery)

Basic Physics of Contrast-Enhanced Ultrasound

Basic physical principles of ultrasound contrast agents and their use in imaging are discussed in Appendix 2.

Contrast-Enhanced Vascular Ultrasound

US contrast agents, often described as being microbubbles, are composed of a low blood solubility gas, enclosed in a biocompatible shell. They are designed to increase the backscattered US to allow better flow determination. The only licenced US contrast agent in the UK is SonoVue, manufactured in Italy by Bracco, and is composed of sulpha hexafluoride encased in a phospholipid monolayer. US microbubble contrast uses non-linear propagation which causes cyclic changes in size due to alternating US pressure waves to generate harmonic signals. This has the advantage of producing strong enhancement of flow without the usual ultrasound artefact. A low acoustic output must be used for contrast imaging to achieve sufficient enhancement, but a trade-off is required. Sufficient energy is needed to demonstrate the strongest contrast compared with surrounding tissues, but there is a ceiling at which the bubbles are destroyed by the sound wave.

Contrast-enhanced ultrasound (CEUS) has exciting scope within vascular surgery to improve flow visualisation and has an established role within cardiac and hepatic ultrasound imaging, but is now becoming mainstream in many vascular centres, filling a void between DUS and X-Ray, or magnetic imaging. CEUS provides clear demonstration of intimal flow borders and is highly sensitive to low flow states; more so than colour or power Doppler. Microbubbles have documented specificity and accuracy [28] and are of sufficient diameter that they can pass through the capillary network, but not into the interstitial space via endothelia fenestrations, therefore reducing the risk of underestimating stenoses. US contrast is not nephrotoxic and is excreted by the lungs rather than the kidneys, meaning patients with poor renal function can still be imaged as it does not reduce renal function further. US contrast agents are cheaper than X-ray contrast, but also much smaller volumes are administered to produce diagnostic images, keeping risk very low. The risks of severe and adverse reactions from US contrast are very low and as it is therefore, considered safe.

Limitations of contrast-enhanced vascular ultrasound

The most important limitation of CEUS is the fact it is still 2D which means Vascular Scientists/Sonographers build a mental impression that is open to misinterpretation. It is also difficult to reproduce the exact transducer location for surveillance. The main limitations of CEUS are related to the physics of US and patient body habitus. Marginally improved image quality is possible with CEUS than DUS alone, but CEUS is still limited by acoustic shadowing. Mirror image and posterior enhancement artefact are also still possible but due to using harmonic imaging other standard B-mode artefacts do not affect CEUS.

Tissue density and oedema make imaging deep vessels a challenge due to the lower acoustic output power than that used in DUS, despite CEUS's better sensitivity than DUS to low flow states. Heart failure and pulmonary hypertension also increase the time delay between injection and intra-luminal visible microbubbles. This can affect the diagnostic process involved such as in Endoleak detection where contrast time delay is important in EVAR surveillance. Mechanical heart valves and trans-catheter aortic valve implantation (TAVI) can also lead to some mild bubble destruction reducing intra-luminal concentration.

Manufacturing processes also impact CEUS imaging. How individual manufactures choose to produce the harmonic imaging can be different depending on manufacturer and the exact method is often patented or bound by confidentiality. This directly impacts on the contrast dosage needed. As a simple rule, the more superficial and distal the target vessel is from the heart, the higher the dosage required. The more distal and superficial the vessel, the higher the frequency used, meaning higher resolution images are possible. There is however, an inverse relationship between half-life and frequency, which leads to a compromise for adequate imaging. Experience with a particular manufacturer's equipment is an important factor to consider.

3D Ultrasound Imaging

3D US improves allows visualisation of pathology from all angles, evading the need to build a mental impression [27, 29, 30]. Accurate surveillance therefore, becomes reproducible as the same anatomy is visualised each time [27, 29, 31] and areas of anatomy inaccessible to DUS and CEUS imaging, such as close to the mandible for high carotid bifurcations, potentially become visible [27, 29]. A whole host of new measurements, such as volume, become available with 3D imaging [29, 31], for. Potentially 3D US benefits patients by identifying those at risk of significant mortality and morbidity sooner through new surveillance and assessment methods.

Types of 3D Ultrasound scanners

There are broadly four types of 3D ultrasound machines;

Mechanical 3D ultrasound

3D mechanical imaging can be performed by either a mechanical arm attached to a DUS transducer or via a motor-driven crystal within the 3D transducer housing [29, 31]. Motors move the arm or piezoelectric crystal a pre-defined set distance between each 2D image frame. A series of 2D image frames, separated by the pre-defined distance, are acquired and each image is placed in sequence into a 3D reconstruction of the anatomy. As the position and orientation of the 2D frames are pre-defined the 3D volume reconstruction is highly accurate [29, 32], resulting in short image acquisition times and high quality 3D reconstructions, but the apparatus can be bulky and cumbersome [29, 32].

Mechanical arms often need to be purchased separately and mechanical crystal transducers are not standard equipment for most vascular ultrasound departments, adding large costs. Motor-driven crystals also mean the transducer housing is larger than traditional DUS probes, which can be difficult to manipulate to achieve perpendicular views of the anatomy and requires large amounts of ultrasound gel, to facilitate heel-toeing.

The transducer can also be fixed in the mechanical arm, or held on the abdomen, at a non-perpendicular angle, allowing colour Doppler imaging when swept [32]. Alternatively, the transducer or crystal can be rotated, tilted or fanned whilst the transducer footprint remains fixed on the patient's abdomen to allow visualisation of slightly larger volumes. However, using rotation/tilting of the probe while the transducer remains fixed on the abdomen means non-specular reflection of the sound wave (see appendix), and further ultrasound wave travel, meaning large amounts of ultrasound energy are lost due to attenuation and 3D volume resolution can subsequently be poor [33]. Mechanical parts mean the systems can be more prone to failure compared to electronic or software 3D ultrasound methods.

Due to the physical limitations of mechanical methods, transducers or crystals can only be driven over short distances and therefore, only small sections of anatomy can be scanned, which are often larger than the 3D volume. As a result, multiple scans must be performed and 'stitched' together to allow visualisation of the whole anatomy which can degrade image quality. The advantages of mechanical 3D scanning are its near real-time volume reconstruction and short reconstruction times [31] and by using a mechanical arm, standard DUS transducers can be used, allowing users to take advantages of US technology/imaging development, cheaply [31].

(Figure 2. A Philips VL 13-5 MHz mechanical 3D transducer)

3D and 4D matrix scanning

Electronic-based imaging techniques were developed to navigate the requirement to move conventional DUS transducers attached to cumbersome mechanical arms over the anatomy. Matrix array transducers are a grid composed of large numbers (up to thousands) of piezoelectric crystals aligned in both lateral and elevational planes that produce non-real-time 3D volumes. Due to the sheer number of crystals in matrix probes multiplexing, signal processing and phasing of element excitation must be employed to reduce the number of wires needed to excite each crystal to keep the transducer cable a usable size [31, 34]. These processes can also make it possible for matrix systems to process and display real-time 3D image volumes, known as 4D matrix imaging [31]. 4D matrix scanning has been shown to improve AAA diameter and volume assessment compared to CT [35] and endoleak detection and visceral vessel revascularisation in fenestrated EVAR (FEVAR) [36]. 3D and 4D volumes are traditionally a truncated pyramid in shape.

In 3D and 4D matrix scanning, the transducer is electronically swept across all the piezoelectric elements. The probe is kept still and produces a limited 3D reconstruction size, with isotropic resolution. A fixed number of elements in the grid mean a maximum fixed reconstruction size which can be smaller than the desired anatomy. Selecting an appropriately sized Matrix is therefore, essential (e.g. 50 x 50 or 128 x 128 elements), but like mechanical scanning, ‘stitching’ multiple scans together is possible to visualise the full anatomy. Matrix transducers are delicate and expensive, meaning large volume reconstructions have not been commercially possible until recently [29]. Royal Philips has been successful in commercialising matrix transducers [34, 35], but other manufacturers are catching up.

Free-hand with position sensors

3D US imaging, via a free-hand holds the greatest potential within vascular surgery. Tracking sensors are attached to a standard DUS transducer and give the sonographer the ability to move the probe wherever they like, hence the name free-hand. To work the DUS instrument either has a 3D software package installed or is coupled to an external 3D system like Curefab CS or Piur tUS. Free-hand tracked methods are also as accurate and reliable as mechanical methods [37].

Sensors (Fig. 3) track transducer position and orientation whilst being swept over the anatomy tagging 2D image frames, from the conventional DUS scanner, with space and time information. Frames are then reconstructed based on this information, allowing the volume to remain accurate with greater operator freedom. Transducers can be manipulated easily over a large area and around obstacles, such as bowel gas and acoustic shadowing, but resolution is not isotopic. Various tracking systems have been utilised, namely potentiometers, acoustic, magnetic (preferable due to greater freedom) and optical based systems (most accurate) [29]. By utilising Standard 2D "off the shelf" transducers that have higher temporal resolution, and therefore higher quality images, than matrix probes are thought to be advantageous.

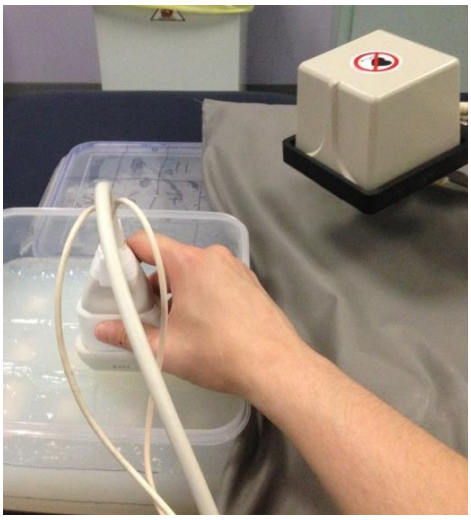

(*Figure 3. Magnetic tracking box and tracking sensors of a 3D free-hand sensor tracked system*)

Free-hand without position sensors

This method holds the same advantages as tracked methods, except no positional or orientation information is tagged to the DUS frames and assumes a pre-defined scan distance, taking a large amount of operator skill when scanning [29]. The lack of positional data means poor 3D volumetric reconstruction accuracy, therefore, measurements cannot be taken, but does produce rapid reconstructions [29]. Effectively, this produces qualitative images that are more applicable to real time imaging, but hold little diagnostic value. Although this method does not require specialist hardware and standard DUS transducers can be used, it is very rarely used within the literature. Accuracy is of high importance within Vascular Surgery; therefore, this method is unlikely to gain traction.

Tomographic 3D ultrasound

Tomographic 3D ultrasound (tUS) utilises a free-hand electromagnetic sensor tracked system using a frame-grab technique (Fig. 4). Once the DUS scanner is resolutionally optimised for the area of anatomical interest, the transducer is swept over the vessel, with the image being captured by the tUS computer, but is not real time. This system is compatible with most ultrasound systems commercially available and utilises software specifically generated for Vascular Surgery, but remains limited by the same constraints as standard DUS. tUS retains the possibility to visualise around obscurity. The software has a method for precisely calculating volume, producing a geometric mesh with high levels of accuracy. Certain features are semi-automated, such as vessel detection and image presentation, which also has manual error correction, that could reduce waiting times (replacing alternative imaging) and speed up patient through-put. This is the only system on the market that has this ability and is specifically engineered for Vascular Surgery, therefore, has the ability to overshadow the large commercial companies such as Philips.

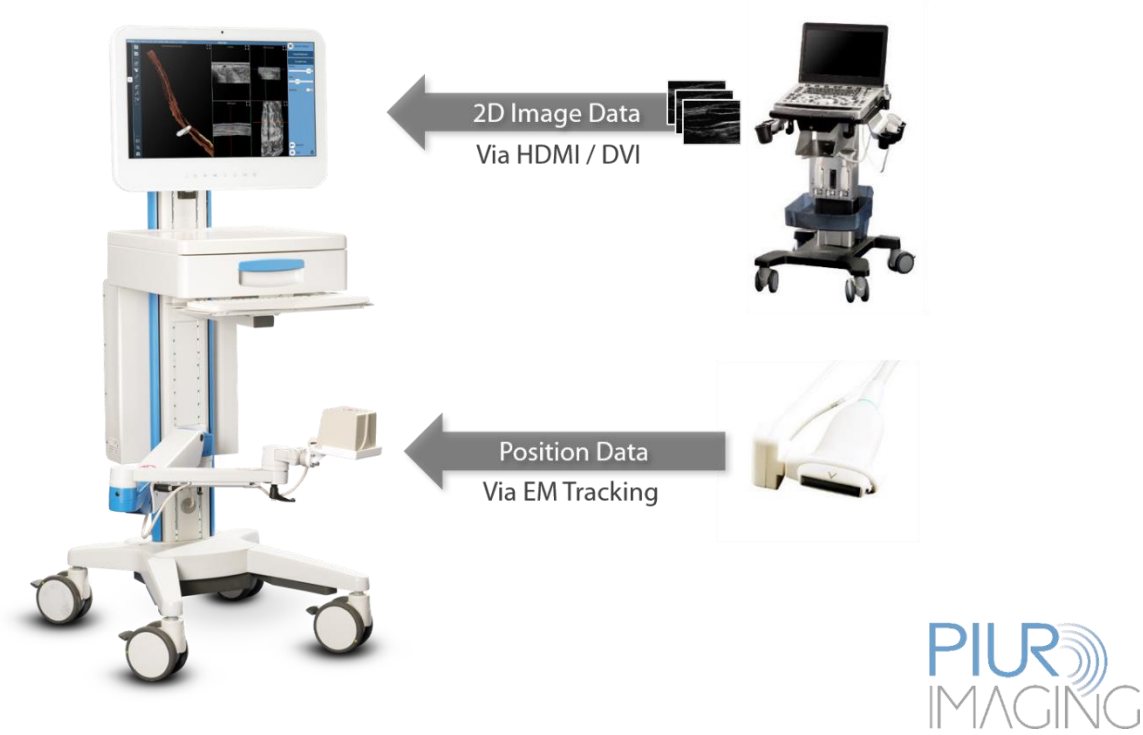

(*Figure 4. Piur imaging tomographic 3D ultrasound electromagnetically tracked device. Reproduced with permission of PIUR imaging GmbH*)

Limitations of 3D US and tUS

3D US addresses some but not all the limitations of DUS and CEUS but also has disadvantages of its own. A crucial downfall is the lack of Doppler information. 3D US imaging currently does not allow flow information to be presented clearly. Although colour Doppler information can demonstrate flow this is difficult to read in 3D as it contains a lot of colour Doppler artefact. Instead, 3D US can be utilised for demonstrating patency. 3D spectral Doppler for velocity calculation is not yet possible, but would be immensely useful.

Motion artefact is also a large limitation of all types of 3D imaging, including CT and MR, which, to some extent, can be combated. Respiratory motion can be limited by breath holding, but does limit to small quick 3D scans, and pulse gating can be utilised to evade cardiac and arterial wall motion. Physical patient movement on the couch is the most difficult to limit but can be minimised by asking the patient to remain still. Patient movement cannot be compensated within tracking, meaning patients with tremor may not be suitable but can be limited by fast image collections with free-hand systems [32].

Computer science is essential to 3D imaging but can also be a source of imperfection. Most 3D US systems use sophisticated software, which relies on complex computer algorithms [32], where glitches within the coding of these algorithms can affect reconstruction accuracy, but these are usually obvious when images are reviewed. Although the ability to calculate volume of disease is an exciting advantage of 3D US, Fenster et al (2011) outlines that segmentation algorithms, the common most method for calculating volume, are lacking as they require significant amount of time from experiences users manually calculating the volume slice by slice. Clinical acceptance of 3D US may depend on the development of automated segmentation methods, but these have previously failed due to artefacts, such as calcium shadowing, that cannot be read by the computer [29]. Artefacts pose a particular problem for automated segmentation methods as they represent a lack of information within a given region of the image need for measurement, i.e. calcium presents a large black void due to acoustic shadowing. This cannot be read by the computer correctly and leads to error in measurement. In the future artificial intelligence may be able to resolve this through prediction. Accurate reconstruction of anatomy also relies on accurate calibration of the system at set up; human error can affect accurate calibration.

Alternate vascular imaging modalities

Catheter Angiography

Digital Subtraction Angiography (DSA) Using Contrast Agents

Catheter angiography is an expensive invasive investigation involving a small incision and insertion of a sheath and catheter, intra-luminally, through which nephrotoxic contrast media is injected whilst being imaged by X-rays. When catheter angiograms are coupled with software, digital subtraction is commercially possible, where bone and soft tissue structures are subtracted from contrast images to leave clear anatomical images of vessels. This method is still considered the gold standard for arterial [38] and aneurysmal [39] imaging, mainly due to its lower contrast dose and due to the limitations of CTa and MRa in vascular imaging. Digital subtraction angiography (DSA) is limited by being uniplanar and the associated renal damage is now known to be cumulative.

The involvement of an arterial puncture means that there is a risk of active bleeding, haematoma, pseudoaneurysm and re-intervention. Although low-osmolality non-ionic contrast agents (considered slightly safer) are available, and the associated reactions are low, their widespread use within vascular radiology is limited by high cost. Bottinor et al reports that "the ability of low-osmolality agents to reduce the incidence of severe life-threatening reactions is still debated" [40]. In turn, high osmolality and ionic contrast agents are still widely utilised despite the higher supposed consequential risks, which are categorised into early and late onset. Early onset reactions occur within, or less than, one hour after administration and late onset has been reported to occur from one hour to seven days post-administration [40]. The rate of mild reaction is reported to be between 2.9 - 15% (ionic high osmolality) and 0.48 - 3% (non-ionic low osmolality), with severe reactions reported as between 0.04 - 0.37% (ionic high osmolality) and 0.004 - 0.04% (non-ionic low osmolality) [41, 42].

Digital Subtraction Angiography Using CO2 (DSA-CO_2)

DSA-CO_2 is not nephrotoxic and still requires arterial puncture, but can negate some of the artefacts of standard DSA due to CO_2's lower viscosity, having a much-reduced operational cost. CO_2 is much less viscous than gadolinium or iodine-based contrast agents therefore, it can pass easily through small channels or tight stenoses, representing patency [43], which may represent a lower false positive rate and has the benefit of being non-allergenic. The relative lack of toxicity means that there is no restriction in the total cumulative volume of CO_2 injected [44], however, there is a ceiling in which the concentration will no longer produce diagnostically better images. The diagnostic accuracy of DSA-CO_2 against standard DSA, using iodinated contrast for PAD, has been reported at 95% when performed well [45, 46], but does dissolve over time, particularly in patients with poor cardiac, output or in heavily diseased, small calibre vessels. This can mean that DSA-CO_2 can overestimate the severity of disease, such as in tibial vessels [47].

A phenomenon known as 'vapour lock' can also occur where CO_2 forms an embolus on a raft of blood cells leading to the over-estimation of disease severity and can lead to ischaemia in anterior wall branches, for instance, of the bowel [43]. Contra-indications include CO_2 retention in respiratory disorders, patients at moderate risk of myocardial infarction and cerebral or upper limb imaging due to neurotoxicity. The risks of DSA-CO_2 are important, but it is cheaper and much safer than DSA using contrast agents. There is a large benefit of DSA- CO_2 for those patients with renal impairment.

Non-invasive alternative imaging

Known side effects and invasiveness of radiological contrast media impact on patient experience and patients prefer other non-invasive imaging modalities [48]. The advent of CTa and MRa allows surrounding tissues to be visualised and reduces invasion. If performed well, CTa and MRa can produce equal image quality to catheter angiography and the number of diagnostic catheter angiograms has dropped significantly as the number of CTa and MRa investigations have gone up.

Computed Tomographic Angiography

CTa involves ionizing radiation and nephrotoxic contrast media (usually iodinated) that causes cumulative renal damage and therefore, is not suitable for a small group of patients with poor renal function [49]. CTa does avoid the limitations of DUS and has a higher sensitivity and specificity, for instance, for peripheral arterial disease (PAD), reported to be between 92 - 99.2% and 91 - 99.1% respectively [50, 51]. Despite the higher sensitivity and specificity and overall better image quality for isolated calf and iliac arterial disease (over DUS), CTa can still be performed badly, significantly reducing its diagnostic capability. The sensitivity and specificity for isolated arterial calf disease has been reported to reduce to 91% and 85% and for isolated iliac arterial disease 92% and 94% [51].

Overestimation of the severity of calcified stenoses by CTa is a major limitation thought due to two main factors; modern CT scanners use maximum intensity projections where vessels that lay close to bones can demonstrate false lesions and calcified disease is highly attenuative. Therefore, CTa requires skilled interpretation and experience to ensure these are not falsely reported.

Magnetic Resonance Angiography

MRa is more expensive than CTa, does not use ionizing radiation and often involves using a gadolinium-based contrast agents. In patients with renal failure, gadolinium contrast agents pose a higher risk of nephrogenic systemic fibrosis [52] and patients whose glomerular filtration rate is close to borderline for use with gadolinium require pre-admission for intra-venous (IV) hydration to protect the kidneys, adding to the expense. The advantage of MRa is in the assessment of infra-popliteal calcified calf vessels (Fig. 5). Kreitner et al (2008) has proven that MRa is as accurate as DSA in assessment of the crural arteries and the foot (k = 0.89) meaning therefore, that diagnostic DSA should not be performed for PAD [53].

Image processing is much quicker than CTa due to semi-automation, but acquisition times are longer and more operator-dependent. MRa scans can easily be mistimed producing an undiagnostic image due to venous contamination, such as when imaging for PAD [54], but this is somewhat dependent on the method of imaging. Traditional bolus chase methods of imaging have a much higher incidence [55]. MRa cannot be used with some metallic implants, including older vascular stents or pacemakers due to the risk of over-heating. Vascular stents also pose the problem as filling voids are often seen (such as with iliac stents), resulting in misdiagnosis of occlusion. DUS can mitigate this with waveform profiling at the groin. Access to an MR scanner due to clinical capacity can also prove problematic; Vascular centres that are within hospitals with Cardiac or Neuro surgical specialities may struggle to gain access to MR scanners, leaving a reliance on CTa with its associated risks and downfalls.

Overestimation of the severity of stenoses by MRa due to the manner in which data is digitally manipulated to produce what can be visually impressive images, is also possible. This is primarily due to the sampling rate [56] when a maximum intensity projection, is used meaning source data must constantly be assessed to avoid misdiagnosis. Misclassification of carotid stenosis is reported to be in the region of 15% [57].

Dependence of Vascular Surgeons on these alternative imaging techniques means Interventional Radiologists spend an increasing amount of time performing diagnostic catheter angiograms and reporting CTa and MRa scans, therefore, intervention waiting lists are increasing.

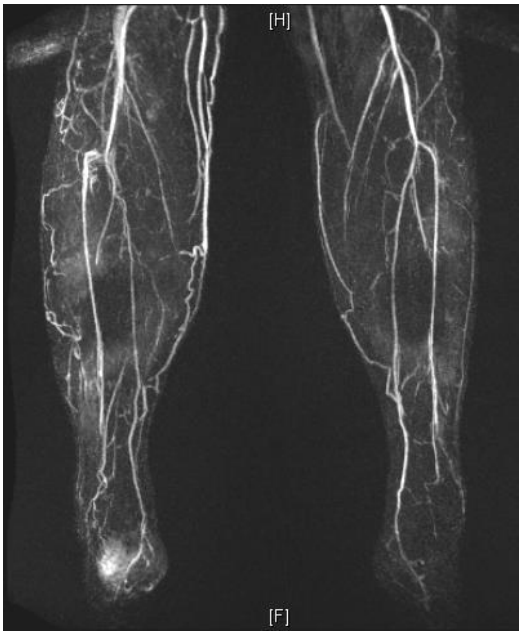

(*Figure 5. MRa of crural arteries bilaterally with venous contamination in a patient with right leg short distance claudication*)

Role of Imaging in this Thesis

tUS possess all the advantages of 3D US, namely lack of nephrotoxic contrast and radiation, and is specifically tailored for vascular surgery, making user interface simple and quick, likely increasing its acceptance within the clinic. However, its accuracy needs to be assessed compared to current practice; either DUS, DSA, MRa or CTa. Secondary outcomes of this thesis will provide evidence around time or new diagnosis methods.

DUS scanning is already quicker than some alternative imaging, but tUS scanning could decrease scan time further having three advantages. Firstly, a lower level of operator-dependence may be created increasing accuracy of diagnosis and secondly, improving cost, which can be improved in two ways. As the time of tUS scan acquisition may be shorter, more patients can be seen within the same length of time. Cost effectiveness of disease management is also improved as tUS is significantly cheaper than alternative imaging. Thirdly, reducing scan time for Vascular Scientists also dramatically improves the risk for developing repetitive strain injury and less alternative imaging means less reporting by Consultant Radiologists. This in turn could shorten intervention waiting lists.

The ability to present data in a new and accurate format to the Surgeon is advantageous as it is not in the Vascular Scientist's/Sonographers mind or in a written report, increasing trust in the result as the Surgeon can see disease for themselves. The most exciting potential role of tUS is new ways to analyse scan data, meaning new clinical parameters can be measured opening new surveillance and assessment methods maybe changing which patients are operated on and when. The ultimate goal for tUS could be in assessing disease risk factors leading to screening and early intervention.

Chapter 2 – Relevant Vascular Diseases and Ultrasound

Abdominal Aortic Aneurysm (AAA)

An abdominal aortic aneurysm (AAA) is an enlargement of more than 50%, in the diameter of the aorta due to a weakening of the arterial wall and is often described as a focal swelling. The exact cause is unknown, but family history and smoking are known risk factors. Traditionally prevalence of AAA in 65 to 79-year-old men is reported to be between 5 and 10% [58, 59]. In 2018 the NHS national AAA screening programme reported a less than 1% prevalence of AAA in the screened population of eligible 65 year-old men [60]. The major associated risk of AAA is death due to rupture. Historically 80% of out of hospital ruptures and 50% of those patients that reach emergency surgery died [59, 61, 62]. The 2018 National Vascular Registry now reports a weekday, in-hospital, mortality from ruptured AAA of 35.2% which increases slightly to 40% at weekends [63].

Ultrasound imaging of AAA

Since the Cochrane review by Cosford et al (2007), the national AAA screening programme was set up in the UK. The current 'gold standard' for AAA surveillance (Fig. 6) remains DUS which is accurate when compared to CT for measuring diameter [md 4mm+/-12(SD)] [64], with surgical intervention only recommended when an aneurysm is greater than 5.5cm, or has increased >1.0cm/year for men [65]. As DUS is accurate in measuring AAA diameter, there is little use for CEUS. Recent data has shown that clinically relevant AAA dimensions have advanced by a decade in terms of patient age [66], controversially suggesting that screening of 65-year-old men may no longer be relevant [67]. There is emerging evidence that the age of AAA screening should increase to 75 in men and include women, but this remains controversial [68, 69]. New evidence suggests that when using the same quality-of-life assessment tools used in male AAA screening, screening women for AAA may not be cost-effective [70].

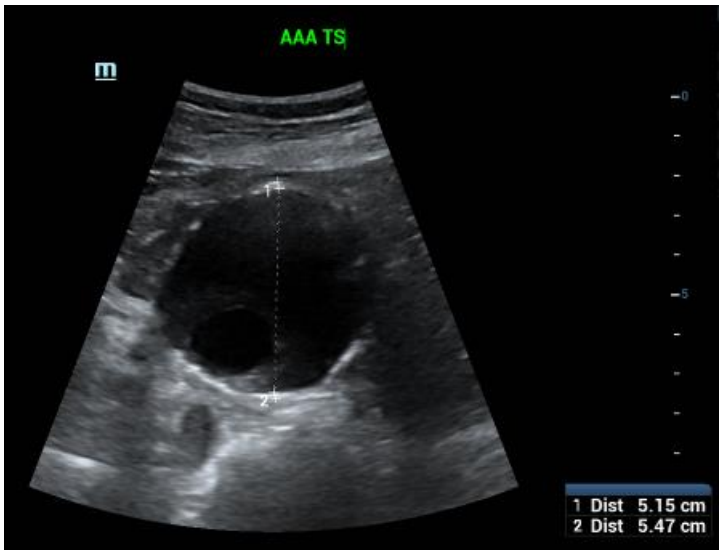

(*Figure 6. Anterior-posterior AAA diameters on ultrasound*)

Treatment of AAA

Once DUS surveillance indicates that an AAA has reached surgical threshold (>5.5cm in men), patients are referred for CTa to aid surgical planning and determine surgical choice. We currently have three options for AAA management. Best medical therapy remains the best option for those patients who have limited life expectancy, or whom surgery is contra-indicted due to extensive co-morbidities, making surgery not an option. The two options available for AAA surgical repair are conventional open surgical repair with a tube graft, or via the less invasive option of Endovascular repair.

Open Surgical Repair

Surgical repair is considered the definitive treatment and requires an extensive abdominal incision (midline, transverse or retroperitoneal), and mobilisation of the bowel. The aorta is clamped above and below the aneurysm sac which is then incised and the atheroma removed. A prosthetic tube graft is sewn into the aneurysm, effectively excluding it from the circulation and the remnant aneurysm wall is oversewn to aid healing and reduce the risk of aorto-enteric fistula or infection. The bowel is then replaced and the abdomen is closed via a layered closure technique. This is major abdominal surgery and requires a period of organ support on an intensive care unit postoperatively. Complications including those directly relating to the operative procedure and general complications which can occur after any anaesthetic. Aneurysm repair specific complications include lower limb ischemia, bowel ischaemia, major haemorrhage, surgical site infections and in the longer-term graft infection and incisional hernia [63]. General complications of major surgery include myocardial infarction, respiratory infection or failure, acute kidney injury and venous thrombosis. While approximately 5% of complications require a return to theatre, the advantage of open repair is the durability of the inlay technique and lack of requirement for image-based follow-up [63].

Endo-Vascular Aneurysm Repair

Endovascular Aneurysm Repair (EVAR) is minimally invasive and was first reported in 1991 [71] which can be performed percutaneously via common femoral artery access and catheter delivery. Patients can be discharged the same day or the following day, but device-related complications require lifelong imaging-based surveillance. EVAR significantly decreases hospital stay, making it suitable for the aged patient and high-risk cases. The short-term cost-effectiveness and health benefits of EVAR are advantageous, but the long-term advantage may be about equal to open repair [72, 73]. Device-related complications maintain a much higher rate of intervention in EVAR, as late as 8 years follow up, with an overall re-intervention rate of approximately 20% up to four years [73]. EVAR does have lower 30-day mortality than traditional open repair [74] but the mortality advantage of EVAR treatment for AAA rupture, over open repair, is ambiguous [75, 76]. The EVAR trial 1 reported that EVAR not only had an early survival benefit and was inferior to open repair beyond 8 years due to sac expansion, but the EVAR group had a higher cancer mortality [77] which is important when considering a CTa based surveillance programme. However, EVAR1 is an old study, and although it is the best published evidence we have, it must be interpreted with caution because of the advances in EVAR technology and improvement in patient outcomes. Despite this, the cost-effectiveness of EVAR over open repair remains questionable and continuous life-long surveillance is required to assess and monitor for potential complications and in the UK, DUS, CEUS and CTa are used [78].

3D ultrasound imaging for AAA pre-treatment

The main focus of 3D US imaging of AAA is in volume, diameter and rupture prediction. 3D US imaging of AAA initially was used in volume assessment for growth and surgical planning. Loretta and colleagues (2001) utilised advantages of tracked free-hand ultrasound to demonstrate AAA geometry [79]. Their investigation lacked true clinical value and did not involve electro-cardio-gram (ECG) gating, but did pave the way for future investigations outlining key areas of work. A recent paper has been published on partial volume assessment, but fails to outline its utility clinically [35].

The most clinically accepted use of 3D US in AAA has been in diameter assessment. Assessment of a complete aneurysm, including neck and iliac bifurcation, can be challenging and often results in poor quality images using DUS. 3D US assessment of diameter may mean that operator variance of diameter assessment is reduced, making surveillance faster due to shorter scan times and more accurate. A more accurate measurement means a true increase in AAA size can be determined earlier resulting in prompt surgical decision.

Long and colleagues have outlined a tool for calculating 'partial volume' in the absence of landmarks, aiming to improve aneurysm diameter accuracy, demonstrating significant inter-class correlation, (0.99) but relied on maximal diameter to be visualised on DUS before 3D acquisition, due to the use of a mechanical transducer with limited field of view [80]. Unfortunately, this study was limited by not being compared to an established 'gold standard', which was addressed by Causey et al (2013), but only in patients post-EVAR [81]. Bredahl et al (2015) reported the use of a 3D matrix probe in AAA diameter assessment, via volume segmentation, and compared to the 'gold standard', where possible [35]. Bredahl reports significant correlation of diameter and volume with strong reproducibility, along with a rapid analysis time of 72 seconds, making 3D US in this way suitable for the clinic [35]. All these works have utilised methods that measure an AAA in the anterior-posterior fashion, based on currently accepted standards in a hospital-based setting. No work has tried to measure the largest maximal diameter in any plane.

Being able to determine which AAA's are more likely to rupture from surveillance and screening remains the unified goal and prediction has been approached from different angles, including computational fluid dynamics, wall stress and strain assessment. Wall stress is thought to be the most important biomechanical parameter to measure – i.e. the most likely to predict rupture [82]. 3D mechanical imaging has been utilised in assessing wall stress, but due to the limited field of view multiple scans must be performed and "stitched" together to allow visualisation of the whole anatomy, degrading image resolution, which can alter wall stress representation [83], making data clinically unusable. Despite this work, we still do not know what an acceptable level of stress is and more research is needed.

A large amount of work has been completed on strain calculation despite it being an assessment of deformation, which is presumed to lead to increased wall stress. In 2013, Bihari and colleagues used an echocardiography 3D speckle-tracked matrix scanner to assess AAA strain in a silicone perfusion model *in-vitro* and in five patients, where data had to be exported to a second piece of specialist software to be analysed [84]. Bihari et al (2013) concluded that strain can be measured *in-vivo*, but failed to add any clinical relevance of rupture prediction in the five patients included. Karatolios et al (2013) used the same setup as Bihari in an unpowered feasibility study on eight patients, but assessed normal with aneurysmal aortas, reporting a significant difference in biomechanical properties and stated that their data may demonstrate the possibility of indices for rupture prediction, but offer no individualised patient-specific predication [85]. Derwich et al (2016) used the same system as Bihari and Karatolios in sixty-five patients and discerns differences between young, old, normal and aneurysmal aortas, recognising that a long-term follow-up investigation is needed before patient specific rupture prediction can be apportioned [86]. This is the closest work to individual rupture prediction to date.

All 3D US work on wall stress and strain uses systems that have limited fields of view using matrix and mechanical 3D US systems, but most utilise ECG gating to ensure a higher degree of accuracy. As outlined by Kok et al (2015), the key area of stress tends to be within a specific location. This leads to multiple acquisitions being needed for a single anatomical aorta, which can falsify results and is applicable to both stress and strain investigation, although this was acknowledged. Further research should focus on, using free-hand sensor tracked ECG gated 3D US systems.

Potential 3D ultrasound research pre-AAA repair

Future 3D US research in patient's pre-AAA repair will focus on rupture prediction. However, there is research missing from the literature on measuring non-AP diameters (medial-lateral) (Fig. 7). Aneurysm screening using AAA volume calculated using AAA diameter measurement by artificial intelligence, may improve inter-modality variability, replacing the need for CT scanning. In addition to AAA luminal volume, as reported above, there appears to be no reported evidence in the assessment of aneurysmal wall volume with 3D US. This is interesting as it is the aneurysm wall that ruptures when it loses structural integrity. Despite being 1-3mm thick the volume of the AAA wall may change as a AAA grows. which may help in rupture prediction. As standard ultrasound is not recommended for highlighting potential inflammatory aneurysms 3D US may identify thickened AAA walls.

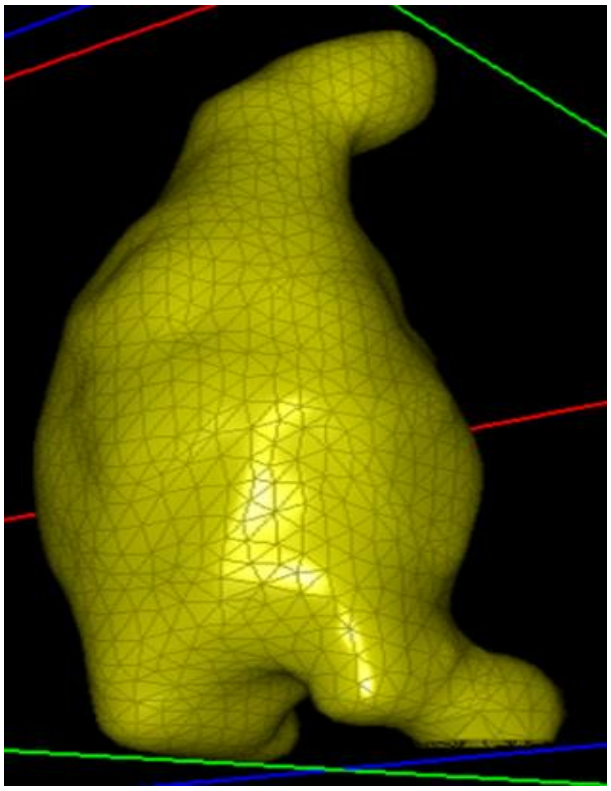

(*Figure 7. 3D ultrasound volume mesh used to create a model to calculate computation fluid dynamics for peak wall stress*)

Endovascular Aneurysm Repair (EVAR) and Post EVAR

Duplex ultrasound imaging of EVAR

Secondary intervention post EVAR is generally due to the inability of the stent graft to exclude the aneurysm sac from the circulation, resulting in endoleak and sac expansion (Fig. 8). DUS is adequate and cost-effective as a first line tool for Endoleak screening but it can be poor for low flow leaks in patients with large body habitus. DUS has a much higher sensitivity, 74% vs 42%, at determining leak type than the current 'gold standard' of CTa, at the point of intervention and has a sensitivity and specificity for detecting leak of 90% and 81% [87]. One limitation of DUS is its inability in detecting stent fracture and migration easily, which can be detected by plain X-ray with ease. DUS, coupled with plain X-ray, are now considered sufficient for EVAR surveillance and are estimated to save €223 per patient [23]. Many vascular centres have adopted a surveillance programme of CTa at three months and then DUS with plain X-ray at 6 months, 12 months and then annually. Should a complication, such as diameter increase, or Endoleak be detected, patients are referred for an 'urgent' CTa, but many centres are now also relying on CEUS and the role of CTa in EVAR surveillance is diminishing.

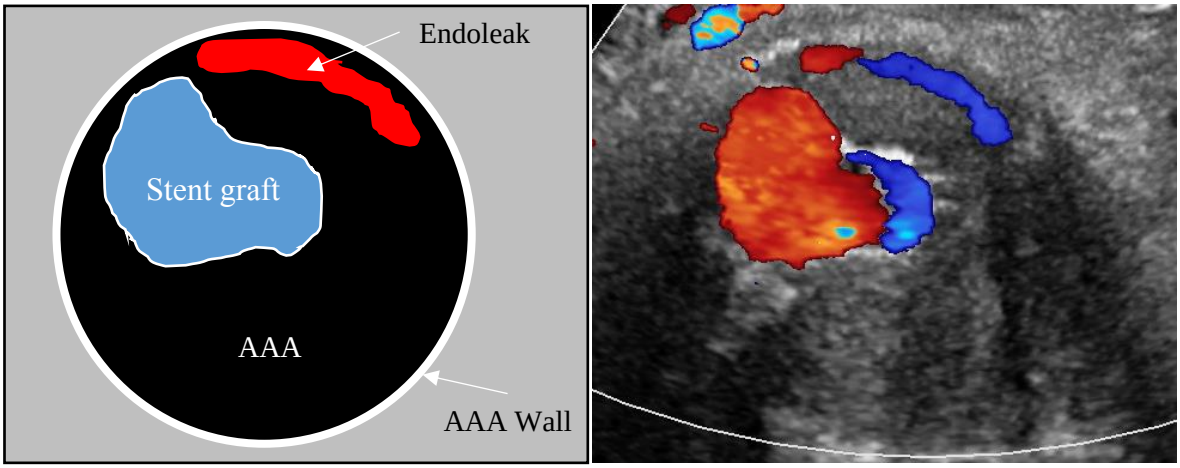

(*Figure 8. Endoleak detection on duplex ultrasound*)

Endoleak types are explained as;

- Type 1a – leak originating from the proximal seal zone – significant and requires re-intervention.
- Type 1b – leak originating from either of the distal seal zones - significant and requires re-intervention.
- Type IIa – leak from an aortic side branch but no exit for flow – only significant if sac grows.
- Type IIb – leak from an aortic side branch exiting via one or more side branches – not significant and usually benign.
- Type 3 – mechanical failure of the graft from fracture, a hole or modular separation - significant and requires re-intervention.
- Type 4 – porosity of the stent graft. These are rare with modern stent grafts.
- Type 5 – an increase in AAA sac size but no leak identified (described as endotension). Often significant and require intervention if leak cannot be identified.

CEUS imaging of EVAR

The major, widely published, application of CEUS in vascular surgery is for the investigation and surveillance post-EVAR, with documented evidence on the equivalence to CTa in Endoleak detection [88]. Other uses of CEUS is aneurysm diameter measurement and evaluation of target vessels for EVAR [89]. Establishment of target vessels for fenestrated or complex EVAR is a reason CTa is requested as it is crucial for determining technical feasibility. Our group has previously shown that 3D CEUS can adequately identify renal arteries intra-operatively in most cases and is sensitive to Endoleak [90, 91]. The use of CEUS, coupled with cone beam CTa, is well documented to be equivalent at diagnosing Endoleak, but has also been proven to reduce nephrotoxic contrast and radiation dosage, leading to shorted hospital stays [92]. However, there still appears to be a reliance of CTa, despite CEUS being equivalent.

3D ultrasound imaging post EVAR

3D US imaging of aneurysms post-EVAR is complex and focuses primarily on the role of complication detection. This has been attempted in three ways, volume and diameter changes as a predictor of rupture risk and more interestingly in the role of endoleak detection and classification. Complication-free success post EVAR is thought to be demonstrated through remnant sac shrinkage. Transversely, sac enlargement, or endotension, significantly increases the risk of rupture within the short term and is considered a surgical emergency.

Changes in aneurysm volume have been detected earlier than with diameter assessment but also when there has been no change in sac diameter when assessed by CTa [93, 94]. This is important because a very small change in AAA diameter may be within ultrasound inter-operator variance (3mm) but a large change in AAA volume may have occurred. This outline represents the principle that aneurysm volume may be more sensitive to changes in EVAR sac and may highlight potential new assessment methods to help detect complications. In 2013, Bredahl et al utilised a matrix transducer with improved field of view over mechanical predecessors and reported successful volumetric assessment using 3D US, compared to CTa. Bredahl et al (2013) reported statistical significance in volume measurement and inter-rater variability [95]. However, the study was limited by the requirement for the user to identify the maximal dimension in both anterior-posterior and long sectional images using a biplane function, although this required user input it is subject to operator error and variability. Causey and colleagues (2013) used a free-hand magnetically tracked system that was ECG triggered to reduce pulsatile variation, which had the advantage of demonstrating the whole anatomy accurately in one acquisition. Causey et al (2013) reported Bland-Altman agreement of 100% between 3D US and CT with inter-rater reliability between 0.92 and 0.999 at 8 weeks post acquisition [81]. Despite the small sample number of seven patients this is highly accurate.

Other groups have demonstrated significant accuracy with 3D US centreline derived diameters, which is the same method utilised by Radiologists in reporting CTa scans and improves inter-modality comparison. The Causey group described above in 2013, reported 92% agreement between 3D US and CT for diameter assessment, but only included seven patients [81]. Another study examined a much larger cohort and reported 1.3mm variability in diameter assessment between 3D US and CT using prototype software that defined the centreline to calculate the maximal inner-to-inner diameter [96]. This team used a 3D matrix transducer, but also required the user to identify the maximal diameter using biplane images before 3D acquisition. This somewhat seems to negate the benefit of using 3D ultrasound if trained and skilled input is required for it to work.

Our group has previously reported the advantages of using a free-hand tracked 3D US system on thirty EVAR cases paired with CTa for endoleak detection and classification [91]. Although this study demonstrates strong inter-rater reliability and high sensitivity, this is likely to be due to the use of ultrasound contrast that improves detection of low flow endoleaks, particularly type II which can be below the threshold for detection by standard duplex. The key advantage of this system was its ability to capture the full aneurysm anatomy in a single scan and demonstrate the source and exit of type II leaks (Fig. 9). 3D CEUS for endoleak can also help differentiate between type 1b and very proximal type II endoleak, which would change patient management. Lowe et al (2017) has continued this investigation to address some of the Abbas study shortcomings by increasing sample numbers to one-hundred patients and decreased the interval to be paired with CT to the same day, and demonstrates the same advantages, outlining a potential reduction in angiography [97].

An Italian group has utilised matrix scanning on twenty-two patients assessing diameter, volume, endoleak and patent visceral vessels in fenestrated EVAR [36]. A 4D matrix transducer was used, which relied on operator-defined biplane maximal diameter for 4D acquisition and uses separate software for analysis. This study reveals strong diameter and volume correlation ($p < 0.01$), 96% agreement on endoleak detection, with only 8% of visceral vessels not identified between 4D US and CTa [36]. Although the detection of endoleak looks impressive, there were only three endoleaks identified in the cohort by CT and one was missed by 4D CEUS due to patient obesity. No meaningful conclusion can be drawn from this study due to it being underpowered and although commercially available, the system utilised relied on user input for acquisition, plus images had a limited field of view. Small patients with large and long aneurysms that involve multi-segments would not be suitable for imaging with matrix probes, resulting in multiple scans being required and even unnecessary additional bolus administrations of ultrasound contrast, which does not add a large advantage over CTa like free-hand techniques would.

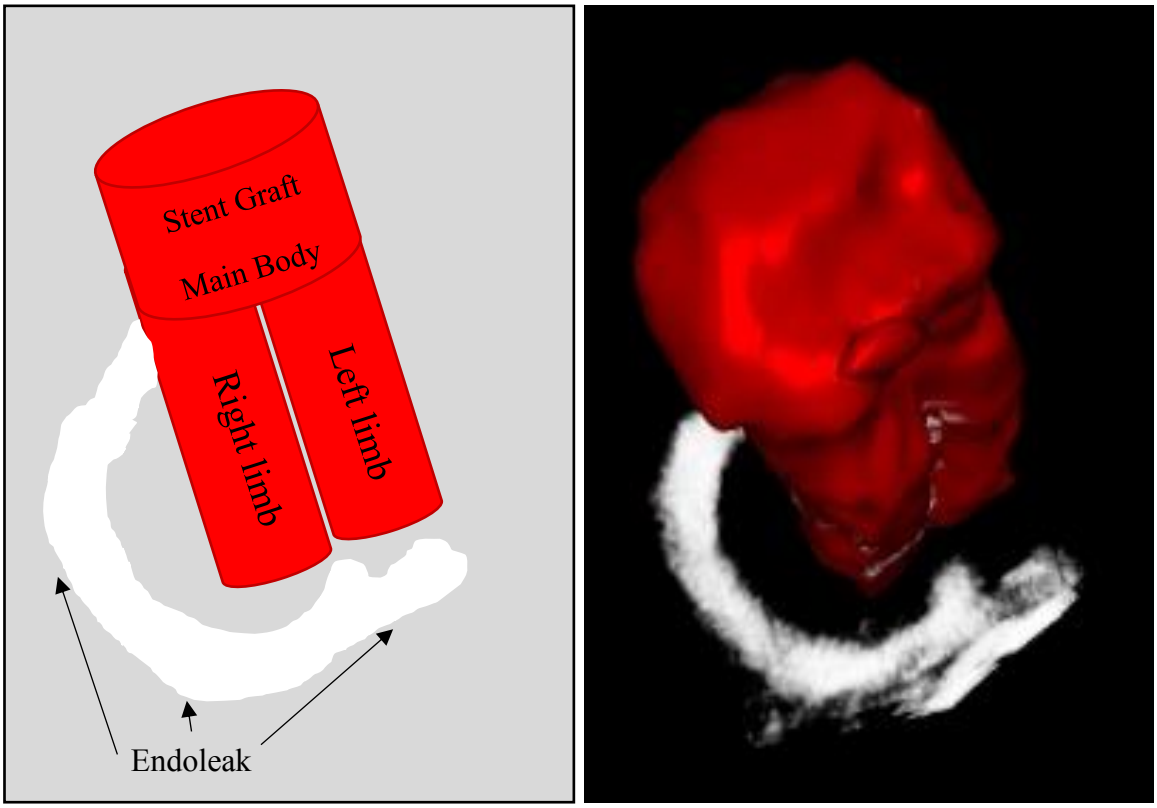

(*Figure 9. 3D CEUS ultrasound of a type II endoleak following EVAR*)

Potential EVAR 3D ultrasound research

Future research of 3D US imaging of EVAR should focus on intra-operative completion assessment to reduce nephrotoxic contrast and radiation exposure. There is scope more towards 3D US deployment of EVAR to negate the use of DSA completely, but more evidence is required for the benefit of 3D CEUS in the completion of EVAR first. There is also scope to utilise free-hand tracked 3D US imaging in FEVAR and FEVAR completion. More work on volume and diameter surveillance in the form of long term follow up studies, is necessary to outline clinical utility before adoption.

Atherosclerosis and cardiovascular risk

Atherosclerosis is the process by which lipid-leaden macrophage deposits and other material, such as cholesterol, calcium, thrombus and protein, build up within an artery (Fig. 10), usually at the point of microtrauma, and promote an inflammatory response [98]. Points of curvature, branching or dilation are more prone to microtrauma. Microtrauma can cause greater flow disturbance, which in turn causes higher shear stresses between the blood flow streams and the artery wall [99, 100]. This turbulence results in cholesterol infiltration into the endothelial cell wall and over time leads to the build-up that, once hardens, forms a plaque that results in a narrowing of the vessel lumen. Increases in shear stress, due to atherosclerosis, also forms a feedback loop, making the artery more susceptible to plaque build-up [101]. Once atherosclerosis builds up to a critically flow-limiting stenosis, or diffuse disease burden, patients may become symptomatic.

Being overweight [102, 103], diabetic [104, 105], having dyslipidaemia [106, 107] or hypertension [108] and smoking [109] are the main risk factors of cardiovascular disease. Being not particularly physically fit is an important surrogate for all of these risks. The symptoms and conditions associated with atherosclerosis include myocardial infarction, angina, stroke (cerebral vascular accident (CVA), reversible ischaemia without neural deficit (RIND) and transient ischemic attack (TIA)) or peripheral arterial disease (PAD) which can all lead to vascular related death.

We now know that surgically treating atherosclerosis at the symptomatic stage is costly to the NHS and is often a protracted terminal treatment plan. Early, long-term use of anti-platelet drugs, like Clopidogrel, are effective at reducing risk [110]. Additionally, there is strong evidence that moderate or high intensity lipid-lowering drug therapy using statins not only reduces cardiovascular but also all-cause mortality, where a target of achieving an LDL-c level below 1.8 mmol/L is important [111]. Although medical optimisation at the point of symptom onset can reduce cardiovascular risk, it is too late to stop the risk developing in the first place. Cardio-vascular screening [112] and aggressive early medical therapy may significantly reduce the number of cardiovascular-related mortality and morbidity.

Imaging for cardiovascular disease can either be prospective or preventative. The use of imaging in cardiovascular screening is vital and has been shown to improve patient compliance of medical management and reduce cardiovascular events [113]. Despite this importance, the main volume of vascular imaging is currently for surgical screening and planning.

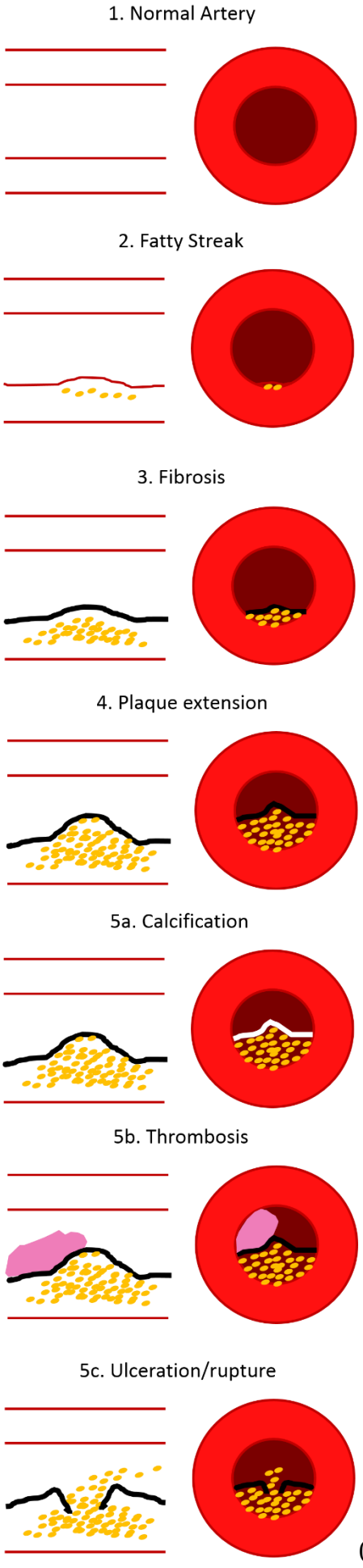

(*Figure 10. Stages of atherosclerosis*)

Carotid Artery Disease, Atherosclerotic Burden and Carotid Plaque Volume (CPV)

Stroke and Carotid artery disease prevalence

A stroke can be a life-threatening condition due to a sudden cut off in blood supply to the brain, either by a blockage or catastrophic haemorrhage. Over 150,000 people have a stroke in the UK each year and 20 - 30% of patients who recover from a transient ischemic attack (TIA) develop a full cerebral vascular accident (CVA) within one year [114]. Approximately 20% of patients with a >50% but < 99% carotid stenosis will have a stroke within 72 hours of symptom onset [115] and nearly 30% of patients will have a recurrent stroke following primary stroke/TIA [116]. The common most treatment for carotid stenosis in the UK is carotid endarterectomy (CEA) which maintains 'gold standard' status, due to its lower risk of procedural stroke or death than stenting by up to 61% [117].

Measuring severity of Carotid stenosis

National Institute of Clinical and healthcare Excellence (NICE) Guidelines indicate TIA patients and those with non-disabling stroke that are neurologically stable should have carotid DUS imaging within one week of symptom onset by a Specialist, only if they are deemed fit for CEA. There has always been controversy in the method of measuring carotid stenosis by DUS, whether this be European Carotid Surgery Trial (ECST) or North American Symptomatic Carotid Endarterectomy Trial (NASCET) criteria (Fig.11). Despite the joint working party collaboration in 2009 [13], establishing a uniformly agreed method of assessment (in the UK this should be NASCET), confusion between Vascular and Stroke Physicians still pertains. NICE guidelines therefore, still recommend CEA (for suitable symptomatic patients) that measure >70%^{ECST} diameter reduction or >50%^{NASCET} diameter reduction.

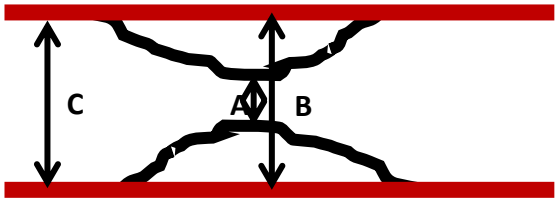

A = Patent lumen
B = Vessel lumen
C = Vessel lumen

ECST DR (%) = [1 - (A÷C)]
NASCET DR (%) = [1 - (A÷B)]

(*Figure 11. NASCET and ECST methods of Carotid stenosis measurement*)

Evidence for symptomatic CEA

Pooled data from ECST, NASCET and Veterans Affairs trials identified that patients with >70%^{NASCET} stenosis significantly benefited from CEA, but for those with >50%-69%^{NASCET} stenosis there is only marginal benefit [118]. Most UK Vascular Centres work from the European Society of Vascular Surgery (ESVS) guidelines operating on all symptomatic patients that are identified with a >50%^{NASCET} stenosis and perioperative stroke and death rate below 6% [119]. Pooling of the ECST and NASCET data reveals that the efficacy of surgery for symptomatic patients is significant ($p = 0.009$) if performed within 2 weeks of symptom onset [120].

Evidence for asymptomatic CEA

The benefit of CEA in asymptomatic patients remains unclear. The Asymptomatic Carotid Atherosclerosis Study (ACAS) study demonstrated a five-year risk of ipsilateral peri-operative stroke or death at 5.1% (53% aggregated risk reduction) in CEA patients with >60%^{NASCET} stenosis and a less than 3% mortality and morbidity risk [121]. The American Heart Association therefore recommend surgery in asymptomatic patients with >60%^{NASCET} stenosis if the stroke and death rate is 3% [122]. The Asymptomatic Carotid Surgery Trial (ACST) reported an overall risk of ipsilateral stroke of 6.4% in patients younger than 75 with >70%^{NASCET} stenosis, but with an overall thirty-day stroke and death rate of 3.1% [123]. Importantly, ACST informs us that the risk of stroke with a >70%^{NASCET} when randomised to BMT was only 9.5%, meaning that the measurement of stenosis (i.e. being >70%^{NASCET}) is not a good predictor. ACST also demonstrated that the benefit of CEA for women is not statistically significant ($p = 0.07$ versus $p = 0.0001$ for men) [123].

As a result of these large scale randomised trials the ESVS have adopted the guideline of recommending CEA in <75-year-old men with a risk of less than 3% and a carotid stenosis of >70%, but <100% and only in young fit women with significant stenosis as the benefit is not significant [119]. Many Surgeons still work on only operating post 80%^{NASCET} in asymptomatic patients. However, we know that a >80%^{NASCET} stenosis remains a poor predictor of stroke, with an ipsilateral risk of <2% [124], with the contralateral risk estimated to be below 1% [125].

Current Surgical Practice

CEA is recommended in symptomatic patients above 50%^{NASCET}, and >70%^{NACET} stenosis in asymptomatic men. However, there is a grey area, especially for women, in the symptomatic >50% to 69%^{NASCET} stenosis group where the benefit from CEA is marginal, but probably beneficial.

Carotid Plaque Vulnerability

The fact that only 9.5% of asymptomatic patients with >70%^{NASCET} stenosis randomised to BMT had a stroke [123] is crucial in informing us that the physical measurement of stenosis is not a good predictor of stroke. What is clear is that it is the content of a stenosis that poses the risk, not the percentage narrowing. Patients with a long 50%^{NASCET} stenosis may have a higher volume of atherosclerotic plaque than a 70%^{NASCET} stenosis, particularly asymptomatic patients, which represents a significant risk of future stroke due to embolic events because a high grade, but short stenosis, may have a smaller volume of plaque. Having more of a risky content may be more important and more specific. Evidence also suggests that the degree of stenosis can be reduced by outward remodelling of the arterial wall [126], making stenosis assessment unreliable at best. Recent work has also demonstrated, that stenosis as measured by current methods, may not be reliable and vulnerability assessment may be the best method [127-129]. It is therefore logical to assess carotid artery disease in terms of embolic risk (vulnerability) rather than stenosis.

DUS of plaque vulnerability

The future of carotid artery disease research and US lies within the field of risk stratification of atherosclerotic burden. Detection of high risk plaques using US techniques include, plaque neovascularisation, of which there have been attempts at quantification [130-133], grey scale median [134-138], fibro-cap thickness [139, 140], thermal strain [141-143] and elastography.

Thermal strain imaging remains an experimental procedure within animal models, but does pose interesting insights into lipid content and therefore, vulnerability. Commercially available technology is required before in-man studies can take place. The most recent vulnerability tool that has been utilised in research despite being relatively new, has been elastography. Elastography is an assessment of strain, the stretch and stiffness, within the plaque and is comparable to grey scale median [144, 145]. It is thought that stretch and stiffness may be a measure of lipid density/calcification and therefore, vulnerability. In *in-vitro* it has excellent inter and intra observer variation (interclass correlation of 0.84 and 0.83) [146]. In *in-vivo* it has proven to be reproducible, feasible and clinically utile [144], with high sensitivity and moderate specificity [147] for lipid cores [148].

CEUS of Carotid disease

Research of carotid plaques using CEUS has focused on assessing vulnerability and neovascularisation as a potential source of embolisation [130]. Neovascular flow theory surrounds the idea that neo-vessels form within the plaque making it unstable and therefore high risk for embolisation. The presence of neo-vascular flow within the carotid plaque has been linked with cerebrovascular events and CEUS has been proven as an accurate method for detection of carotid plaque neovascular flow. Published studies investigating neovascularization have only been performed on patients following their cerebrovascular event. We therefore do not know if neovascular tissue causes embolisation or is part of a healing process to stabilise the plaque after it has discharged emboli. This remains unanswered within the literature.

There is also documented evidence that the use of CEUS in occlusive carotid disease can distinguish between true occlusion and near occlusion with greater sensitivity than DUS and is equal to CTa [149]. There has been more scope in the assessment of CPV using B-mode US or DUS [150]. The next logical step in CPV assessment is the use of contrast to improve the accuracy in measurement of carotid plaque volume with 3D US (Fig. 12). Using the search terms of ultrasound, carotid plaque volume and contrast within PubMed, there is no documented evidence of the use of CEUS in calculation of CPV, at present.

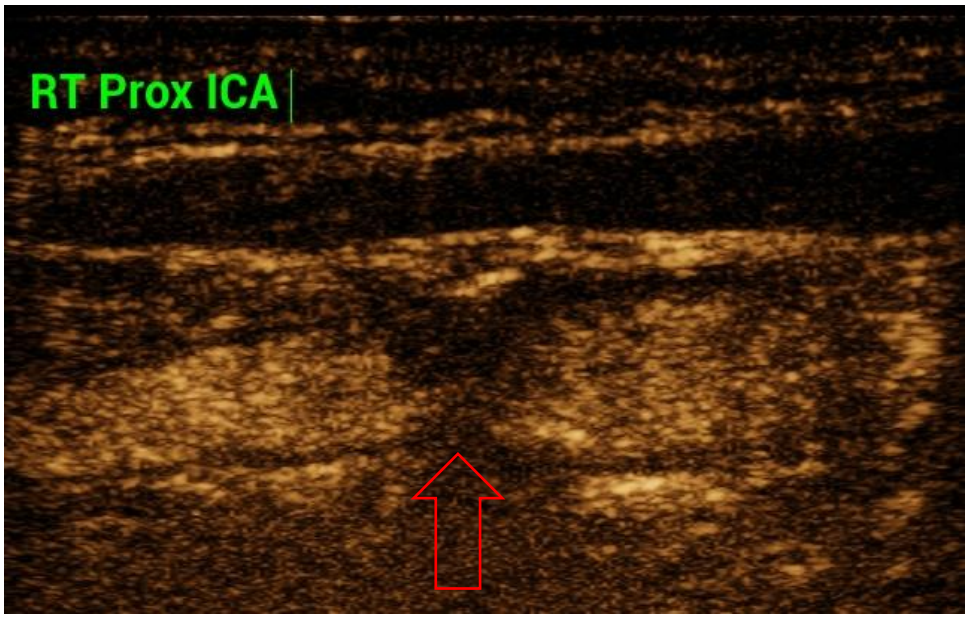

(*Figure 12. A long section contrast-enhanced ultrasound image of the right internal carotid artery. Red arrow indicates location of a 90-95%^{NASCET} stenosis*)

3D ultrasound measures of plaque vulnerability

Assessment of neovascularisation has focused on 2D. One study reported the quantification of neovascularisation in 3D, but acquisition was still based on 2D assessment [151]. There is only one reported case of 3D US assessment of Carotid plaque neovascularisation which is in Japanese [152]. This study uses a matrix transducer which yields a small high-resolution volume that would be adequate for carotid imaging, but investigate if neovascular flow causes stroke or is part of the healing process. There have been no reported attempts at 3D grey scale median quantification either with software or 3D US. Only one reported case assesses fibrous cap thickness using matrix 3D US on a small cohort investigating macrophage infiltration compared with immunohistochemistry [153]. This paper does evaluate the role of 3D US in the assessment of plaque vulnerability, but offers little clinical value. Although there has been experimental assessment of elastographic strain using 3D US [154] significant development is needed before *in vivo* assessment.

Carotid Plaque Volume (CPV)

The origin of CPV stems from Cardiology. Coronary artery plaque burden has long been shown to link with cardiac event and not coronary artery stenosis [155]. Previous work also links CPV and coronary artery burden to cardiac events [156] and the link between calcification and coronary artery burden voided the use of stenosis assessment [157]. The importance of CPV in acute stroke has been outlined with MRI [158, 159], but MRI is costly, time consuming and if involving contrast agents involves greater risk. MRI/a has been shown to underestimate the presence of carotid atherosclerosis [128, 129, 160]. Therefore, MRI may not be the most accurate tool for measuring CPV.

Our group has shown that at four weeks the CPV is significantly higher in symptomatic versus asymptomatic patients ($1.01cm^3$ versus $0.78cm^3$ ($p=0.003$) [161]. We also demonstrated that symptomatic CPV decreases over time (8 weeks) to a comparable level to asymptomatic CPV [161], consistent with the recommendation to operate within two weeks of symptom onset. We also know that CPV progresses longitudinally [162], increasing embolic risk and patients whose carotid plaque progresses longitudinally are at a 2.1 times higher risk of stroke, MI or death [163]. Progression of CPV has previously been proven to be a predictor of stroke/TIA and remains a risk factor, despite adjustment [164]. CPV is also sensitive to plaque regression when treated with aggressive medical therapy [162], is superior to intima-media thickness (IMT) and juxta-luminal plaque area and can be used to assess medical therapy [164].

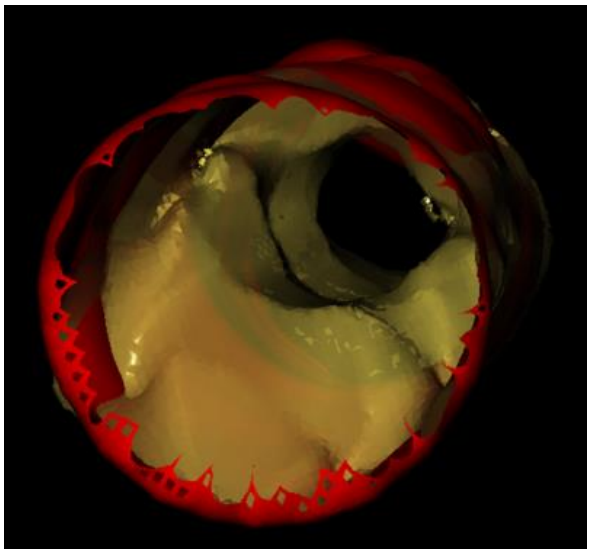

(*Figure 13. Carotid Plaque Volume as generated by 3D ultrasound*)

3D ultrasound measurement of CPV

The importance of being able to measure CPV accurately and non-invasively is essential to the ongoing utilisation of CPV clinically. There have been multiple studies assessing the ability to measure CPV with 3D US although these previous reports are limited, as they do not compare to true endarterectomised plaque immersion volume [162, 165-168]. Our group has previously shown excellent correlation between endarterectomy specimen and CPV measured by tUS (r=0.93, p,0.001) with minimal inter and intra-observer bias in a pilot study [169]. Our data was backed up by a smaller study that reported ICC between 3D US and endarterectomy volume of 0.93 [170]. The technical failure rate, due to calcification shadowing, large neck and poor image quality etc, could not be drawn from these studies and larger sample numbers are needed.

It is an essential step to link CPV to cerebrovascular events in both symptomatic and asymptomatic patients, so that the effective "cut-off" level of plaque volume for CEA can be determined. Heliopoulos et al correlated carotid plaque morphology with cerebrovascular event risk using 3D US, but did not utilise CPV [171]. Before this step can be taken, it is vitally important to prove CPV can be accurately measured with 3D US when compared to both the endarterectomy specimen and MRI. However, there are many imaging technicalities when measuring CPV with 3D US. ECG gating has previously been thought to be an important factor in CPV assessment [172, 173], but we know that atherosclerotic disease has decreased motility and pulsation of carotid vessels [174]. ECG gating therefore, may not be necessary for CPV assessment increasing its utility and decreasing operator-dependence and expense.

The operator-dependence of measuring CPV on 3D US can be time-consuming [173]. The difficulty/cost in calculating CPV comes from the challenge of differentiating between media-intimal boundary (MIB) and Plaque/Intima-luminal boundary (ILB). Before CPV becomes clinically accepted, operator-dependence and time consumption need to be reduced [31]. One method for doing this is automated analysis using artificial intelligence. Two groups have successfully produced systems that can define MIB and ILB that may circumvent these issues and demonstrate excellent correlation and minimal variation between manual and automated CPV measurement, but there was no correlation to a ground truth such as the endarterectomised plaque [175, 176].

More work is required comparing these automated methods to a water suspension volume measurement, but once accuracy is proven with automated artificial intelligence-based methods adoption will improve for the use of CPV, but for now CPV measurement with 3D US remains manual. One reason for this is in defining the extent of plaque extension with 3D US in manual CPV measurements. Definition of plaque extent is challenging due to fixed inter-slice distance, i.e. you can only jump in 1mm slices when calculating CPV manually on 3D US, but the plaque can start in between slices. The inter-slice distance, i.e. the distance between the previous and current slice, has previously been shown to be a source or variability for CPV measurement, where the exact starting position of the first planimetry slice can be a source of error [167]. The variability of CPV measurement however, remains constant with an inter-slice distance between 1mm and 3mm, maintaining a high inter and intra-observer variability [166, 168].

Potential 3D ultrasound research

There are three unanswered questions relating to CPV. Firstly, a large study assessing the role of 3D US in measuring CPV with good reliability should look towards the use of CEUS for the calculation of CPV, with the aim of creating a larger acoustic impedance and therefore, easier plaque-lumen differentiation and may improve accuracy. Secondly, CEUS could dramatically speed up CPV calculation further opening up scope for automated analysis making assessment cost-effective and give better clinical utility. Thirdly, long term follow-up studies of CPV are required to establish its true potential as a replacement of stenosis assessment for CEA by establishing a surgical threshold. As discussed above, very little 3D US work has been done on plaque vulnerability. 3D US assessment of neovascularisation, grey scale median and fibrous cap thickness may be achieved with software developments. 3D US elastography and thermal strain assessment at present remain long term goals without significant manufacturing developments of commercially available US machines.

Peripheral Arterial Disease (PAD)

Peripheral arterial disease (PAD) affects 20% of the over-sixties, with symptoms ranging from intermittent claudication through to critical limb ischaemia (5 – 10% of cases) [177]. In severe cases, this can require catheter-based revascularisation using angioplasty (45.4%) or stenting (6.7%), or arterial bypass surgery (47.9%) to improve quality of life and avoid limb loss [63]. PAD is particularly problematic in patients with Diabetes Mellitus (DM), which can lead to diabetic foot complications, such as infection, osteomyelitis, neuropathy, and Charcot arthropathy [178]. A significant proportion of vascular patients that require bypass surgery therefore, have DM.

2D ultrasound imaging of PAD

Duplex ultrasound (DUS) has a sensitivity and specificity of nearly 80% for PAD, with a positive predictive value of 88% and negative predictive value of 66.7% [179], making DUS the ideal cost effective and safe tool for initial PAD screening and initial treatment planning [180]. Franz and colleagues found a significant relationship between peak systolic velocity and angiographic stenosis ($p < 0.001$) and the low negative predictive value described represents the weakness of DUS in below-knee lesion detection [179]. DUS has moderate accuracy at diagnosing crural artery disease [181] and currently has no routine utility in the assessment of pedal, arch and digital arteries. Current initial clinical assessment with US, by both Vascular Scientists and Surgeons, tends to be using hand held continuous wave Doppler. Although this has shown to have a higher sensitivity and specificity in diabetic (74%) and non-diabetic (84%) patients than Ankle-Brachial Pressure Indices (ABPI) and Toe-Brachial Pressure Indices (TBPI) [182], it has major limitations, i.e. cannot identify disease or stenosis location. Surgeons must therefore, rely on alternative imaging of these arteries to determine the appropriate treatment.

The Plantar arch and arteries of the foot/toes are routinely not assessed by DUS, likely due to the very limited information that standard DUS can provide of the patency of small vessels, often of which are heavily calcified. Small vessels, the size of those in the foot, are challenging to assess with bulky ultrasound transducers. Small hockey stick transducers are commercially available but other limitations such as calcification and the associated poor penetration of sound (see appendix) remain a limiting factor in its clinical utility. Currently, the 'gold standard' imaging modality for imaging these arteries is catheter angiography. Despite catheter angiography being the gold standard, treatment decisions are often based on MRA or CTA. Angiography which provides the required information to govern treatment type, i.e. level of arterial disease and anastomosis location. Location of graft anastomosis, particularly for femoral-distal, below knee, bypass grafts, affects long-term patency and can determine technicality of surgery, which can be attributed to the level of disease, or stenosis downstream to anastomosis location. Downstream stenosis to anastomosis location, is a proven significant predictor of angioplasty or graft failure [183], therefore confirmation of distal vessel patency is of high importance to the Surgeon.

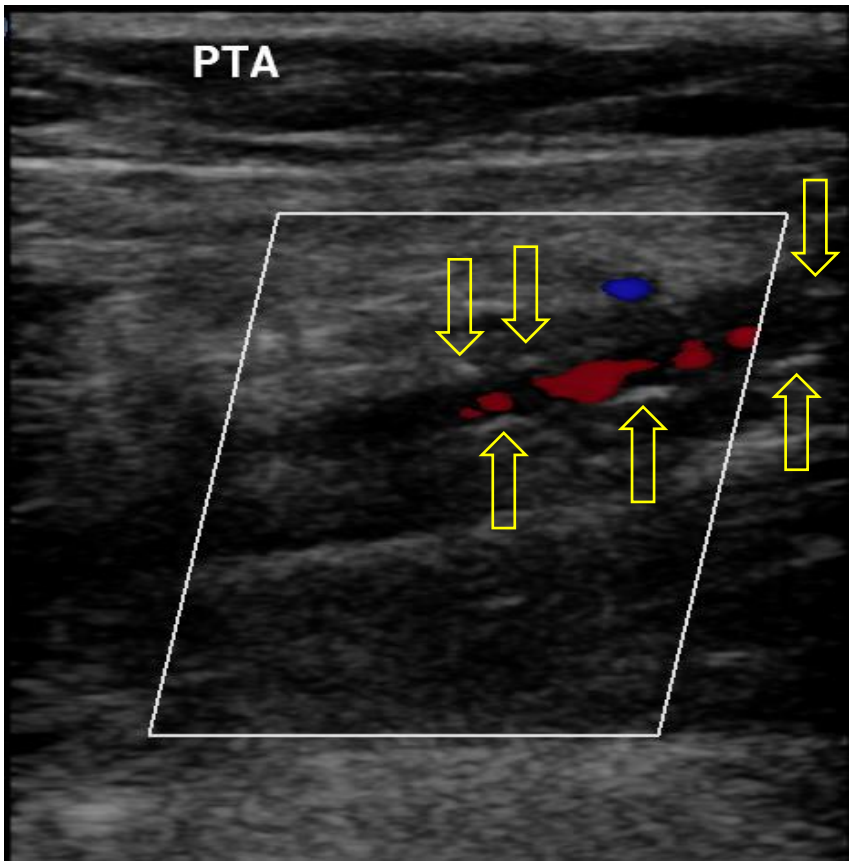

(*Figure 14. 2D duplex ultrasound of a calcified posterior tibial artery. Poor colour filling [red colour] is due to calcification which is highlighted by yellow arrows.*)

CEUS imaging of PAD

The main focus of CEUS within PAD has been on muscle and end organ perfusion within atherosclerotic disease [184, 185]. Studies that use CEUS to measure the collateralisation and skeletal calf muscle perfusion, as a direct measure of PAD, do not use CEUS in the direct assessment of macrovascular crural artery patency. There has been very little published on the direct use of contrast in lower limb imaging, despite its use clinically.

The use of Contrast-Enhanced Ultrasound (CEUS) for below-knee arterial imaging has previously been documented [186-188]. Mestre et al (2015) reported a change in surgical plan by 53%, with agreement to surgical findings rising by 8.1% to 95.2% when ultrasound contrast is utilised [187]. Eiberg et al (2003) also reported a reduction by 70% of inconclusive arterial duplex scans when using ultrasound contrast [188]. The Coffi et al [186], Mestre et al [187] and Eiberg et al [188] works report discrepancies between index imaging and contrast ultrasound, but report only moderate agreement (ƙ 0.45 – 0.50), which may be a reflection of lack of 3D visualisation of the disease. The Coffi and Eiberg works also utilised infusion administration of contrast agents to give prolonged enhancement time so that the CEUS scan could be performed, as bolus injections have a half-life less than <5mins.

Despite the acknowledged superiority of CEUS over duplex and the documented inferiority of duplex at assessing the crural arteries, there is limited report of CEUS use within the literature and widespread clinical use has never succeeded, which may represent its lack of 3D information and inadequacy/mistrust in its ability to aid surgical planning. Vascular Specialists would probably rely on alternative angiography to answer these questions.

3D ultrasound imaging of PAD

Overall, 3D ultrasound assessment of the peripheral vasculature for PAD has been grossly understudied. An attempt has been made using invasive Intra-Vascular Ultrasound (IVUS) and expensive disposable catheter probes (a unique type of free-hand untracked 3D US) meaning clinical traction is unlikely [189]. Although this paper describes the technical success of such a technique, it offers no clinical utility and involves an invasive procedure. The fact that this procedure involves expensive, disposable, ultrasound catheter probes and is invasive means that it is unlikely to gain clinical traction, but this type of work may represent the future of treatment-based 3D IVUS PAD angioplasty. [189].

Janvier and colleagues have developed an accurate mechanical 3D US system that uses a robotic arm and a free hand transducer to assess stenosis of a femoral artery in a tissue phantom, producing images that represent filling defects [190]. Despite being *in-vitro*, this system does describe the potential of their system of assessing infra-inguinal supra-popliteal segments. A Washington (USA) based group has also reported a case in the use of a free-hand magnetically tracked system (Flock of Birds, Ascension Technology coupled to a HDI 5000 Philips scanner) in the assessment of bypass graft stenosis and remodelling demonstrating clear imaging of the stenosis (85% luminal diameter reduction) and post stenotic dilation [191]. Given that standard duplex is more than adequate at diagnosing above-knee arterial disease, there is probably little clinical utility except for targeted assessment when duplex is inconclusive, similar to the CEUS works by Coffi, Eiberg and Mestre.

Potential 3D ultrasound research

Despite the technology used in the Washington (USA) study above being old, and this being a single reported case, there is significant scope for tUS in this method. If a large-scale study could be performed, it would dramatically save time making post-op vein graft surveillance much more cost-effective. The issue of post scan analysis would require auto-segmentation improvement. At present, no work has been done on looking into arteriosclerotic plaque volume of peripheral arterial disease (PAD), another potential use of tUS. tUS may play a role in determining treatment type and the anastomosis location, e.g. angioplasty versus bypass, currently determined by alternative imaging by producing accurate reconstructions of the calf and foot arteries, avoiding the use of unnecessary radiation and nephro-toxic contrast. This method could help reduce cost, radiation and contrast dosage and diagnostic waiting lists.

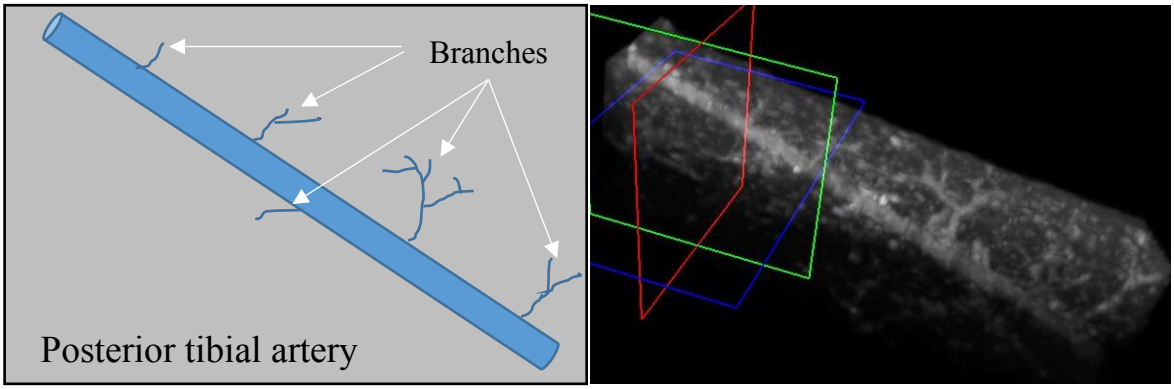

(*Figure 15. tUS angio image of the posterior tibial artery in a healthy subject showing muscular branches*)

Evaluation of potential autologous bypass grafts

Autologous vein bypass grafts have a higher patency and lower re-intervention rates than prosthetic grafts [192] and are therefore, primary choice for a Surgeon. Location of graft anastomosis affects long-term patency and can determine technicality of surgery, and therefore, is crucial. Occlusive peripheral or coronary artery disease may require peripheral arterial bypass (PBG) and Coronary Artery Bypass Grafting (CABG) when significant, to improve quality of life, avoid limb loss or prevent further myocardial infarction.

Duplex ultrasound conduit mapping

Routine saphenous vein DUS mapping, prior to CABG or PBG surgery, has shown strong correlation to surgical measurements [193] and has been shown to clearly demonstrate abnormalities [194], which include areas of varicosity [195], making them unsuitable for harvest as a conduit. DUS has also been proven to reduce the length of incision, time of incision, length of hospital stay [196] and cost. It is therefore, novelistic that DUS imaging of conduit vessels is accurate and beneficial to both Surgeon and patient, particularly at identifying the best conduit for surgery. DUS mapping is considered the current 'gold standard' for vein assessment, but due to its dynamic nature and operator-dependence a high level of trust must exist between Vascular Scientist and operating Surgeon, at identifying the optimum vessel.

CEUS and the peripheral venous system

In the last five years the Pubmed and Medline databases yielded no reports in the use of CEUS for the assessment of potential autologous bypass vessels for research conducted in humans. Search terms include, contrast AND ultrasound OR CEUS and vein, conduit or autologous bypass. Specifically relating to the peripheral venous system, there are reports assessing DVT [197], IVC filter assessment [198], central vein catheter placement [199] and perforator incompetence [200].

3D ultrasound mapping

Searching Pubmed and Medline databases using the terms 3D OR three-dimensional and vein, conduit or autologous bypass in humans in the last five years there is no published research in the peripheral venous system.

Potential 3D ultrasound research

Galeandro et al have previously reported that Physicians with little vascular knowledge better understand vein mapping when demonstrated in a 3D report [201]. Operator-dependence of tUS is minimal and quality is improved as it is possible to produce good quality images with minimal training. The trust, therefore, between Surgeon and operator could be highly improved by tUS as Surgeons can visualise and identify the optimum vessel candidate themselves (Fig. 16). tUS may also play a role in surgical planning for endoscopic vessel harvest as the Surgeon can see where to make incisions and what segments of vessel can be bridged, which will improve the technical success and shorten procedure times.

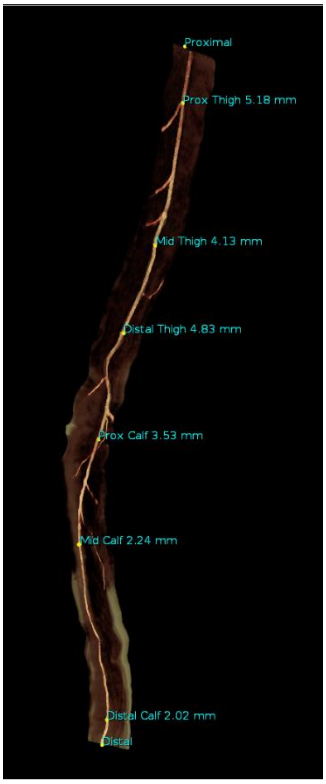

(*Figure 16. tUS vein map of a long saphenous vein with branches and perforators*)

Arterio-Venous Fistulae (AVF)

A chronic kidney disease (CKD) diagnosis is given when the glomerular filtration rate decreases below <60mL/min/1.73 m^2 [202]. CKD costs are estimated between £1.44 and £1.45 billion annually, equating to 1.3% of the annual NHS budget [203]. 2% of patients with CKD will progress to kidney failure and more than half of the total cost of CKD is spent on renal replacement therapy each year [203]. The solution to renal replacement therapy is renal transplant, which is considered the definitive treatment. Dialysis is still the foremost method for renal replacement therapy and around 5000 patients commenced haemodialysis in 2016, a 14% increase from 2011 [204]. Although peritoneal dialysis (PD) holds short-term survival benefit over haemodialysis (HD) in the young non-diabetic patient, this decreases with time, resulting in no long-term advantage [205]. Additionally, not every patient is suitable for peritoneal dialysis and the associated risks are higher. Age and diabetes create a survival difference towards HD [206]. The cost benefit of PD versus HD globally is very mixed [207], although data does suggest that PD is cheaper in developed nations [208].

A well-functioning Arterio-Venous Fistula (AVF) is essential for haemodialysis whilst patients wait for renal transplant, but haemodialysis is costly (>£35,000/patient/year) [209]. This cost can vary depending on location, i.e. hospital versus community, with the highest costs relating to nursing staff and consumables [209]. Turbulence in blood flow, leading to high shear stress, is thought to lead to intimal damage, and thereby leading to flow-limiting stenoses or aneurysmal changes in an AVF. When undetected and untreated, these stenoses lead to thrombosis of the AVF, a lifeline for the patient. Thromboses of AVF is the largest cause of morbidity in patients on haemodialysis [210]. Angioplasty is recommended when diameter reduction is greater than 50% [211], to prevent thrombosis. Despite regular DUS surveillance to detect issues before they cause thrombosis, up to 50% of AVFs will fail within one year [24, 212, 213].

Pre-operative duplex ultrasound and AVF

DUS mapping of the upper limb arterial and venous systems takes considerable skill and time. Renal association guidelines now state that patients should undergo DUS mapping prior to AVF creation, particularly those whom have had previous central vein catheterisation [214]. DUS mapping of the arterial and venous systems within the arm prior to AVF creation has been shown to positively reduce surgical complications, reduce immediate failure rates [215] and can positively influence AVF location/type [216]. Pooled data also demonstrates that routine mapping was more beneficial than selective mapping alone ($p < 0.05$) [215]. In a small cohort study (76 patients), DUS pre-operative mapping has been shown to increase surgical success by 3% ($p = 0.001$), with a 12.7% higher patency rate at 6 months compared to physical examination [217]. DUS mapping has been shown to decrease the use of prosthetic grafts by 36% ($p < 0.001$) [218] and can predict and increase the likelihood of fistula maturation [218, 219].

Post-operative duplex ultrasound and AVF

Post-operatively, 50% of AVF's will fail within one year and a vigorous surveillance strategy is essential. If AVF flow rate meets one of four criteria 1) >15% reduction in access flows on two consecutive occasions, 2) >30% reduction in access flow on one occasion, 3) access flow of <600 ml, 4) presence of recirculation, patients undergo DUS assessment. If a flow-limiting stenoses is detected, arrangements are made for a fistuloplasty. DUS is cheap, safe and allows assessment of flow dynamics which a fistulogram cannot. [210]. Clinicians also have to rely on written reports and poor DUS images to make the decision for intervention. A high degree of trust therefore, exists between the Vascular Scientist/Sonographer and the Clinician due to the operator-dependence of DUS. Equally importantly, we are currently amidst a national shortage of skilled ultrasound operators, which compounds increased service demand, which contributes to Sonographer-related repetitive strain injury, from which as much as 83% of the workforce suffers [220-222]. Reducing scan time is now a research priority.

CEUS and AVF

In the last five years for research conducted in humans, the Pubmed and Medline databases yielded no reports in the use of CEUS for the assessment of AVF. Search terms included CEUS OR contrast ultrasound and AVF OR Arterio-Venous-Fistula.

3D ultrasound imaging

Searching Pubmed and Medline databases using the terms 3D OR three-dimensional and AVF OR Arterio-Venous-Fistula in humans in the last five years we have found no published research.

Potential 3D ultrasound research

An important unmet need in AVF imaging is the ability to improve pre-operative AVF mapping (Fig. 17). The ability to map large sections of vessels of the upper limb at once with minimal operator variance, reduces labour costs through decreased scan time improving cost-effectiveness and avoiding unnecessary incisions and associated complications. Additionally, reducing or removing post-operative surveillance is essential to reduce cost and improve Vascular Scientist-related repetitive strain injury.

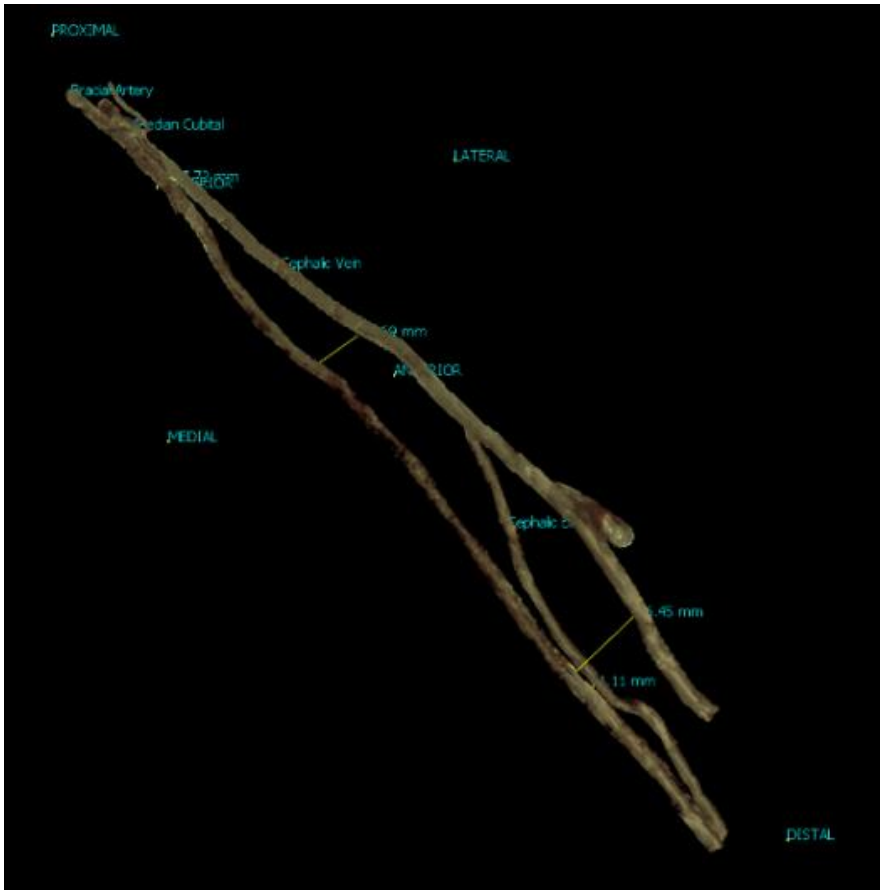

(*Figure 17. A pre-operative radial artery and cephalic vein map showing anatomical orientation and proximity with the venae comitantes*)

Chapter 3 – Overview of Thesis Aims

The aim of this PhD will be to explore the accuracy and clinical utility of tUS within vascular related disease. My thesis will focus on the reproducibility, intra-observer variability, diagnostic accuracy and utility of tUS for each clinical application. I have collaborated with the Research Fellows, within various study groups working on 3D US applications, within our department and in Europe.

Working with the largest vascular US company in Europe who perform over eighty thousand examinations a year for the NHS, there was more than sufficient clinical material for my proposed research. Patients underwent standard DUS followed by a tUS scan paired with alternative imaging, where appropriate. Research angiographic scans were not required as all patients undergo clinical investigations, therefore tUS scans were performed the same day, avoiding unnecessary visits. Angiographic and tUS images were analysed using specialist software and all volumes or reconstructions were analysed by myself, plus another Vascular Scientist to calculate variability. Reproducibility was assessed via sample numbers determined by previous literature and power calculations. I measured accuracy against the accepted 'gold standard' which is catheter angiography, MRa, CTa and the multi-disciplinary team decision. However, we already know these are not 'gold standard' for deep vein thrombosis, AAA screening and surveillance or EVAR complication detection. My aim was to provide the evidence, in the scope outlined above, that tUS should be the accepted 'gold standard', freeing up Interventional Radiologists to focus on intervention rather than diagnostic imaging.

Research questions addressed in my thesis:

- To establish whether tUS is the most accurate investigation for each indication based on diagnostic accuracy, utility, reproducibility, inter- and intra-observer variability.
- To demonstrate the potential value of tUS in vascular surgery.
- To assess if tUS is the definitive investigation for vascular related disease.

Section 2 – Published Research

(Methods, Results and Discussion)

Chapter 4 – An *ex-vivo* evaluation of tomographic 3D ultrasound, B-mode ultrasound, CT and MR imaging to measure artery diameter, legth and wall volume.

Chapter contributions and role:

Division of Cardiovascular Sciences

S Rogers: conception, study design, phantom build, establishing collaboration, immersion volume measurement, data collection, statistical analysis and manuscript writing.

Dr C. Miller: CT and MR analysis

Mr J. Ghosh MD: Co-Supervisor and critical review

Prof C. McCollum: Supervisor and critical review

Independent Vascular Services Ltd

J. Carreira: DUS and tUS scanning, DUS measurements.

R. Thompson: tUS primary analysis

A. Morais: tUS secondary analysis

Imfusion GmbH

Dr W. Wein: Software development

Abstract

Objectives

Precise measurement of luminal diameter in arteries is important when planning interventional vascular procedures in patients. Measuring wall volume may be important in detecting early artery disease and in the assessment of treatments to prevent atherosclerosis.

Methods

An *ex-vivo* phantom using porcine arteries was used to evaluate the accuracy with which i) B-mode ultrasound, ii) tomographic 3D ultrasound (tUS), iii) Computed-Tomography and iv) Magnetic-Resonance imaging measured length, diameters and volume.

Results

The mean error in inner-to-inner diameter measurements by B-mode, tUS, CT and MRI were 0.08±0.26mm, -0.73±0.96mm, 0.09±0.55mm and 0.60±1.01mm respectively. The mean error in outer-to-outer diameter measurements by B-mode, tUS, CT and MRI were -1.33±0.61mm, -1.03±0.35mm, 0.02±1.00mm and -0.47±1.32mm respectively. The mean error in volume measurements by B-mode, tUS, CT and MRI were -0.54±0.62cm^3, -0.06±0.09 cm^3, 0.01±0.18 cm^3 and -0.20±0.32 cm^3 respectively.

Conclusion

Errors in length and diameters remain within clinically acceptable thresholds where MR was the least accurate. tUS was the most accurate method of volume measurement

Key Words: Measurement of arteries, tomographic 3D ultrasound, accuracy.

Introduction:

Cardiovascular disease (CVD) costs the European economy €210 billion/year with stroke alone costing €45 billion [223]. Atherosclerosis is the predominant cause, initiated from early middle age even though symptoms develop in later life [224]. The ability to detect and accurately measure atherosclerosis, while asymptomatic long before it causes symptomatic disease is vital to prevention and to research on treatments designed to prevent or slow the progression of atherosclerosis [162]. The early detection of atherosclerosis offers the opportunity to reduce risk through smoking cessation, modifying diet, taking exercise and weight loss. For the pharmaceutical industry, the accurate measurement of intimal-medial thickness or atherosclerotic disease is motivating for the evaluation of new medications to prevent or slow the progression of atherosclerosis.

Carotid Intimal-Medial Thickness (CIMT) is known to be associated with CVD risk, but changes over time are small with wide measurement errors using existing techniques [225]. As CIMT is measured in millimetres there will be substantial measurement errors based on where the Scientist or Radiologist places the cursor to measure thickness. If the volume of the length of artery of known diameter could be measured, the error associated with measurement would be minimised.

Current imaging techniques for measuring arterial geometry in patients or in animal models include B-Mode ultrasound, CT and MRI. However, B-mode ultrasound cannot be used to measure volume, CT requires ionising radiation and MRI is time consuming. 3D ultrasound (3D US) avoids radiation, with the ability to measure arterial geometry. Tomographic 3D ultrasound (tUS) is a novel free-hand electromagnetically tracked 3D US system which works via video capture and can be coupled to any commercially available ultrasound system that provides a video output. The principle advantage of this technology is that every ultrasound reflection from the artery being examined is captured in space and time by the computer system to generate a 3D image that can be interpreted by clinicians and used to accurately measure length, luminal diameter, wall volume and other important measures of arterial geometry. tUS imaging is quick, easy to use, inexpensive and entirely safe for patients. tUS is ideally placed for vascular conditions due to its specifically designed software.

The ability to accurately detect, measure and survey atherosclerosis is essential for population screening and early intervention to reduce the economic burden of CVD. However, it is not known what is the most accurate method for measuring atherosclerotic geometry. Before population screening for atherosclerosis can commence the question of measurement accuracy needs addressing.

To date, there is no published data on the relative accuracy of tUS at measuring diameter, lengths or volume which would be needed before acceptance in routine clinical practice. This *ex-vivo* static non-perfused phantom study compares B-mode ultrasound, tUS, Computed Tomography (CT) and Magnetic Resonance (MR) imaging against the physical "gold standard" calliper diameter and lengths plus water displacement volumes to identify the most accurate imaging modality.

Materials & methods:

Ex-vivo artery phantom Creation and Scanning:

One Aorta, Carotid, Renal and Internal Mammary (IMA) arteries (4 in total) were harvested from pig carcasses being used for cadaveric teaching within 10 minutes of slaughter and transferred to the laboratory where they were dissected to remove all fat and loose tissue adherent to the artery. Once laid on the laboratory bench relatively straight sections of vessel were identified and dissected out leaving one small segment of each artery. The length of each artery segment was cut proportionally to vessel diameter using a scalpel and surgical tape measure (aorta = 25mm, Carotid 20mm, Renal & IMA 15mm). The arterial segments were stored in 0.9% saline for an hour whilst a liquid Agar gel was cooked. The length of the arterial segments were measured using precise digital callipers. Artery volume was calculated using a validated water immersion technique and digital balance by an experienced Senior Vascular Scientist (SR) [169, 226].

The liquid Agar was prepared using a ratio of 7g of Agar-Agar powder to 1000mL of water to a total volume of 2500mL, which was brought to the boil and then left to cool. The arteries were suspended above the bottom of a plastic container to ensure that they were all the same distance from the ultrasound transducer using surgical silk. Once cool, but not yet set, the Agar liquid was poured into the plastic container to immerse the arteries so that they were approximately 2cm from the surface and left to gel overnight. As we were assessing test accuracy we did not perfusion fix the vessels.

Length and proximal diameters (inner-to-inner [ITI] and outer-to-outer [OTO]) of the arteries were carefully measured by a second blinded Vascular Scientist (JC) using a 9MHz transducer and standard B-mode ultrasound (Resona 7, Mindray, Shenzhen, China). The volume of the artery was then calculated using a mathematical formula ($V = ([\pi \times (DiameterA/2)^2 \times LengthA] - [\pi \times (DiameterB/2)^2 \times LengthB]$). Subsequently, tomographic 3D ultrasound (tUS) scans (Fig. 18) were performed using the PIUR tUS system (PIUR imaging GmbH, Vienna, Austria) connected to a high-end ultrasound platform (Resona 7, Mindray, Shenzhen, China) via a video cable using a 9MHz transducer. PIUR tUS is a non-ECG gated, electromagnetically tracked free-hand 3D ultrasound device that allows 3D visualisation and multi-planar reconstructions (Fig. 19). Ten standard B-mode scans and ten tUS scans per vessel were completed. As tUS is a new technology, a third blinded Vascular Scientist (RT) acquired a second set of ten tUS scans.

The *ex-vivo* phantom was then transferred to another unit to allow the acquisition of CT and 1.5 Tesla MR scans where the phantom was orientated with the proximal end of the vessels being scanned first. The CT scan was performed using a Soft Tissue standard series with 1mm slice thickness protocol localised to just larger than the phantom container (Aquilion One Vision, Toshiba Medical Systems, The Netherlands). A 1.5T MR scan was performed using a T1 weighted, turbo spin echo black blood protocol using a head RF coil, with 1 mm slice thickness, again with the localiser just larger than the phantom container (MAGMETOM Avanto 1.5T equipped with TIM Dot integration, Siemens Healthcare, United Kingdom). All standard B-mode, tUS, CT and MR scans were performed within one hour.

Upon return of the *ex-vivo* phantom to the laboratory the four arteries were cut from the gel 'on block' using a scalpel. To facilitate accurate comparison of geometry the proximal end and side of each vessel was exposed from the gel allowing the exact same diameter/length to be measured in the same way as in each type of scan. The precise length and ITI plus OTO diameters were measured using digital callipers by the first Senior Vascular Scientist (SR) blinded to any scan measurements.

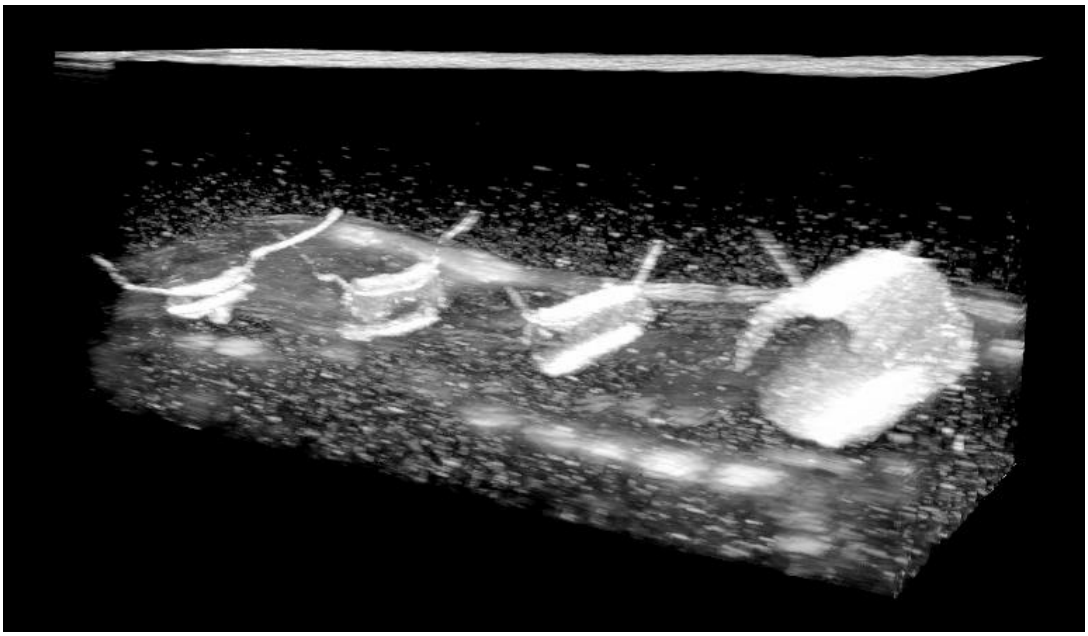

(Figure 18. Tomographic ultrasound image of the four sections of artery (IMA, Renal, Carotid, Aorta) suspended on surgical silk set within an Agar gel)

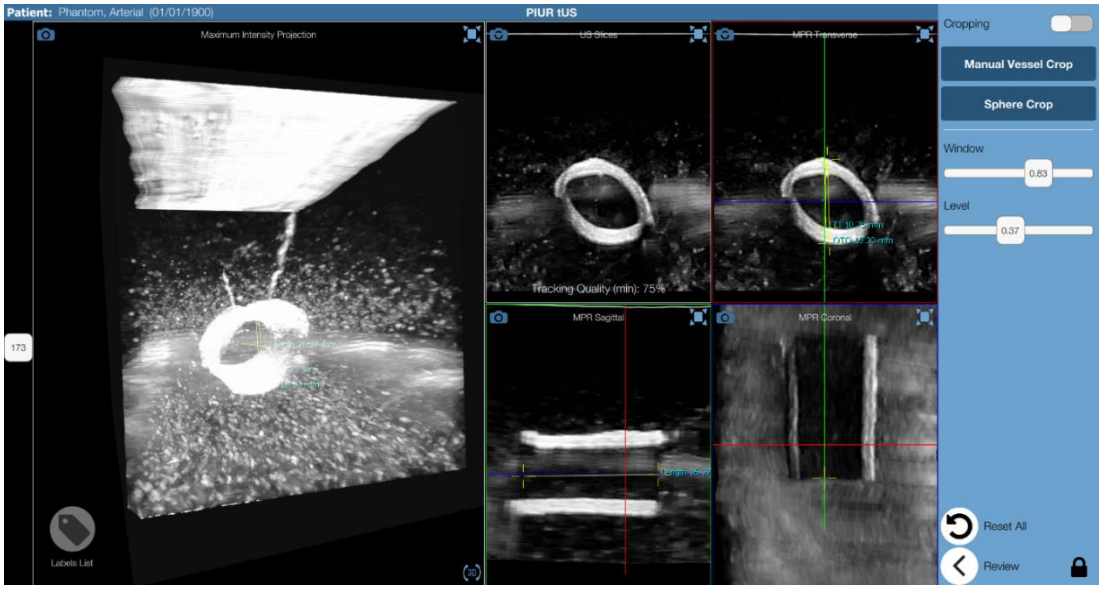

(Figure 19. Visual representation of tomographic ultrasound scan within the PIUR imaging software of the Aortic arterial segment. The images demonstrate a 3D reconstruction and multi-planar reconstructions. The coloured lines allow angle correction within the axial, sagittal or coronal planes. The yellow line with cross-hairs demonstrates line measurements)

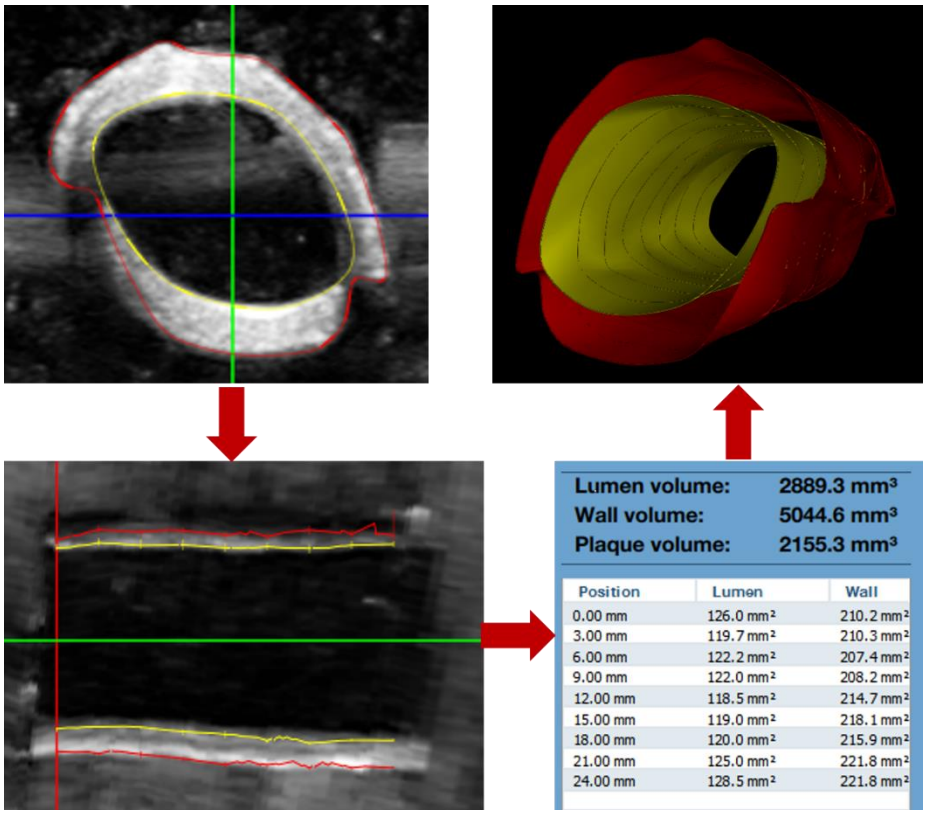

(Figure 20. Flow diagram for the volume calculation of the tomographic ultrasound scan within the PIUR imaging software. Top left shows the manual annotation of the vessel lumen and outer wall. Bottom left demonstrates the 3mm slice thickness in the coronal plane. Bottom right and top right show the volume calculation from the manual planimetry and the 3D reconstruction)

tUS measurements:

tUS measurements (length, internal and external diameter and volume) were calculated using specialist 3D tUS software by two clinical vascular scientists (RT & AM) blinded to the each other, the physical measurements (Archimedes volume and calliper measurements) and standard B-mode measurements. tUS presents the images as Multi-Planar Reconstructions (MPRs) that allow the user to correct for angle as well as a 3D reconstruction (Fig. 19). Users navigated through the axial MPRs to the proximal end of the vessel that could be seen within the 3D reconstruction. Manual planimetry was then used, with 3 mm spacing along the length of the vessel, to calculate the tUS volume (Fig. 20). Lengths and diameters were measured on the angle corrected MPRs to avoid oblique measurements (Fig. 19).

CT and MR measurements:

CT and MR measurements (length, internal and external diameter and volume) were calculated by a Consultant Cardiologist with a special interest in imaging, who was blinded to the physical and tUS measurements, using ImFusion Suite software (ImFusion GmbH, Munich, Germany) that also allows the user to angle correct using MPRs (Fig. 21). Volume was measured using manual planimetry (Fig. 22) with 3 mm spacing with lengths and diameters calculated on angle corrected MPRs (Fig. 21).

Statistical analysis:

Means and mean differences were used to compare imaging modalities and tUS accuracy. Bland-Altman analysis was used to assess inter-observer variability. For the comparison of tUS with CT and MR the mean tUS measurement of each artery was used to determine the statistical difference. Statistical analysis was performed using GraphPad prism v7 (GraphPad software inc, La Jolla, CA, USA).

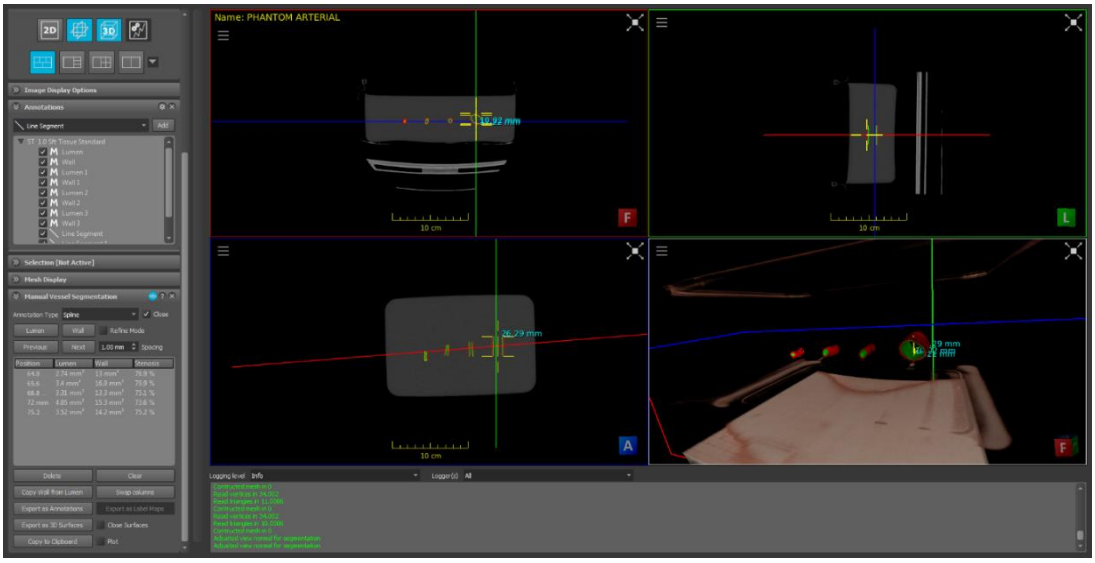

(Figure 21. Visual representation of the CT scan of the whole phantom demonstrating the coloured lines for angle correction within the axial [top left panel], sagittal [top right panel] or coronal planes [bottom left panel] and the 3D image reconstruction [bottom right panel] with the line measurements within the Imfusion software)

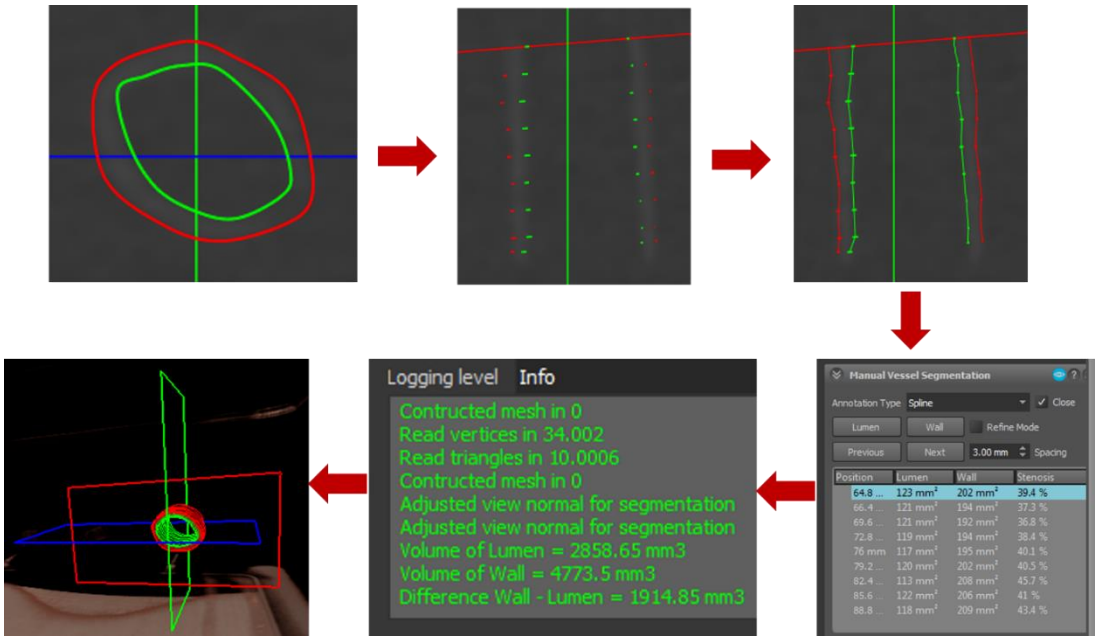

(Figure 22. Flow diagram for the volume calculation of the CT or MR scans within the Imfusion software. Top left shows the manual annotation of the vessel lumen and outer wall. Top middle and top right demonstrate the 3mm slice thickness in the coronal and sagittal planes. Bottom right, middle and left show the volume calculation from the manual planimetry and the 3D reconstructed volume)

Results:

Observer agreement:

Good Intra-observer agreement was identified for tUS, with sub millimetre length/diameter and minimal volume standard deviations (tab. 1). Minimal variation was identified indicating little spread within the data for each measure.

Inter-observer agreement for tUS is represented in table 2 for all measures/arteries and is graphically represented for the Renal artery in figure 23 to demonstrate the spread of data. Inter-observer mean differences for tUS ranged for length (-0.58 to 1.32 mm), ITI diameter (-0.34 to 0.91 mm), OTO diameter (-0.36 to 0.45 mm) and volume (-0.28 to 0.02 cm^3).

Inter-observer agreement for CT is represented in table 3 for all measures and arteries. Inter-observer differences for CT ranged for length (0.04 to 2.35 mm), ITI diameter (-0.48 to 0.70 mm), OTO diameter (-0.5 to 0.45 mm) and volume (0.034 to 0.54 cm^3). Inter-observer agreement for MR is represented in table 3 for all measures and arteries. Inter-observer differences for MR ranged for length (-3.38 to 5.77 mm), ITI diameter (-1.54 to 1.25 mm), OTO diameter (-0.41 to 1.35 mm) and volume (-0.24 to 0.18 cm^3).

Comparison to the Gold Standard:

Mean measurements, for each vessel and imaging modality (Tab.4) were compared to the mean calliper or water displacement measurements (gold standards) (Fig. 24). The mean difference (of all four vessels) length measurements ranged from -1.62 mm to 0.51 mm for B-mode compared to -1.04 mm to 1.16 mm for tUS, -0.22 mm to 2.81 mm for CT and -3.82 mm to 2.57 mm for MR. The mean difference ITI diameters ranged from -0.62 mm to 0.51 mm for B-mode, -2.29 mm to 0.32 mm for tUS, -0.60 mm to 0.93 mm for CT and -1.11 mm to 1.37 mm for MR. OTO diameter mean difference ranged from-2.16 mm to -0.55 mm for B-mode, -1.40 mm to -0.51 mm for tUS, -1.33 mm to1.42 mm for CT and -2.11 mm to 0.99 mm for MR. The mean volume difference ranged from -1.62 cm^3 to -0.12 cm^3 for B-mode, -0.16 cm^3 to 0.08 cm^3 for tUS, -0.24 cm^3 to 0.25 cm^3 for CT and -0.72 cm^3 to 0.13 cm^3 for MR. The mean difference between each imaging modality and the 'Gold Standard' measurements with the maximum and minimum possible differences as a measure of spread for each artery, are demonstrated in table 5.

Table 1. Intra-observer agreement of tUS.

		Mean	sd	Range	Coefficient of Variation
Aorta	**Length**	25.96	0.5	1.67	0.07
	ITI	11.15	0.21	0.65	0.02
	OTO	15.97	0.28	0.94	0.02
	Volume	2.14	0.11	0.4	0.05
Carotid	**Length**	21.45	0.8	2.68	0.04
	ITI	4.74	0.32	0.92	0.07
	OTO	7.82	0.26	0.84	0.03
	Volume	0.5	0.02	0.07	0.04
Renal	**Length**	14.83	0.45	1.24	0.03
	ITI	6.76	0.17	0.51	0.03
	OTO	9.1	0.28	0.99	0.03
	Volume	0.32	0.02	0.07	0.06
IMA	**Length**	13.87	0.28	0.89	0.02
	ITI	2.7	0.11	0.35	0.04
	OTO	4.61	0.26	0.55	0.06
	Volume	0.12	0	0.01	0.03

(Length, ITI & OTO units = mm, Volume units cm^3, sd = standard deviation.)

Table 2. Interobserver agreement of tUS between blinded users.

		tUS 1		tUS 2					
		Mean	**sd**	**Mean**	**sd**	**Mean Diff**	**sd**	**LOA**	**LOA**
Aorta	**Length**	25.96	0.53	25.24	0.88	0.72	1.01	-1.27	2.70
	ITI	11.15	0.23	11.09	0.32	0.06	0.41	-0.73	0.86
	OTO	15.97	0.29	15.75	1.51	0.22	1.53	-2.78	3.22
	Volume	2.14	0.11	2.43	0.07	-0.28	0.12	-0.53	-0.04
Carotid	**Length**	21.45	0.84	20.13	0.93	1.32	0.70	-0.05	2.69
	ITI	4.74	0.33	5.08	0.39	-0.34	0.39	-1.10	0.42
	OTO	7.82	0.28	8.18	0.17	-0.36	0.36	-1.05	0.34
	Volume	0.50	0.02	0.48	0.03	0.02	0.03	-0.03	0.07
Renal	**Length**	14.83	0.48	14.80	0.64	0.03	0.85	-1.63	1.69
	ITI	6.76	0.18	5.84	0.35	0.91	0.29	0.35	1.48
	OTO	9.10	0.30	8.65	0.26	0.45	0.38	-0.29	1.20
	Volume	0.32	0.02	0.37	0.03	-0.05	0.03	-0.11	0.02
IMA	**Length**	13.87	0.30	14.46	0.73	-0.58	0.89	-2.32	1.16
	ITI	2.70	0.12	2.16	0.14	0.54	0.21	0.12	0.96
	OTO	4.61	0.28	4.16	0.25	0.45	0.46	-0.45	1.35
	Volume	0.12	0.00	0.17	0.02	-0.06	0.02	-0.09	-0.02

(Length, ITI & OTO units = mm, Volume units cm^3, sd = standard deviation, LOA = limit of agreement)

Table 3. Inter-observer agreement for CT & MR.

		CT			MR		
		Mean	**sd**	**Diff.**	**Mean**	**sd**	**Diff.**
Aorta	**Length**	25.3	0.02	0.04	26.9	2.89	5.77
	ITI	10.5	0.015	0.03	10.1	0.005	-0.01
	OTO	14.3	0.25	-0.5	14.1	0.34	0.67
	Volume	2	0.271	0.541	2.6	0.09	0.177
Carotid	**Length**	19.79	0.86	1.71	18.6	0.05	0.11
	ITI	4.32	0.24	-0.48	3.58	0.77	-1.54
	OTO	6.87	0.1	-0.19	7.17	0.68	1.35
	Volume	0.42	0.04	0.076	0.55	0.03	-0.061
Renal	**Length**	14.2	1.18	2.35	16.9	0.94	1.89
	ITI	4.7	0.34	0.67	4.3	0.67	-1.34
	OTO	8	0.13	-0.25	7.7	0.21	-0.41
	Volume	0.3	0.04	0.074	0.4	0.12	-0.237
IMA	**Length**	11.4	0.3	0.6	13.6	1.69	-3.38
	ITI	2	0.35	0.7	2.8	0.65	1.29
	OTO	4.4	0.23	0.45	5	0.43	0.85
	Volume	0.1	0.02	0.034	0.2	0.025	-0.05

(Length, ITI & OTO units = mm, Volume units cm^3, sd = standard deviation, Diff. = Difference between mean gold standard value and CT or MR value)

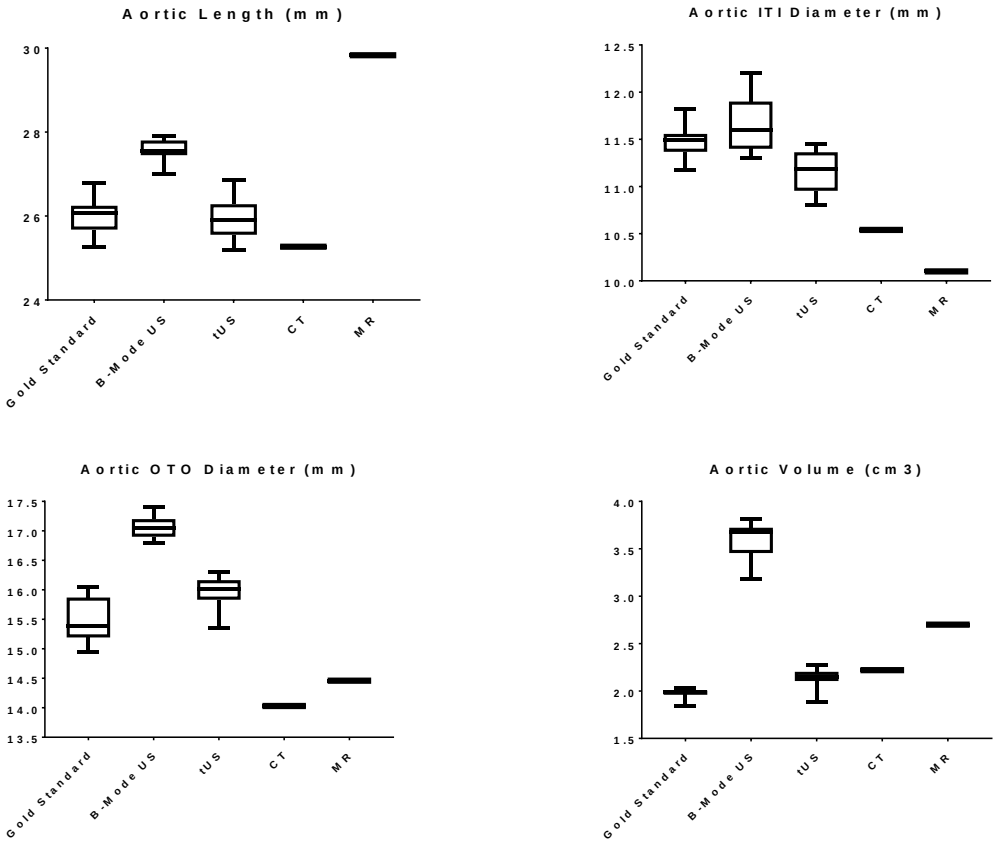

(Figure 23. Intra-observer agreement for each type of measure for the aorta by modality)

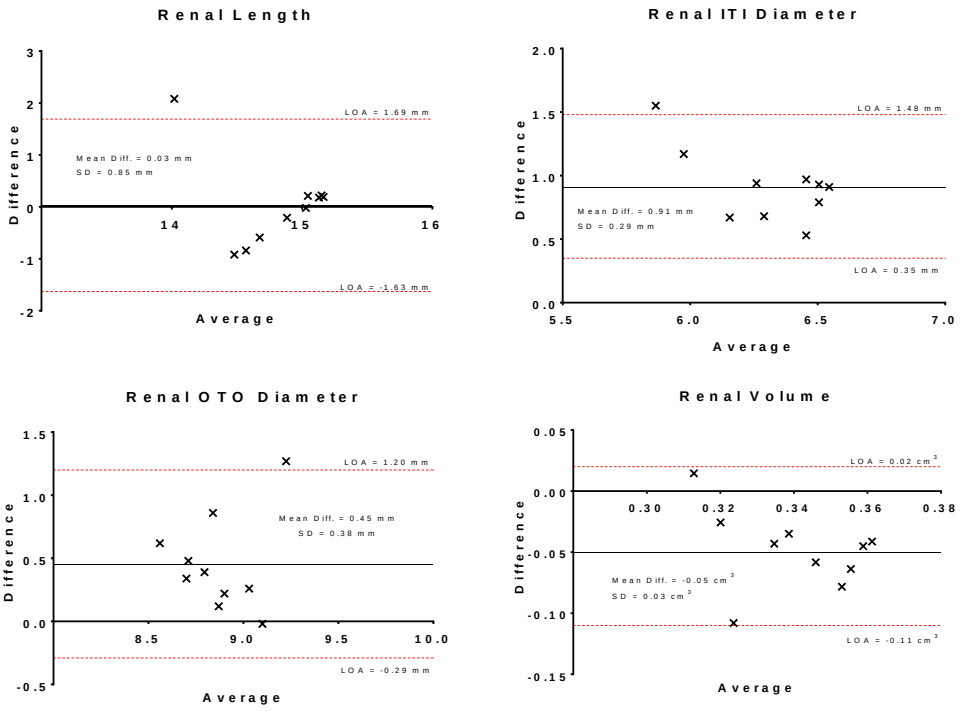

(Figure 24. Bland-Altman Interobserver agreement of all four measures of tUS accuracy for the Renal artery)

Table 4. Modality comparison data of all measures for all arteries.

		Gold Standard		B-Mode US		tUS		CT	MR
		Mean	**sd**	**Mean**	**sd**	**Mean**	**sd**		
Length	**Aorta**	26.01	0.48	27.55	0.26	25.96	0.53	25.27	29.83
	Carotid	20.42	0.30	20.98	0.31	21.45	0.84	20.64	18.68
	Renal	15.99	0.23	16.61	0.38	14.83	0.48	15.40	17.81
	IMA	14.47	0.19	14.60	0.26	13.87	0.30	11.66	11.90
ITI	**Aorta**	11.47	0.19	11.65	0.28	11.15	0.23	10.54	10.10
	Carotid	4.13	0.24	4.17	0.18	4.74	0.33	4.08	2.81
	Renal	4.47	0.26	3.96	0.16	6.76	0.18	5.07	3.66
	IMA	2.35	0.07	2.31	0.14	2.70	0.12	2.39	3.46
OTO	**Aorta**	15.45	0.36	17.06	0.19	15.97	0.29	14.03	14.46
	Carotid	6.42	0.32	7.41	0.19	7.82	0.28	6.77	7.84
	Renal	8.18	0.29	8.73	0.16	9.10	0.30	7.85	7.53
	IMA	3.31	0.08	5.47	0.18	4.61	0.28	4.64	5.42
Volume	**Aorta**	1.98	0.05	3.60	0.19	2.14	0.11	2.22	2.70
	Carotid	0.37	0.02	0.58	0.04	0.50	0.02	0.45	0.52
	Renal	0.40	0.02	0.52	0.03	0.32	0.02	0.31	0.27
	IMA	0.07	0.01	0.28	0.03	0.12	0.00	0.15	0.14

(Mean data is presented where repeat measures were taken. Length, ITI & OTO units = mm, Volume units cm^3, sd = standard deviation.)

Table 5. Comparative accuracy of each imaging modality.

		Gold Standard		B-Mode US			tUS			CT			MR		
		Mean	**sd**	**Mean diff.**	**Min***	**Max***	**Mean diff.**	**Min***	**Max***	**Mean diff.**	**Min***	**Max***	**Mean diff.**	**Min***	**Max***
Aorta	**Length**	26.01	0.48	-1.54	-2.65	-0.21	0.06	-1.6	1.61	0.74	-0.02	1.52	-3.82	-4.58	-3.04
	ITI	11.47	0.19	-0.18	-1.03	0.52	0.32	-0.28	1.02	0.93	0.63	1.28	1.37	1.07	1.72
	OTO	15.45	0.36	-1.61	-2.45	-0.76	-0.51	-1.35	0.68	1.42	0.92	2.01	0.99	0.49	1.58
	Volume	1.98	0.05	-1.62	-1.97	-1.15	-0.16	-0.43	0.15	-0.24	-0.38	-0.19	-0.72	-0.86	-0.67
Carotid	**Length**	20.42	0.30	-0.56	-1.72	0.41	-1.04	-2.96	0.65	-0.22	-0.76	0.17	1.74	1.2	2.13
	ITI	4.13	0.24	-0.04	-0.63	0.65	-0.60	-1.37	0.33	0.05	-0.31	0.47	1.32	0.96	1.74
	OTO	6.42	0.32	-0.99	-1.62	-0.02	-1.40	-2.28	-0.44	-0.35	-0.69	0.31	-1.42	-1.76	-0.76
	Volume	0.37	0.02	-0.21	-0.33	-0.12	-0.13	-0.22	-0.07	0.25	-0.14	-0.06	-0.15	-0.21	-0.13
Renal	**Length**	15.99	0.23	-0.62	-1.78	0.3	1.16	0.16	2.28	0.59	0.02	0.9	-1.82	-2.39	-1.51
	ITI	4.47	0.26	0.51	-0.02	1.15	-2.29	-2.82	-1.64	-0.60	-0.89	-0.22	0.81	0.52	1.19
	OTO	8.18	0.29	-0.55	-1.12	0.15	-0.92	-2.08	-0.22	0.33	-0.07	0.8	0.65	0.25	1.12
	Volume	0.40	0.02	-0.12	-0.2	-0.05	0.08	0.01	0.15	0.09	0.04	0.11	0.13	0.08	0.15
IMA	**Length**	14.47	0.19	-0.13	-0.8	0.5	0.59	0	1.42	2.81	2.54	3.07	2.57	2.3	2.83
	ITI	2.35	0.07	0.04	-0.25	0.48	-0.36	-0.6	-0.02	-0.04	-0.14	0.09	-1.11	-1.21	-0.98
	OTO	3.31	0.08	-2.16	-2.6	-1.72	-1.29	-1.96	-0.82	-1.33	-1.44	-1.16	-2.11	-2.22	-1.94
	Volume	0.07	0.01	-0.21	-0.27	-0.16	-0.04	-0.07	-0.02	-0.08	-0.1	-0.07	-0.07	-0.09	-0.06

(Length, ITI & OTO units = mm, Volume units cm^3, Min & Max* represent the minimum and maximum possible difference.)*

Discussion:

We assessed the range of variability of different sized vessels relevant to the majority of cardiovascular surgical practice comparing readily accessible imaging technologies. This study is the first to compare B-mode, tUS, CT and MR to gold-standard physical measures for artery geometry in an *ex-vivo* phantom model. We demonstrate excellent inter and intra-observer agreement for length plus diameter with good inter and intra-observer agreement for volume, using tUS. Observer agreement for CT and MR was good. We identified that tUS has the smallest, and B-mode had the largest, error of all imaging modalities at calculating volume compared to the water suspension volume. CT and B-mode were comparable at diameter measurement when compared to physical measurements. tUS had a larger diameter error than CT or B-mode but this was still smaller than MR. The errors seen in diameter measurement by all modalities were within clinical acceptable limits. The largest error in length measurement, when compared to physical measurement, was measured by MR. B-mode and tUS length measurements were comparable with a small difference to physical measurement. CT had a larger difference than B-mode or tUS, but the length error was still within clinical thresholds. Length measurements were within clinically acceptable limits despite the accuracies we report for all four imaging techniques.

The use of B-mode US measurements and formulas for volume are widely inaccurate due to the assumption of fixed tubular geometry, which is seldom true *in-vivo*. Various authors have previously validated, with ranging accuracy error (tab. 6), length and volume measurements using phantom studies, but most fail to also compare to gold standard physical measurements or clinical imaging modalities such as CT or MR [37, 227-230]. Where validation against CT and MR has been investigated, this has only been image registration methods with no comparison of length/diameter or volume [231]. Our investigation compares both physical gold standard measurements, plus both CT and MR, in addition to inter-observer agreement, meaning that clinical reference can be made; essential when there is a difference of clinical importance such as diameter-related risk stratification for the decision to treat in abdominal aortic aneurysm surveillance.

In comparison to previous reports (tab. 6), the absolute error range for lengths and diameters from our investigation is comparable. Our length/diameter measurements are also well within clinically acceptable limits, such as those for measuring abdominal aortic aneurysm diameter between imaging modalities, but also inter-observer variation [232-235]. However, our volume measurements have significantly smaller mean difference range than previous reports for free-hand 3D US (tab. 6), suggesting that our reported volume method may have a significantly higher degree of precision. As there is no current guideline within vascular surgery that limits the degree of volume variation (likely due to no current clinical utility), the highest degree of precision is essential.

Our theory that greater error would be seen with smaller vessels, as you approach the limit of ultrasound resolution, was not identified as the mean difference ranges and their standard deviations do not yield any strong difference in relation to vessel size, meaning that the clinical use of tUS on small vessel disease or early atherosclerotic change is possible. This suggests we did not approach the limit of resolution and smaller objects need to be imaged to test this hypothesis further.

A major limitation of any tUS technique is the reliance on B-mode US image data (unlike matrix/4D US imaging) because of the process of video capture. Any error that is present within B-mode US image will be translated into the tUS (or other 3D US type) reconstruction. If a vessel with a 10 mm diameter is 1 mm smaller due to 2D US image reconstruction error, a clinically small error of little consequence in 2D, for a vessel of 10 mm in length, the calculated volume difference, as measured with tUS, could be as large as 0.15 cm^3 which could be of clinical relevance (or not). Although this working example depicts a large error in theory, the diameter and length errors in our study are within this range at most. Increased sensitivity of this potential error with tUS to subtle changes in volume, such as atherosclerotic disease, which may not be detected by standard intimal-medial thickness measurements on 2D ultrasound [236]. A small thickness change on B-mode US may not indicate atherosclerotic change, but in reality, could be a large volume change and warrant aggressive medical therapy and avoiding subsequent, severe atherosclerosis with luminal deficit that could result in CVD events.

B-mode US artefact which degrades resolution or image quality, will also be incorporated into the tUS reconstruction. This causes error in two ways; firstly, resolution error in B-mode US will mean measurement imprecision that is incorporated into tUS, secondly, what may be clinically adequate images with artefact on B-mode US may become clinically inadequate in 3D. Therefore, B-mode US images need to be optimised to reduce any potential error when translated into 3D. It is accepted that standard B-mode US transducers have higher image resolution than commercial matrix/4D ultrasound traducers meaning free-hand techniques, like tUS, have a higher degree of resolution, which is essential for precision. This could facilitate clinical adoption of improved image quality faster as new B-mode US transducers can readily be updated as opposed to the much more expensive matrix/4D probes.

B-mode US lateral resolution error, due to beam thickness, is also translated into the tUS measurements reconstruction [229]. As our study measured anterior-posterior diameters and vessel length, which are not affected by lateral resolution, the error seen in these measurements cannot be explained by beam thickness. Any slight variation in volume could however, be explained by the beam thickness error, but it is likely we found small errors in volume measurement.

Source data variability is a limitation of any video capture 3D US method, including tUS, which is susceptible to degradation. US transducer age and US scanner software level used for the tUS scan will therefore, impact on measurement error. The Mindray Resona 7 scanner used in this investigation was less than 6 months old, meaning it is a modern high-end platform with the latest processing technology (responsible for displaying sharp, clear and bright images on the monitor) and some of the best resolution images available. The accuracy was therefore the highest achievable at the point of data collection, however, this error range cannot be guaranteed with ageing and a higher degree of precision could be achieved with future updates. Consistent quality assurance calibrations are vitally important for continuing clinical accuracy, both for the B-mode US system, but also for tUS [237]. Although error variations are likely to vary between US manufactures, these are hopefully very small and of clinical insignificance. Caution should be sought when using mid-range and portable US systems, which are regarded as generally having lower resolution images.

Electromagnetic tracking means tUS is dynamic and is not constrained by limits of angulation, unlike optical tracking systems which require a constant line of sight [238], which are often not practical for vascular scanning due to the inherent tortuosity of vessels. Although electromagnetic tracking has slightly lower reconstruction accuracy than optical, this error difference is well within clinically acceptable limits. The Root Mean Square difference of the tracking system used in our tUS system is 1.15 mm. This error would not impact linear measurements like length or diameter as the same error would occur to the spatial positioning of each and every B-mode US frame, i.e. if the whole reconstruction is out by 1.15 mm in terms of representation in space, then there is no change in length as each frame is out by the same distance. As the error range for volume from our study is so minimal, it is unlikely that tracking error plays a part in our precision and therefore, the error we identify in linear measurements is likely due to other sources.

The manual planimetry/segmentation method for calculating vessel volume in this work is very time-consuming, although accurate. Some previous works [236] have tried to utilise semi-automatic methods for volume estimation. This is essential for the clinical acceptance of 3D US within a fast-paced surgical environment. The adoption of artificial intelligence and smart based algorithms for medical diagnostics would be of huge benefit to this process and will open up the adoption of tUS to users with little ultrasound experience, meaning it could benefit a much wider population. Centralisation of vascular services could also benefit as patients may no longer need to come to a tertiary referral centre for ultrasound scans. This effectively extends the tertiary referral centre's initial diagnostics into outreach locations with ease, improving departmental capacity, diagnosis and surgical decision making.

Table 6. Summary of published *in-vitro* 3D US accuracy & error.

	Type of 3D US	Length	Volume accuracy error	Comparison to ground truth	Comparison to CT/MR
King et al 1991	Free-hand tracked	0.02 – 1.08mm	0.64 mL	Yes	No
Gilja et al 1994	Mechanical	N/A	0.001 to 0.040 (mean log)	Yes	No
Riccabona et al 1996	Mechanical	1.0%	6.4%	Yes	No
Zotz et al 2001	Mechanical	1.12% to 4.9%	5.1% to 8.9%	Yes	No
Kot et al 2008	Mechanical	N/A	-2.1 to 1.86 mL	Yes	No
	Free-hand tracked	N/A	-2.57 to 1.86 mL	Yes	No
Feurer et al 2012	Free-hand tracked	1.52 mm	N/A	Yes	Yes

We have assessed the relative accuracy of four imaging techniques for the measurement of artery geometry under ideal conditions. The artery segments were dissected to remove all fat and loose adherent tissue and embedded in an agar gel. This presented clear images without surrounding soft tissue enhancement. Under clinical conditions, *in-vivo*, there may be greater uncertainty and ambiguity in measuring diameter, length or volume. Evaluation of measurement accuracy under clinical conditions should be the subject of future work to establish if similar and acceptable measurement can be found. Given the likely sensitivity of volumes to small changes, tUS may be the most suitable method for assessing CVD event risk. Small difference in volume could mean changes in CVD risk can be monitored either over time, as an assessment of progression or in response to aggressive medical therapy. Artery geometry (particularly volume) may prove to be an important tool in CVD risk models. Next steps in this technology would be for the studies assessing arterial change which could be of particular interest to the pharmaceutical industry.

Conclusion:

Tomographic ultrasound is an accurate and reproducible free-hand 3D ultrasound technique with excellent or good observer agreement. MR had the largest error of all modalities compared to physical measurements which may be explained by point-to-point reconstruction errors in image formation. Error in length measurement was largest with MR with B-mode and CT being comparable to physical measurement. tUS length errors were within clinically acceptable thresholds. When compared to physical measurement, tUS has a larger error than CT and B-mode for diameter measurement but errors by all modalities were within clinically acceptable thresholds. tUS is a accurate system with no side effects for measuring artery geometry meaning a new range of imaging and measurements of vascular disease becomes possible, which could be revolutionary for screening or surveillance of atherosclerosis.

Acknowledgments: We thank Mr Philip Foden for his invaluable advice as departmental statistician and Mr David Clarke from Alliance Medical for his invaluable advice as senior radiographer for CT and MR protocols.

Chapter 5 - Comparison of contrast-enhanced tomographic 3D ultrasound against rotational angiography imaging immediately after Endovascular Aneurysm Repair (EVAR)

Chapter contributions and role:

Division of Cardiovascular Sciences

S Rogers: conception, study design, ethics, establishing collaboration, tUS scans, data collection, statistical analysis and manuscript writing.

Mr. C. Lowe MD: conception

Prof C. McCollum: Co-supervisor and critical review

Mr J. Ghosh MD: Supervisor and critical review

Independent Vascular Services Ltd

J. Carreira: Secondary tUS analysis.

Abstract:

Objectives

This proof of principle study assesses the utility of CEUS and contrast-enhanced tomographic ultrasound (CEtUS), as a intra-procedural imaging tool, following endovascular-aneurysm-repair (EVAR), compared to rotational angiography.

Methods

Twenty consecutive patients undergoing infra-renal EVAR underwent immediate post deployment rotational angiography, followed by CEUS and CEtUS scans. Outcomes were presence of endoleak, renal artery patency and endograft deformity.

Results

CEUS and CEtUS detected 12 endoleaks, 8 of which were not detected by rotational angiography. CEUS and CEtUS classify 7 and 8 type IIb endoleaks not detected by rotational angiography. CEUS/CEtUS could not identify 12 and 13 renal arteries respectively, detected by rotational angiography. Rotational angiography and CEtUS both identified one endograft limb deformity, corrected immediately.

Conclusion

CEUS and CEtUS are more sensitive to type II endoleak than rotational angiography although there is a lower detection of renal arteries. CEUS or CEtUS has the utility for immediate post-EVAR endoleak detection where reduction of contrast agent is indicated.

Key Words: Tomographic 3D ultrasound, tUS, EVAR, CEUS, CEtUS, Rotational angiography

Introduction:

The success of Endovascular Aneurysm Repair (EVAR) is dependent upon accurate imaging immediately after endograft deployment to identify device deformity or significant (type I or III) endoleak and to ensure that the endograft has not covered the renal ostium. Digital subtraction angiography (DSA), was traditionally considered the reference standard for immediate post procedure imaging [39] but is limited by being a two-dimensional representation and the associated contrast-induced nephrotoxicity is known to be cumulative.

Post-operative standard duplex ultrasound (duplex) has been found to detect endoleaks not seen by intraoperative angiography [239]. Standard duplex has an estimated sensitivity of between 0.67 to 0.82 and specificity of 0.93 [240]. Due to this potentially low sensitivity units are now utilising contrast-enhanced ultrasound (CEUS), which demonstrates better sensitivity than computed tomography (CT) for post-operative surveillance [241]. Duplex is known to be limited by low-flow states but by adding-on CEUS to compliment Duplex both can be utilised side by side to reduce CTa scanning in surveillance [242]. Some studies have shown that the sensitivity of duplex increases from 0.67 to 0.97 when ultrasound contrast is used [240]. When utilised as an immediate post-operative tool CEUS has shown equivalence to cone-beam rotational angiography for EVAR assessment [92].

However, despite CEUS showing better sensitivity than CT for endoleak and equivalence to rotational angiography, it is limited by only demonstrating two dimensional images. Although the anatomy can be interrogated from different angles by CEUS, the Vascular Scientist is required to create a mental impression of the graft for correct diagnosis, which can be misinterpreted. 3D or tomographic ultrasound (tUS) scans produce a 3D volumetric reconstruction, which can be viewed from multiple angles, potentially giving a higher degree of confidence and lower risk of misinterpretation. Our unit has previously shown that tUS was preferred by Surgeons when interpreting images due to the increased trust from not replying on written reports produced from the Vascular Scientist's mental interpretation, but also more closely agrees with the multi-disciplinary team decision than CT [97]. In the 2014 aortic guideline, the European Society of Cardiology have previously outlined 3D imaging research as a priority [243].

To date, we are aware of only two papers that utilise CEUS for EVAR immediate post-deployment imaging, which have shown CEUS and 3D CEUS (now termed contrast-enhanced 3D tomographic ultrasound [CEtUS]) can adequately identify renal arteries. In most cases CEUS and 3D CEUS is sensitive to Endoleak [90, 244]. Our group has previously compared 3D CEUS to uniplanar DSA intra-procedural imaging for EVAR deployment on a mobile C-arm which has since been superseded by 3D rotational angiography within a hybrid theatre environment [90]. 3D rotational angiography (also known as cone-beam CT) utilises a fixed C-arm and X-rays that rotates around the patient within the operating room and produces 3D CT-like images.

To date there has been no comparison of rotational angiography to 3D contrast-enhanced tomographic ultrasound (CEtUS) for intraoperative immediate EVAR imaging. The sensitivity, specificity, positive predictive value and negative predictive value of CEtUS for EVAR imaging has previously been described [90, 91, 97]. This proof of principle study aims to identify the role of CEUS and CEtUS, in patients undergoing infra-renal EVAR. CEtUS is a novel type of tracked, non-ECG gated, free-hand 3D ultrasound which in addition to CEUS was compared to the 'reference standard' of 3D rotational angiography imaging immediately after EVAR. Our aim was to assess if it is feasibly safe to use CEUS and CEtUS for completing imaging compared to rotational angiography.

Materials & methods:

Consecutive patients from a single institution, due to undergo conventional infra-renal EVAR, gave informed consent for CEUS/CEtUS under national research ethics approval (13/NW/0485). Immediately after endograft deployment, rotational 3D angiography was performed using the Discovery 730 platform (GE healthcare, Chalfont St Giles, UK) and 70 mL dilute iodinated contrast media: 2/3 Visipaque 270 contrast (GE healthcare, Chalfont St Giles, UK) to 1/3 0.9% saline, given over 5 seconds. Images were interpreted by the same Consultant Interventional Radiologist and Consultant Vascular Surgeon undertaking all 20 cases. Immediately following this, and while still on the operating table, CEUS and CEtUS was undertaken at the same time by the same accredited Vascular Scientist who was blinded to the rotational angiogram in all 20 cases. The scientist was asked to remain outside the operating room while the rotational angiogram was performed and analysed to avoid bias. Results were relayed to the surgical team and any necessary interventions based on imaging were then carried out. Measured outcomes were; presence of any endoleak, renal artery ostium patency and endograft limb deformity. Significant endoleaks were considered to be type I or III. Type II (a or b) endoleaks were considered benign. Inter-observer agreement was performed by a second blinded Vascular Scientist with no access to other imaging reports for CEtUS, 1 month following surgery.

CEUS scans were performed to a standard departmental protocol using either a Phillips iu22 (Phillips, Bothwell, USA) or a Mindray Resona 7 (Mindray, Shenzhen, China) ultrasound system using a 5 MHz transducer. A maximum of 5 mL sulpha hexafluoride microbubbles (Sonovue, Bracco Diagnostics, Milan, Italy) was administered by a 16 gauge, peripherally inserted, venous cannula in 1 mL boluses, with a 5 mL 0.9% Sodium Chloride flush after each bolus injection for CEUS and CEtUS. A total of 5 scans could be performed per patient.

A novel tomographic 3D ultrasound system was used for CEtUS scans (Piur imaging GmbH, Vienna, Austria) which was attached to the ultrasound system via a video cable. Sensors were attached to standard ‘off the shelf’ transducer casing of either ultrasound system where the transducer orientation and position in time and space were electromagnetically tracked (Fig. 25). Multi-planer reconstructions (MPR) were computed with a 3D ultrasound volume reconstruction from the 2D CEUS image frames almost instantly (Fig. 26). CEtUS scans were acquired by placing the transducer in transverse section and sweeping the transducer distally from just below the diaphragm, along the length of the aorta, to the common iliac arteries.

Statistical Analysis:

Descriptive statistics (median, range and percentage) were used for patient demographics and endoleak. Modality agreement was confirmed using McNemar's test and inter-observer agreement using Kappa statistic. A *p* value less than 0.05 was considered significant and a ƙ value of 1 was considered perfect agreement. Statistical analysis was performed using SPSS statistics v22 (IBM Corp., Armonk, NY, USA).

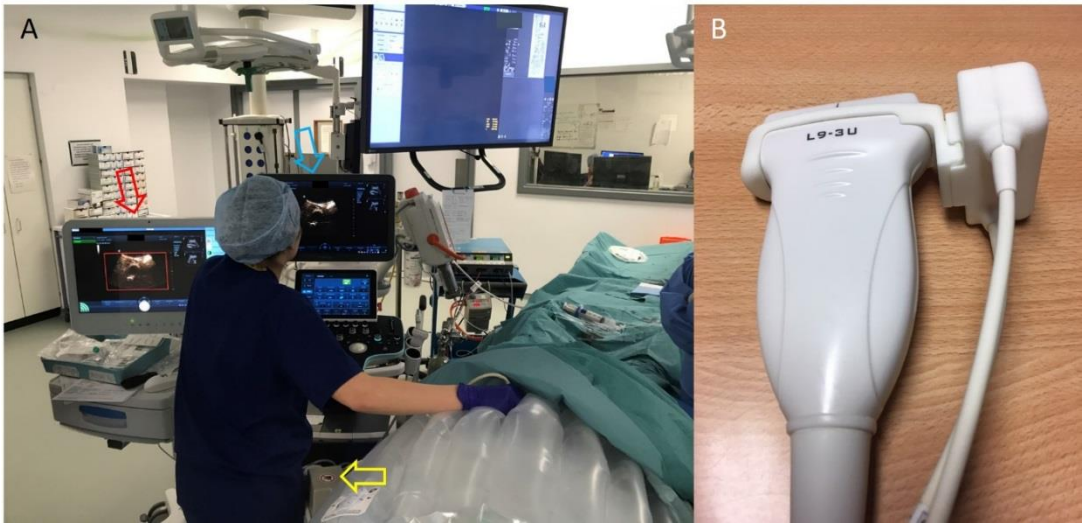

(Figure 25. Set up of tomographic ultrasound. Panel A red arrow - tomographic ultrasound scanner, blue arrow – standard duplex scanner, yellow arrow – magnetic tracking box. Panel B – off-the-shelf ultrasound transducer with tracking sensors attached)

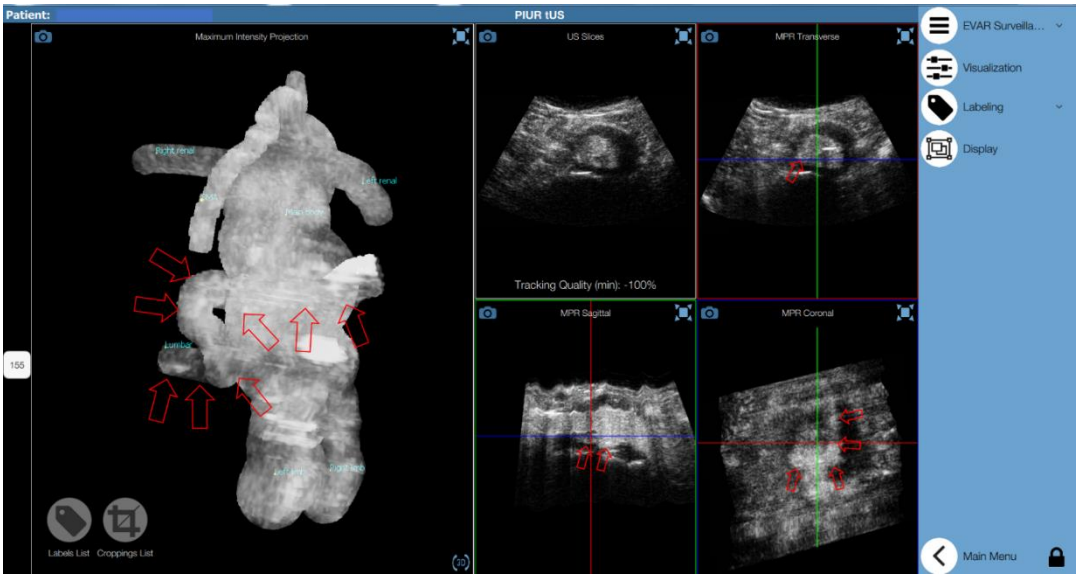

(Figure 26. Screen shot of CEtUS software showing multi-planar reconstructions and a 3D volume of a deployed stent graft, patent renal arteries and SMA with a type IIb endoleak. Red arrows highlight the endoleak track curving around the stent graft from IMA to lumbar)

Results:

Twenty consecutive patients (17 men: 3 women) undergoing intra-procedural imaging for EVAR were recruited from a single institution, over a 12-month period, for a one-off assessment. Median patient age was 77.5 years (range 53-87) with a mean inner to inner, anterior-posterior abdominal aortic aneurysm (AAA) diameter of 5.6 cm and median body mass index was 27.0 (range 19.8-40.4). Five Altura (Lombard Medical), four Ovation (Endologix), nine Endurant II (Medtronic), one Aorfix (Lombard Medical) and one Zenith Alpha (Cook) stent grafts were deployed. Endoleak detection is categorised by imaging modality in Table 1.

CEUS and CEtUS identified 10 type II endoleaks (i.e. endoleak from aortic side branches unrelated to endograft or seal zones) compared to rotational angiography which detected a total of 4. Of the 10 type II endoleaks, CEUS classified three as type IIa with only an inflow vessel seen (i.e. endoleak entering into AAA sac via inferior mesenteric or lumbar artery) and seven as type IIb (i.e. endoleak entering the AAA sac via the inferior mesenteric or lumbar artery and exiting via another aortic side branch) with both inflow and outflow vessels seen. CEtUS detected two type IIa endoleaks with a single inflow vessel and eight type IIb endoleaks. The difference between CEUS and CEtUS was that in one patient the endoleak was reclassified as type IIb by CEtUS (from type IIa by CEUS) as both inflow and outflow vessels were identified (Table 7). Type II endoleaks were not treated at the time of stent-graft deployment.

Table 7. Total endoleak classification by imaging modality.

Modality			
Endoleak	**CEUS**	**CEtUS**	**Rotation**
Type I	0	0	0
Type IIa	3	2	4
Type IIb	7	8	0
Type III	0	0	0
Diagnosis uncertain			
Indeterminate type	2	2	0
Undiagnostic (high BMI)	1	1	0
	13	**13**	**4**

Table 8. Renal artery patency by modality.

	Modality		
Renal patency	**CEUS**	**CEtUS**	**Rotation**
Patent	27	26	39
Not identified	12	13	0
Total	**39**	**39**	**39**

In another patient CEUS and CEtUS images were undiagnostic due to high Body Mass Index (BMI) (40.4) and extensive bowel gas meaning the stent graft (Endurant II) could not be identified; rotation angiography did not demonstrate any endoleak in this patient. In two further patients, the diagnosis of endoleak classification was indeterminate. One patient had rotational angiography which showed no endoleak where CEUS identified endoleak which could not be classified due to the proximity of the leak to the stent graft and the lack of contrast time delay. CEtUS further identified a side branch and therefore, this was treated as a type IIa endoleak. In a different patient there was an uncertain diagnosis of endoleak presence. On CEUS and CEtUS an indeterminate endoleak was seen but unclassified where no endoleak was identified on rotational angiography. The stent graft was balloon moulded and subsequent CT and duplex follow up surveillance did not identify any continued endoleak.

There was poor agreement between imaging modalities for endoleak detection (Cohens Kappa p=0.107). Rotational angiography identified 20% of patients as having an endoleak, compared to CEUS/CEtUS which identified endoleak in 60% of patients. When CEUS or CEtUS was compared to rotational angiography that was taken as the 'reference standard', the difference in the proportion of endoleaks was statistically significant (McNemar's test p=0.021). Both rotational angiography and CEUS classified endoleak in 15% and CEtUS in 10% of patients. Rotational angiography and CEUS/CEtUS agreed that there was no endoleak in 40% of patients. Inter-observer agreement for endoleak detection, plus classification and renal artery patency, was perfect for CEtUS (ƙ=1.00).

Out of a possible 39 patent renal arteries (one previous nephrectomy), CEUS, CEtUS and rotational angiography identified 27, 26 and 39 vessels respectively (Table 8). Only one endograft limb incomplete expansion was detected by all modalities, which was corrected at the time of surgery by additional balloon angioplasty. No limb migration was identified by any modality. No reactions or adverse event was seen from any patient with the use of microbubble contrast (Sonovue).

Discussion:

Immediate post EVAR imaging is essential to detect device-related complications that can be corrected intra-operatively [245]. Up to 9% of endoleaks are still missed by uniplanar DSA compared to duplex ultrasound [239]. This figure is as high as 19% when uniplanar DSA was compared to rotational angiography [246]. Multiplanar or rotational angiography may improve detection but possibly involves higher doses of nephrotoxic contrast media. The lack of published evidence for the utility of rotational angiography for EVAR was identified as a research priority in the 2011 ESVS aortic guideline [235]. Our unit has previously published the benefit of 3D ultrasound to supplement or replace standard DSA in a population that did have clinically significant (type I or III) endoleaks [90]. Our new study supports the role of CEtUS in intra-operative imaging immediately following EVAR.

This validation study demonstrates that CEtUS and CEUS were non-inferior to rotational angiography at detecting endoleak, particularly type II. CEUS has previously been shown to be significantly cheaper and more cost effective than CTa for EVAR surveillance [247]. Although this series did lack clinically significant (type I or III) endoleaks and did not assess cost-effectiveness, the patient safety benefits and improved capacity CEtUS potentially provides, may mean it is superior to rotational angiography with development. This current study also reports a good renal artery detection rate of CEtUS, with only 33% of renal vessels not identified, which is a significant improvement on the previously reported 50% renal artery identification rate by 3D CEUS [90]. In this series, the incomplete stent expansion detected by CEtUS outlines its sensitivity to such issues, which is vitally important for long term patency of EVAR. The safety of microbubble contrast agents has been well described [248] and although our series was small, the fact we identified no reactions to Sonovue is important given the intra-operative use.

CEtUS can capture the full AAA anatomy in a single 3D CT-like, intuitive image, that can be interrogated from any angle/plane for clear diagnosis. This can demonstrate the renal patency, inflow, outflow and type of endoleak removing operator dependence (demonstrated by the excellent observer agreement) over CEUS. Although no formal scan times were recorded as part of this research, CEtUS scans took approximately 30 seconds to perform and two minutes to process and form a diagnosis compared to 5 – 10 minutes for CEUS in skilled hands (these are estimated values from the Vascular Scientist performing the scans as this was not a recorded outcome of our study). Identifying the renal artery origin on CEUS can be technically demanding. Although in this study, we identified a similar number of renal arteries with CEUS and CEtUS, there is a clear advantage in using CEtUS due to the lower skill required to produce a diagnostically acceptable image, i.e. CEtUS involves a single sweep then retrospective image processing compared to CEUS which involves continual interpretation whilst scanning. In our practice we therefore now utilise CEtUS to identify renal arteries for intra-operative imaging when indicated, rather than CEUS.

The higher number of low flow, type II endoleaks, detected by CEUS/CEtUS identified may be due to the absence of delayed-phase imaging on rotational angiography. Delayed phase imaging is not routinely performed as only critical type 1 or 3 endoleaks are treated at the time of deployment. As type II endoleaks are low flow they may not be present in arterial phase rotational angiographic images. This may account for the disagreement in endoleak detection we identified. Alternatively, CEUS/CEtUS may have a higher false positive detection rate. However, this is unlikely given the previous work by Lowe et al (2017) which utilised the Multi-Disciplinary team opinion as the index test as CTa missed endoleaks later identified on catheter directed DSA [97]. Type II endoleaks, at the point of immediate post-deployment imaging, may also be the normal course of EVAR completion that has previously not been detected by a sensitive enough imaging modality (Fig. 27). However, due to no late phase imaging, it may not be appropriate to use rotational angiography as the reference standard.

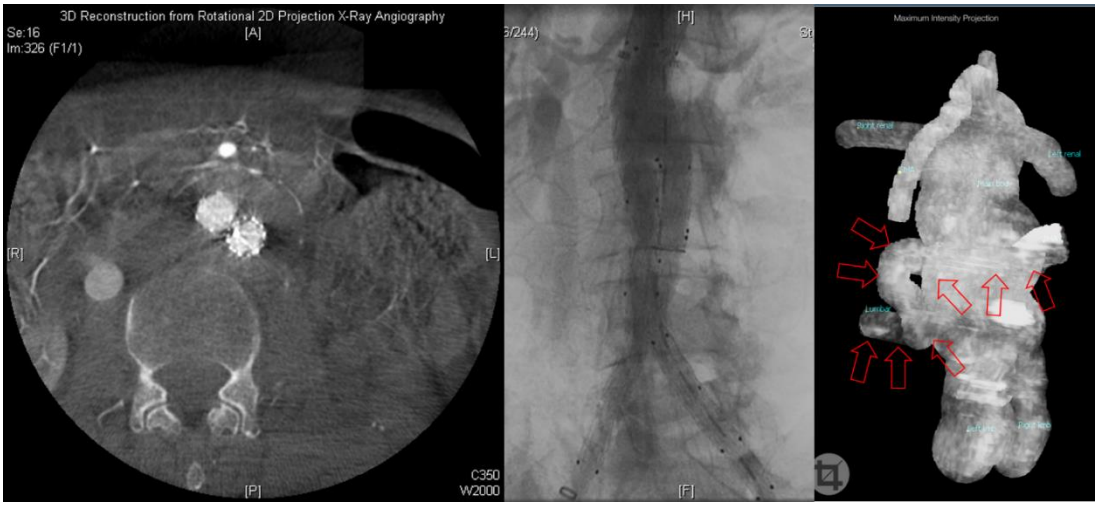

(Figure 27, Left: 3D reconstruction from rotational 2D projection X-ray rotational angiography with no endoleak, Middle: 3D volume of X-ray rotational angiography with no endoleak, Right: 3D CEtUS volume with a type IIb endoleak from the same patient. Red arrows highlight the endoleak track curving around the stent graft from IMA to lumbar)

The non-visualised case was due to high BMI and bowel gas and is a recognised limitation of any aortic ultrasound-based imaging technique. CEtUS however, does produce a 3D image that can be interrogated, which may hold potential to improve aortic and stent graft visualisation, as scans can be performed at extreme laterality to avoid bowel gas. In our study, rotational angiography did not detect endoleak in one case with extreme BMI nor the two other indeterminate scans on CEtUS. Of these two indeterminate leaks, CEtUS did identify additional information that lead to the clinical decision of type II endoleak in one case. Traditionally, where seen on routine standard duplex surveillance, this type of leak would have normally indicated an urgent outpatient CEtUS or Computed Tomographic angiogram (CTa) scan. As CEtUS had already been completed intra-operatively, and we knew about the type II endoleak, the patient is being followed up routinely unless the aneurysm sac begins to grow. Inter-observer agreement for endoleak detection from this study (ƙ=1.0) is slightly better than that of our two previously reported studies (ƙ=0.88 and 0.89) [91, 97], which may, in part, represent advances in software processing demonstrating clearer images and increasing experience with 3D ultrasound within our institution, but our sample number is small.

The disparity between CEtUS and the figure detected by rotational angiography for renal artery patency may reflect the learning curve of the Vascular Scientist who does not normally scan renal arteries and the limitation of ultrasound in patients with a high BMI. We do not feel the discrepancy is a reflection of the technology due to the perfect inter-observer agreement (ƙ=1.0). Although, for the 33% of patients whom renal ostium's were not visualised, the consequences of missed coverings by the stent graft would be significant, which may reduce the efficacy of the technique.

When compared with CTa, CEUS is equivalent at diagnosing endoleak, but has also been proven to reduce nephrotoxic contrast and radiation dosage, leading to shortened hospital stays [92]. Kopp et al (2010) have utilised CEUS intra-operatively replacing DSA successfully for stent deployment, plus as a intra-operative imaging tool [244]. However, there still appears to be a reliance clinically of DSA, despite CEUS being equivalent, which could be due to its lack of 3D information. CEUS and CEtUS have been demonstrated to be sensitive and specific for EVAR surveillance [97, 241]. Our current study suggests that CEtUS may be a safe alternative and with further research non-inferior to rotational angiography as an intra-procedural imaging tool. This proof-of-principle suggests that CEtUS has sensitivity in endoleak detection and this would be compatible with the previous surveillance observations by Abbas et al. (2014), Ormesher et al. (2014) and Lowe et al. (2017). Assessment of target vessels for fenestrated or complex EVAR is often a reason CTa is requested pre-operatively as it is crucial for determining technical feasibility. No conclusion can be made from this study for fenestrated or complex EVAR as further research is needed in this patient group.

The key benefit of duplex technology is in patients with contrast allergy or poor renal function, when avoidance of nephrotoxic iodinated contrast is paramount. In this setting, uniplanar digital subtraction angiography (DSA) using CO_2 (DSA-CO_2) avoids nephrotoxicity and can negate some of the artefacts of standard DSA due to the lower viscosity of CO_2. The diagnostic accuracy of DSA-CO_2 versus DSA, using iodinated contrast, is reported at 95% when performed well [45, 249], decreasing over time, particularly in patients with poor cardiac output. CO_2 angiography has been reported to have a specificity of 72% and interobserver agreement for type II endoleak as low as 29% [250]. Although the use of CO_2 angiography is a good choice for endograft deployment, it is deemed inadequate for imaging immediately following EVAR deployment [235]. DSA-CO_2 is also uniplanar and is limited by the same constraints as standard DSA in this nature if multiple views are not taken. The combination of DSA-CO_2 for endograft deployment and CEtUS for intra-operative imaging following EVAR is now a vital nephrotoxic contrast reduction strategy in our institution for 'at risk' patients who require EVAR.

This is a proof of principle study on the utilisation of CEtUS in a patient group undergoing standard infra-renal EVAR. No conclusions can be made about those patients undergoing complex endovascular aneurysm repair from this small study, where more work is needed to develop the role of intra-operative CEtUS. There is however, a role for CEtUS use in those patients who may have impaired renal function but a much larger study may be needed to gain confidence. The role of CEtUS is highly advantageous in our unit for imaging immediately following EVAR in high risk patients (i.e. those with significant renal impairment). Further work on better identifying renal arteries in all patients and use of this technique in juxta-renal AAA's would lend itself towards greater adoption. CEtUS does however, have the ability to reduce radiation exposure.

Conclusion:

CEUS and CEtUS are more sensitive to type II endoleak than rotational angiography, possibly as delayed angiograms were not routine, though there is lower detection of renal arteries. CEUS or CEtUS have a utility for post-EVAR deployment intra-operative imaging where avoidance of contrast agent is indicated, particularly for those patients with significantly reduced renal function or contrast allergy. CEtUS is fast and can be interrogated from any angle retrospectively giving confidence in diagnosis. CEtUS is a valuable strategy for radiation and nephrotoxic contrast reduction in our institution.

Acknowledgments: We thank Dr Julie Morris and Mr. Phillip Foden for their invaluable advice as Departmental Statisticians.

Section 3 – Unpublished Research

(Methods, Results and Discussion)

Chapter 6 - Abdominal Aortic Aneurysm (AAA) diameter

Chapter contributions and role:

Division of Cardiovascular Sciences

S Rogers: conception, study design, tUS scans, tUS reporting data collection, statistical analysis and manuscript writing.

Mr C. Lowe MD: conception, study design, ethics and critical review

Mr J. Ghosh MD: Co-Supervisor and critical review

Prof C. McCollum: Supervisor and critical review

Independent Vascular Services Ltd

J. Carreira: tUS scanning and second reporting.

Imfusion GmbH

Dr W. Wein: Software development

Funding: Manchester Surgical Research Trust (MSRT) (Registered Charity Number 2415906)

Abstract

Objectives:

An abdominal aortic aneurysm (AAA) poses a risk of fatal rupture. Surveillance relies on accurate aortic diameter measurement. Unlike Computed Tomographic angiography (CTa), conventional ultrasonography struggles to provide a true orthogonal diameter. We investigated the reproducibility and agreement of tomographic 3D ultrasound (tUS), compared with CTa at measuring orthogonal AAA diameter.

Materials and methods:

41 patients were recruited from an AAA surveillance programme underwent same day tUS and CTa scans. Two blinded operators measured AAA diameter in an anterior-posterior (AP) and maximal orthogonal (MO) fashion using an inner wall (ITI) and outer wall method (OTO).

Results:

Intra-operator difference for AP diameters was -0.53 (ITI) and 0.07 (OTO) mm compared with MO 0.70 (ITO) and 0.38 (OTO) mm. Inter-operator difference for AP diameters was -0.15 (ITI) and 2.60 (OTO) mm compared with MO 0.79 (ITO) and 3.96 (OTO) mm. The mean tUS AP diameters were 2.91 (ITI) and 0.47 (OTO) mm smaller than CTa. Mean MO tUS diameter difference was 0.99 (ITI) or -3.22 (OTO) compared with CTa.

Conclusions:

tUS has excellent inter- and intra-operator agreement. When compared to CTa, tUS shows good agreement, with AP ITI diameters being the most accurate. The AP OTO technique offers the best accuracy when compared to CTa, but ITI holds better reproducibility. tUS may be clinically acceptable for those patients in AAA or EVAR surveillance with complex geometry.

Key Words: Abdominal aortic aneurysm, diameter, 3D, tomographic ultrasound.

Introduction

The prevalence of abdominal aortic aneurysm (AAA) in 65 to 79-year-old men is reported to be between 5 and 10% [58, 59], and increasing aneurysm diameter is associated with fatal rupture [59, 62, 251]. The risk of rupture is almost four times higher in women than men (p<0.001) [252], has decreased since 1979 due to decreases in smoking prevalence and has a mortality rate below 1% [253]. The indication to treat an AAA in the UK is Duplex Ultrasound (DUS) anterior-posterior AAA diameter that measures greater than 5.5cm. Accuracy in measuring the AAA is therefore, crucially important so that the risk of rupture can be managed appropriately or balanced with continued surveillance. There are three methods of measuring an AAA, inner wall to inner wall, outer wall to outer wall, or leading edge to leading edge. Inner wall (ITI) or outer wall (OTO) diameter measurement are the most commonly accepted methods in the UK, with a mean difference between methods reported between 2.7 - 4.21mm [19, 254, 255]. ITI dimensions have greater reproducibility [254], with operator variance reported to be <1 - 4mm [256] and has therefore, been utilised by the UK National AAA Screening Programme (NAAASP). However, AAA have complex geometry that can be tortuous and irregularly shaped. Both pulsatility and geometry can impact accurate standard DUS anterior-posterior AAA diameter measurement that needs careful consideration as they can lead to under or over estimation of diameter.

Computed Tomographic (CT) scanning with X-Rays and nephro-toxic contrast is the accepted gold standard, with an intention to treat, for AAA imaging as it allows orthogonal diameter measurement. Two-dimensional DUS has a reported mean difference of 4±12 mm compared to Computed Tomographic Angiography (CTa) for AAA diameter measurement [64]. CTa has been shown to consistently measure AAA diameters larger than DUS [257], with DUS being shown to underestimate aortic diameter by 5mm when compared to CTa [258]. The difference between DUS and CTa could be attributed to oblique measurement on DUS due to complex AAA geometry. The advantage of any form of 3D imaging (CTa or 3D ultrasound) is the ability to negate the issue of complex geometry and oblique measurement.

The use of 3D ultrasound (3DUS) has shown excellent correlation with CTa, demonstrating a reduction in AAA diameter measurement error [80, 259, 260]. These works, however, utilise specialist 3D ultrasound transducers (mechanical or matrix) which have a limited field of view, meaning the whole AAA sac cannot be visualised in one 3D volume. As a result, the user must identify the largest expanse of the AAA prior to acquisition, but demonstrate good operator agreement. Tracked free-hand 3D ultrasound using standard DUS transducers, has been used to demonstrate the geometry of AAA [261]. No matter what type of 3DUS utilised for AAA diameter measurement, a reduction in operator error could make AAA surveillance more accurate and efficient as angle correction could avoid oblique measurement.

This study measured anterior-posterior and maximal orthogonal, inner-to-inner and outer-to-outer AAA diameters by utilising free-hand tomographic 3D ultrasound (tUS), to demonstrate inter-modality and inter-operator agreement. We aimed to investigate the issue of oblique measurement and AAA geometry, compared to CTa in AAA patients pre and post EVAR.

Methods

Between 2016 and 2017 consented patients with AAA above surgical threshold who were being worked up for repair, attended the Vascular Studies Unit one hour prior to a clinical CTa scan, where a tUS scan was performed by an experienced Vascular Scientist who was blinded. CTa was treated as the index test and CTa diameters were measured retrospectively in the same software as the tUS scans three months later to reduce bias. National ethical approval was obtained from the Health Research Authority Ethics Committee (13/NW/0468).

Imaging

tUS is a free-hand (meaning any size of vessel can be scanned in one go) electromagnetically-tracked non-ECG gated 3DUS device (Piur imaging GmbH, Vienna, Austria) that was attached to a Philips iu22 ultrasound system (Philips, Bothwell, USA) via a video cable. Sensors were attached to the iu22 standard ‘off the shelf’ ultrasound transducer (5MHz) to track orientation and position in time and space. Multi-planer reconstructions (MPR’s) are computed with a 3D ultrasound volume from the DUS images, almost instantly, and presented on the tUS screen (Fig. 28). B-mode scans were performed due to improved resolution over colour Duplex imaging and are acquired by placing the transducer in transverse section and sweeping the transducer distally from the sternum to the aorto-iliac bifurcation, or beyond, to capture the full AAA anatomy.

A non-ECG gated arterial phase CTa was then performed using a Siemens SOMATOM Perspective scanner (Siemens Medical, Munich, Germany) where images were acquired at 1mm slices from T12 to the pubic symphysis. A bolus dose of 100 mL of iodinated contrast medium (Omnipaque 240, GE Healthcare, UK) was administered at a flow rate of 3 mL/s. The arterial phase acquisition was bolus triggered from the abdominal aorta at T12 level.

Diameter measurement

tUS and CTa scans were loaded into specialist software (Imfusion suite, Imfusion GmbH, Munich, Germany) where MPR's allowed angle correction, avoiding oblique measurements for AAA geometry (tortuosity and angulation), represented by the red, blue and green lines in figure 28. AAA's were measured by both ITI and OTO methods in an anterior-posterior (AP) and maximal orthogonal (MO) diameter following angle correction. Measurements were interrogated in specific software by the Vascular Scientist and a Vascular Surgeon blinded to each other's result and experienced in diameter measurements.

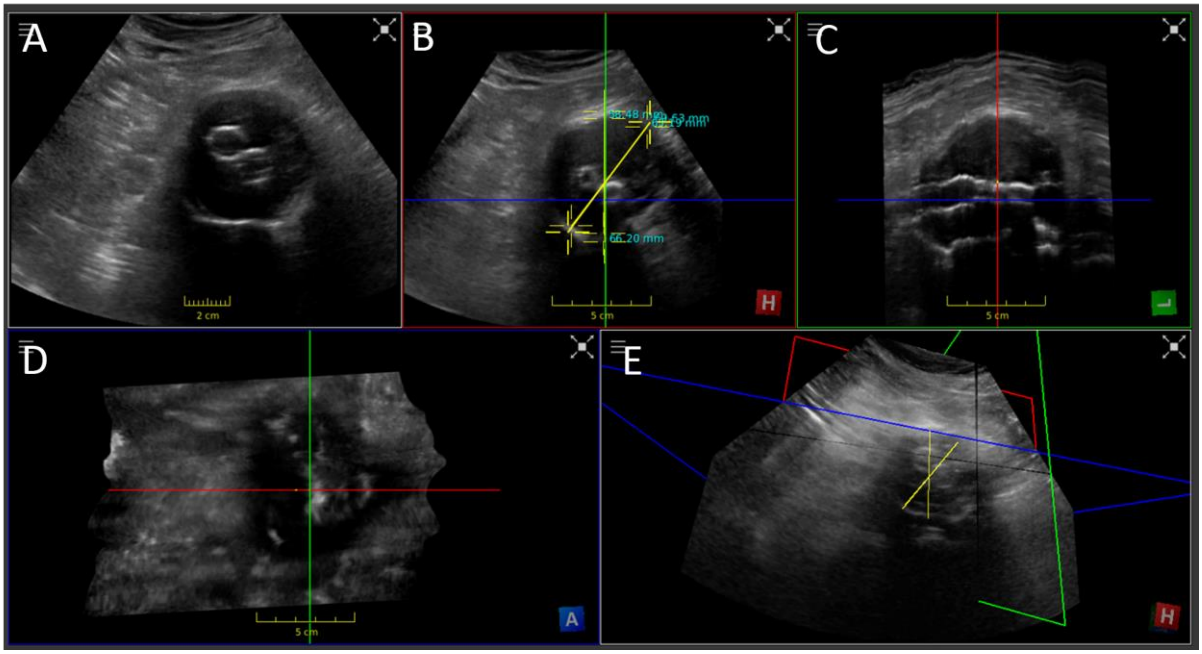

(Figure 28. Post EVAR tUS image display. Panel A – DUS standard image. Panel B – Transverse (axial) MPR slice. Panel C – Long section (sagittal) MPR slice. Panel D – Coronal MPR slice. Panel E – 3DUS volume. Yellow lines are AP and MO, ITI and OTO diameters. Red, blue and green lines allow angle correction in all three orientations)

Statistical analysis:

Observer variability and inter-modality agreement was analysed using Bland-Altman agreement to establish a mean difference between users and modalities. To allow clinical inference errors of acceptability where calculated via a repeatability coefficient/range of variability where a clinical acceptance of 5mm was used [80]. Range of Variability was calculated as 1.96 x standard deviation of mean differences. A paired students t-test was utilised to identify any significant difference where a *p*-value less than 0.05 was considered significant. Statistical analysis was performed using GraphPad prism v7 (GraphPad software inc., La Jolla, CA, USA).

Results:

A total of 41 patients; sixteen patients with native untreated AAA's being worked-up for surgery and 25 patients post EVAR under surveillance programmes were recruited from a single institution.

Aneurysm diameter

All 41 patients were included in mean AAA diameter assessment. Combined, pre and post EVAR mean diameters as measured by CTa were calculated for each method of measurement (AP, MO, ITI and OTO) (Tab. 9).

Table 9. Mean AAA AP and MO diameter measured for both ITI and OTO dimensions by CTa.

	AP ITI	**AP OTO**	**MO ITI**	**MO OTO**
Combined* (mm)	57.0 ± 9.9	59.7 ± 10.1	61.4 ± 11.0	63.7 ± 10.9
EVAR* (mm)	56.6 ± 11.8	59.1 ± 11.9	61.9 ± 13.3	64.1 ± 13.2
AAA* (mm)	57.7 ± 6.1	60.5 ± 6.2	60.6 ± 6.1	63.0 ± 6.1

*(*mean ± standard deviation)*

tUS Intra-observer agreement

tUS intra-operator variability was assessed for all patients by one author's measures (Tab. 10). Mean intra-operator difference ± standard deviation for AP ITI and OTO diameters (Fig. 29a and 29b) was -0.53±2.34 mm (p = 0.155) and 0.07 ± 2.31 mm (p = 0.853). Mean intra-operator difference ± standard deviation for MO ITI and OTO diameters (Fig. 29c and 29d) was 0.70±5.12 mm (p = 0.384) and 0.38±5.92 mm (p = 0.682). Mean diameters were not significantly different between repeat measurements. Repeatability coefficients were only within clinically acceptable limits for AP diameters (4.59 and 4.53mm). Maximal orthogonal diameter, repeatability coefficients (10.04 and 11.60mm), were widely outside clinical thresholds.

tUS Inter-observer agreement

tUS inter-operator variability was assessed for all patients comparing two blinded author's measurements (Tab. 10). Mean inter-operator difference ± standard deviation for AP ITI and OTO diameters (Fig. 30a and 30b) were -0.15±2.25 mm (p = 0.672) and 2.60±2.26 mm (p<0.001). Mean inter-operator difference ± standard deviation for MO ITI and OTO diameters (Fig. 30c and 30d) was 0.79±6.20 mm (p = 0.419) and 3.96±6.85mm (p = 0.001). Mean diameters were not significantly different between ITI measurements by both methods, but were for all OTO diameters. Repeatability coefficients were only within clinically acceptable limits for AP diameters (4.41 and 4.43mm). Maximal orthogonal diameter, repeatability coefficients, were widely outside clinical thresholds (12.15 and 13.43mm).

Table 10. tUS and CTa intra- and inter-observer mean AP and MO diameter difference for both ITI and OTO dimensions.

		AP ITI	**AP OTO**	**MO ITI**	**MO OTO**
Intra	Mean difference ± sd (mm)	-0.53±2.34	0.07±2.31	0.70±5.12	0.38±5.92
	p value*	0.155	0.853	0.384	0.682
	Statistically different*	No	No	No	No
	Coefficient of Repeatability (mm)	4.59	4.53	10.04	11.60
Inter	Mean difference ± sd (mm)	-0.15±2.25	2.60±2.26	0.79±6.20	3.96±6.85
	p value*	0.672	<0.001	0.419	0.001
	Statistically different*	No	Yes	No	Yes
	Coefficient of Repeatability (mm)	4.41	4.43	12.15	13.43

*(*Value relates to comparison of means.)*

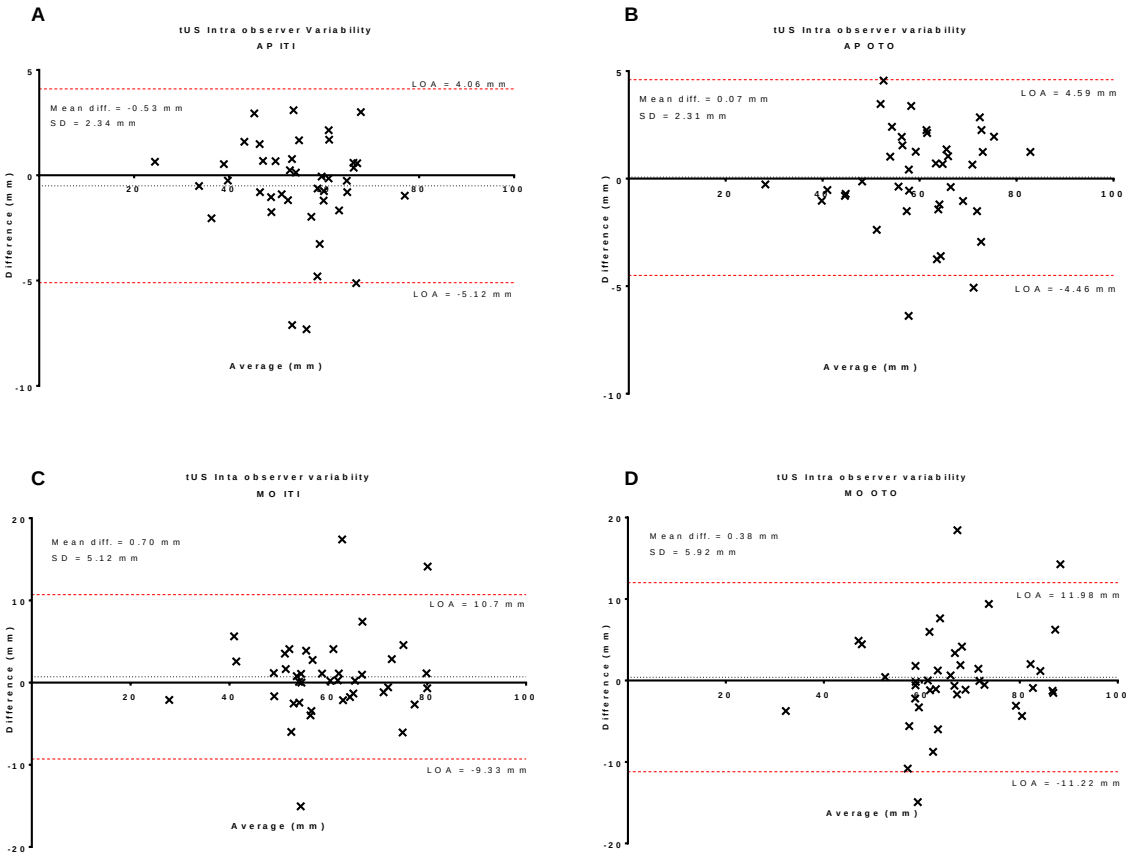

(Figure 29. tUS Intra-observer variability for all patients with ITI and OTO diameters measured by AP and MO planes. SD = standard deviation, LOA = limit of agreement)

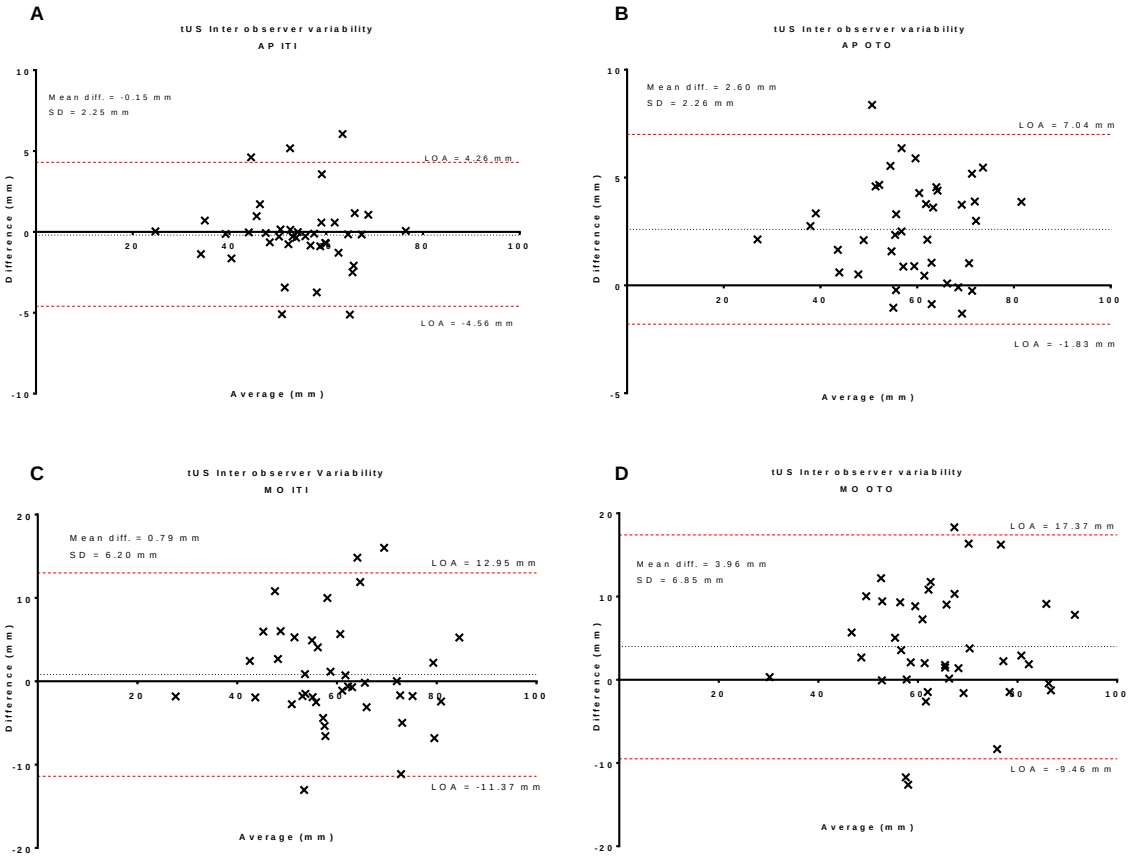

(Figure 30. tUS Inter-observer variability for all patients with ITI and OTO diameters measured by AP and MO planes. SD = standard deviation, LOA = limit of agreement)

Inter-modality variability (tUS vs CTa)

Inter-modality agreement (tUS vs CTa) was calculated for all patients combined (Tab. 11 and Fig. 31) and as sub-groups of pre (Fig. 32) and post EVAR (Fig. 33). When combined (AAA + EVAR), mean AP ITI and MO OTO diameters were significantly different between modalities, compared with AP OTO and MO ITI, which were not statistically different. Repeatability coefficients were outside clinical thresholds for AP ITI, AP OTO, MO ITI and MO OTO diameter measures for combined measures.

Sub-group analysis showed slight differences between pre and post EVAR-patients. EVAR mean AP ITI and MO OTO diameters were significantly different between modalities, compared with AP OTO and MO ITI, which were not statistically different. Repeatability coefficients were outside clinical thresholds for AP ITI, AP OTO, MO ITI and MO OTO diameter measures for combined AAA and EVAR. Pre-treatment AAA patients results differed to the combined and EVAR analysis where only AP ITI mean diameter was significantly different and AP ITI and AP OTO coefficients of repeatability were within clinically accepted limits (4.17 and 4.66mm).

Table 11. Inter-modality mean AP and MO diameter difference for both ITI and OTO dimensions.

		AP ITI	**AP OTO**	**MO ITI**	**MO OTO**
Combined	Mean difference ± sd (mm)	-2.91±3.19	-0.47±4.22	0.99 ± 6.88	-3.22±8.18
	p value*	<0.001	0.476	0.363	0.016
	Statistically different*	Yes	No	No	Yes
	Coefficient of Repeatability (mm)	6.25	8.27	13.48	16.03
EVAR	Mean difference ± sd (mm)	-2.90±3.76	0.68 ± 5.09	-1.37±5.62	3.14±7.28
	p value*	0.001	0.509	0.233	0.041
	Statistically different*	Yes	No	No	Yes
	Coefficient of Repeatability (mm)	7.37	9.98	11.02	14.27
AAA	Mean difference ± sd (mm)	-2.94±2.13	0.15±2.38	-0.39±8.68	3.35±9.67
	p value*	<0.001	0.809	0.860	0.186
	Statistically different*	Yes	No	No	No
	Coefficient of Repeatability (mm)	4.17	4.66	17.01	18.95

*(*Value relates to comparison of tUS with CTa mean)*

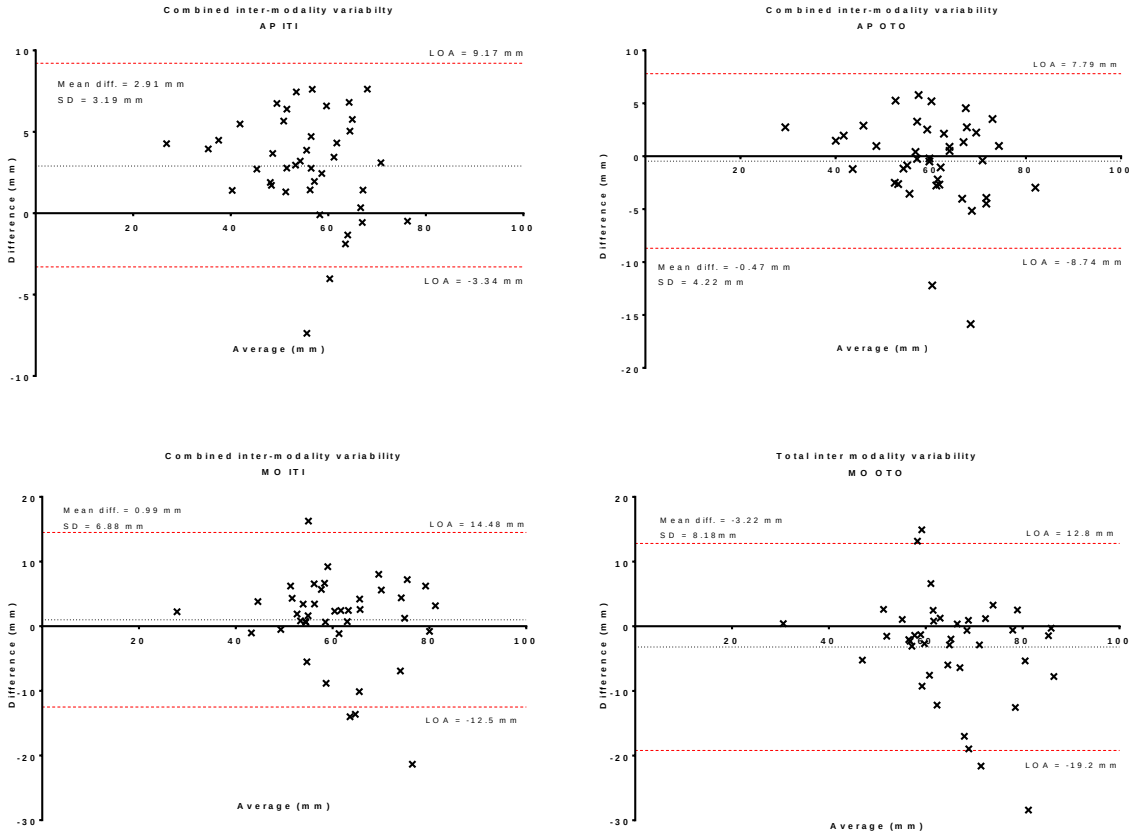

(Figure 31. Combined Inter-modality diameter difference for all patients. SD = standard deviation, LOA = limit of agreement)

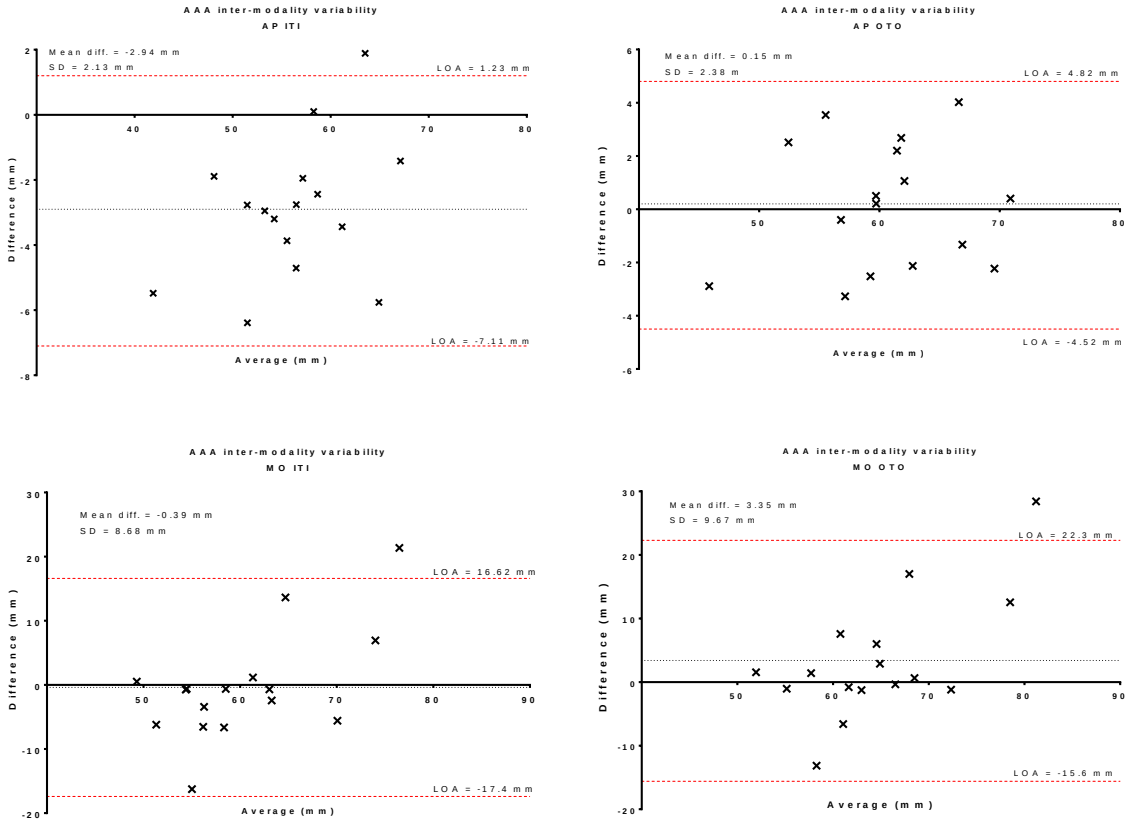

(Figure 32. Inter-modality diameter difference for AAA patients. SD = standard deviation, LOA = limit of agreement)

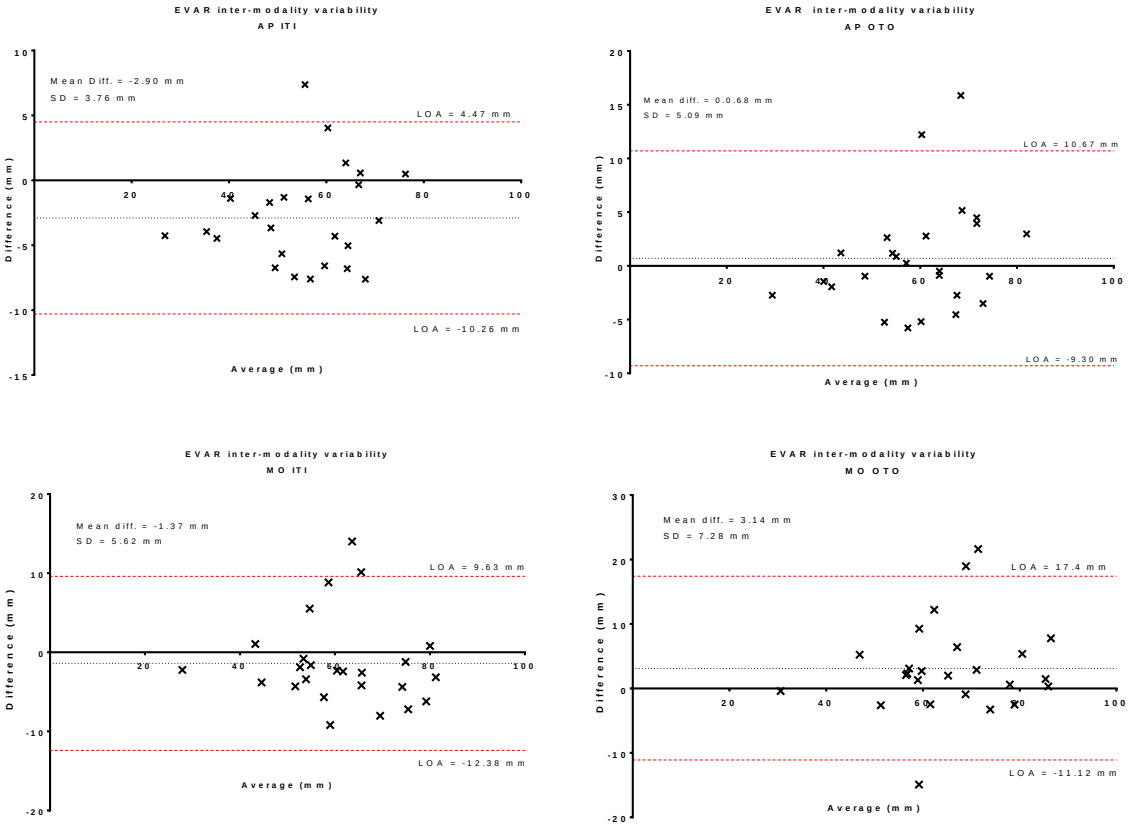

(*Figure 33. Inter-modality diameter difference for EVAR patients. SD = standard deviation, LOA = limit of agreement*)

Discussion:

Due to population ageing and cost, the need for of a non-invasive imaging modality, without radiation or nephrotoxic contrast media for surveillance, is vital. 3D US is a novel and emerging technology in the field of vascular disease, despite its routine use in Obstetrics and Cardiology. 3D US's potential to aid management of AAA is crucial for routine surveillance, but there is a need to demonstrate close agreement to CTa before CTa can be replaced entirely.

We have shown that tUS has excellent inter- and intra-observer agreement for AP and MO ITI diameters, but only AP dimensions, ITI and OTO, are within clinical thresholds (repeatability coefficients 4.41 to 4.59mm). OTO dimensions show less inter-observer agreement, but AP dimensions remain below the 5mm clinical threshold. MO diameters remain clinically unacceptable, with large repeatability coefficients (10.04 to 13.43mm), well above acceptable limits. We report that the most reproducible method for measuring diameter by tUS is AP ITI due to slightly better inter-observer agreement (mean difference [ITI] -0.15 vs [OTO] 2.60mm) but AP OTO is an acceptable alternative (repeatability coefficient 4.41 vs 4.43mm). The Inter and Intra observer agreement we calculate for AP ITI diameter is slightly improved on those reported by Long et al (2013) and comparable with Bredahl et al (2015) [35, 80]. The discrepancy with Long et al (2013) may reflect the improvement in DUS image quality since 2013. Although comparisons can be made to these previous studies, caution must be taken due to the different methods of measuring the diameter (ITI, OTO or leading edge to leading edge).

When compared to CTa, we have shown that there is greater variability in diameter measurements for patients who have had EVAR than those pre-treatment and that AP diameters remain the most accurate method of assessment (mean difference AP OTO -0.47±4.22mm). This investigation demonstrates that the currently accepted difference between DUS and CTa of 5mm could be reduced if using tUS and that an AAA should still be measured in the AP plane. When compared to Bredahl (2015), which looked at small AAA's, our mean differences are better (-0.47 versus 1.8mm), but we report nearly double the standard deviation. The mean difference and repeatability coefficient we report in patients with EVAR, for AP diameters, are comparable with those reported by Bredahl et al (2013). Again, caution must be given in the comparison to these studies due to the methods of diameter measurement but we report similar results.

According to key studies, our results appear to be relatable to those previously reported which is encouraging, given that Long et al used a mechanical 3D transducer and Bredahl et al used matrix 3D transducers [35, 80, 262]. It may therefore, be possible to use interchangeably the type of 3D ultrasound system to measure AAA diameter.

DUS has some significant pitfalls, including the operator building a mental impression [27] of AAA geometry, which has been shown to be erroneous and can result in some discrepancy between DUS and CTa. Although current rupture risk is based on an anterior-posterior measurement by DUS, not all AAA's are perfectly spherical and as such, the AP dimension may not represent the true risk for particular patients whose aneurysms are curved or oval in geometry. The geometry of AAA's has been studied significantly, but the fundamental issue of highly tortuous or angulated AAA's can lead to oblique incidence angles with DUS, which can falsely elongate an AAA, reducing the accuracy of diameter calculations. CTa is often the only answer to address this, but it is expensive and involves radiation and nephrotoxic contrast. Alternative 3D imaging modalities, such as 3D ultrasound, are therefore, vitally important.

The large error seen in MO diameters we report could be attributable, in part, to a type of ultrasound artefact called edge-enhancement. As a standard assumption, ultrasound travels in straight lines perpendicular to the transducer footprint on the anterior abdomen. The medial and lateral walls of an AAA are parallel to the path of ultrasound travel and therefore, are represented as weaker echoes (darker pixels) on the monitor, due to loss of energy, as a result of non-specular reflection, which means it is less accurate to measure MO diameters due to the poor image resolution at these medial-lateral boundaries. It is plausible that worse resolution and therefore, calliper placement, at points perpendicular to ultrasound transmission, i.e. the medial-lateral AAA wall, accounts for some of the error in the MO measurements. However, not all AAA's are largest in the AP plane. A future solution to improve this limitation would be to acquire tUS volumes from different scan planes, e.g. anterior and right and left lateral, that are fused together like a 3D compound imaging technique, which may combat this error. The same method could be utilised to negate issues surrounding ultrasound and bowel gas, making follow-up more consistent.

The cardiac cycle is a major contributor to the variability in DUS AAA diameter measurement which has a reported pulsatile distance of 1.95mm [263], and is thought to account for some variability between DUS and CTa diameters. ECG gating is not currently possible with tomographic 3D ultrasound; however, it is not standard practice to ECG gate for CTa to image the abdominal either. CTa gating is common practice in cardiac imaging but is not utilised routinely for AAA. CTa ECG gating can make detection of submillimetre motion possible which is important for accurate diameter measurement [264]. Without ECG gating, CTa is very fast, making pulsatility a very minor issue. tUS comparatively takes a little longer, making the likelihood of error higher as the AAA is imaged at any point in the cardiac cycle.

ECG-gating can combat pulsatile measurement error, but is time-consuming and has a reported inter-operator variance of 3mm [265]. ECG gating has been shown to significantly reduce DUS intra-operator error below 0.4mm [265]. The lack of ECG-gating in our study could account for the slightly higher error that has been seen in other studies [262, 265]. Despite the reported use of ECG-gating within research, it has not found favour in routine clinical practice, presumably due to the added complexity and time consumption. In our study, we assumed that post-EVAR patients have non-pulsatile aneurysms as none had endoleak and would therefore, have smaller measurement error due to pulsatility. We hoped that our study would demonstrate lower variability in the EVAR group compared to those pre-treatment, which we did not see. As such, the question around the use of ECG-gating persists.

Despite acceptable errors identified in this study, more work is needed to reduce measurement error, which may be confounded by the manual process of diameter measurement. Centreline-derived diameters could improve our measurement and have been shown to have lower modality variability (1.6mm) than techniques that rely on manual measurement (2.6mm) through finding the maximal diameter [260]. Automated centreline measurement and compound 3D multi-scanning (scanning from different angles and stitching the scans together) with the possibility of ECG-gating, may negate some limitations of our study and produce even greater agreement.

Conclusion:

Tomographic ultrasound has excellent inter- and intra-operator variability. When compared to CTa, tUS shows good agreement, with AP ITI diameters being the most accurate. The AP OTO technique offers the best accuracy when compared to CTa, but ITI methods hold better operator reproducibility. Tomographic ultrasound may be clinically acceptable for those patients in aneurysm or EVAR surveillance, or where accurate growth measurements are required. Centreline derived diameters, compound scanning and ECG gating may diminish variability altogether with development.

Acknowledgments: We thank Dr Julie Morris for her invaluable advice as Departmental Statistician.

Chapter 7 - Carotid Plaque Volume can be accurately measured by three-dimensional tomographic ultrasound.

Chapter contributions and role:

Division of Cardiovascular Sciences

S Rogers: conception, study design, DUS and tUS scanning, tUS CPV measurement, immersion volume measurement training, data collection, statistical analysis and manuscript writing.

A. Phair: patient recruitment, plaque immersion volume, data collection and critical review.

C. Olech: patient recruitment, plaque immersion volume and data collection.

Mr J. Ghosh MD: Co-Supervisor and critical review

Prof C. McCollum: Supervisor and critical review

Independent Vascular Services Ltd

J. Carreira: DUS and tUS scanning, tUS measurements.

Funding: This project has received funding from the European Union's Horizon 2020 research and innovation programme under grant agreement No [760380].

Abstract

Objectives:

A <2% risk of ipsilateral stroke/year in asymptomatic patients demonstrates that carotid stenosis severity is a poor predictor of stroke. We know that carotid plaques undergo outward remodelling to preserve luminal diameter, adding further evidence that plaques should be assessed in terms of vulnerability and not stenosis. This study has utilised a novel 3D tomographic ultrasound (tUS) system, with and without microbubble-contrast to establish the most accurate method for calculating CPV non-invasively.

Materials and methods:

Pre-operatively, B-mode and CEUS scans were performed by an experienced Vascular Scientist. B-mode, CEUS and fused tUS scans were used to measure CPV by two observers using a standardised technique. The precise volume of the endarterectomised plaque was measured using immersion.

Results:

CPV measurements were performed on 34 of 50 recruited patients. Minimal bias was identified for intra-observer B-mode, CEUS and fused tUS scans, 0.10(0.25) [95%CI -0.38 to 0.58]cm^3, 0.14(0.29) [95%CI -0.43 to 0.7]cm^3 and 0.06(0.18) [95%CI -0.28 to 0.41]cm^3. Minimal bias was identified for inter-observer B-mode, CEUS and Fused tUS scans; -0.06(0.28) [95%CI -0.60 to 0.48]cm^3, -0.02(0.26) [95%CI -0.5 to 0.53]cm^3 and -0.05(0.19) [95%CI -0.43 to 0.33]cm^3. B-mode, CEUS and fused tUS methods had minimal bias when compared with endarterectomy volume; -0.22(0.34) [95%CI -0.88 to 0.44]cm^3, -0.05(0.24) [95%CI -0.51 to 0.42]cm^3 and -0.10(0.22) [95%CI -0.52 to 0.32]cm^3.

Conclusions:

CPV can be accurately measured by tUS with excellent intra- and inter-observer agreement and minimal bias when compared to endarterectomy volume. The highest degree of precision was seen with CEUS and fused images but B-mode tUS scans have sufficient precision for Carotid screening.

Key Words: Carotid plaque volume, CPV, three-dimensional (3D) tomographic ultrasound, tUS

Introduction:

A joint working party collaboration between the UK Vascular Societies (VS and SVT) in 2009 uniformly agreed that the North American Symptomatic Carotid Endarterectomy Trial (NASCET) method for grading carotid artery disease should be used in the UK [13]. Approximately 20% of patients with a >50%^{NASCET} but <99%^{NASCET} carotid stenosis will have a stroke within 72 hours of symptom onset [115] and nearly 30% of patients will have a recurrent stroke [116]. As a direct result carotid artery disease poses a huge financial burden to the NHS.

Despite knowing that stroke, secondary to carotid artery disease is embolic, we still base the decision to operate on the degree of stenosis, i.e. the percentage. The fact that patients with the same degree of stenosis can be symptomatic or asymptomatic infers that stenosis measurement is not the most reflective measure of stroke prediction. Previous cardiology research suggests that the degree of stenosis can also be reduced by outward remodelling of the arterial wall to preserve luminal diameter making stenosis assessment unreliable [126]. The Asymptomatic Carotid Surgery Trial (ACST) established a risk of ipsilateral stroke in patients randomised to differed intervention of 9.5% in patients younger than 75 with >70%^{NASCET} stenosis (i.e. only 10 out of 100 patients with >70% stenosis have a stroke) [123]. It is therefore logical to assess carotid artery disease in terms of embolic risk rather than percentage stenosis.

Carotid plaque volume (CPV) is a measure of vulnerability (embolic risk) and may be a better predictor of stroke than stenosis assessment; potentially clarifying surgical thresholds. Patients with a cranially extending <70%^{NASCET} stenosis may have a large volume of atherosclerotic plaque compared to a short high-grade stenosis and could therefore pose similar risk to those >70%^{NASCET}. Our group has previously demonstrated that CPV relates to cerebral symptomology but does not correlate with peak systolic velocity, i.e. percentage stenosis [161]. We also demonstrated in 34 patients that CPV can be measured non-invasively and accurately by 3D tomographic ultrasound (tUS) [161].

B-mode tUS scans are preferential when calculating CPV due to improved image resolution, however, they lack flow information meaning the blood-plaque border can be difficult to identify; a particular challenge when imaging soft plaques or thrombus. Alternatively, contrast-enhanced ultrasound (CEUS) scans have good flow definition but have low resolution due to the low acoustic output power utilised, which makes definition of the intima-lumen boundary difficult to visualise. Image fusion is a new technique that adopts the benefits of both B-mode with CEUS tUS scans to negate the complexities of soft plaques and flow, i.e. good intimal-lumen boundaries from B-mode and excellent blood-plaque definition from CEUS.

This study has utilised a novel tUS system with and without microbubble contrast to establish the most accurate method, B-mode, CEUS or image fusion, for calculating CPV non-invasively whilst confirming with precise immersion volumes of the surgical endarterectomy specimens.

Materials & methods:

The study was given ethical approval by the national Research Ethics Committee (11/NW/0308). All patients (male, female, symptomatic and asymptomatic) admitted for carotid endarterectomy (CEA) were approached and provided written informed consent. Symptomatic patients with >50%^{NASCET} stenosis and asymptomatic patients with >80%^{NASCET} stenosis were consented for a tUS scan (with and without microbubble contrast) and carotid plaque immersion. A Carotid Duplex ultrasound scan and tUS scans were performed pre-operative immediately prior to surgery. All Duplex and tUS scans were performed by experienced accredited Senior Vascular Scientists. Plaque immersion volume and surgical lengths were calculated by a Vascular Surgical Fellow experienced in this technique within 20 minutes of the specimen being removed from the neck. tUS scans were analysed by two Vascular Scientists blinded to the immersion volume and trained/validated in house.

Pre-operative scanning:

A Duplex ultrasound scan was performed as per the joint recommendations protocol [13] using a 9MHz Linear array transducer on a Resona 7 high definition ultrasound instrument with contrast imaging enabled (Mindray, Shenzhen, China). A magnetically-tracked non-ECG gated freehand 3D tomographic ultrasound (tUS) system (PIUR imaging GmbH, Vienna, Austria) was attached to the Resona 7 ultrasound scanner. Sensors were attached to the 9MHz linear ultrasound probe to track the transducer orientation and position in time and space. Using screen capture from the Resona 7, the tUS system computes Multi-planer reconstructions (MPR) with a 3D ultrasound volume almost instantly.

A 16-gauge peripheral venous cannula was inserted with an extension line to facilitate contrast imaging. The patient was then asked to remain perfectly still while 6 tUS scans were performed with microbubble contrast being administered half way through. Three B-mode tUS scans were performed in transverse section from the supra-clavicular fossa to the level of the mandible. The contrast package was then enabled on the Resona 7 and three contrast-enhanced tUS (CEtUS) scans were performed following administration of 2mL microbubble contrast (Sonovue, Bracco, Italy) followed by a 5mL,0.9% Saline flush.

tUS CPV measurement:

To calculate the corrected CPV, Vascular Scientists were given the total and bifurcation lengths to ensure start and stop points of measurement. CPV was calculated by tracing around the intima-lumen border and also around the blood-plaque border in transverse sections. A process termed manual planimetry, within the MPR with an inter-slice distance of one millimetre. Multiple slices are created along the full length of the carotid plaque for its correct surgical length (Fig. 34). CPV was measured on B-mode, CEUS and Fused tUS scans for each patient by two Vascular Scientists blinded to the endarterectomy volume and each other. One Vascular Scientist repeated the volumes months later, still blinded, for observer assessment. All tUS CPV measurements (B-mode, CEUS and fused) were calculated using the research software ImFusion Suite (ImFusion GmbH, Munich, Germany).

Immersion technique:

The endarterectomised plaque was taken immediately from theatre, where total and bifurcation lengths were accurately measured using a disposable tape in millimetre units by a Vascular Surgery Fellow. Specimen dry weight was calculated using a digital balance. A braided suture was then secured around the specimen which is immersed in 10mL, 0.9% saline, which was zeroed on the digital balance. CPV was then calculated from immersion technique (immersion weight/density of Saline) based on Archimedes principle using Saline stored at 23 degrees. The endarterectomy volume was withheld from the Vascular Scientists.

Statistical analysis:

Bland-Altman analysis was calculated to determine bias between methods of CPV measurement using GraphPad prism v7 (GraphPad software Inc., La Jolla, CA, USA). Intra-Class Correlation (ICC) estimates and their respective 95% confidence (95%CI) intervals were calculated using SPSS statistical package version 22, (SPSS Inc, Chicago, IL, USA) based on a single-measurement, absolute agreement, 2 away mixed-effects model.

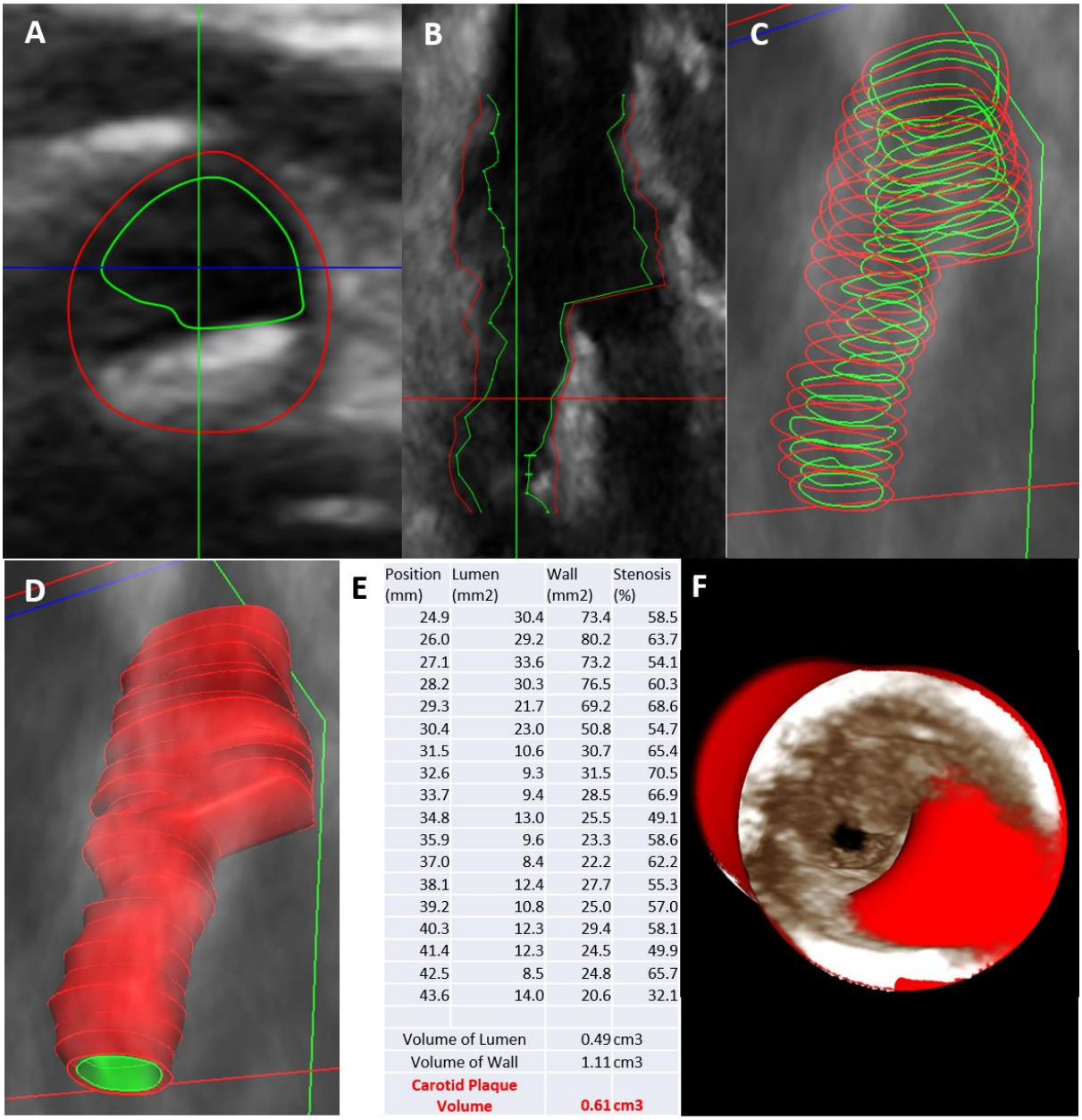

Position (mm)	Lumen (mm2)	Wall (mm2)	Stenosis (%)
24.9	30.4	73.4	58.5
26.0	29.2	80.2	63.7
27.1	33.6	73.2	54.1
28.2	30.3	76.5	60.3
29.3	21.7	69.2	68.6
30.4	23.0	50.8	54.7
31.5	10.6	30.7	65.4
32.6	9.3	31.5	70.5
33.7	9.4	28.5	66.9
34.8	13.0	25.5	49.1
35.9	9.6	23.3	58.6
37.0	8.4	22.2	62.2
38.1	12.4	27.7	55.3
39.2	10.8	25.0	57.0
40.3	12.3	29.4	58.1
41.4	12.3	24.5	49.9
42.5	8.5	24.8	65.7
43.6	14.0	20.6	32.1
Volume of Lumen		0.49	cm3
Volume of Wall		1.11	cm3
Carotid Plaque Volume		**0.61**	**cm3**

(Figure 34. Diagram for calculating CPV with tUS. Panel A – Transverse manual planimetry of plaque. Panel B – Coronal manual planimetry of plaque. Panel C – 3D manual planimetry. Panel D – tUS volume reconstruction. Panel E – CPV calculation from manual planimetry. Panel F – tUS volume rendered CPV)

Results:

The first fifty patients have completed the protocol where only five patients were asymptomatic. All fifty patients had carotid stenosis greater than 50%[NACSET] (Tab. 12). Of the fifty patients, sixteen had to be excluded from analysis leaving thirty-four suitable for interpretation. Of the sixteen, five were completely obscured by calcium shadowing meaning tUS measurement was not possible. Three plaques were not retained by theatre staff and four operations were cancelled due to bed availability. The remaining four patients either withdrew before the scan or were unable to be cannulated. Total mean(±standard deviation) endarterectomy CPV was 0.79(0.45)cm^3 compared with B-mode 1.01(0.63)cm^3, CEUS 0.84(0.47)cm^3 and fused 0.87(0.48)cm^3 measured by tUS.

Table 12. Number of patients by stenosis severity

Stenosis severity	Number of patients (N=34)
50 – 59%	5
60 – 69%	13
70 – 79%	2
80 – 89%	4
90 – 95%	10

Intra-observer agreement:

Intra-observer agreement demonstrated minimal bias(±SD) [95%CI], for B-mode, CEUS and fusion, 0.10(0.25) [95%CI -0.38 to 0.58]cm^3, 0.14(0.29) [95%CI -0.43 to 0.7]cm^3 and 0.06(0.18) [95%CI -0.28 to 0.41]cm^3 respectively (Fig. 36). Intra-observer agreement showed excellent correlation, ($p<0.001$), with narrow confidence intervals. ICC for B-mode, CEUS and fusion for the same observer was 0.91(95%CI 0.82-0.95), 0.87(95%CI 0.6-0.88) and 0.92(95%CI 0.85-0.96) respectively (Fig. 37).

Inter-observer agreement:

Minimal bias(±SD) [95%CI] was identified for repeat measures from the two users for all three imaging methods (B-mode, CEUS and fusion). Respectively these were -0.06(0.28) [95%CI -0.60 to 0.48]cm^3, -0.02(0.26) [95%CI -0.5 to 0.53]cm^3 and -0.05(0.19) [95%CI -0.43 to 0.33]cm^3 (Fig. 36). Inter-observer agreement had excellent ICC with narrow confidence intervals for B-mode, CEUS and fusion. Respectively ICC was 0.90(95%CI 0.81-0.95), 0.83(95%CI 0.69-0.91) and 0.92(95%CI 0.84-0.96) (Fig. 37).

Agreement with Index:

CPV measured by all three methods (B-mode, CEUS and fused) by tUS strongly correlated with endarterectomy CPV, ($p<0.001$), and have narrow confidence intervals (Fig. 35). ICC for CPV tUS measurements by B-mode, CEUS and fusion compared with endarterectomy were 0.81(95%CI 0.67-0.9), 0.87(95%CI 0.75-0.93) and 0.89(95%CI 0.79-0.95) respectively. All three tUS methods had minimal bias with the highest degree of precision seen with fusion (Fig. 36). Mean difference, bias(±SD) [95%CI], for all B-mode, CEUS and fusion was -0.22(0.34) [-0.88 to 0.44]cm^3, -0.05(0.24) [-0.51 to 0.42]cm^3 and -0.10(0.22) [-0.52 to 0.32]cm^3.

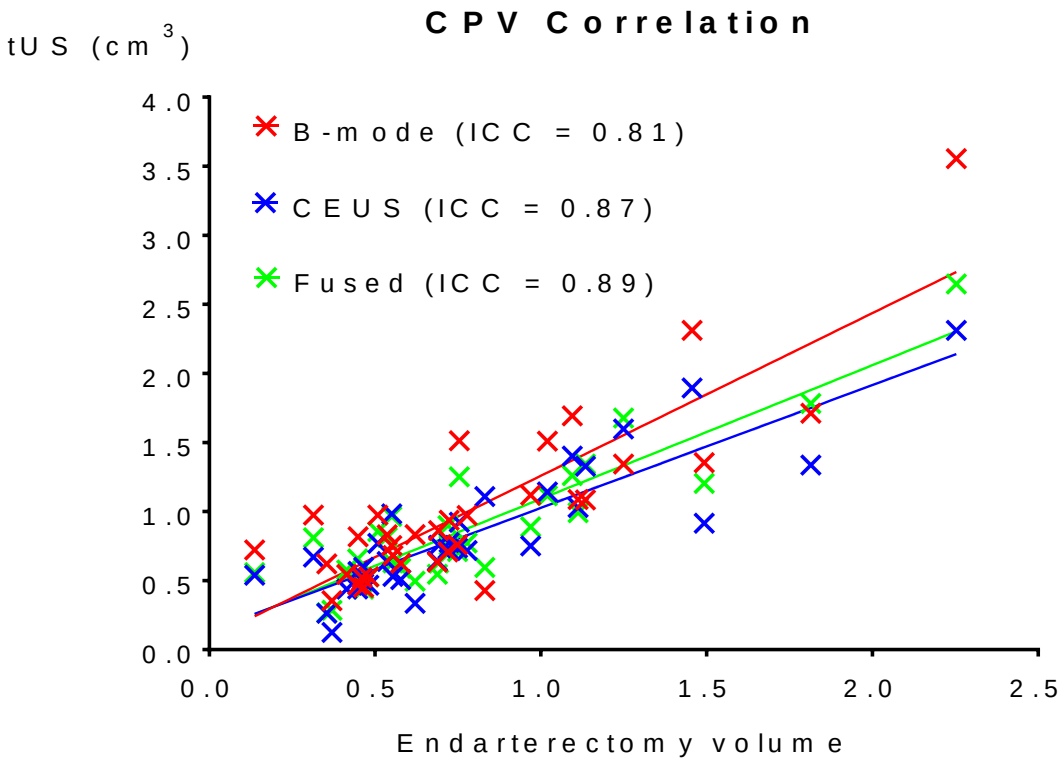

(*Figure 35, CPV correlation for all three tUS methods*)

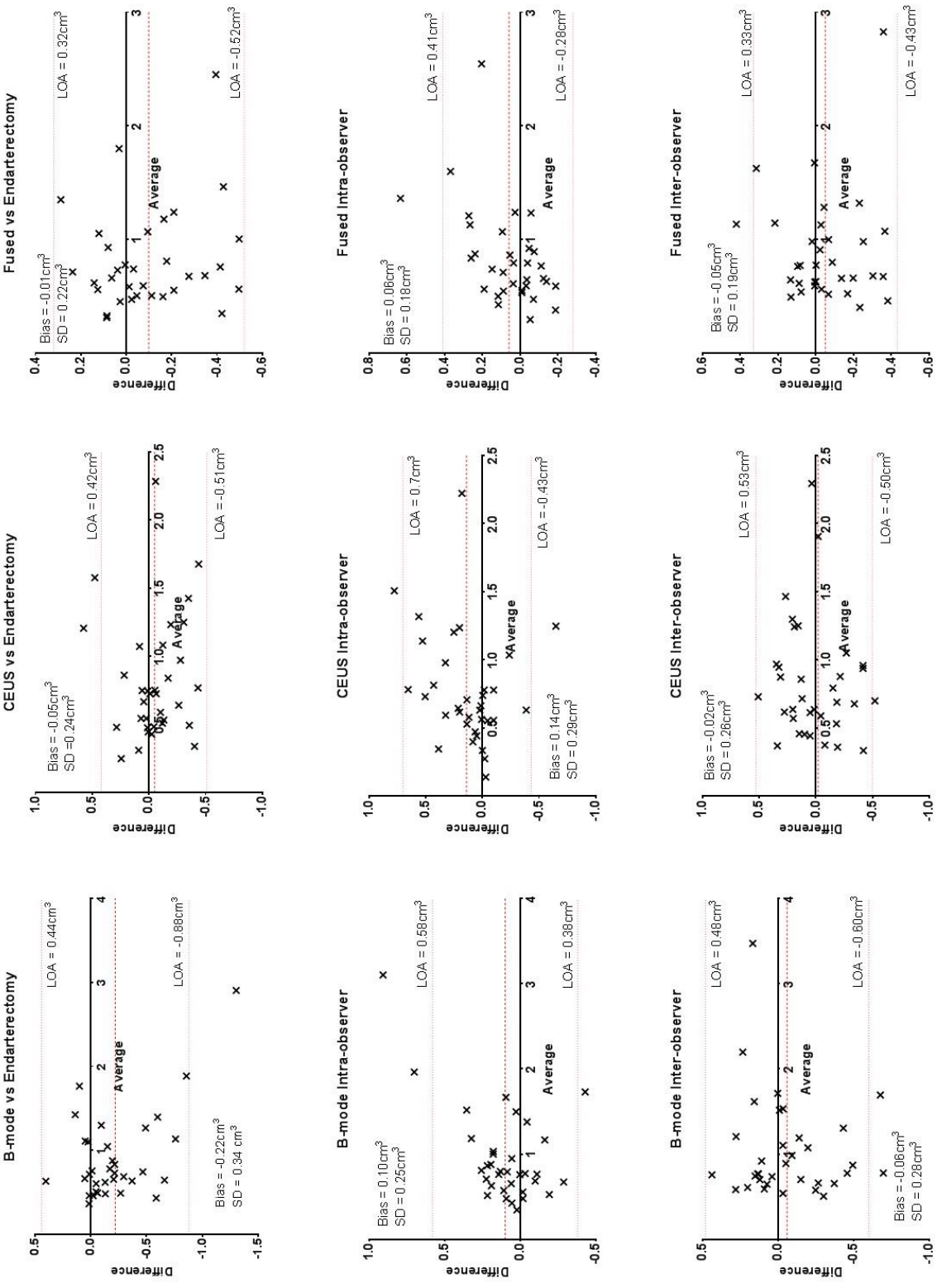

(Figure 36. Bland-Altman agreement of tUS B-mode, CEUS and Fused volume compared to endarterectomy, intra- and inter-observer volumes)

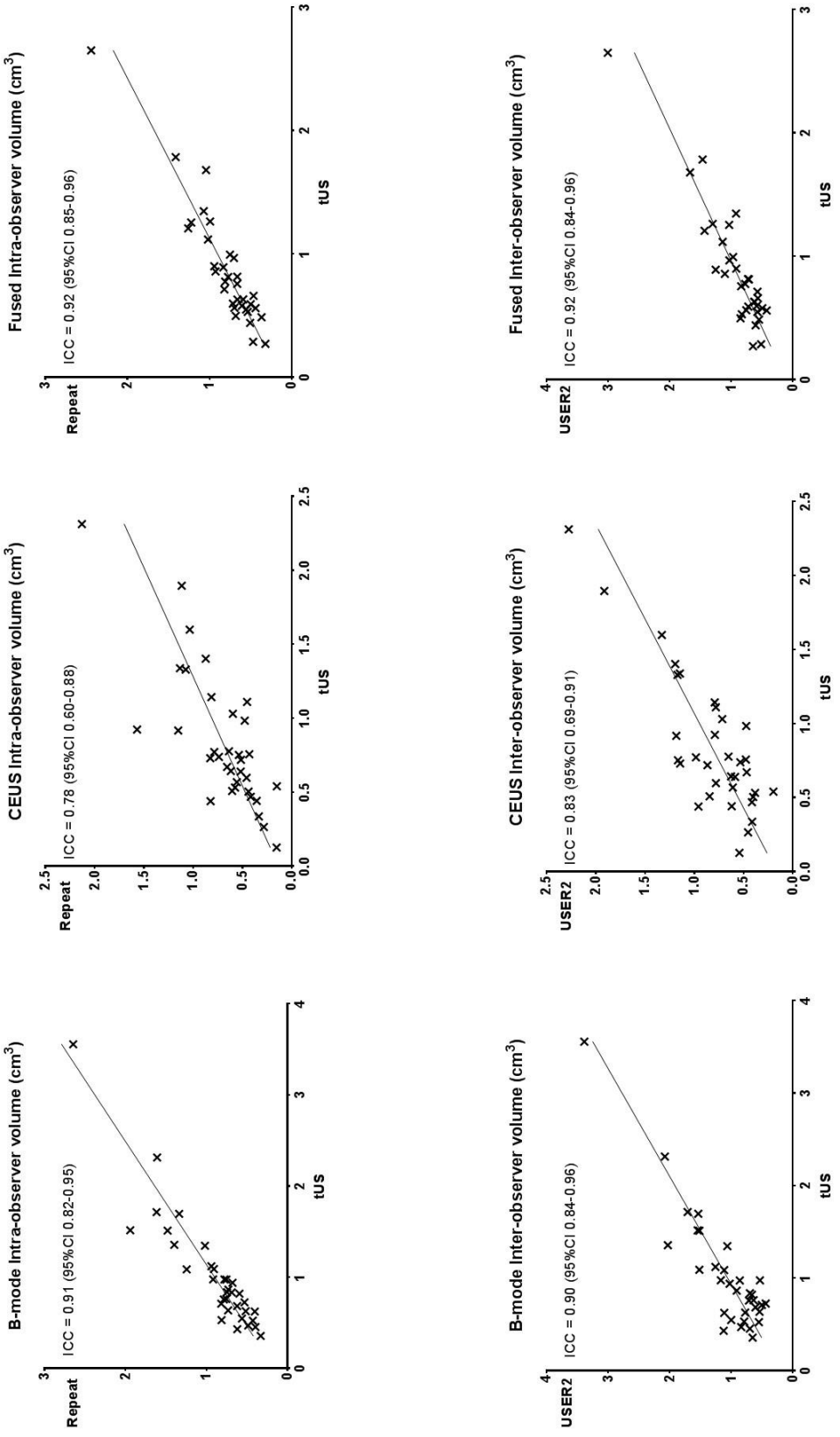

(Figure 37. Inter-class correlation of tUS B-mode, CEUS and Fused volume for Intra- and Inter-observer agreement)

Discussion:

Assessing Carotid disease in the form of embolic risk through measuring CPV may be a better predictor of stroke than stenosis assessment; potentially clarifying surgical thresholds. However, its clinical use is only relevant if it can be precisely measured non-invasively. We report the accuracy of three tUS methods for calculating CPV when compared to the plaque specimen. We have shown that tUS is highly reproducible for measuring CPV with minimal bias and a high degree of precision seen through narrow confidence intervals. B-mode, CEUS and fused tUS methods had minimal bias when compared with endarterectomy volume indicating a degree of precision.

Despite the good agreement and precision, we report, there are some potential sources of explainable error in the measurement bias that we have identified. Definition of the plaque extent due to a pre-defined inter-slice distance (when using manual planimetry) has previously been shown to be a source or variability where the exact starting position of the first planimetry slice is a source of variation [167]. Our bias shown between observers and tUS/immersion could in part be explained through different starting positions for the calculations of surgical lengths, i.e. 1.0cm proximal to the ICA origin for the starting point may not be the exact same point for plaque specimen and tUS (e.g. 0.9cm and 1.1cm depending on where the user decides to start their measurement). Although correcting for surgical lengths is not a real-world solution it facilitates the ability to measure tUS accuracy for CPV calculations. tUS can therefore be used for accurate CPV calculations but would need to follow a uniformly agreed clinical protocol to ensure that variability is kept low. Further research should establish the starting and stopping positions for measuring CPV as the clinical protocol. Variability of CPV has been proven to remain constant with an inter slice distance between 1mm and 3mm maintaining a high inter and intra-observer variability [166, 266]. The choice of 1mm in our protocol would limit this type of error.

The excellent correlation and minimal bias seen between operators for tUS outlines a highly accurate method of CPV calculation. The slightly higher, but still minimal bias between tUS and immersion shows that there is no consistent over-estimation in CPV by tUS meaning source of error could in part also be the ‘gold standard’ immersion technique, however, this is highly unlikely ultimately meaning that the planimetry starting position must be the primary source of the bias confounded by surgical technique, i.e. missing plaque.

Operator dependence or measurements is a known limitation of any ultrasound technique and is true of tUS. Although tUS removes the dependence of scanning, this type of error still pertains in CPV measurement. As previously reported, operator dependence of CPV measurement using manual planimetry for analysis is time consuming [267]. Before CPV becomes clinically accepted operator dependence and time consumption need to be reduced [31]. One method to reduce time consumption could be by utilizing artificial intelligence that can perform automated CPV measurement. However, the difficulty in automatically calculating CPV due to differentiation between blood-plaque boundary and Intima-luminal boundary (ILB) needs addressing. Two groups have successfully produced systems that can define blood-plaque boundary and ILB that may circumvent these issues and demonstrate excellent correlation and minimal variation between manual and automated segmentation, but both groups failed to validated against a ground truth, i.e. the endarterectomy specimen [175, 176]. More work is required comparing automated methods to a ground truth, but once accuracy is proven with clinical traction will improve for the use of CPV.

The largest error seen in our data was with B-mode tUS CPV calculation compared with endarterectomised CPV. This can partly be explained by ultrasound plaque morphology presentation on screen. Ultrasound presents tissues separated by their density in a grey scale meaning it is possible for echolucent, lipid rich plaques to be displayed as black. When identifying the blood-plaque boundary when measuring CPV it is possible that a small amount of lipid plaque may be miss-classified as lumen when using B-mode tUS slices, effectively underestimating the volume. Another possibility of variation could be that on resection liquid plaque or haematoma is not included as part of the retained specimen, purely due to surgical technique, rather than surgeon decision, effectively underestimating the immersion volume. There would be no way of excluding this from our research and as such must be accepted as a minimal source of variability.

A major unavoidable limitation of tUS is the ability to capture the real time dynamic information. Modern matrix 3DUS systems commercially available can achieve this but are expensive and probably not necessary for CPV measurement. However, 3D haemodynamic information, such as computational fluid dynamics, could be another plaque vulnerability assessment tool and should be explored. Vessel pulsatility however, could be another source of error. ECG gating was thought to be an important factor in CPV assessment [267, 268], but the negligible bias seen in our investigation demonstrates a significant accuracy without gating. This may be a reflection on the decreased motility and pulsation of carotid vessels with atherosclerotic disease [174]. There is only evidence that motility is reduced in moderate disease, therefore with the assessment of early arterial disease, ECG gating may still be required due to pulsatility, but this is beyond the scope of this investigation. The ability to detect early atherosclerotic change however, may be of importance to the pharmaceutical industry through intimal volume. Given the aging population and number of annual strokes set to increase in line with population growth this is an area of future research that could help outline new targets for novel drugs giving scope for early aggressive therapy.

The bias we report suggests that B-mode tUS can be accurately utilised for clinical screening/surveillance. CEUS and fused volumes hold the highest degree of precision with negligible bias and may remain for highly precise research studies as the impracticality of CEUS for screening means its utility is currently limited to tertiary centres. The slightly higher level of bias we report with B-mode still falls within the realm of acceptability for screening and surveillance but a larger study that establishes a surgical threshold will only address the question of clinical acceptability. Our results on intra- and inter-observer variability correspond with previous reports [161, 166, 269-271], although these previous reports do not compare to true plaque immersion volume. When compared to theoretical volumes CPV has remained statistically significant [266] but for clinical traction comparison to true surgical specimen is vital. Where immersion volume has been reported our results corroborate those findings [272].

It is possible to measure CPV with both Computed X-Ray Tomography and Magnetic Resonance Imaging and there have been works on their validation with cardiovascular risk and cerebrovascular symptoms [273-275]. Whilst these modalities offer ability for other cerebral measurements, they are expensive or involve radiation exposure. As we report tUS to be an accurate alternative, its accessibility makes it a more useful tool for future clinical assessment.

This work outlines a clear and accurate method for the assessment and surveillance of carotid artery disease in the form of CPV. Assessment of atherosclerotic vulnerability in this way could outline those patients who would benefit from CEA more clearly once a threshold is established. Identifying those patients, particularly those for whom there is currently no benefit or marginal surgical benefit (>50% - <70% ^{NASCET} stenosis) [276], more clearly and accurately is essential for modern vascular practice. Previous work performed linking CPV and coronary artery burden to cardiac events [277] and the link between calcification and coronary artery burden demonstrates a use of replacing the use of stenosis assessment [157].

Conclusion

Despite the fact that our study demonstrates CPV can be accurately measured with excellent inter- and intra-observer agreement by tUS, the process of manual planimetry is laborious and time consuming. Future planned research should focus on automatic tUS CPV measurement. This will dramatically speed up CPV calculation and potentially adding better clinical utility. This may involve CEUS to more clearly define the blood-plaque boundary however, this may not be practical when used as a screening tool. Future work in the form of long-term follow-up studies are essential to identify the acceptable level of surgical differentiation and a greater understanding of the link to cardiovascular risk. Utilisation of tUS for the accurate calculation of arthrosclerosis holds potential that aggressive medical therapy could reduce future health burden.

Acknowledgments: We thank Dr Julie Morris for her invaluable advice as departmental statistician.

Chapter 8 - Comparison of below knee contrast-enhanced 3D tomographic ultrasound to CT, MR or Catheter angiography for peripheral arterial imaging.

Chapter contributions and role:

Division of Cardiovascular Sciences

S. Rogers: conception, study design, tUS scanning, tUS reporting, data collection, statistical analysis and manuscript writing.

A. Phair: patient recruitment, data collection and critical review.

C. Olech: patient recruitment and data collection.

Mr J. Ghosh MD: Co-Supervisor and critical review

Prof C. McCollum: Supervisor and critical review

Independent Vascular Services Ltd

J. Carreira: tUS scanning, tUS reporting.

Funding: This project has received funding from the European Union's Horizon 2020 research and innovation programme under grant agreement No [760380].

Abstract

Objectives:

Clear imaging of below-knee and foot arteries is essential to plan distal reconstructions. Contrast-enhanced tomographic ultrasound (CEtUS) is novel and entirely safe with no exposure to ionising radiation or nephrotoxic contrast. We compared below knee CEtUS with angiography.

Materials and methods:

In the same week as CT, MR or catheter angiography, CEtUS was performed using intravenous 1.5mL bolus injections of Sonovue with a maximum of 5mL administered/patient. CEtUS was reported by a Vascular Scientist blinded to the angiograms which were reported by a Consultant Radiologist and the results compared using a modified Society of Vascular Surgery (SVS) run-off score.

Results:

One-hundred and eighteen patients have been recruited where 19 were excluded from analysis. The remaining 99 patients were split into two groups. 72 had crural imaging and 27 had pedal imaging representing 360 and 54 imaged arteries respectively. Weighted quadratic Kappa and ICC values for intra- and inter-observer agreement were excellent (k/ICC=0.80 to 0.97) and had narrow confidence intervals indicating precision, for both groups. When comparing all types of angiography and CEtUS, weighted quadratic Kappa and ICC agreement was moderate with acceptable confidence intervals in both groups ([Crural k=0.57, ICC=0.52], [Pedal k/ICC=0.59). Agreement decreased from Popliteal to pedal vessels as diameter decreased (k=0.81 to 0.42).

Conclusions:

CEtUS is a novel imaging modality with strong observer agreement that achieves clear peripheral and foot images without ionising radiation exposure or nephrotoxic X-ray contrast media. CEtUS enhances visualisation of run-off vessels which may play a role in planning of limb salvage.

Key Words: Tomographic 3D ultrasound, tUS, Peripheral arterial disease.

Introduction:

In severe cases of Peripheral arterial disease (PAD) catheter-based revascularisation using angioplasty plus/minus stenting, or arterial bypass surgery may be required to improve quality of life and avoid limb loss. Downstream stenosis, to anastomosis location, is a proven significant predictor of angioplasty or graft failure [183], therefore confirmation of distal vessel patency is of high importance to the specialist. Accurate run-off imaging is therefore vitally important in this treatment decision.

Initial clinical assessment is often by standard duplex which has a sensitivity and specificity of nearly 80% for PAD, with a positive predictive value of 88% and negative predictive value of 66.7% [179], making duplex the ideal cost-effective and safe tool for primary PAD screening and initial treatment planning [180]. Despite this, duplex only has moderate accuracy at diagnosing crural artery disease [181] and currently has limited utility in the assessment of pedal, arch and digital arteries.

Due to the crural and pedal limitation of duplex, vascular specialists rely on alternative angiographic imaging to help determine the appropriate treatment. Both Computed Tomographic (CTa) and Catheter-directed digital subtraction (DSA), angiography utilise high doses of radiation and the nephrotoxic contrast media damage is known to be cumulative. We also now know that patients with chronic kidney disease who develop contrast-induced acute kidney injury when being imaged for PAD are significantly associated with poor outcome [278]. The debate around Gadolinium-based contrast agents and brain deposits, utilised for Magnetic Resonance (MRa) angiography is another need for safer alternative. CTa and MRa also give limited information for run-off vessels particularly when high levels of calcium are present. The sensitivity of these imaging modalities coupled with the 3D information they can present, often makes them an essential tool for the vascular specialist.

The use of Contrast-Enhanced Ultrasound (CEUS) for below knee arterial imaging has previously been documented [186, 187, 279]. Yet, despite the acknowledged superiority of CEUS over duplex and the documented inferiority of duplex at assessing the crural arteries, there is limited report of its use within the literature and widespread clinical use has never succeeded. This may represent its lack of 3D information and inadequacy in its ability to aid surgical planning. Vascular specialists would probably rely on alternative angiography to answer these questions. We utilised a novel type of tomographic 3D ultrasound with microbubble contrast (CEtUS) to evaluate its role for imaging crural and pedal artery disease in comparison to the index tests of CTa, MRa or Catheter angiography (DSA) that were completed the same week.

Materials & methods:

Patients diagnosed with PAD following a duplex ultrasound scan from a single tertiary vascular referral centre between 2016 and 2018 being referred for a diagnostic angiogram (either CTa, MRa or DSA) by a Consultant Vascular Surgeon were recruited. Ineligible patients were those with pacemakers or internal cardiac defibrillators due to the electromagnetic tracking system used by CEtUS, plus allergies to any form of contrast media. Patients attended the vascular laboratory the same week as their clinical angiogram where a contrast-enhanced tomographic 3D ultrasound (CEtUS) scan was performed by an experienced Vascular Scientist blinded to the angiogram.

The tomographic 3D ultrasound (tUS) system (PIUR imaging, Vienna, Austria) was connected to a Mindray Resona 7 (Mindray Inc, Shenzhen, China) high end ultrasound system with tUS tracking sensors attached to a L9-3 transducer. A peripherally inserted venous cannula was utilised to administer ultrasound contrast (Sonovue, Bracco, Italy) in 1.2 mL bolus followed by a 5 mL 0.9% saline chase. Each contrast bolus administration allowed multiple scans of each arterial segment. For all scans to be completed it took approximately 20 minutes. Patients were recruited to two groups due to the limit on contrast volume needed to scan all vessels. Group one for crural assessment and group two for pedal. The ultrasound probe was moved over the Anterior Tibial, Dorsalis pedis or Primary pedal arch (Plantar arch) when the patient was laid supine. The patient is then turned prone so the distal Popliteal, Tibio-Peroneal trunk, Posterior Tibial and Peroneal arteries could be imaged.

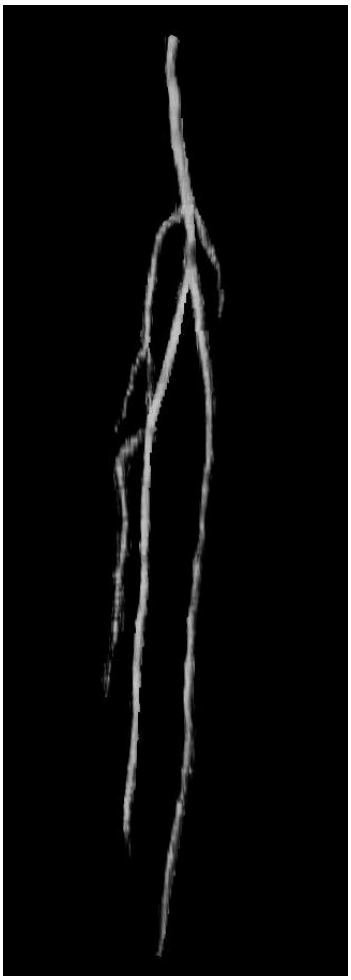

(Figure 38. A CEtUS arteriogram image of the below knee vessels)

The CEtUS scans were then processed using the specific PIUR imaging software that allowed the soft tissue to be cropped out of the image leaving what is described as an arteriogram like image (fig. 38) in under 5 minutes. A vascular scientist would then identify the presence of any stenosis or occlusions and using a validated Society of Vascular Surgery (SVS) run off score (tab. 13) [280] which was modified for Kappa analysis. The SVS score allows categorisation of disease severity were an effectively widely patent vessel (<20% greatest stenosis) scores one, mild stenosis (20-49%) is scored two, moderate to severe stenosis (50-99%) scores three, an occlusion half the vessel length a four and occlusion a five. Two blinded Vascular Scientists performed inter-observer assessment of CEtUS. A minimum of four weeks was maintained between repeat CEtUS analysis for intra-observer variability. Once the clinical angiograms (CTa, MRa or DSA) were completed they were reported by a Consultant Vascular Radiologist blinded to the CEtUS scan. Subsequently the SVS run off scores for the angiograms were recorded for comparison to the CEtUS scans assuming angiography to be the gold standard.

Table 13. Modified Society of Vascular Surgery run off score.

	<20% greatest stenosis	20 - 49% greatest stenosis	50 – 99% greatest stenosis	Occluded less than half vessel length	100% occluded
Score	1	2	3	4	5

Statistical analysis

Weighted quadratic Kappa statistic was used to assess the agreement between imaging methods in addition to inter/intra observer agreement. Intra-Class Correlation (ICC) estimates and their respective 95% confidence (95%CI) intervals were calculated based on a single-measurement, absolute agreement, 2 way mixed-effects model. SPSS statistical package version 22 was used (SPSS Inc, Chicago, IL, USA).

Results:

To date 118 patients have been recruited. Of the 118, a total of 19 had to be excluded from analysis. Undiagnostic images were obtained from 14 patients, 4 were unable to be cannulated and 1 patient withdrew consent prior to being scanned. This left 99 remaining patients split into 72 in the crural group and 27 in the pedal group representing 360 and 54 imaged arteries respectively. In group 1, CEtUS was compared with 18 Catheter, 35 MR and 19 CT angiograms. CEtUS was compared with 4 CT and 23 catheter angiograms in group 2. All angiograms were requested clinically due to severe limiting claudication or critical limb ischemia for surgical planning.

Table 14. Mean modified Society of Vascular Surgery run off scores for each artery.

Artery	CEtUS	Angiography
Popliteal	2.10±1.42	1.90±1.40
Tibio-peroneal trunk	1.81±1.31	1.56±1.21
Anterior tibial	2.32±1.36	2.00±1.36
Posterior tibial	2.86±1.45	2.44±1.64
Peroneal	2.63±1.49	2.11±1.52
Plantar Arch	1.19±1.34	1.43±1.54
Dorsalis pedis	1.38±1.50	1.66±1.72

The mean (+/- standard deviation) modified SVS scores for CEtUS and all types of angiography, are demonstrated by artery in table 14. Weighted quadratic Kappa and ICC values for intra- and inter-observer agreement were excellent and had narrow confidence intervals indicating precision, for both groups (Tab 15. and 16, Fig. 39). When comparing all types of angiography and CEtUS, weighted quadratic Kappa and ICC agreement was moderate with acceptable confidence intervals in both groups (tab. 15 and 16, Fig 40). Kappa and ICC agreement was assessed for each artery type individually which decreased consistently from the Popliteal to pedal vessels (tab. 17).

Table 15. CEtUS crural artery agreement with angiography

	Weighted Quadratic Kappa	Std Error	95% CI		P Value	ICC	95% CI	
			Lower	Upper			Lower	Upper
Intra-observer	0.94	0.02	0.91	0.97	<0.0001	0.94	0.93	0.95
Inter-Observer	0.88	0.02	0.85	0.92	<0.0001	0.88	0.86	0.90
CEtUS vs Angio	0.57	0.05	0.48	0.66	<0.0001	0.59	0.52	0.65

Table 16. CEtUS Pedal artery agreement with angiography

	Weighted Quadratic Kappa	Std Error	95% CI		P Value	ICC	95% CI	
			Lower	Upper			Lower	Upper
Intra-observer	0.97	0.01	0.95	1.0	<0.0001	0.97	0.96	0.99
Inter-Observer	0.80	0.07	0.66	0.94	<0.0001	0.80	0.68	0.88
CEtUS vs Angio	0.59	0.11	0.38	0.80	<0.0001	0.59	0.38	0.74

Table 17. CEtUS agreement with angiography per vessel type

	Weighted Quadratic Kappa	Std Error	95% CI		P Value	ICC	95% CI	
			Lower	Upper			Lower	Upper
PoP A	0.81	0.07	0.68	0.95	<0.0001	0.82	0.73	0.88
TPT	0.54	0.13	0.29	0.79	<0.0001	0.55	0.36	0.69
ATA	0.52	0.11	0.32	0.73	<0.0001	0.54	0.35	0.68
PTA	0.49	0.10	0.29	0.69	<0.0001	0.51	0.31	0.66
PeR A	0.42	0.11	0.21	0.64	<0.0001	0.45	0.24	0.62
DP	0.67	0.15	0.38	0.96	<0.0001	0.67	0.40	0.84
Plantar Arch	0.47	0.17	0.15	0.80	<0.012	0.48	0.13	0.72

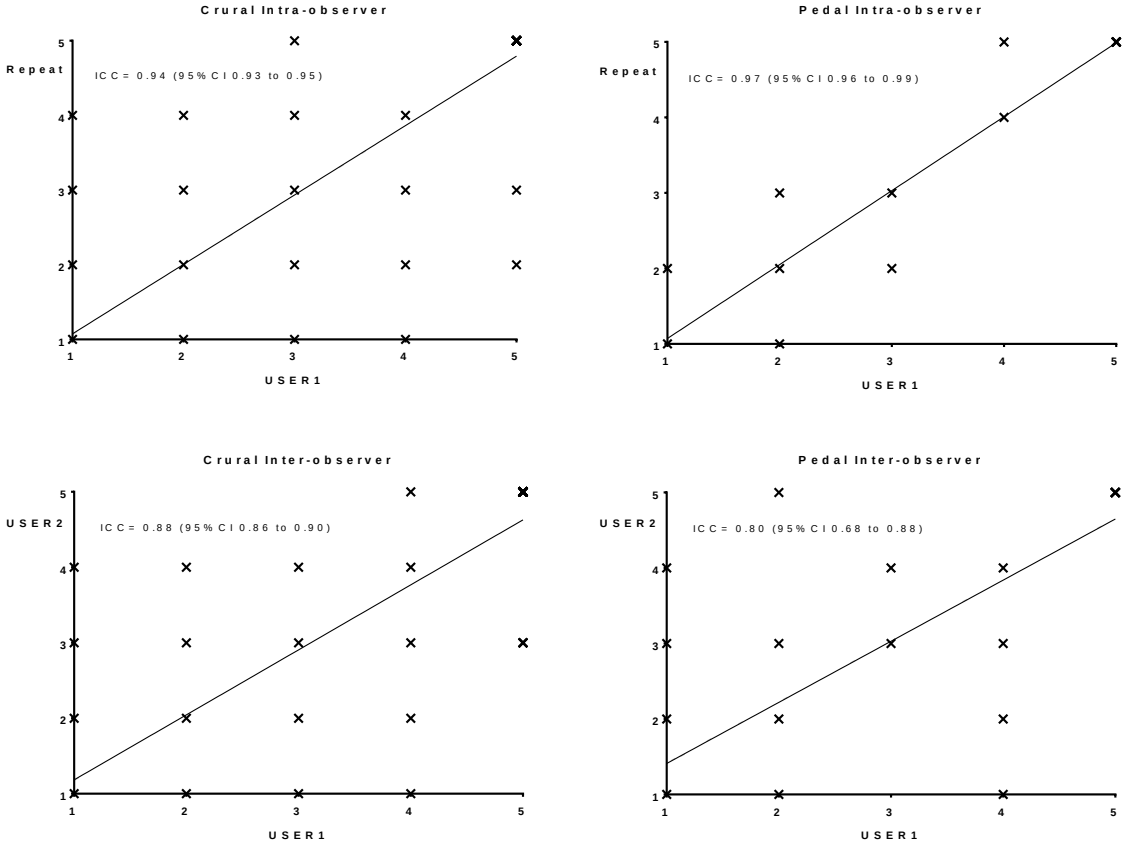

(Figure 39. Intra- and inter-observer ICC agreement for CEtUS in both groups)

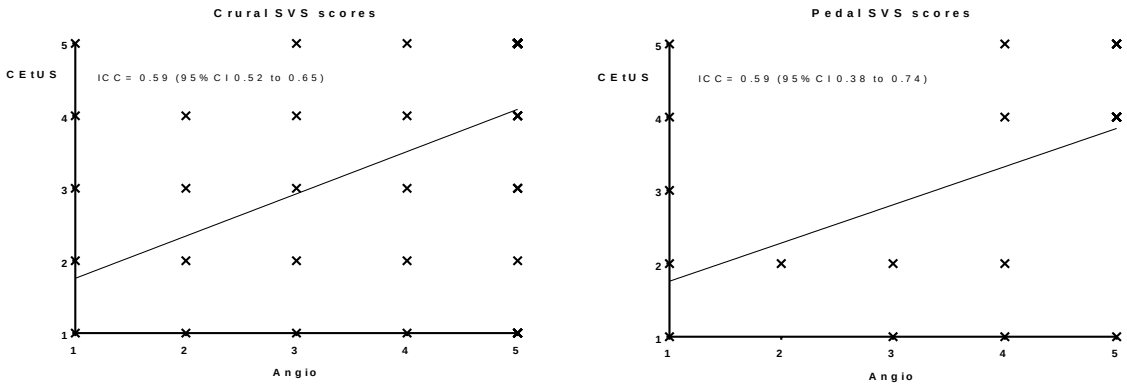

(Figure 40. ICC agreement for CEtUS versus angiography in both groups)

In group 1 there were 53 instances where CEtUS reported severe arterial stenosis or occlusion not demonstrated on angiography (fig. 41). Conversely there were 21 different instances where angiography demonstrated severe stenosis or occlusion but CEtUS did not. In group 2 there were 7 instances where CEtUS reported severe arterial stenosis or occlusion not demonstrated on angiography (fig. 42). Conversely there was 6 different instances where angiography demonstrated severe stenosis or occlusion not reported by CEtUS.

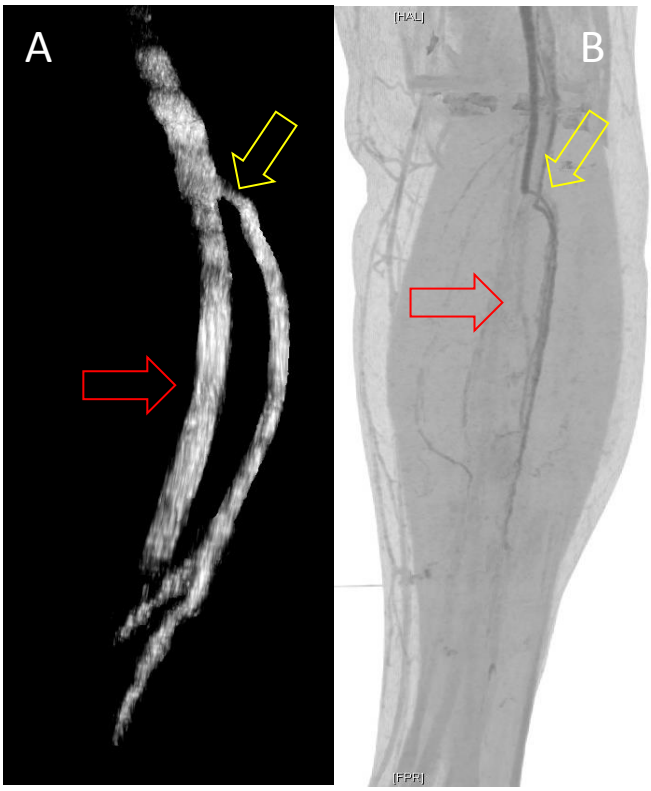

(Figure 41. Panel A. CEtUS scan that demonstrates a patent tibio-peroneal trunk [red arrow] and a stenosed anterior tibial artery origin [yellow arrow]. Panel B. The corresponding MR angiogram that demonstrates an occluded tibio-peroneal trunk [red arrow] and a widely patent anterior tibial artery origin [yellow arrow]).

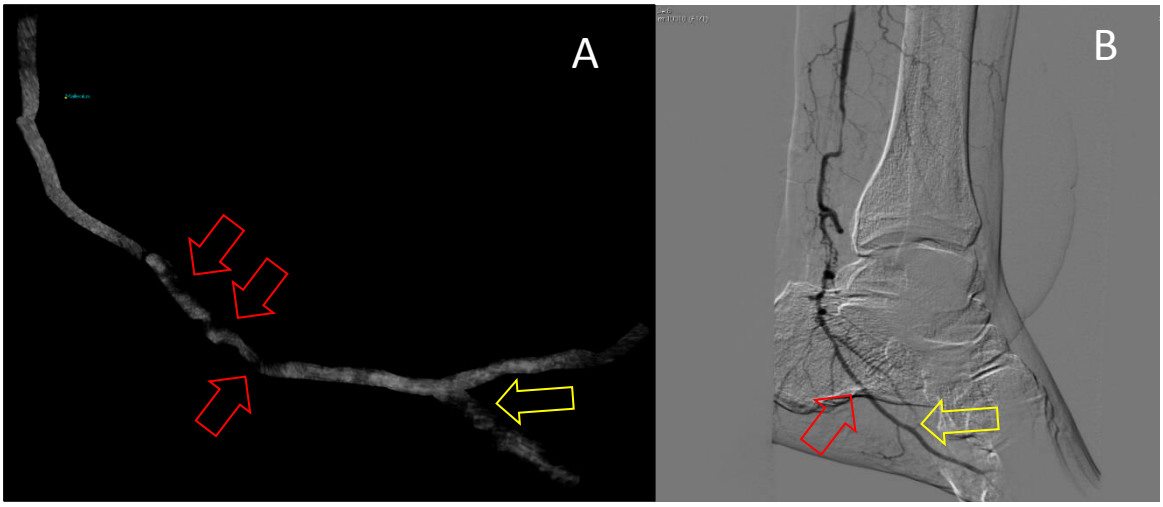

(Figure 42. Panel A. A CEtUS pedal image that demonstrates arch stenoses [red arrows]. Panel B. The comparison digital subtraction angiogram that demonstrates a completely patent vessel at the same location [red arrow]. The yellow arrow demonstrates the level of the same collateral for orientation)

Discussion:

Our study is the first to investigate the accuracy of CEtUS at the detection of clinically significant stenoses and occlusions of run-off vessels in comparison to the gold standard imaging technologies, as a real-world example. Our aim was not to repeat the standard duplex assessment. Duplex has good diagnostic accuracy within the femero-popliteal segment but has a moderate limitation for isolated calf disease and currently little utility in foot arterial imaging. Our aim was to utilise contrast and 3D technology to improve on a known weakness of duplex. The role of contrast-enhanced ultrasound for the investigation of peripheral arterial disease is highly advantageous and we report no ill-effects from its use in our study. We report that CEtUS is highly reproducible with a significant degree of precision as seen through narrow confidence intervals of observer agreement. We also report that the comparison to index tests has moderate agreement but note some discrepancies between both CEtUS and angiography.

This study is limited by its size and a larger sample is required, particularly for group 2, which is actively recruiting. Even with CEtUS, the Peroneal and most of the Posterior tibial arteries are deep in the calf and difficult to visualise which is reflected in the lower agreement seen in these vessels. Calcification is a known limitation for ultrasound and its impact in this study does account for some discrepancies seen between angiography and CEtUS.

Mestre et al (2015) have previously reported a change in surgical plan that was based on CT or MR angiography by 53% when CEUS was used, with agreement to surgical findings rising by 8.1% to 95.2% with ultrasound contrast [187]. Eiberg et al (2003) have also previously reported a reduction by 70% of inconclusive arterial duplex scans when using ultrasound contrast [279]. The Coffi et al [186], Mestre et al [187] and Eiberg et al [279] works report discrepancies between index imaging and contrast ultrasound similar to our findings but report only moderate agreement (ƙ 0.45 – 0.50). Although they have small numbers, we identified similar outcomes using 3D ultrasound, however our agreement was slightly better at ƙ = 0.57 and 0.59. This may, be a reflection of 3D visualisation of the disease. The Coffi and Eiberg works utilised infusion administration of contrast agents to give prolonged enhancement time so that the CEUS scan could be performed, as bolus injections have a very short half-life (<5mins). Our work differs from this as we utilised 1.2mL bolus injections which give bright enhancement of flow. This was possible because CEtUS scans of a single artery can be completed in under 30 seconds. This may account for the higher Kappa agreement we identified.

With angiography, in addition to simple factors such as venous contamination and patient movement, there are a few reasons that could explain disagreement. Firstly, fluoroscopy is uniplanar and out of plane disease is a known limitation. Additionally, all angiography types struggle with slow flow due to blood dilution of contrast resulting in a low concentration for detection, where the risk is increased with extensive collateralisation. This can be misregistered as occlusion on imaging. Modern CT and MR scans are also performed via a bolus chase method. In cases of femoral occlusion (important in below knee imaging), the bolus will take collateral routes and therefore travel down the limb slower than predicted. Therefore, it is possible that below knee vessels are imaged out of phase with the contrast bolus thus lowering the sensitivity to disease. The advantage of CEtUS is in its operator dependence. Effectively CEtUS is a bolus chase method under the control of the Vascular Scientist who only scans once a bright contrast filled vessel is identified. This control avoids the limitations seen with MR and CT.

Another limitation is blurring artefact which is a phenomenon relevant to any imaging modality [281-283]. As the voxel/pixels are of a fixed size the impact of blurring is greater for smaller vessels as a larger proportion of the disease/lumen is affected. Sometimes known as penumbra on X-ray, blurring of the images means that rather than a crisp, sharp image of a single target, a blurred representation is made. This partially explains why CT is poor at small vessel disease as precise measurement of stenosis is difficult to visualise. This may account for the disagreement between CEtUS and CT/MR angiography stenosis measures as one modality could have more or less blurring of a stenosis than the other, meaning a different percentage is established, and therefore a potentially different SVS score, reducing the Kappa agreement. This phenomenon may also explain the decreasing agreement seen with vessel size with CEtUS.

Our study is also limited by the use of three different index tests. We compared CEtUS to three different types of angiography, each with their own advantages and limitations. Our sample size was insufficient to differentiate differences between imaging modalities and the combined assessment should be interpreted with caution. The majority of image comparisons were against MR angiography in group 1. It is widely accepted that catheter angiography is more sensitive than MR or CT for crural vessel disease and a higher number of catheter angiograms for comparison may improve our agreement. However, we have shown that CEtUS has good agreement with strong observer correlation which may mean it could ultimately be used for peripheral angiography.

3D ultrasound assessment of the peripheral vasculature for PAD has been understudied. Invasive intra-Vascular Ultrasound (IVUS) and expensive disposable catheter probes have been trialled in pre-op assessment where clinical traction is unlikely; this type of work may represent the future of treatment based 3D IVUS angioplasty [189]. A Washington (USA) based group have used 3D ultrasound for the assessment of bypass graft stenosis and remodelling, demonstrating clear imaging of severe stenosis with post stenotic dilation [191]. Given that standard duplex is more than adequate at diagnosing above knee arterial disease there is probably little clinical utility except, for targeted assessment when duplex is inconclusive, similar to the works by Coffi, Eiberg and Mestre. Studies that use CEUS to measure skeletal calf muscle perfusion, as a direct measure of PAD, do not use CEUS in the direct assessment of macrovascular crural artery patency [184, 185]. As this gives no information to the vascular specialist for planning intervention and that the body is adept at collateralisation, muscle perfusion is unlikely to yield any clinical benefit other than perhaps assisting the interventionalist in angiosome theory.

We have shown adequate agreement for the detection of significant disease with excellent observer agreement in addition to identifying potential disease not seen with current gold standard imaging. More importantly greater confidence in the duplex result can be achieved and if used clinically could drastically reduce radiation and nephrotoxic contrast exposure. Future work could focus on using CEtUS to aid interventions or address other ultrasound limitations such as aorto-iliac disease to facilitate clinical adoption and to replace angiography completely. In its current format CEtUS could be used clinically to target specific lesions for detailed velocity shift detection.

Conclusion:

Contrast-Enhanced Tomographic 3D ultrasound (CEtUS) is a novel imaging modality with strong observer agreement that achieves clear peripheral and foot images without exposing patients to ionising radiation or nephrotoxic X-ray contrast media. CEtUS is quick, safe and easily interpreted and enhances visualisation of run-off vessels which may play a role in the planning of limb salvage with further research. Wider adoption of ultrasound-contrast agents is needed to improve limb salvage imaging.

Acknowledgments: We thank Dr Julie Morris, Mr. Phillip Foden and Dr John Belcher for their invaluable advice as Departmental Statisticians.

Chapter 9 - Tomographic 3D ultrasound compared with standard duplex for imaging potential autologous bypass grafts.

Chapter contributions and role:

Division of Cardiovascular Sciences

S. Rogers: conception, study design, DUS and tUS scanning, data collection, statistical analysis and manuscript writing.

A. Phair: patient recruitment, data collection and critical review.

C. Olech: patient recruitment and data collection.

Mr J. Ghosh MD: Co-Supervisor and critical review

Prof C. McCollum: Supervisor and critical review

Independent Vascular Services Ltd

J. Carreira: DUS and tUS scanning.

Funding: This project has received funding from the European Union's Horizon 2020 research and innovation programme under grant agreement No [760380].

Abstract

Objectives:

Vein mapping using duplex ultrasound (DUS) is helpful in selecting optimal autologous bypass grafts, but is time-consuming and operator-dependent. Tomographic 3D Ultrasound (tUS) is a free-hand, high resolution, electromagnetically tracked 3D ultrasound system which uses a frame-grab technique. The aim of this study was to compare tUS with DUS for conduit mapping for coronary artery and lower limb arterial bypass.

Methods:

DUS and tUS scans performed on the morning of bypass surgery were compared. Time taken to acquire each scan was recorded. Operating surgeons post-operatively scored the agreement for each imaging modality with their score of the graft harvested. A score of 5 was complete agreement, with scores of 4 counting as good.

Results:

199 potential grafts in 110 patients were imaged. DUS scanning took a mean (+/-sd) of 9:46±5:44mins compared with 0:56 ±0:30mins for tUS, $p<0.0001$. DUS reporting took a mean of 11:32±10:00mins compared with 17:32±11:21mins for tUS, $p=0.0487$. Most surgeons agreed that tUS reconstructions of potential autologous conduits compared more highly with the intra-operative findings (58 versus 49), helped better with decisions (59 versus 52) and was more valuable to the decision on which vessel to harvest (56 versus 47) than DUS. On balance Surgeon's felt tUS scans would be useful and could replace DUS.

Conclusions:

Surgeons preferred to see the potential autologous graft tUS images themselves over conventional DUS. tUS scans were significantly quicker than DUS and requires less operator skill.

Key Words: Tomographic 3D ultrasound, tUS, conduit mapping.

Introduction:

Coronary artery bypass grafting (CABG) for coronary heart disease is necessary when there is significant and profound cardiac ischemia to restore adequate blood supply to the myocardium. Peripheral arterial disease (PAD) is a risk factor for coronary artery disease and affects 20% of the over sixties, with symptoms ranging from intermittent claudication through to critical limb ischaemia (5 – 10% of cases) [177]. PAD can result in disabling claudication or critical limb ischaemia which may require bypass surgery to improve quality of life or avoid limb loss.

Routine saphenous vein Duplex ultrasound (DUS) mapping is essential prior to bypass surgery has shown strong correlation to surgical measurements [284] and has been shown to clearly demonstrate abnormalities [285] which include areas of varicosity [195], making veins unsuitable for harvest as a conduit. DUS has also been proven to reduce the length of incision, time of incision, length of hospital stay [286, 287] and cost. Pre-operative DUS assessment of conduit vessels is accurate and beneficial to both surgeon and patient, particularly at identifying the best conduit for surgery. The very nature of DUS being a dynamic assessment means that ultrasound operators build a 3D mental impression of the vessel and vascular pathology [27]. This process is highly operator dependent [26] meaning scan quality is variable from hospital to hospital and is prone to error. As a result, a high level of trust must exist between vascular technician/scientist and surgeon, at identifying the optimum vessel.

Tomographic 3D Ultrasound (tUS) is a free-hand, high resolution, electromagnetically tracked 3D ultrasound system which uses a frame-grab technique. Each DUS image is resolutionally optimised on the DUS scanner for the area of anatomical interest. The transducer with tracking sensors attached is then swept over the vein and the image is acquired by the tUS computer, but this is not real time. tUS can reduce operator dependence and improve scan quality as the vessel is reconstructed into a 3D volume that can be manipulated to view the vessel from all angles. Galeandro et al have previously reported that Physicians with little vascular knowledge better understand vein mapping when demonstrated in a 3D report [201]. Operator dependence of tUS is minimal and quality is improved as it is possible to produce good quality 3D images with minimal training. The trust, therefore, between surgeon and operator is highly improved by tUS as they can visualise the optimal vessel for themselves.

We compared tUS and DUS vein mapping to the operating Surgeon's agreement of the harvested vein using a scoring system in patients undergoing CABG or peripheral bypass.

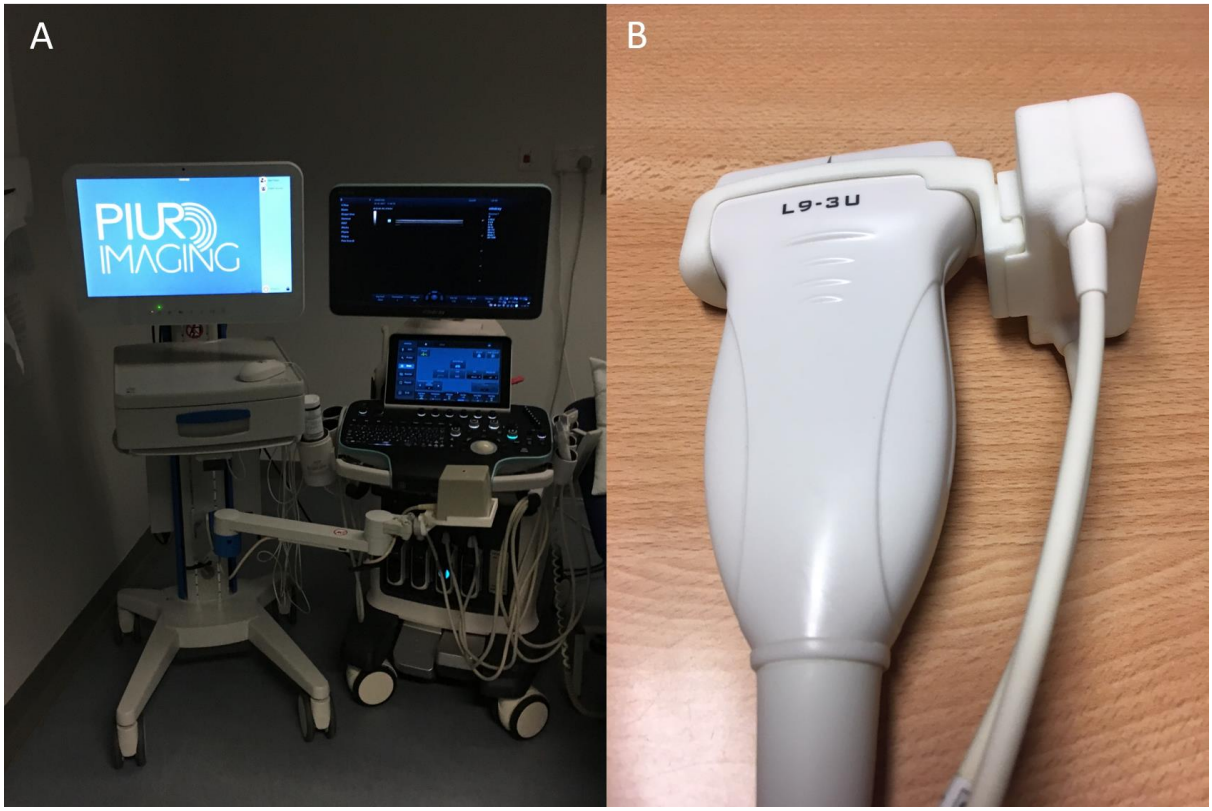

(Figure 43. Panel A. Set up of the Piur tUS with electromagnetic tracker next to Resona 7 DUS instrument. Panel B. A Resona 7 9-3MHz transducer with PIUR tUS tracking sensors attached to the probe)

Materials & methods:

Patients were recruited from a single tertiary centre following National Research Ethics Committee (REC) [approval no. 16/NW/0153] approval since November 2016. Patients provided informed written consent prior to undergoing either autologous peripheral, or coronary artery bypass. Patients with pacemakers and internal cardiac defibrillators were excluded due to risks associated with tUS electromagnetic tracking in addition to those who were unstable and unable to attend the vascular laboratory for scanning. Patients unable to stand for the scan were also excluded. Patient height, weight and blood pressure was recorded prior to scans.

Pre-operatively patients attended the vascular laboratory for standard duplex vein mapping which was performed by a vascular scientist using a high definition Resona 7 scanner (Mindray Inc, Shenzhen, China). In the same sitting a tomographic 3D ultrasound vein mapping was performed using PIUR tUS (Piur Imaging GmbH, Vienna, Austria) (Fig.43). Patients were scanned in an erect position. Bilateral Long Saphenous Veins (LSV), including Sapheno-femoral junction, were imaged from the groin to the ankle. Bilateral Short Saphenous Veins (SSV), including Sapheno-popliteal junction, were imaged from the vein of Giacomini, if present, to the ankle. As we did not know what procedure patients were having or the length of vessel required, we scanned bilateral LSV and SSV on each patient.

Time to perform both mappings was recorded. Time to report the duplex and analyse the tUS images was also recorded. Pre-operatively surgeons were only shown the standard duplex report, in line with standard clinical care, as not to influence decision on which conduit to harvest at the request of the REC.

Post-operatively, the Surgical Care Practitioners (SCP) or Surgeon who had harvested the conduit were then shown the standard duplex report again, followed by the tUS images (Fig. 43). Subsequently they were asked a series of questions (Tab. 1&2) and asked to grade their answers out of 5 using a simple scoring system we created. Scores of 4 or 5 were considered good or excellent agreement. Scores of 3 were considered moderate agreement and scores of 1 or 2, poor agreement. For the first three questions the SCP's or surgeons were asked to provide scores for each modality independently. For the following three questions they were asked to compare either each modality to one another or tUS to the conduit used. Moderate agreement (score of 3) was considered when DUS was equal to tUS and good or excellent (score of 4 or 5) agreement wen tUS was considered to have been better than DUS.

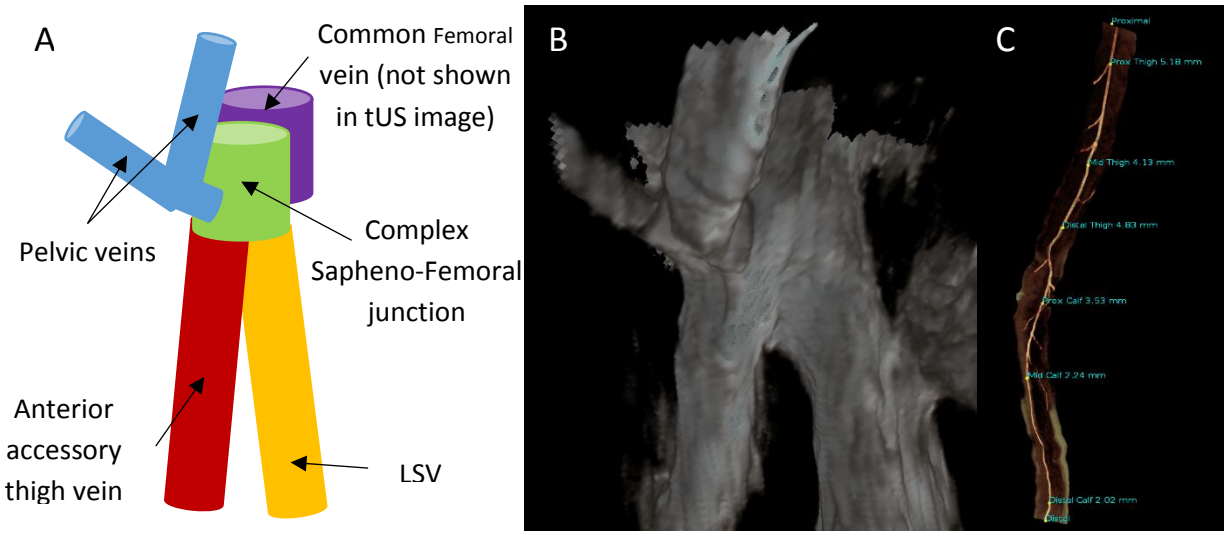

(Figure 44. Panel A: A Diagram of Panel B. Panel B: A tUS image of a complex Sapheno-femoral junction with pelvic, anterior accessory thigh and long saphenous branches. Panel C. A tUS image of the Long Saphenous vein with branches and perforators from groin to ankle)

Statistical analysis

Our sample number is in line with other pilot studies of this nature and represents only interim analysis of a larger data set yet to be recruited. As this was questionnaire data, only descriptive statistics have been applied. Scores of 4 or 5 represent good or excellent responses. Mean and standard deviations were used to assess scan and reporting times where a *p* value less than 0.05 was considered significant. Statistical analysis was performed using GraphPad prism v7 (GraphPad software inc., La Jolla, CA, USA).

Results:

To date one-hundred-and-ten patients have been recruited with ninety patients having undergone surgery. Surgical responses were not available for analysis from twenty patients. Of the twenty, two questionnaires were incorrectly completed by the SCPs, two had corrupted tUS scans due to metallic interference, two had pacemakers and could not be scanned, and fourteen had their surgery cancelled or moved to another institution meaning data could not be collected. The remaining 90 patients were statistically analysed mean height and weight was 168.2±20.7 cm and 82.8±20.5 Kg respectively. Mean blood pressure was 129/75 mmHg. A total of 199 potential autologous conduits were imaged (86 right LSV, 86 left LSV, 8 right SSV, 8 left SSV, 5 right Radial artery and 5 left radial arteries) in the 90 patients.

As DUS mapping is part of standard care prior to being listed for surgery, some patients had their DUS scan prior to being identified by the research team. Following the exposure rules within research of As-Low-As-Reasonably-Achievable (ALARA), the DUS scan was not repeated. There were 44 patients where the scan and reporting time was recorded for both DUS and tUS which were available for comparison. Mean (±sd) DUS scan time was 9:46±5:44 min compared with 0:56±0:30 min for tUS, $p<0.0001$ (Fig. 45). Mean (±sd) DUS analysis time was 11:32±10:00 min compared with 17:32±11:21 min for tUS, $p=0.0487$ (Fig. 46).

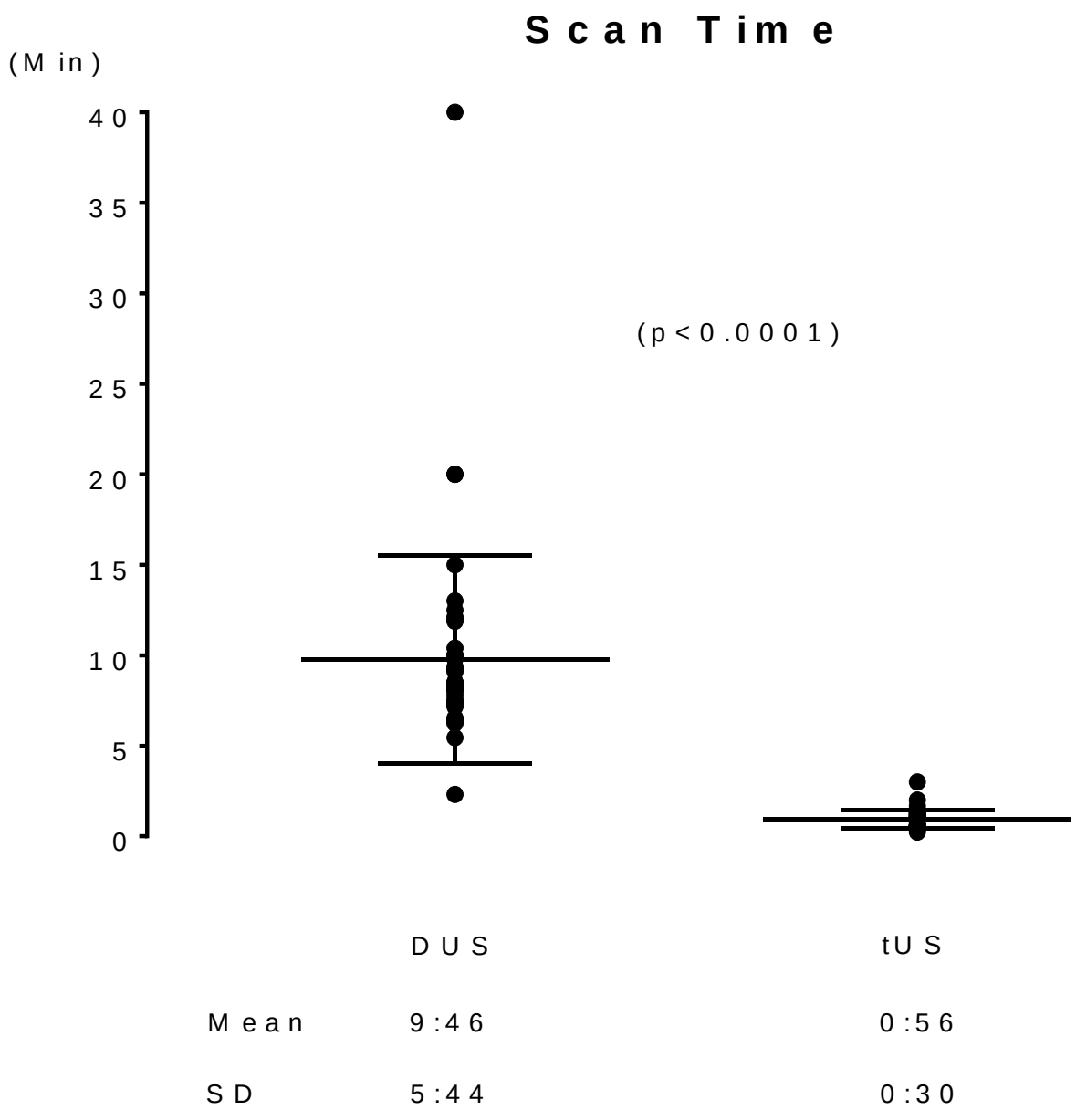

(Figure 45. Paired DUS and tUS scan times per vein)

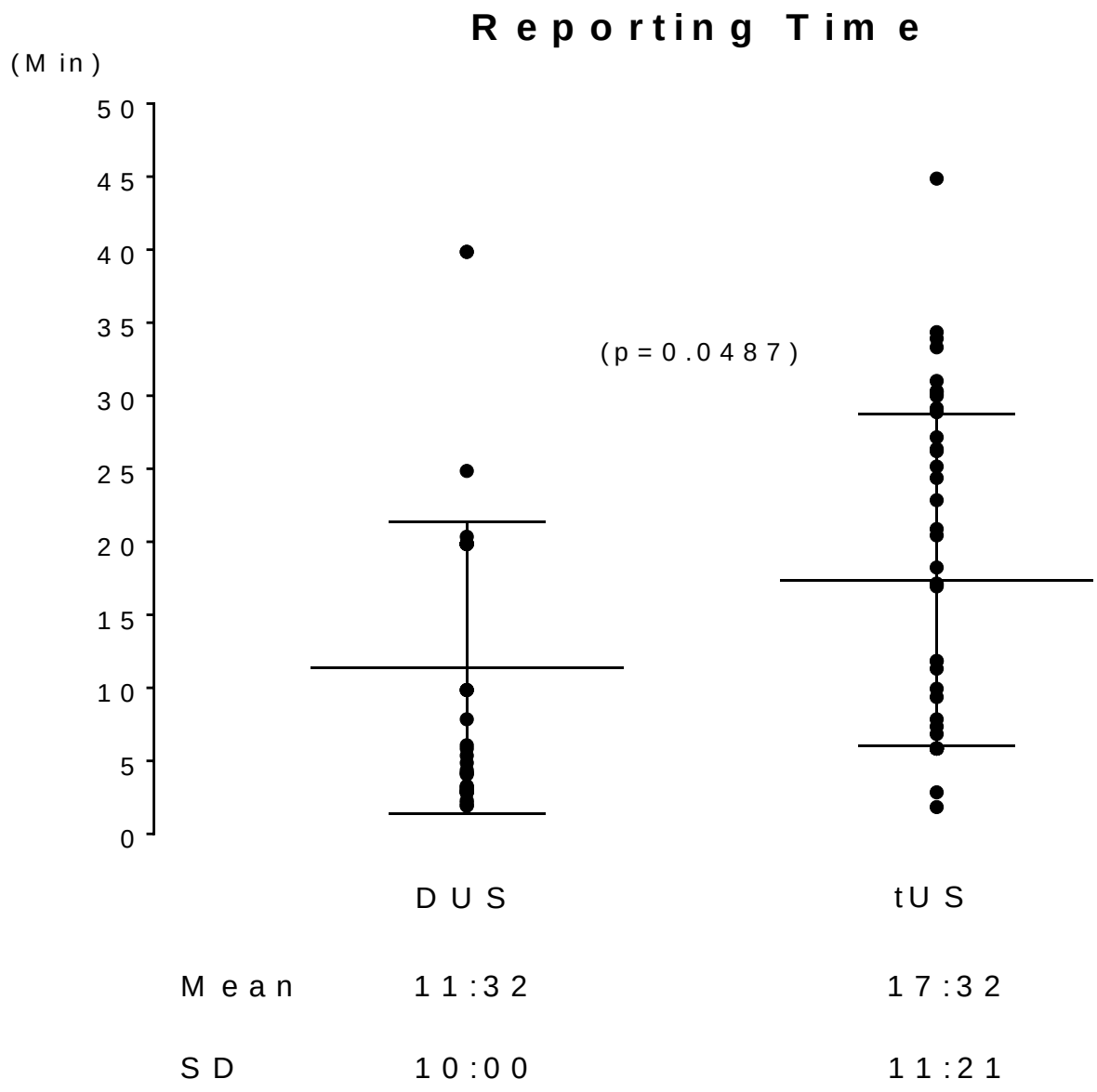

(Figure 46. Paired DUS and tUS reporting times per vein.)

Intra-operative findings of the 90 harvested autologous conduits were then compared to the DUS and tUS scans of the respective vessels. When asked how valuable each imaging modalities (DUS vs tUS) were on deciding which vessel to harvest to use for the bypass, SCP's or Surgeons rated tUS a 4 or a 5 in 59 instances compared to 52 for DUS. There were 10 instances where SCP's or Surgeon's found DUS to be more valuable compared to 17 for tUS.

When asked if the imaging modalities added anything to help their decision on which vessel to harvest SCP's or Surgeons rated tUS a 4 or 5 in 56 instances compared to 47 for DUS. There were 15 instances where SCP's or Surgeon's found the tUS images added more to help their decision compared to 6 for DUS.

When asked about the agreement of each imaging modality (DUS and tUS) with intra-operative findings; SCP's or Surgeon's rated tUS a 4 or 5 in 58 patients compared with 49 for DUS. There were 11 occasions where SCP's or Surgeon's thought DUS was more valuable compared with 20 occasions where SCP's or Surgeon's rated tUS as more valuable.

On 37 occasions SCP's or Surgeon's completely agreed that when compared to DUS that tUS would have changed their decision on which vessel to use. However, 40 disagreed which would have reflected no change in surgical plan. When asked if tUS could replace DUS altogether, in 59 out of 90 (66%) instances SCP's or Surgeon's completely agreed. When asked about intra-operative findings SCP's and Surgeon's felt that tUS could replace DUS for conduit mapping on 56 occasions.

Table 18. Scores for each question by imaging modality.

	Score					
	1&2 (poor)		3 (moderate)		4&5 (good)	
Question	**DUS**	**tUS**	**DUS**	**tUS**	**DUS**	**tUS**
Independently, how valuable was the modality mapping in your decision on which vessel to use for the bypass?	11 (12.2%)	16 (17.8%)	27 (30.0%)	15 (16.7%)	52 (57.8%)	59 (65.6%)
Independently, did the modality mapping add anything to help your decision?	17 (18.9%)	17 (18.9%)	26 (28.9%)	17 (18.9%)	47 (52.2%)	56 (62.2%)
How well did the modality mapping agree with intra-operative findings?	14 (15.6%)	12 (13.3%)	27 (30.0%)	20 (22.2%)	49 (54.4%)	58 (64.4%)

Table 19. Scores demonstrating value of tUS.

	Score		
Question	**1&2 (poor)**	**3 (moderate)**	**4&5 (good)**
Compared to DUS mapping would tUS have changed your decision on which vessel to use?	40 (44.4%)	13 (14.4%)	37 (41.1%)
Could tUS replace DUS mapping?	18 (20.0%)	13 (14.4%)	59 (65.6%)
Compared to intra-operative surgical findings could tUS replace DUS mapping?	15 (16.7%)	19 (21.1%)	56 (62.2%)

Discussion:

We have shown that the 3D tUS reconstructions of potential autologous conduits agreed more highly with the intra-operative findings, helped better with decisions and added more to the decision on which vessel to harvest than DUS. On balance SCP's and Surgeon's felt tUS scans would be useful and could replace DUS. Additionally, the tUS scans are significantly faster than DUS which represents a substantial time saving for the health service.

This study is limited but is significant. A larger population is needed before clinical adoption but we continue to recruit. Importantly this study also lacked significant numbers of radial arteries which will be part of our ongoing research. Our surgeons rarely harvest the radial artery for use as a conduit but tUS would be very useful in this assessment. Another limitation is questionnaire bias. The communication barrier between our researchers and the SCP's has been minimised by our study design. We have avoided technical terms in our questions and have a scale that allows differentiation of response [288]. However, the level of understanding of ultrasound by the SCP's may impact in their responses. This is unavoidable but all SCP's use DUS mapping routinely and have had some training on interpreting tUS images to minimise this bias as much as possible. An independent score for DUS, tUS and the harvested conduit on the suitability of the vessel as an autologous bypass graft could have been beneficial in clarifying the best assessment method but would introduce bias in future comparisons as this is missing for currently recruited patients.

In addition to bias we identified limitations and advantages with the ultrasound set up. Utilising the imaging from DUS instruments for tUS imaging means tUS does not need specialist 3D transducers and takes advantage of the best image resolution achievable, compared with commercially available matrix/4D ultrasound transducers. However, by being reliant on the DUS image to compile the tUS reconstruction, tUS by its very nature is therefore limited by the resolution of the DUS transducers. This could mean that branches smaller than the resolution limit, sub 1mm, of the DUS scanner are not identified in tUS accounting for some discrepancy in the number of branches detected. It is however, generally accepted that standard DUS transducers could have better resolution than specific 3D transducers meaning we have the most optimal setup achievable. Additionally, the portability of our 3D method is an accepted disadvantage but by being coupled to the DUS instrument it would be challenging to perform the tUS scan in small anaesthetic rooms prior to surgery as both the DUS instrument and tUS would need to be taken to theatre. Picture-Archiving-and-Communication System (PACS) connectivity of tUS is essential for clinical adoption as it allows the Surgeon to plan the operation or see the scan during the harvest. Until further advances in technology are available this has to be an accepted limitation.

Our data corroborates the previously published works that show DUS can accurately identify problematic segments of vein and influence surgical decision in addition to reducing complications and costs [195, 285-287, 289, 290]. Despite these advantages of DUS we know that being able to identify the optimal bypass graft in 3D is more readable than a written DUS report prone to misinterpretation [201]. We are aware of no previous publications on the use of 3D ultrasound technology for mapping the peripheral venous anatomy. However there are reports of the use of Computed X-Ray Tomography (CT) without contrast for conduit assessment prior to CABG [291], but more worryingly with the use of nephrotoxic contrast for varicose vein surgical planning [292]. The use of radiation and nephrotoxic contrast to produce a 3D reconstruction for conduit assessment cannot be advocated. tUS is significantly cheaper than CT but more importantly it allows surgeons to visualize the optimal conduit for themselves in 3D, avoiding sonographer misinterpretation and improving sonographer/surgeon trust.

The increased reporting time of tUS compared to DUS is a reflection of the manual process by which the tUS reconstructions are prepared. Large numbers of branches and perforator vessels increase the time it takes to complete. Although the tUS device has an automated function, improvements are still needed.

From a scanning perspective and ignoring reporting times, there are potential significant capacity savings from using tUS over DUS. Assuming that a minimum of two veins (bilateral LSV) must be scanned for conduit selection we found a mean difference in scan time between DUS and tUS of 8:50 minutes meaning a potential of 8:50 minutes per patient could have been saved for our sample number (n=90). This represents a total potential of 795 minutes could have been saved if tUS was utilised instead of DUS. The UK National Health Services (NHS) reimbursement tariff assumes vascular ultrasound scans take 20 minutes to complete [293]. By utilising tUS instead of DUS in our population we could have saved the equivalent of nearly 40 scans representing a potential increased capacity for the NHS. If the analysis could be performed automatically by artificial intelligence then addition time savings could be made further improving NHS efficiency. There is a recognised need for the redesign of ultrasound scanning protocols to limit occupational repetitive strain injury (RSI) for vascular sonographers [220]. Shorter scan times through the use of tUS is one method of combating this RSI; less time in uncomfortable scanning positions reduces risk.

We have focused on conduit mapping for autologous bypass but have encountered varicose veins during out assessment. We have identified future research in using tUS for scanning varicose veins to plan radio-frequency ablation in addition to other types of vessel mapping for planning surgery such as for arterio-venous fistula creation. tUS may play a role in endoscopic vessel harvest surgical planning as the surgeon can see where to make incisions in addition to identifying what segments of vessel could be bridged. This will improve the technical success and shorten harvest times. Additional research should focus on the discrepancy in outcomes we found between SCP scores comparing tUS to DUS on whether tUS would have changed the surgical plan, where 44% said no change but 41% said there would have been a change. Finally, an ergonomics study should be performed comparing tUS to DUS to provide further evidence of the benefit of tUS for vascular scientists/sonographers to limit RSI. Our current study continues to recruit a larger population to provide greater evidence to facilitate better clinical adoption.

Conclusion:

tUS allows the operating surgeon to visualise potential autologous grafts to be used for bypass for themselves. Conduits can be viewed from any angle removing the risk of misinterpretation by the vascular sonographer and improving surgeon-sonographer trust. tUS scans were significantly quicker than DUS and requires less operator skill but without automated preparation using artificial intelligence of tUS images there is no time saving on image/report production. Nevertheless, tUS could play a role in avoidance of unnecessary incisions and the associated complications while reducing RSI.

Acknowledgments: We thank Dr Julie Morris and Mr. Phillip Foden for their invaluable advice as departmental statisticians. We also thank Bhuvana Bibbleraaj, Pascaline Njoki, Nehru Devan, Janesh Ivair and Rick Air for their assistance with providing surgical data.

Chapter 10 - Arterio-Venous Fistula surveillance using tomographic 3D ultrasound

Chapter contributions and role:

Division of Cardiovascular Sciences

S Rogers: conception, study design, ethics, obtaining funding, establishing collaboration, tUS training, data collection, statistical analysis and manuscript writing.

A. Haque: ethics and critical review

Prof C. McCollum: supervisor and critical review

Independent Vascular Services Ltd

K. Simm: tUS scanning and analysis.

S. Kiyegga: secondary tUS analysis

Wirral University Teaching Hospital NHS Foundation Trust

Dr S. Lea: fistulogram analysis.

R. Chandrasekar: conception, study design and critical review

Funding: This project has received funding from the European Union's Horizon 2020 research and innovation programme under grant agreement No [760380].

Abstract

Background

A well-functioning Arterio-Venous Fistula (AVF) is essential for haemodialysis. Despite regular Duplex Ultrasound (DUS) a significant number of AVF's fail. Tomographic 3D ultrasound (tUS) creates a 3D image of the AVF that can be interpreted by the Clinician. We compared DUS, tUS and fistulograms for the identification and estimation of flow-limiting stenosis.

Methods

Patients with suspected AVF dysfunction at routine Transonic® surveillance meeting certain criteria underwent DUS [1) >15% reduction in access flows on two consecutive occasions, 2) >30% reduction in access flow on one occasion, 3) access flow of <600ml, 4) presence of recirculation]. On the day of fistulography, DUS was repeated, in addition to tUS imaging of the fistula including the stenosis. Delayed tUS measurements were performed by a Vascular Scientist blinded to the fistulography result, reported by one Consultant Radiologist. Maximum diameter reduction at any stenosis was measured using all 3 techniques.

Results

In 40 patients with 32 stenoses mean (sd) stenosis was measured as 61.9(±16.6)%, 66.9(±9.51)% and 67.1(±11.9)% for the fistulograms, tUS and DUS respectively. tUS observer agreement was excellent [intra ICC=0.94 (95%CI 0.86-0.97) and inter ICC=0.87 (95%CI 0.72-0.94), $p<0.0001$]. Bland-Altman agreement for tUS was -5.1(±17.9)% (95%CI -40.2-30.1) compared with -5.2(±17.3)% (95%CI -39.1-28.6) for DUS with the fistulogram as the index standard. Mean (sd) tUS scan time was 3.7(±2.2)min compared to 9.9(±3.7)min for duplex, $p<0.0001$.

Conclusion

DUS and tUS were equally accurate at detecting complications compared to fistulography. tUS has excellent observer agreement, takes less skill and is significantly quicker than DUS in detecting stenoses in an AVF.

Key Words: Tomographic 3D ultrasound, tUS, surveillance, AVF, Arterio-Venous Fistula

Introduction:

Chronic kidney disease (CKD) is diagnosed when the glomerular filtration rate decreases below <60mL/min/1.73 m^2 [202] and costs between £1.44 and £1.45 billion annually, equating to 1.3% of the annual UK NHS budget [294]. Two percent of patients with CKD will progress to kidney failure and more than half of the total cost of CKD is spent on renal replacement therapy each year [294]. Dialysis is still the foremost method for renal replacement therapy and around 5000 patients commenced haemodialysis in 2016, a 14% increase from 2011 [204].

A well-functioning Arterio-Venous Fistula (AVF) is essential for haemodialysis whilst patients wait for renal transplant, but haemodialysis is costly (>£35,000/patient/year) [209]. This cost can vary depending on location (hospital versus community) with the highest costs relating to nursing staff and consumables [209].

Turbulence in blood flow leading to high shear stress is thought to lead to intimal damage, and thereby leading to flow-limiting stenoses or aneurysmal changes in an AVF. When undetected and untreated, these stenoses lead to thrombosis of the AVF, a lifeline for the patient. Thromboses of AVF is the largest cause of morbidity in patients on haemodialysis [210]. Angioplasty is recommended when diameter reduction is greater than 50% [211], to prevent thrombosis. Despite regular DUS surveillance to detect issues before they cause thrombosis, up to 50% of AVFs will fail within one year [24, 212, 213].

DUS is cheap, safe and allows assessment of flow dynamics which a fistulogram can not. [210]. Clinicians often cannot visualise the anatomy/pathology from duplex scans like skilled ultrasound operators who are able to build a mental impression within their minds, which we know is also prone to misdiagnosis [27, 29, 31]. In the absence of this skill, Clinicians have to rely on written reports and poor 2D ultrasound images to make the decision for intervention. A high degree of trust therefore, exists between the Vascular Scientist/Sonographer and the Clinician due to the operator-dependence of DUS. Equally importantly, we are currently amidst a national shortage of skilled ultrasound operators, which compounds increased service demand. This contributes to Sonographer-related repetitive strain injury from which as much as 83% of the workforce suffers [220-222]. New technologies could potentially improve these occupational issues whilst continuing routine AVF surveillance.

Tomographic 3D ultrasound (tUS) is a high resolution, tracked free-hand, 3D ultrasound system, which works by frame-grabbing the images from a standard duplex ultrasound system. The standard ultrasound transducer has sensors attached to track its position, which is then swept over the vessel, where an entire length of vessel can be scanned in seconds. The ultrasound images are acquired by the tUS computer, tagged with the tracking information and reconstructed into a near real time 3D image. The software has the ability to generate a reconstructed volume of the AVF within seconds, which can be manipulated into any orientation to allow better visualisation and therefore, diameter reduction measurement.

We compared DUS and tUS against fistulography for the identification and estimation of flow-limiting stenosis (Fig. 47) reporting our interim results. We timed duplex and tUS scanning as a measure of practicality.

(Figure 47. AVF stenosis in a single patient by imaging modality. Panel A = Duplex ultrasound image of a right cephalic vein stenosis (62%). Panel B = tUS image of a bifid right cephalic vein with a stenosis within one vessel (61.7%). Panel C = Fistulogram image of the same bifid right cephalic vein with a stenosis within one of the vessels (52%). Red arrow indicates the same point within each image. Yellow arrow indicates the bifid non-stenosed cephalic vein. Units = percentage stenosis)

Materials & methods:

Patients in whom AVF dysfunction was suspected on clinical grounds, or at routine surveillance using Transonic® that met one of four criteria, 1) >15% reduction in access flows on two consecutive occasions, 2) >30% reduction in access flow on one occasion, 3) access flow of <600 ml, 4) presence of recirculation, underwent duplex scanning. If a flow-limiting stenoses was detected, arrangements were made for a fistuloplasty. Prior to fistuloplasty, a repeat duplex scan and tomographic 3D ultrasound (PIUR imaging GmbH, Vienna, Austria) was carried out. This was performed using a 9MHz transducer and a standard duplex ultrasound scanner (Affinity 5g, Philips UK Ltd, Guildford, UK) connected to the tUS device. tUS scans were performed in transverse section using B-mode ultrasound settings. Separate tUS scans were performed on the inflow vessel, outflow vessel and anastomosis. The time to perform the duplex and tUS scans was recorded.

A diagnostic fistulogram was performed to identify the lesion/s, prior to fistuloplasty. This was carried out using Axiom Artis fluoroscopy set (Siemens healthineers, Frimley, UK), with images acquired at 3 frames per second. Contrast was hand injected via either a 6F sheath side arm or through 4F catheters using Visipaque 270 (GE healthcare, Chalfont St Giles, UK) diluted 50% with 0.9% saline. The fistulogram was used as the index comparator test for duplex and tUS where diameter reduction was retrospectively measured in batches by a Consultant Interventional Radiologist blinded to the duplex and tUS measurement.

A minimum of two months was left between the tUS scan and the analysis/measurement of the diameter reductions to reduce bias. The primary measurement was performed by an experienced Vascular Scientist blinded to the results of DUS and fistulogaphy. Repeat analysis was performed by a second blinded Vascular Scientist. All patients provided informed written consent and the study protocol was approved by the National Research Ethics committee (18/LO/0100).

Statistical Analysis:

Descriptive statistics (median and standard deviations) were used for patient demographics and diameter reduction per imaging modality. Intra- and inter-observer agreement was assessed using inter-class correlation (ICC). ICC estimates and their respective 95% confidence (95%CI) intervals were calculated based on a single-measurement, absolute agreement, 2 way mixed-effects model. A *p* value less than 0.05 was considered significant. Bland-Altman agreement was used to establish measurement bias for each modality using fistulography as the index test. Inter-class correlation was calculated using SPSS statistics v22 (IBM Corp., Armonk, NY, USA). Descriptive statistics, Bland-Altman agreement and all graphs were created using GraphPad Prism v7 (GraphPad software inc., La Jolla, CA, USA).

Results:

This study is a part of a larger project funded by the European Commission on the value of tomographic ultrasound in diagnosing vascular disease. We report our interim results with regarding to imaging of stenoses in AVF, where we continue to recruit. From the first forty patients, nine were removed from analysis. Of the nine, two patients did not have any diameter reductions on any imaging modality (fisultography was still requested due to suspected dysfunction of fistula, and to rule out central vein stenosis), there were 5 technical failures of tUS or fistulogram (no pre-plasty image saved), one axillary vein not scanned (deviation of protocol) and one AVF occluded between ultrasound imaging and fistulography. Of the remaining thirty-one patients, there were thirty-two stenoses (one patient had two diameter reductions) available for comparison.

Six of the initial forty AVF's were in the right arm and two had previously been revised. Fifteen were brachio-basilic transpositions, sixteen were radio-cephalic and nine were brachio-cephalic AVFs. The mean (±sd) time between duplex/tUS scans and fistulogram was 21.9(±17.9) days. Mean (±sd) percentage diameter reduction (fig. 48) was reported at 61.9(±16.6)%, 66.9(±9.51)% and 67.1(±11.9)% for the fistulograms, tUS and duplex respectively, $p=0.1959$ (no significant difference).

Intra and Inter-observer agreement (fig. 49) for tUS was excellent for percentage stenosis with ICC values of 0.94 (95%CI 0.86-0.97) and 0.87 (95%CI 0.72-0.94) respectively, $p<0.001$. DUS and tUS agree closely with the fistulogram for the severity of stenosis. With the fistulogram as the index test, Bland-Altman agreement (fig. 50) for tUS was -5.1(±17.9)% (LOA -40.2-30.1) compared with -5.2(±17.3)% (LOA -39.1-28.6) for DUS. Mean (±sd) tUS scan time (fig. 51) was 3.7(±2.2) min compared to 9.9(±3.7) min for duplex, $p<0.001$ (significantly different).

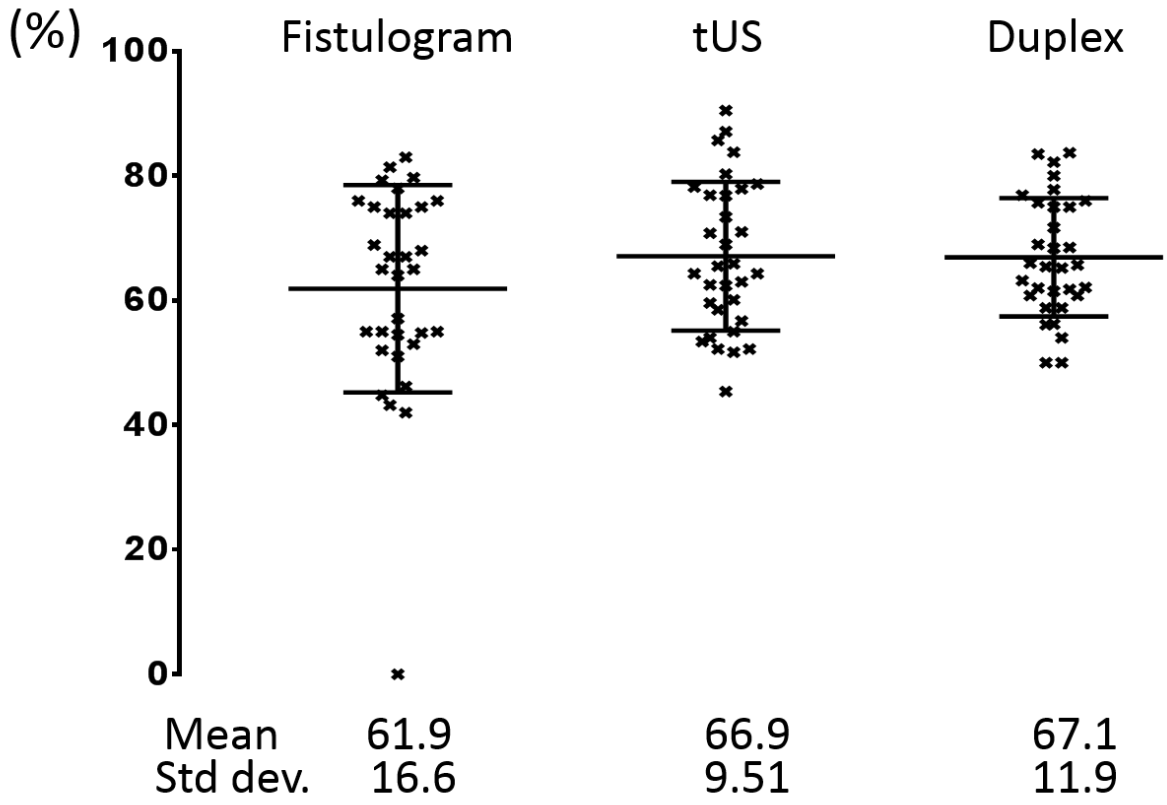

(Figure 48. Mean percentage stenosis by imaging modality. Units = percentage stenosis)

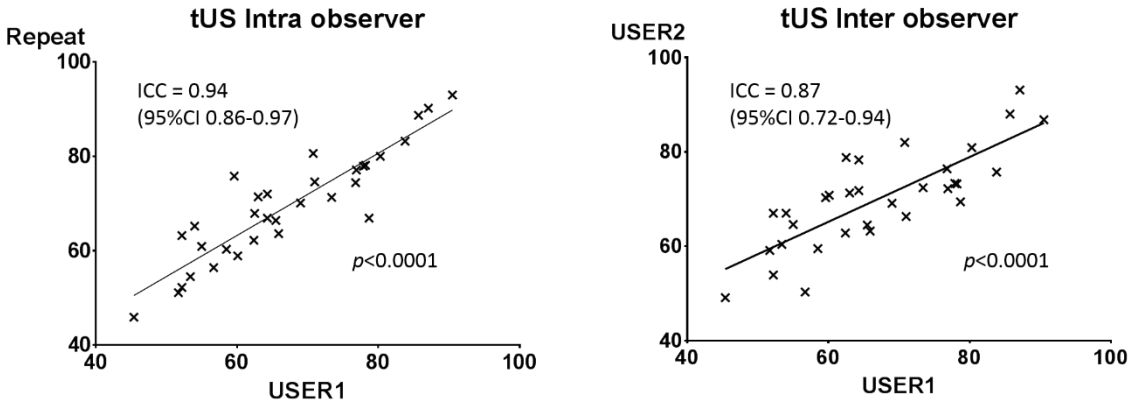

(Figure 49. Intra and Inter observer agreement for tUS. Units = percentage stenosis)

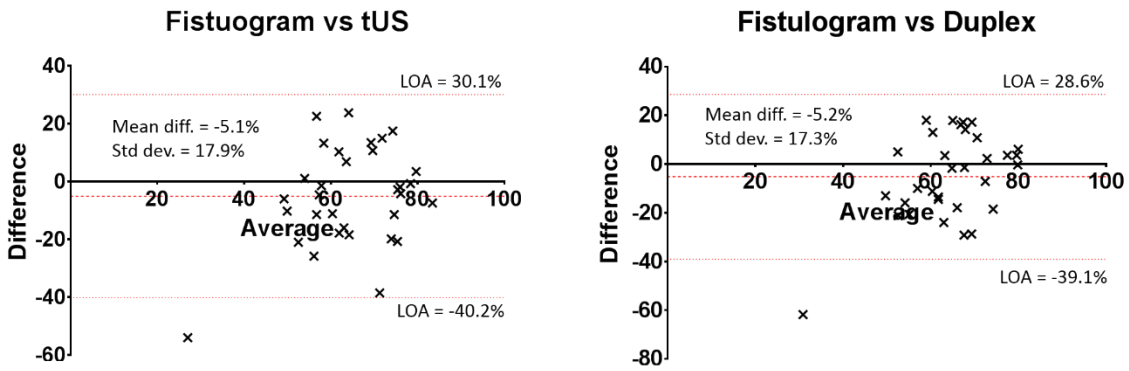

(Figure 50. Bland-Altman agreement for tUS and DUS compared to Fistulography as the index test. Units = percentage stenosis)

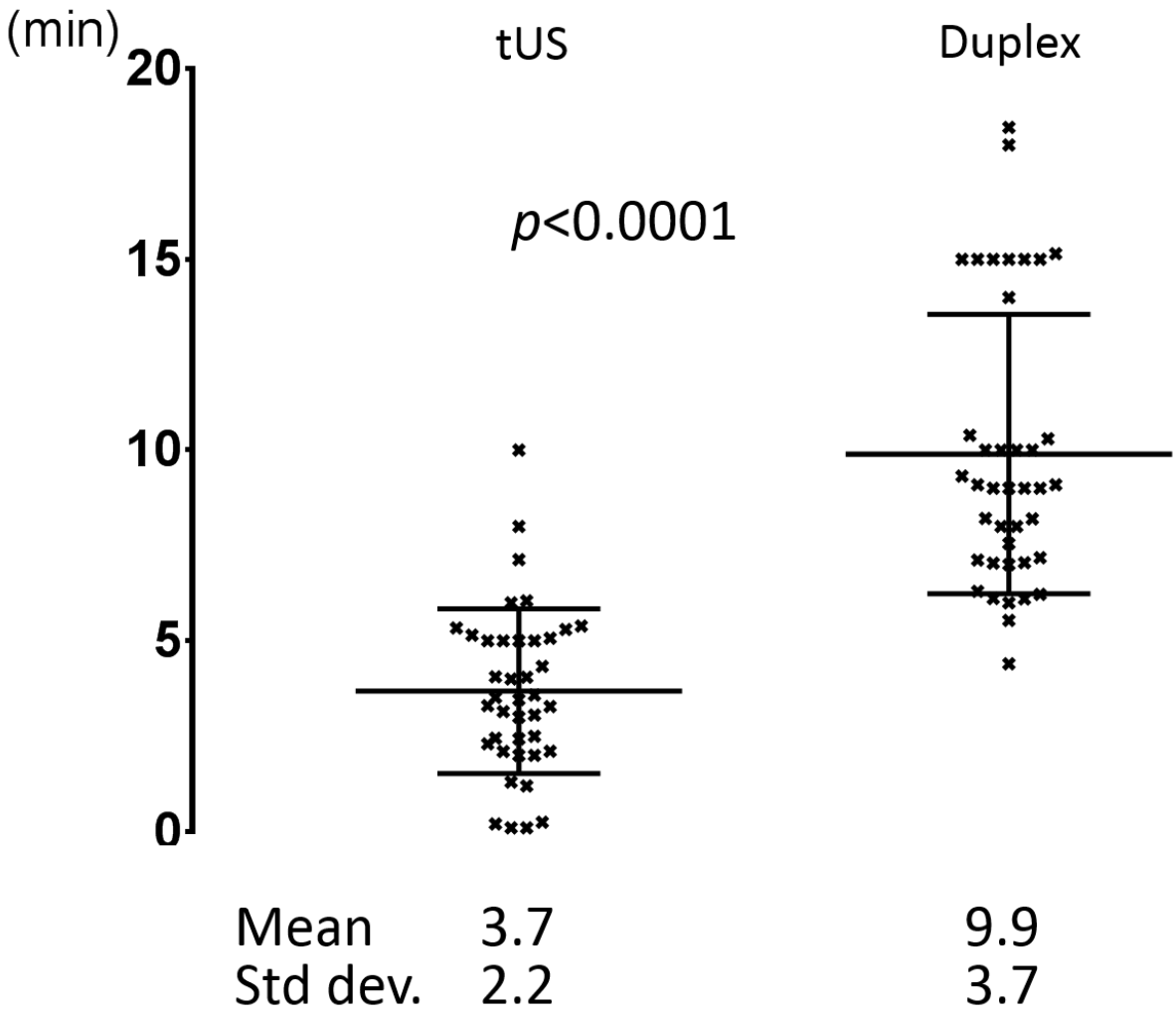

(Figure 51. Mean scan time for tUS and DUS by one Vascular Scientist. Units = minutes)

Discussion:

This pilot study reports no meaningful difference between tUS and DUS when compared to fistulography, potentially outlining a use for tUS to replace duplex for routine surveillance of AVF, but greater patient numbers are needed. The relatively less skill and also the shorter time required to assess the AVF by tUS, in comparison to the standard DUS, has added benefits for both the patient and the workforce representing a potential increased scanning capacity and decreased RSI risk.

This study is a part of a larger project which requires two-hundred participants, meaning this current work is small. Despite this, we suggest a non-inferiority of tUS compared to both the current accepted standard used in routine practice daily (DUS) and the index test of fistulography, but a larger data set is needed. Larger sample numbers may present further data to support our findings.

The nine patients that were removed from analysis represents a flaw in our methodology, where two patients recruited had no diameter reductions for comparison and one AVF had occluded between scans. In all three instances, tUS could still have been performed and resulted in the same clinical conclusion. The four instances of tUS technical failure all occurred within the first 20 recruited patients suggesting this was related to early adoption of the technique.

The nature of AVF disease being aneurysmal, plus the requirement to scan in one fixed plane (transverse section) for tUS acquisition made ultrasound scanning challenging. A significantly larger sample number will demonstrate the true failure rate to reach adequate diagnosis. Although tUS is compatible with most ultrasound systems commercially available and utilises software specifically generated for Vascular Surgery, it remains limited by the same constraints as standard DUS. Aneurysmal disease, causing poor transducer skin contact and acoustic shadowing, as a result of calcification, remain a challenge for tUS techniques. These will impact the failure rate of tUS in any sample population.

One of the contributing factors to Sonographer-related RSI was total time scanning and the leaning/twisting of the sonographer position while scanning [221]. Implementing methods that reduce risk and improve workforce occupational health has previously been recommended [220, 222]. Due to the speed and lower operator skill required for tUS, it may be possible for scans to be performed in dialysis centres by users with minimal training to improve patient quality of life, but also improve departmental capacity of the Vascular Laboratory through fewer or faster scans. The added bonus is that this will reduce sonographer related RSI as faster scans mean shorter exposure to occupational risk of RSI and reduce further hospital visits for dialysis patients.

Based on a potential saving of 6.2 mins/patient, a total time saving in this cohort could have been 248 mins if tUS was used for surveillance instead of DUS. Using the current UK reimbursement tariff that assumes a DUS takes 20 minutes on average, we estimate that an additional 12 patients could have been scanned [293] . Fundamentally, tUS could improve departmental capacity, reduce RSI and shorten waiting lists.

Although we know DUS has a role in predicting maturation of AVF [295], perhaps tUS also opens new methods of interpretation that may further improve outcomes. Traditionally, DUS could be used to detect changes in volume flow within an AVF [25]. Advances in dialysis equipment now mean that this volume flow can easily be detected during dialysis, avoiding the need for patients to travel to the Vascular Laboratory for additional testing [296]. Although we know that changes in Doppler volume flow (cm/s) are predictive of AVF failure [25], tUS presents us with new ways to sensitively measure changes within the AVF. By being 3D, tUS opens up the possibility of AVF volume (cm^3) measurements. Further assessment via randomised control trials should be used to assess the role of tUS like those performed with traditional DUS to further outline its role vascular access creation [25]. Future work should focus on AVF volumes and their correlation with maturation rates and future complications as they represent potential early warning. It is clear that volume is sensitive to small changes, but a threshold needs establishing.

Endovascular created AVF's have recently been shown to be a viable alternative to surgically created AFV and have reduced post-operative costs at 12 months [297, 298]. Pre-operative vasculature mapping for this treatment decision (endo vs surgical) is essential. Future work should explore the role of tUS in the form of a randomised control trial to truly assess its utility for surgical planning.

Conclusion:

DUS and tUS were equally accurate at detecting complications compared to fistulography in our interim analysis. Tomographic 3D ultrasound has excellent intra and inter-observer agreement and requires less skill to perform. tUS is significantly quicker than standard duplex at detecting potential problems in an AVF, representing an improved capacity and reduced repetitive strain risk. Our results suggest that tUS may replace all other imaging modalities for AVF surveillance but further work is needed.

Acknowledgments: We thank Mr. Phillip Foden for his invaluable help in providing statistical advice.

Section 4 – Overall Discussion

Chapter 11 – Thesis discussion

This thesis addresses the application of tUS for the investigation of vascular disease. The literature on vascular disease relevant to ultrasound imaging and current gold standard modalities has been reviewed, which highlighted the research questions outlined. My aim was to establish whether tUS is the most accurate investigation for each indication based on diagnostic accuracy, utility, reproducibility and intra-/inter-observer agreement while demonstrating the potential value of tUS in vascular surgery. My secondary aim was to determine if tUS is the definitive investigation for vascular disease. Two broad uses have emerged from my research. tUS can be used with and without microbubble contrast and the implications of each are crucially important to implementation into daily use.

Non-contrast tUS imaging

Artery geometry and anatomical mapping/surveillance appear to be clinically acceptable features my work has presented. tUS can readily be utilised to accurately measure artery geometry; namely, length, diameter and volume. Due to capacity and availability, my thesis has shown that tUS should be the imaging modality of choice when a measure of artery geometry is required, where the data presented corroborates those of similar published works using other types of 3D US. Given the likely sensitivity of volumes to small changes, tUS may be the most suitable method for assessing CVD event risk. Small differences can assess changes in CVD risk that could be monitored either over time as an assessment of progression or in response to early aggressive medical therapy. Next steps would be for studies assessing arterial change which could be of particular interest to the pharmaceutical industry. Additional work could also be performed on a pulsatile model to assess impact of arterial motion.

When compared to CTa, we have shown that there is greater variability in diameter measurements for patients who have had EVAR than those pre-treatment, and that AP diameters remain the most accurate method of assessment. According to key studies, our results appear to be relatable to those previously reported [35, 80, 262]. tUS diameter measurements may be clinically acceptable for those patients in AAA or EVAR surveillance with complex geometry. Further work should be conducted into AAA volume over time.

My thesis presents work on vessel mapping for bypass and AVF surveillance which has never been reported within the literature. The data corroborates the previously published works that show DUS can accurately identify problematic segments of vein and influence surgical decision in addition to reducing complications and costs [195, 285-287, 289, 290]. The relatively less skill and also the shorter time required to assess the potential conduits or AVF by tUS, in comparison to the standard DUS, has added benefits for both the patient and the workforce representing a potential increased scanning capacity and decreased RSI risk.

Contrast-enhanced tUS imaging

The limitation of tUS for haemodynamic information is a potential confounding factor for its widespread adoption, similarly to other types of angiography. Like other types of angiography tUS can be used with contrast agents to demonstrate haemodynamic significance via filling voids or aberrant flow. My thesis outlines the importance of contrast imaging for complex arterial assessment. Greater adoption of contrast agents by the Vascular Scientist community are now essential for the utilisation of tUS.

Our work demonstrated CEtUS and CEUS were non-inferior to rotational angiography at detecting endoleak, particularly type II. Although our work lacked clinically significant (type I or III) endoleaks, the patient safety benefits of CEtUS may mean it is superior to rotational angiography in certain circumstances. Our current study reported a good renal artery detection rate of CEtUS, with only 33% of renal vessels not identified, which is a significant improvement on the previously reported 50% renal artery identification rate by 3D CEUS [90].

My thesis was the first to investigate the accuracy of CEtUS at the detection of clinically significant stenoses and occlusions of run-off vessels in comparison to the gold standard imaging technologies. Our aim was not to repeat the standard duplex assessment. The role of CEtUS for the investigation of PAD is highly advantageous and we report no ill-effects from its use in our study. Our report that CEtUS is highly reproducible with a significant degree of precision for popliteal-pedal imaging, as seen through narrow confidence intervals of observer agreement is important. The moderate agreement with the index test adds validity to our technique especially given the discrepancies between both CEtUS and angiography. As specialists can see the PAD for themselves with CEtUS, greater confidence in the duplex result is achieved and if used clinically could drastically reduce radiation and nephrotoxic contrast exposure possibly playing a role in planning of limb salvage.

The work presented in this thesis presents a strategy to avoid radiation and nephrotoxic contrast agents essential for those patients with limited renal function or allergy. CEtUS has now become part of our clinical strategy when CO_2 is used for EVAR stent-graft deployment but this result could clearly be extrapolated to other interventional circumstances, e.g. lower limb stenting, with further work. In its current format, CEtUS should be used to target specific lower limb lesions for detailed velocity shift detection providing increase confidence on PAD pathology prior to surgical decision. Clearly CEtUS has the ability to not only reduce radiation/nephro-toxic contrast exposure, but may represent a potential financial saving for the health service with further research.

The CPV work we carried out is the first study to demonstrate the accuracy of three tUS methods for calculating CPV but also comparing to the plaque specimen. We have shown that tUS is highly reproducible for measuring CPV with minimal bias and a high degree of precision with narrow confidence intervals. The excellent correlation and minimal bias seen between operators for tUS outlines a highly accurate method of CPV calculation. Our results on intra- and inter-observer variability correspond with previous reports [161, 166, 269-271], although these previous reports do not compare to true plaque immersion volume. Where immersion volume has been reported our results corroborate those findings [272]. The highest degree of precision my thesis found, was seen with CEUS and fused images but B-mode tUS scans have sufficient precision for Carotid screening. Long-term follow-up studies are needed to identify the surgical threshold and a greater understanding of the link to cardiovascular risk.

Future work

There are continual themes of future work that have been highlighted by this thesis. The need for automation and advanced image analysis tools, such as artificial intelligence (AI), are essential for the future adoption of tUS. Namely for centreline AAA diameter/volume and CPV measurement. The use of AI for data capture should also be investigated to identify any improvements that can be made on removing or limiting the effect or image artefacts.

The use of a perfusion/pulsatile model should be utilised to understand the discrepancy between tUS and other imaging modalities like CTa for *in-vivo* diameter/volume measurements. The development of thresholds and the premise of use in artery disease/screening are essential next steps for tUS. In my opinion, a key feature to aid the adoption of tUS is virtual endoscopy. The ability to show surgeons the high-risk plaque or anastomosis location from inside the vessel holds great opportunity. Other measures of plaque vulnerability should also be investigated with tUS. Grey Scale Median (GSM) is an exciting opportunity to develop a tool that measures the morphology of the plaque. Validating tUS GSM with 3D histology is a novel approach. However, all of these techniques lack haemodynamic information. Combining tUS measurements with computational fluid dynamics could provide information not currently available on flow patterns and shear stress.

Potential future directions of non-contrast-enhanced tUS are clearly in the form of planning all types of vascular interventions while at the same time extending the reach of the vascular team into the community through screening and remote services. The discrepancy between surgical responses on change of surgical plan from using DUS or tUS conduit mapping should be investigated further. It is important to understand if the discrepancy was due to surgical interpretation or due to differences in imaging modalities. Other interventional procedures that are immediate research targets for tUS include planning radio-frequency ablation of varicose veins, endoscopic vein harvesting and surgical and endo-AVF creation. Additionally, the role of tUS within AVF surveillance should be investigated further using volume measurements and assessing the predictive value for maturation or AVF failure.

Future research using ultrasound contrast agents should be on using completion imaging EVAR scans, from tUS and rotational angiography, to develop predictive algorithms for delayed endoleak and AAA growth at the point of intervention. This could help develop personalised surveillance strategies for high risk patients. Future lower limb arterial imaging research should assess the improvement in image quality of small vessels with the use of post reactive hyperaemia. This way well demonstrates patent vessels that have very slow low volume flow that may appear occluded without the use of hyperaemia. 3D perfusion studies of muscle perfusion should also be researched to identify thresholds of viable perfusion as an assessment of amputation level.

The fact that tUS is faster than alternative imaging techniques is an added bonus but the development of the tUS hardware into a portable and wireless technology that is significantly cheaper than the device used in this work is vitally important. Cheaper, more accurate automated devices will extend the scope of acceptance and may well lead to the use of tUS for planning and intra-operative imaging, avoiding the need for radiation exposure altogether. However, health economics research should be conducted along with ergonomics-based human-performance assessment to establish the financial benefit for the NHS and reduced RSI risk for vascular scientists/sonographers above current DUS technology.

The applicability of the technology to 3D guidance within the operative setting with virtual reality is an exciting avenue to follow along with tUS guided interventional work. Randomised control trials are now essential for the evidence creation necessary to facilitate widespread clinical adoption of tUS.

Overall conclusion

My thesis has investigated the value of tUS for vascular disease imaging. We have shown the accuracy, reproducibility and precision of tUS for various disease modalities. My work has added evidence to the published literature while addressing my aims, laying the foundations for future work with tUS for vascular surgery. Based on the evidence available from my thesis tUS can readily be utilised for arterial geometry assessment and vessel mapping/surveillance. CEtUS should be used as part of a careful imaging strategy on EVAR completion as well as for targeted angiographic imaging of PAD.

With little development my thesis suggests tUS could be utilised for carotid screening and the assessment of atherosclerosis will attract the pharmaceutical industry. The prospect of complete tUS angiography without the need for alternative imaging is obtainable with close collaboration with contrast and Duplex manufacturers. Further developments of the technology, both hardware and software, will only improve the applicability of tUS while at the same time widening its reach across many hospital departments and into the community to influence the management of large numbers of patients. Beyond the initial development, long term utility of tUS has to be interventional and surgical guidance with augmented reality. The possibility of safe endovascular procedures through avoidance of radiation and nephrotoxic contrast is attractive for both workforce and patients.

The possibility of tUS to significantly improve working conditions for Vascular Scientist while highlighting more accurate and appropriate ways to investigate/survey vascular disease for our patients, is an exciting prospect. tUS has a firm place within the diagnosis, management and hopefully treatment of vascular disease.

Section 5 – References and Appendix

Chapter 12 – References and Appendix.

References

1. Dussik, K., *Über die Möglichkeit, hochfrequente mechanische Schwingungen als diagnostisches Hilfsmittel zu verwerten.* Zeitschrift für die gesamte Neurologie und Psychiatrie, 1942. **174**(1): p. 153-168.
2. Donald, I., J. Macvicar, and T.G. Brown, *Investigation of abdominal masses by pulsed ultrasound.* The Lancet, 1958. **271**(7032): p. 1188-1195.
3. Holmes, J. and D. Howry, *Ultrasonic diagnosis of abdominal disease.* Am J Dig Dis, 1963. **8**(1): p. 12-32.
4. Barber, F.E., et al., *Ultrasonic Duplex Echo-Doppler Scanner.* Biomedical Engineering, IEEE Transactions on, 1974. **BME-21**(2): p. 109-113.
5. Umemura, S., et al., *Multi-element ultrasonic transducer*. 1986, Google Patents.
6. Mumoli, N., et al., *Accuracy of nurse-performed compression ultrasonography in the diagnosis of proximal symptomatic deep vein thrombosis: a prospective cohort study.* J Thromb Haemost, 2014. **12**(4): p. 430-5.
7. El Tabei, L., et al., *Accuracy in diagnosing deep and pelvic vein thrombosis in primary care: an analysis of 395 cases seen by 58 primary care physicians.* Dtsch Arztebl Int, 2012. **109**(45): p. 761-6.
8. Pomero, F., et al., *Accuracy of emergency physician-performed ultrasonography in the diagnosis of deep-vein thrombosis: a systematic review and meta-analysis.* Thromb Haemost, 2013. **109**(1): p. 137-45.
9. Kordowicz, A., et al., *Quality assurance of lower limb venous duplex scans performed by vascular surgeons.* Int Angiol, 2015. **34**(1): p. 60-6.
10. De Maeseneer, M.G., et al., *Accuracy of duplex evaluation one year after varicose vein surgery to predict recurrence at the sapheno-femoral junction after five years.* Eur J Vasc Endovasc Surg, 2005. **29**(3): p. 308-12.
11. Lurie, F., et al., *Multicenter assessment of venous reflux by duplex ultrasound.* J Vasc Surg, 2012. **55**(2): p. 437-45.
12. Jahromi, A.S., et al., *Sensitivity and specificity of color duplex ultrasound measurement in the estimation of internal carotid artery stenosis: a systematic review and meta-analysis.* J Vasc Surg, 2005. **41**(6): p. 962-72.
13. Oates, C.P., et al., *Joint recommendations for reporting carotid ultrasound investigations in the United Kingdom*, in *Eur J Vasc Endovasc Surg*. 2009: England. p. 251-61.
14. Sidhu, P.S. and P.L. Allan, *Ultrasound assessment of internal carotid artery stenosis.* Clin Radiol, 1997. **52**(9): p. 654-8.
15. Favaretto, E., et al., *Analysis of agreement between Duplex ultrasound scanning and arteriography in patients with lower limb artery disease.* J Cardiovasc Med (Hagerstown), 2007. **8**(5): p. 337-41.
16. Katsamouris, A.N., et al., *Can ultrasound replace arteriography in the management of chronic arterial occlusive disease of the lower limb?* Eur J Vasc Endovasc Surg, 2001. **21**(2): p. 155-9.
17. Gray, C., et al., *Comparison of colour duplex ultrasound with computed tomography to measure the maximum abdominal aortic aneurysmal diameter.* Int J Vasc Med, 2014. **2014**: p. 574762.
18. Greenhalgh, R. and J. Powell, *Screening for abdominal aortic aneurysm.* BMJ, 2007. **335**(7623): p. 732-3.
19. Meecham, L., et al., *Abdominal Aortic Aneurysm Diameters: A Study on the Discrepancy between Inner to Inner and Outer to Outer Measurements.* Eur J Vasc Endovasc Surg, 2014. **49**(1): p. 28-32.
20. Wild, J.B., et al., *A Multicentre Observational Study of the Outcomes of Screening Detected Sub-aneurysmal Aortic Dilatation.* Eur J Vasc Endovasc Surg, 2013. **45**(2): p. 128-134.

21. Zimmermann, H., et al., *Value of high-resolution contrast-enhanced ultrasound in detection and characterisation of endoleaks after EVAR.* Clin Hemorheol Microcirc, 2014. **58**(1): p. 247-60.
22. Sidloff, D.A., et al., *Type II endoleak: conservative management is a safe strategy.* Eur J Vasc Endovasc Surg, 2014. **48**(4): p. 391-9.
23. Harrison, G.J., et al., *Surveillance after EVAR based on duplex ultrasound and abdominal radiography.* Eur J Vasc Endovasc Surg, 2011. **42**(2): p. 187-92.
24. Al-Jaishi, A.A., et al., *Patency rates of the arteriovenous fistula for hemodialysis: a systematic review and meta-analysis.* Am J Kidney Dis, 2014. **63**(3): p. 464-78.
25. Aragoncillo, I., et al., *The impact of access blood flow surveillance on reduction of thrombosis in native arteriovenous fistula: a randomized clinical trial.* J Vasc Access, 2016. **17**(1): p. 13-9.
26. Shahi, F. and K. Murali, *Variations in ultrasound scanning protocols in the UK for suspected deep vein thrombosis in outpatients.* Phlebology, 2013. **28**(8): p. 397-403.
27. Fenster, A., et al., *Three-dimensional ultrasound imaging of the vasculature.* Ultrasonics, 1998. **36**(1–5): p. 629-633.
28. Iezzi, R., et al., *Contrast-enhanced ultrasound versus color duplex ultrasound imaging in the follow-up of patients after endovascular abdominal aortic aneurysm repair.* J Vasc Surg, 2009. **49**(3): p. 552-560.
29. Fenster, A., D.B. Downey, and H.N. Cardinal, *Three-dimensional ultrasound imaging.* Phys Med Biol, 2001. **46**(5): p. R67-99.
30. Prager, R.W., et al., *Three-dimensional ultrasound imaging.* Proc Inst Mech Eng H, 2010. **224**(2): p. 193-223.
31. Fenster, A., G. Parraga, and J. Bax, *Three-dimensional ultrasound scanning.* Interface Focus, 2011. **1**(4): p. 503-519.
32. Downey, D.B., A. Fenster, and J.C. Williams, *Clinical Utility of Three-dimensional US.* RadioGraphics, 2000. **20**(2): p. 559-571.
33. Blake, C.C., et al., *Variability and accuracy of measurements of prostate brachytherapy seed position in vitro using three-dimensional ultrasound: an intra- and inter-observer study.* Med Phys, 2000. **27**(12): p. 2788-95.
34. Savord, B. and R. Solomon. *Fully sampled matrix transducer for real time 3D ultrasonic imaging*. in *Ultrasonics, 2003 IEEE Symposium on*. 2003.
35. Bredahl, K., et al., *Three-Dimensional Ultrasound Evaluation of Small Asymptomatic Abdominal Aortic Aneurysms.* Eur J Vasc Endovasc Surg, 2015. **49**(3): p. 289-296.
36. Gargiulo, M., et al., *Could Four-dimensional Contrast-enhanced Ultrasound Replace Computed Tomography Angiography During Follow up of Fenestrated Endografts? Results of a Preliminary Experience.* Eur J Vasc Endovasc Surg, 2014. **48**(5): p. 536-542.
37. Kot, B.C., D.M. Sin, and M. Ying, *Evaluation of the accuracy and reliability of two 3-dimensional sonography methods in volume measurement of small structures: an in vitro phantom study.* J Clin Ultrasound, 2009. **37**(2): p. 82-8.
38. Tatò, F., et al., *Comparison of angiography, duplex sonography and intravascular ultrasound for the graduation of femoropopliteal stenoses before and after balloon angioplasty.* Ultrasound Med Biol, 2006. **32**(12): p. 1837-1843.
39. Mirvis, S.E., S.O. Pais, and D.R. Gens, *Thoracic aortic rupture: advantages of intraarterial digital subtraction angiography.* Am J Roentgenol, 1986. **146**(5): p. 987-991.
40. Bottinor, W., P. Polkampally, and I. Jovin, *Adverse reactions to iodinated contrast media.* Int J Angiol, 2013. **22**(3): p. 149-54.
41. Wolf, G.L., et al., *Comparison of the rates of adverse drug reactions. Ionic contrast agents, ionic agents combined with steroids, and nonionic agents.* Invest Radiol, 1991. **26**(5): p. 404-10.
42. Morcos, S.K. and H.S. Thomsen, *Adverse reactions to iodinated contrast media.* Eur Radiol, 2001. **11**(7): p. 1267-75.
43. Huber, P.R., et al., *CO(2) angiography.* Catheter Cardiovasc Interv, 2002. **55**(3): p. 398-403.

44. Caridi, J.G., et al., *Carbon dioxide digital subtraction angiography: The practical approach.* Tech Vasc Interv Radiol, 2001. **4**(1): p. 57-65.
45. Hawkins, I.F. and J.G. Caridi, *Carbon dioxide (CO2) digital subtraction angiography: 26-year experience at the University of Florida.* Eur Radiol, 1998. **8**(3): p. 391-402.
46. Seeger, J.M., et al., *Carbon dioxide gas as an arterial contrast agent.* Annals of Surgery, 1993. **217**(6): p. 688-698.
47. Kerns, S.R. and I.F. Hawkins, *Carbon dioxide digital subtraction angiography: expanding applications and technical evolution.* AJR Am J Roentgen, 1995. **164**(3): p. 735-741.
48. Nielsen, Y.J., *Whole-body MR angiography in patients with peripheral arterial disease.* Dan Med Bull, 2010. **57**(12): p. B4231.
49. RCR, *Standards for intravascular contrast agent administration to adult patients*. Third edition ed. 2015, London: The Royal Collage of Radiologists.
50. Ota, H., et al., *MDCT Compared with Digital Subtraction Angiography for Assessment of Lower Extremity Arterial Occlusive Disease: Importance of Reviewing Cross-Sectional Images.* AJR Am J Roentgen, 2004. **182**(1): p. 201-209.
51. Sun, Z., *Diagnostic Accuracy of Multislice CT Angiography in Peripheral Arterial Disease.* J Vasc Interv Radiol, 2006. **17**(12): p. 1915-1921.
52. Pomposelli, F., *Arterial imaging in patients with lower extremity ischemia and diabetes mellitus.* J Vasc Surg, 2010. **52**(3 Suppl): p. 81s-91s.
53. Kreitner, K.-F., et al., *MR angiography of the pedal arteries with gadobenate dimeglumine, a contrast agent with increased relaxivity, and comparison with selective intraarterial DSA.* J Magn Reson Imaging, 2008. **27**(1): p. 78-85.
54. Iglesias, J. and C. Pena, *Computed tomography angiography and magnetic resonance angiography imaging in critical limb ischemia: an overview.* Tech Vasc Interv Radiol, 2014. **17**(3): p. 147-54.
55. Eshed, I., et al., *Time-resolved MR angiography of the calf arteries using a phased array cardiac coil: comparison of visibility with standard three-step bolus chase MR angiography.* Acta Radiol, 2011. **52**(9): p. 973-7.
56. Kaufmann, T.J. and D.F. Kallmes, *Utility of MRA and CTA in the Evaluation of Carotid Occlusive Disease.* Seminars in Vascular Surgery, 2005. **18**(2): p. 75-82.
57. JM, U.K.-I., et al., *Contrast-enhanced MR angiography for carotid disease: diagnostic and potential clinical impact.* Neurology, 2004. **62**(8): p. 1282-90.
58. Vardulaki, K.A., et al., *Incidence among men of asymptomatic abdominal aortic aneurysms: estimates from 500 screen detected cases.* J Med Screen, 1999. **6**(1): p. 50-4.
59. Cosford, P.A. and G.C. Leng, *Screening for abdominal aortic aneurysm.* Cochrane Database Syst Rev, 2007(2): p. Cd002945.
60. PHE, *NHS Abdominal Aortic Aneurysm Screening Programme Standards Data Report April 2017 to March 2018*. 2018, Public Health England.
61. Basnyat, P.S., et al., *Mortality from ruptured abdominal aortic aneurysm in Wales.* Br J Surg, 1999. **86**(6): p. 765-770.
62. Johnston, K.W., *Ruptured abdominal aortic aneurysm: six-year follow-up results of a multicenter prospective study. Canadian Society for Vascular Surgery Aneurysm Study Group.* J Vasc Surg, 1994. **19**(5): p. 888-900.
63. Waton, S., et al., *National Vascular Registry: 2018 Annual report.* 2018, The Royal College of Surgeons of England: London.
64. Wilmink, A.B., et al., *Accuracy of serial screening for abdominal aortic aneurysms by ultrasound.* J Med Screen, 2002. **9**(3): p. 125-7.
65. Ballard, D.J., et al., *Surgery for small asymptomatic abdominal aortic aneurysms.* Cochrane Database of Systematic Reviews, 2008(4).
66. Anjum, A. and J.T. Powell, *Is the Incidence of Abdominal Aortic Aneurysm Declining in the 21st Century? Mortality and Hospital Admissions for England & Wales and Scotland.* Euro J Vasc Endovasc Surg, 2012. **43**(2): p. 161-166.

67. Darwood, R.J. and M.J. Brooks, *The Impact of Decreasing Abdominal Aortic Aneurysm Prevalence on a Local Aneurysm Screening Programme.* Euro J Vasc Endovasc Surg, 2012. **44**(1): p. 45-50.
68. Howard, D.P., et al., *Age-specific incidence, risk factors and outcome of acute abdominal aortic aneurysms in a defined population.* Br J Surg, 2015. **102**(8): p. 907-15.
69. Howard, D.P., et al., *Population-Based Study of Incidence of Acute Abdominal Aortic Aneurysms With Projected Impact of Screening Strategy*. J Am Heart Assoc, 2015. **4**(8).
70. Sweeting, M.J., et al., *Analysis of clinical benefit, harms, and cost-effectiveness of screening women for abdominal aortic aneurysm.* Lancet (London, England), 2018. **392**(10146): p. 487-495.
71. Parodi, J.C., J.C. Palmaz, and H.D. Barone, *Transfemoral intraluminal graft implantation for abdominal aortic aneurysms.* Ann Vasc Surg, 1991. **5**(6): p. 491-9.
72. De Bruin, J.L., et al., *Long-term outcome of open or endovascular repair of abdominal aortic aneurysm.* N Engl J Med, 2010. **362**(20): p. 1881-9.
73. Greenhalgh, R.M., et al., *Endovascular versus open repair of abdominal aortic aneurysm.* N Engl J Med, 2010. **362**(20): p. 1863-71.
74. Lubke, T. and J. Brunkwall, *Metaanalysis of EVAR versus open repair for patients undergoing elective repair of abdominal aortic aneurysms.* Zentralbl Chir, 2014. **139**(5): p. 552-61.
75. McHugh, S.M., et al., *Endovascular versus open repair of ruptured abdominal aortic aneurysm.* Surgeon, 2015.
76. Edwards, S.T., et al., *Comparative effectiveness of endovascular versus open repair of ruptured abdominal aortic aneurysm in the Medicare population.* J Vasc Surg, 2014. **59**(3): p. 575-82.
77. Patel, R., et al., *Endovascular versus open repair of abdominal aortic aneurysm in 15-years' follow-up of the UK endovascular aneurysm repair trial 1 (EVAR trial 1): a randomised controlled trial.* The Lancet, 2016. **388**(10058): p. 2366-2374.
78. Moll, F.L., et al., *Management of Abdominal Aortic Aneurysms Clinical Practice Guidelines of the European Society for Vascular Surgery.* Euro J Vasc Endovasc Surg, 2011. **41, Supplement 1**: p. S1-S58.
79. Leotta, D.F., et al., *Measurement of abdominal aortic aneurysms with three-dimensional ultrasound imaging: Preliminary report.* J Vasc Surg, 2001. **33**(4): p. 700-707.
80. Long, A., et al., *Abdominal aortic aneurysm imaging with 3-D ultrasound: 3-D-based maximum diameter measurement and volume quantification.* Ultrasound Med Biol, 2013. **39**(8): p. 1325-36.
81. Causey, M.W., et al., *Three-Dimensional Ultrasonography Measurements After Endovascular Aneurysm Repair.* Ann Vasc Surg, 2013. **27**(2): p. 146-153.
82. Fillinger, M.F., et al., *Prediction of rupture risk in abdominal aortic aneurysm during observation: Wall stress versus diameter.* J Vasc Surg, 2003. **37**(4): p. 724-732.
83. Kok, A.M., et al., *On the feasibility of wall stress analysis of abdominal aortic aneurysms using three-dimensional ultrasound.* J Vasc Surg, 2015. **65**(5): p. 1175-84.
84. Bihari, P., et al., *Strain Measurement of Abdominal Aortic Aneurysm with Real-time 3D Ultrasound Speckle Tracking.* Euro J Vasc Endovasc Surg, 2013. **45**(4): p. 315-323.
85. Karatolios, K., et al., *Method for Aortic Wall Strain Measurement With Three-Dimensional Ultrasound Speckle Tracking and Fitted Finite Element Analysis.* Ann Thorac Surg, 2013. **96**(5): p. 1664-1671.
86. Derwich, W., et al., *High Resolution Strain Analysis Comparing Aorta and Abdominal Aortic Aneurysm with Real Time Three Dimensional Speckle Tracking Ultrasound.* Euro J Vasc Endovasc Surg, 2016. **51**(2): p. 187-193.
87. Schmieder, G.C., et al., *Endoleak after endovascular aneurysm repair: duplex ultrasound imaging is better than computed tomography at determining the need for intervention.* J Vasc Surg, 2009. **50**(5): p. 1012-7; discussion 1017-8.
88. Chung, J., et al., *Contrast-enhanced ultrasound (CEUS) versus computed tomography angiography (CTA) in detection of endoleaks in post-EVAR patients. Are delayed type II*

endoleaks being missed? A systematic review and meta-analysis. J Ultrasound, 2015. **18**(2): p. 91-9.
89. Perini, P., et al., *Contrast-enhanced ultrasound vs. CT angiography in fenestrated EVAR surveillance: a single-center comparison.* J Endovasc Ther, 2012. **19**(5): p. 648-55.
90. Ormesher, D.C., et al., *Use of three-dimensional contrast-enhanced duplex ultrasound imaging during endovascular aneurysm repair.* J Vasc Surg, 2014. **60**(6): p. 1468-72.
91. Abbas, A., et al., *3D contrast enhanced ultrasound for detecting endoleak following endovascular aneurysm repair (EVAR).* Eur J Vasc Endovasc Surg, 2014. **47**(5): p. 487-92.
92. Hertault, A., et al., *Benefits of Completion 3D Angiography Associated with Contrast Enhanced Ultrasound to Assess Technical Success after EVAR.* Eur J Vasc Endovasc Surg, 2015. **49**(5): p. 541-8.
93. Prinssen, M., et al., *Decision-making in follow-up after endovascular aneurysm repair based on diameter and volume measurements: a blinded comparison.* Eur J Vasc Endovasc Surg, 2003. **26**(2): p. 184-7.
94. Wever, J.J., et al., *Maximal aneurysm diameter follow-up is inadequate after endovascular abdominal aortic aneurysm repair.* Eur J Vasc Endovasc Surg, 2000. **20**(2): p. 177-82.
95. Bredahl, K., et al., *Volume Estimation of the Aortic Sac after EVAR Using 3-D Ultrasound – A Novel, Accurate and Promising Technique.* Euro J Vasc Endovasc Surg, 2013. **45**(5): p. 450-455.
96. Bredahl, K., et al., *Three-dimensional ultrasound improves the accuracy of diameter measurement of the residual sac in EVAR patients.* Eur J Vasc Endovasc Surg, 2013. **46**(5): p. 525-32.
97. Lowe, C., et al., *Three-dimensional contrast-enhanced ultrasound improves endoleak detection and classification after endovascular aneurysm repair.* J Vasc Surg, 2017. **65**(5).
98. Pant, S., et al., *Inflammation and atherosclerosis--revisited.* J Cardiovasc Pharmacol Ther, 2014. **19**(2): p. 170-8.
99. Heo, K.S., K. Fujiwara, and J. Abe, *Shear stress and atherosclerosis.* Mol Cells, 2014. **37**(6): p. 435-40.
100. Zhou, J., Y.S. Li, and S. Chien, *Shear stress-initiated signaling and its regulation of endothelial function.* Arterioscler Thromb Vasc Biol, 2014. **34**(10): p. 2191-8.
101. Feaver, R.E., et al., *Atheroprone hemodynamics regulate fibronectin deposition to create positive feedback that sustains endothelial inflammation.* Circ Res, 2010. **106**(11): p. 1703-11.
102. Ayer, J., et al., *Lifetime risk: childhood obesity and cardiovascular risk.* Eur Heart J, 2015. **36**(22): p. 1371-6.
103. Mandviwala, T., U. Khalid, and A. Deswal, *Obesity and Cardiovascular Disease: a Risk Factor or a Risk Marker?* Curr Atheroscler Rep, 2016. **18**(5): p. 21.
104. Balakumar, P., U.K. Maung, and G. Jagadeesh, *Prevalence and prevention of cardiovascular disease and diabetes mellitus.* Pharmacol Res, 2016. **113**(Pt A): p. 600-609.
105. Chillaron, J.J., et al., *Type 1 diabetes, metabolic syndrome and cardiovascular risk.* Metabolism, 2014. **63**(2): p. 181-7.
106. Kopin, L. and C. Lowenstein, *Dyslipidemia.* Ann Intern Med, 2017. **167**(11): p. Itc81-itc96.
107. Allaire, J., et al., *LDL particle number and size and cardiovascular risk: anything new under the sun?* Curr Opin Lipidol, 2017. **28**(3): p. 261-266.
108. Sarzani, R., et al., *Cardiac Natriuretic Peptides, Hypertension and Cardiovascular Risk.* High Blood Press Cardiovasc Prev, 2017. **24**(2): p. 115-126.
109. Messner, B. and D. Bernhard, *Smoking and cardiovascular disease: mechanisms of endothelial dysfunction and early atherogenesis.* Arterioscler Thromb Vasc Biol, 2014. **34**(3): p. 509-15.
110. *A randomised, blinded, trial of clopidogrel versus aspirin in patients at risk of ischaemic events (CAPRIE). CAPRIE Steering Committee.* Lancet, 1996. **348**(9038): p. 1329-39.
111. Conte, M.S., et al., *Global Vascular Guidelines on the Management of Chronic Limb-Threatening Ischemia.* European Journal of Vascular and Endovascular Surgery, 2019. **58**(1): p. S1-S109.e33.

112. Viera, A.J., *Screening for Hypertension and Lowering Blood Pressure for Prevention of Cardiovascular Disease Events.* Med Clin North Am, 2017. **101**(4): p. 701-712.
113. Naslund, U., et al., *Visualization of asymptomatic atherosclerotic disease for optimum cardiovascular prevention (VIPVIZA): a pragmatic, open-label, randomised controlled trial.* Lancet, 2019. **393**(10167): p. 133-142.
114. NICE. *Stroke*. 2008; A clinical guideline, CG68]. Available from: https://www.nice.org.uk/guidance/cg68.
115. Ois, A., et al., *High Risk of Early Neurological Recurrence in Symptomatic Carotid Stenosis.* Stroke, 2009. **40**(8): p. 2727-2731.
116. Marnane, M., et al., *Plaque Inflammation and Unstable Morphology Are Associated With Early Stroke Recurrence in Symptomatic Carotid Stenosis.* Stroke, 2014. **45**(3): p. 801-806.
117. Kakisis, J.D., et al., *The European Society for Vascular Surgery Guidelines for Carotid Intervention: An Updated Independent Assessment and Literature Review.* Euro J Vasc Endovasc Surg, 2012. **44**(3): p. 238-243.
118. Rothwell, P.M., et al., *Analysis of pooled data from the randomised controlled trials of endarterectomy for symptomatic carotid stenosis.* Lancet, 2003. **361**(9352): p. 107-16.
119. Liapis, C.D., et al., *ESVS guidelines. Invasive treatment for carotid stenosis: indications, techniques.* Eur J Vasc Endovasc Surg, 2009. **37**(4 Suppl): p. 1-19.
120. Rothwell, P.M., et al., *Endarterectomy for symptomatic carotid stenosis in relation to clinical subgroups and timing of surgery.* Lancet, 2004. **363**(9413): p. 915-24.
121. *Endarterectomy for asymptomatic carotid artery stenosis. Executive Committee for the Asymptomatic Carotid Atherosclerosis Study.* Jama, 1995. **273**(18): p. 1421-8.
122. Moore, W.S., et al., *Guidelines for carotid endarterectomy. A multidisciplinary consensus statement from the ad hoc Committee, American Heart Association.* Stroke, 1995. **26**(1): p. 188-201.
123. Halliday, A., et al., *Prevention of disabling and fatal strokes by successful carotid endarterectomy in patients without recent neurological symptoms: randomised controlled trial.* Lancet, 2004. **363**(9420): p. 1491-502.
124. Moneta, G.L., et al., *Operative versus nonoperative management of asymptomatic high-grade internal carotid artery stenosis: improved results with endarterectomy.* Stroke, 1987. **18**(6): p. 1005-10.
125. Schroeder, T., et al., *Asymptomatic carotid lesions after endarterectomy of contralateral carotid artery. Five-year follow-up study and prognosis.* Arch Surg, 1987. **122**(7): p. 795-801.
126. Glagov, S., et al., *Compensatory enlargement of human atherosclerotic coronary arteries.* N Engl J Med, 1987. **316**(22): p. 1371-5.
127. Dong, L., et al., *Geometric and Compositional Appearance of Atheroma in an Angiographically Normal Carotid Artery in Patients with Atherosclerosis.* American Journal of Neuroradiology, 2010. **31**(2): p. 311-316.
128. Saam, T., et al., *Prevalence of American Heart Association type VI carotid atherosclerotic lesions identified by magnetic resonance imaging for different levels of stenosis as measured by duplex ultrasound.* J Am Coll Cardiol, 2008. **51**(10): p. 1014-21.
129. Babiarz, L.S., et al., *Comparison of gadolinium-enhanced cardiovascular magnetic resonance angiography with high-resolution black blood cardiovascular magnetic resonance for assessing carotid artery stenosis.* J Cardiovasc Magn Reson, 2007. **9**(1): p. 63-70.
130. van den Oord, S.C., et al., *Quantitative contrast-enhanced ultrasound of intraplaque neovascularization in patients with carotid atherosclerosis.* Ultraschall Med, 2015. **36**(2): p. 154-61.
131. Saito, K., et al., *Contrast-enhanced ultrasound for the evaluation of neovascularization in atherosclerotic carotid artery plaques.* Stroke, 2014. **45**(10): p. 3073-5.
132. Akkus, Z., et al., *Carotid intraplaque neovascularization quantification software (CINQS).* IEEE J Biomed Health Inform, 2015. **19**(1): p. 332-8.
133. Li, C., et al., *Quantification of carotid plaque neovascularization using contrast-enhanced ultrasound with histopathologic validation.* Ultrasound Med Biol, 2014. **40**(8): p. 1827-33.

134. Salem, M.K., et al., *Identification of patients with a histologically unstable carotid plaque using ultrasonic plaque image analysis.* Eur J Vasc Endovasc Surg, 2014. **48**(2): p. 118-25.
135. Ostling, G., et al., *Comparison of grey scale median (GSM) measurement in ultrasound images of human carotid plaques using two different softwares.* Clin Physiol Funct Imaging, 2013. **33**(6): p. 431-5.
136. Andersson, J., et al., *The carotid artery plaque size and echogenicity are related to different cardiovascular risk factors in the elderly: the Prospective Investigation of the Vasculature in Uppsala Seniors (PIVUS) study.* Lipids, 2009. **44**(5): p. 397-403.
137. Griffin, M., A. Nicolaides, and E. Kyriacou, *Normalisation of ultrasonic images of atherosclerotic plaques and reproducibility of grey scale median using dedicated software.* Int Angiol, 2007. **26**(4): p. 372-7.
138. Mayor, I., et al., *Carotid plaque: comparison between visual and grey-scale median analysis.* Ultrasound Med Biol, 2003. **29**(7): p. 961-6.
139. Brinjikji, W., et al., *Contemporary carotid imaging: from degree of stenosis to plaque vulnerability.* J Neurosurg, 2016. **124**(1): p. 27-42.
140. Sharma, A.M., et al., *A Review on Carotid Ultrasound Atherosclerotic Tissue Characterization and Stroke Risk Stratification in Machine Learning Framework.* Curr Atheroscler Rep, 2015. **17**(9): p. 55.
141. Dutta, D., et al., *Motion Artifact Reduction in Ultrasound Based Thermal Strain Imaging of Atherosclerotic Plaques Using Time Series Analysis.* IEEE Trans Ultrason Ferroelectr Freq Control, 2013. **60**(8): p. 1660-1668.
142. Mahmoud, A.M., et al., *Noninvasive detection of lipids in atherosclerotic plaque using ultrasound thermal strain imaging: in vivo animal study.* J Am Coll Cardiol, 2013. **62**(19): p. 1804-9.
143. Kim, K., et al., *Arterial vulnerable plaque characterization using ultrasound-induced thermal strain imaging (TSI).* IEEE Trans Biomed Eng, 2008. **55**(1): p. 171-80.
144. Ramnarine, K.V., et al., *Shear wave elastography imaging of carotid plaques: feasible, reproducible and of clinical potential.* Cardiovasc Ultrasound, 2014. **12**: p. 49.
145. Garrard, J.W. and K. Ramnarine, *Shear-wave elastography in carotid plaques: comparison with grayscale median and histological assessment in an interesting case.* Ultraschall Med, 2014. **35**(1): p. 1-3.
146. Ramnarine, K.V., et al., *Shear wave elastography assessment of carotid plaque stiffness: in vitro reproducibility study.* Ultrasound Med Biol, 2014. **40**(1): p. 200-9.
147. Liu, F., et al., *Real-time tissue elastography for the detection of vulnerable carotid plaques in patients undergoing endarterectomy: a pilot study.* Ultrasound Med Biol, 2015. **41**(3): p. 705-12.
148. Naim, C., et al., *Characterisation of carotid plaques with ultrasound elastography: feasibility and correlation with high-resolution magnetic resonance imaging.* Eur Radiol, 2013. **23**(7): p. 2030-41.
149. Ventura, C.A., et al., *Can contrast-enhanced ultrasound with second-generation contrast agents replace computed tomography angiography for distinguishing between occlusion and pseudo-occlusion of the internal carotid artery?* Clinics (Sao Paulo), 2015. **70**(1): p. 1-6.
150. Yamaguchi, M., et al., *Quantitative assessment of changes in carotid plaques during cilostazol administration using three-dimensional ultrasonography and non-gated magnetic resonance plaque imaging.* Neuroradiology, 2012. **54**(9): p. 939-45.
151. Hoogi, A., G. Zurakhov, and D. Adam, *Evaluation of a 3D technique for quantifying neovascularization within plaques imaged by contrast enhanced ultrasound.* Conf Proc IEEE Eng Med Biol Soc, 2013. **2013**: p. 1124-7.
152. Nakaoka, T., et al., *Carotid artery wall perfusion of the plaque: three dimensional contrast sonographic imaging.* No Shinkei Geka, 2008. **36**(11): p. 991-1000.
153. Koyama, S., et al., *Preoperative prediction of macrophage infiltration by 3-D tomographic ultrasound in endoarterectomized carotid plaques in elderly patients.* Geriatr Gerontol Int, 2013. **13**(4): p. 834-41.

154. Khallaghi, S., et al., *Experimental validation of an intrasubject elastic registration algorithm for dynamic-3D ultrasound images.* Med Phys, 2012. **39**(9): p. 5488-97.
155. Stone, G.W., et al., *A prospective natural-history study of coronary atherosclerosis.* N Engl J Med, 2011. **364**(3): p. 226-35.
156. Sillesen, H., et al., *Carotid Plaque Burden as a Measure of Subclinical Atherosclerosis: Comparison With Other Tests for Subclinical Arterial Disease in the High Risk Plaque BioImage Study.* JACC: Cardiovasc Imaging, 2012. **5**(7): p. 681-689.
157. Sangiorgi, G., et al., *Arterial calcification and not lumen stenosis is highly correlated with atherosclerotic plaque burden in humans: a histologic study of 723 coronary artery segments using nondecalcifying methodology.* J Am Coll Cardiol, 1998. **31**(1): p. 126-33.
158. Lindsay, A.C., et al., *Plaque features associated with increased cerebral infarction after minor stroke and TIA: a prospective, case-control, 3-T carotid artery MR imaging study.* JACC Cardiovasc Imaging, 2012. **5**(4): p. 388-96.
159. Zhao, X., et al., *Discriminating carotid atherosclerotic lesion severity by luminal stenosis and plaque burden: a comparison utilizing high-resolution magnetic resonance imaging at 3.0 Tesla.* Stroke, 2011. **42**(2): p. 347-53.
160. Dong, L., et al., *Geometric and compositional appearance of atheroma in an angiographically normal carotid artery in patients with atherosclerosis.* AJNR Am J Neuroradiol, 2010. **31**(2): p. 311-6.
161. Ball, S., et al., *Carotid plaque volume in patients undergoing carotid endarterectomy.* Br J Surg, 2018.
162. Ainsworth, C.D., et al., *3D ultrasound measurement of change in carotid plaque volume: a tool for rapid evaluation of new therapies.* Stroke, 2005. **36**(9): p. 1904-9.
163. Spence, J.D., et al., *Carotid plaque area: a tool for targeting and evaluating vascular preventive therapy.* Stroke, 2002. **33**(12): p. 2916-22.
164. Wannarong, T., et al., *Progression of carotid plaque volume predicts cardiovascular events.* Stroke, 2013. **44**(7): p. 1859-1865.
165. AlMuhanna, K., et al., *Carotid plaque morphometric assessment with three-dimensional ultrasound imaging.* J Vasc Surg, 2015. **61**(3): p. 690-697.
166. Landry, A., J.D. Spence, and A. Fenster, *Measurement of carotid plaque volume by 3-dimensional ultrasound.* Stroke, 2004. **35**(4): p. 864-9.
167. Landry, A. and A. Fenster, *Theoretical and experimental quantification of carotid plaque volume measurements made by three-dimensional ultrasound using test phantoms.* Medical physics, 2002. **29**(10): p. 2319-2327.
168. Landry, A., J.D. Spence, and A. Fenster, *Quantification of carotid plaque volume measurements using 3D ultrasound imaging.* Ultrasound Med Biol, 2005. **31**(6): p. 751-762.
169. Ball, S., et al., *Carotid plaque volume in patients undergoing carotid endarterectomy.* Br J Surg, 2018. **105**(3): p. 262-269.
170. Kumar, A., et al., *Plaque Volume of Carotid Endarterectomy Specimens Measured by 3D Ultrasound Technology.* JACC: Cardiovasc Imaging, 2016. **9**(9): p. 1118-1119.
171. Heliopoulos, J., et al., *A three-dimensional ultrasonographic quantitative analysis of non-ulcerated carotid plaque morphology in symptomatic and asymptomatic carotid stenosis.* Atherosclerosis, 2008. **198**(1): p. 129-35.
172. Delcker, A. and C. Tegeler, *Influence of ECG-Triggered Data Acquisition on Reliability for Carotid Plaque Volume Measurements with a Magnetic Sensor Three-Dimensional Ultrasound System.* Ultrasound Med Biol, 1998. **24**(4): p. 601-605.
173. Bar, M., et al., *Inter-rater reliability of carotid atherosclerotic plaque quantification by 3-dimensional sonography.* J Ultrasound Med, 2014. **33**(7): p. 1273-1278.
174. Mallett, C., et al., *Prospective cardiac gating of carotid three-dimensional ultrasound.* Medical physics, 2009. **36**(7): p. 3168-3175.
175. Hossain, M.M., et al., *Semiautomatic segmentation of atherosclerotic carotid artery wall volume using 3D ultrasound imaging.* Med Phys, 2015. **42**(4): p. 2029-43.
176. Ukwatta, E., et al., *Three-dimensional ultrasound of carotid atherosclerosis: semiautomated segmentation using a level set-based method.* Med Phys, 2011. **38**(5): p. 2479-93.

177. NICE. *Peripheral arterial disease*. January 2014 01/03/2015]; NICE quality standard [QS52]]. Available from: https://www.nice.org.uk/guidance/qs52.
178. NICE. *Diabetic foot problems: Inpatient management of diabetic foot problems*. March 2011 01/03/2015]; Available from: https://www.nice.org.uk/guidance/cg119/chapter/1-guidance.
179. Franz, R.W., et al., *Accuracy of duplex ultrasonography in estimation of severity of peripheral vascular disease.* Int J Angiol, 2013. **22**(3): p. 155-8.
180. Wong, T.H., et al., *Duplex ultrasonography arteriography as first-line investigation for peripheral vascular disease.* Singapore Med J, 2013. **54**(5): p. 271-4.
181. Mustapha, J.A., et al., *Comparison between angiographic and arterial duplex ultrasound assessment of tibial arteries in patients with peripheral arterial disease: on behalf of the Joint Endovascular and Non-Invasive Assessment of LImb Perfusion (JENALI) Group.* J Invasive Cardiol, 2013. **25**(11): p. 606-11.
182. Tehan, P.E., A. Bray, and V.H. Chuter, *Non-invasive vascular assessment in the foot with diabetes: sensitivity and specificity of the ankle brachial index, toe brachial index and continuous wave Doppler for detecting peripheral arterial disease.* J Diabetes Complications, 2016. **30**(1): p. 155-60.
183. Norgren, L., et al., *Inter-Society Consensus for the Management of Peripheral Arterial Disease (TASC II).* J Vasc Surg, 2007. **45 Suppl S**: p. S5-67.
184. Song, Y., et al., *[Preliminary study of contrast-enhanced ultrasound in correlation between muscle perfusion deficits in lower extremity arterial disease and its collateralization].* Zhonghua Yi Xue Za Zhi, 2014. **94**(7): p. 507-9.
185. Duerschmied, D., et al., *Contrast ultrasound perfusion imaging of lower extremities in peripheral arterial disease: a novel diagnostic method.* Eur Heart J, 2006. **27**(3): p. 310-5.
186. Coffi, S.B., et al., *Contrast-enhanced duplex scanning of crural arteries by means of continuous infusion of Levovist.* J Vasc Surg, 2004. **39**(3): p. 517-22.
187. Mestre, X.M., et al., *Role of contrast-enhanced ultrasound arterial mapping in surgical planning for patients with critical limb ischemia.* Ultrasound Med Biol, 2015. **41**(6): p. 1570-6.
188. Eiberg, J.P., et al., *Ultrasound contrast-agent improves imaging of lower limb occlusive disease.* Euro J Vasc Endovasc Surg, 2003. **25**(1): p. 23-28.
189. Rim, Y., D.D. McPherson, and H. Kim, *Volumetric three-dimensional intravascular ultrasound visualization using shape-based nonlinear interpolation.* Biomed Eng Online, 2013. **12**: p. 39.
190. Janvier, M.A., et al., *Validation of a new 3D-US imaging robotic system to detect and quantify lower limb arterial stenoses.* Conf Proc IEEE Eng Med Biol Soc, 2007. **2007**: p. 339-42.
191. McGah, P.M., et al., *A longitudinal study of remodeling in a revised peripheral artery bypass graft using 3D ultrasound imaging and computational hemodynamics.* J Biomech Eng, 2011. **133**(4): p. 041008.
192. Neville, R.F., et al., *A comparison of tibial artery bypass performed with heparin-bonded expanded polytetrafluoroethylene and great saphenous vein to treat critical limb ischemia.* J Vasc Surg, 2012. **56**(4): p. 1008-14.
193. Head, H.D. and M.F. Brown, *Preoperative vein mapping for coronary artery bypass operations.* Ann Thorac Surg, 1995. **59**(1): p. 144-148.
194. Cohn, J.D. and K.F. Korver, *Optimizing saphenous vein site selection using intraoperative venous duplex ultrasound scanning.* Ann thorac surg, 2005. **79**(6): p. 2013-2017.
195. Barros, F.S., et al., *Echocolor Doppler saphenous vein mapping prior to myocardial revascularization.* Revista Brasileira de Cirurgia Cardiovascular, 1999. **14**(4): p. 303-307.
196. Luckraz, H., et al., *Pre-operative long saphenous vein mapping predicts vein anatomy and quality leading to improved post-operative leg morbidity.* Interact Cardiovasc Thorac Surg, 2008. **7**(2): p. 188-191.

197. Lux, J., et al., *Thrombin-Activatable Microbubbles as Potential Ultrasound Contrast Agents for the Detection of Acute Thrombosis.* ACS Appl Mater Interfaces, 2017. **9**(43): p. 37587-37596.
198. Yan, J.P., et al., *Application of contrast-enhanced ultrasound before inferior vena cava filter recovery.* Int Angiol, 2017. **36**(5): p. 474-481.
199. Bou Chebl, R., et al., *Use of Contrast-Enhanced Ultrasound for Confirmation of Central Venous Catheter Placement: Systematic Review and Meta-analysis.* J Ultrasound Med, 2017. **36**(12): p. 2503-2510.
200. Zhang, J., et al., *Value of Contrast-Enhanced Ultrasound in Detecting Competent and Incompetent Lower-Extremity Perforating Veins.* Ultrasound Med Biol, 2018. **44**(8): p. 1721-1726.
201. Galeandro, A.I., et al., *A three-dimensional electronic report of a venous echo color Doppler of the lower limbs: MEVeC(R).* Vasc Health Risk Manag, 2014. **10**: p. 549-55.
202. Burt, V.L., et al., *Prevalence of Hypertension in the US Adult Population: Results From the Third National Health and Nutrition Examination Survey, 1988-1991.* Hypertension, 1995. **25**(3): p. 305-313.
203. Kerr, M., et al., *Estimating the financial cost of chronic kidney disease to the NHS in England.* Nephrol Dial Transplant, 2012. **27**(Suppl 3): p. iii73-iii80.
204. Evans, K., et al., *UK Renal Registry 20th Annual Report: Introduction.* Nephron, 2018. **139 Suppl 1**: p. 1-12.
205. Liem, Y.S., et al., *Comparison of hemodialysis and peritoneal dialysis survival in The Netherlands.* Kidney Int, 2007. **71**(2): p. 153-8.
206. Vonesh, E.F., et al., *Mortality studies comparing peritoneal dialysis and hemodialysis: what do they tell us?* Kidney Int Suppl, 2006(103): p. S3-11.
207. Peeters, P., et al., *Analysis and interpretation of cost data in dialysis: review of Western European literature.* Health Policy, 2000. **54**(3): p. 209-27.
208. Karopadi, A.N., et al., *Cost of peritoneal dialysis and haemodialysis across the world.* Nephrol Dial Transplant, 2013. **28**(10): p. 2553-69.
209. Baboolal, K., et al., *The cost of renal dialysis in a UK setting--a multicentre study.* Nephrol Dial Transplant, 2008. **23**(6): p. 1982-9.
210. Visciano, B., et al., *Complications of native arteriovenous fistula: the role of color Doppler ultrasonography.* Ther Apher Dial, 2014. **18**(2): p. 155-61.
211. Besarab, A., A. Asif, and P. Roy-Chaudhury, *The native arteriovenous fistula in 2007. Surveillance and monitoring.* 2007, J Nephrol. p. 656–67.
212. Huijbregts, H.J., et al., *Hemodialysis arteriovenous fistula patency revisited: results of a prospective, multicenter initiative.* Clin J Am Soc Nephrol, 2008. **3**(3): p. 714-9.
213. Pisoni, R., J. Barker-Finkel, and M. Allo, *Statin therapy is not associated with improved vascular access outcomes.* Clin J Am Soc Nephrol, 2010. **5**(8): p. 1447-50.
214. Kumwenda, M., S. Mitra, and C. Reid, *Renal associations clinical practive guideline, Vascular access for haemodialysis.* 2015, UK renal association.
215. Georgiadis, G.S., et al., *The Necessity for Routine Pre-operative Ultrasound Mapping Before Arteriovenous Fistula Creation: A Meta-analysis.* Eur J Vasc Endovasc Surg, 2015. **49**(5): p. 600-5.
216. Hull, J.E., E.N. Kinsey, and W.L. Bishop, *Mapping of the snuffbox and cubital vessels for percutaneous arterial venous fistula (pAVF) in dialysis patients.* J Vasc Access, 2013. **14**(3): p. 245-51.
217. Ilhan, G., et al., *The clinical utility of vascular mapping with Doppler ultrasound prior to arteriovenous fistula construction for hemodialysis access.* J Vasc Access, 2013. **14**(1): p. 83-8.
218. Kakkos, S.K., et al., *Routine preoperative venous and arterial mapping increases both, construction and maturation rate of upper arm autogenous arteriovenous fistulae.* Vasc Endovascular Surg, 2011. **45**(2): p. 135-41.
219. Mendes, R.R., et al., *Prediction of wrist arteriovenous fistula maturation with preoperative vein mapping with ultrasonography.* J Vasc Surg, 2002. **36**(3): p. 460-3.

220. Roll, S.C., et al., *An analysis of occupational factors related to shoulder discomfort in diagnostic medical sonographers and vascular technologists.* Work, 2012. **42**(3): p. 355-65.
221. Russo, A., et al., *The prevalence of musculoskeletal symptoms among British Columbia sonographers.* Appl Ergon, 2002. **33**(5): p. 385-93.
222. Wareluk, P. and W. Jakubowski, *Evaluation of musculoskeletal symptoms among physicians performing ultrasound.* J Ultrason, 2017. **17**(70): p. 154-159.
223. Wilkins, E., et al., *European Cardiovascular Disease Statistics.* European Heart Network, 2017.
224. Fernandez-Friera, L., et al., *Prevalence, Vascular Distribution, and Multiterritorial Extent of Subclinical Atherosclerosis in a Middle-Aged Cohort: The PESA (Progression of Early Subclinical Atherosclerosis) Study.* Circulation, 2015. **131**(24): p. 2104-13.
225. Lorenz, M.W., et al., *Predictive value for cardiovascular events of common carotid intima media thickness and its rate of change in individuals at high cardiovascular risk – Results from the PROG-IMT collaboration.* PLOS ONE, 2018. **13**(4): p. e0191172.
226. Hughes, S., *Archimedes revisited: a faster, better, cheaper method of accurately measuring the volume of small objects.* Physics Education, 2005. **40**(5): p. 468-74.
227. Zotz, R.J., et al., *In vitro measurement accuracy of three-dimensional ultrasound.* Echocardiography, 2001. **18**(2): p. 149-56.
228. Riccabona, M., T.R. Nelson, and D.H. Pretorius, *Three-dimensional ultrasound: accuracy of distance and volume measurements.* Ultrasound Obstet Gynecol, 1996. **7**(6): p. 429-34.
229. King, D.L., D.L. King, Jr., and M.Y. Shao, *Evaluation of in vitro measurement accuracy of a three-dimensional ultrasound scanner.* J Ultrasound Med, 1991. **10**(2): p. 77-82.
230. Gilja, O.H., et al., *In vivo comparison of 3D ultrasonography and magnetic resonance imaging in volume estimation of human kidneys.* Ultrasound Med. Biol., 1995. **21**(1): p. 25-32.
231. Feurer, R., et al. *Reliability of a freehand three-dimensional ultrasonic device allowing anatomical orientation "at a glance": Study protocol for 3D measurements with Curefab CS®*. J Biomed Graph Comput, 2012. **2**, DOI: 10.5430/jbgc.v2n2p1.
232. Ellis, M., J.T. Powell, and R.M. Greenhalgh, *Limitations of ultrasonography in surveillance of small abdominal aortic aneurysms.* Br J Surg, 1991. **78**(5): p. 614-6.
233. Beales, L., et al., *Reproducibility of ultrasound measurement of the abdominal aorta.* Br J Surg, 2011. **98**(11): p. 1517-25.
234. Singh, K., et al., *The difference between ultrasound and computed tomography (CT) measurements of aortic diameter increases with aortic diameter: analysis of axial images of abdominal aortic and common iliac artery diameter in normal and aneurysmal aortas. The Tromso Study, 1994-1995.* Eur J Vasc Endovasc Surg, 2004. **28**(2): p. 158-67.
235. Moll, F.L., et al., *Management of abdominal aortic aneurysms clinical practice guidelines of the European society for vascular surgery.* Eur J Vasc Endovasc Surg, 2011. **41 Suppl 1**: p. S1-s58.
236. Lopez-Melgar, B., et al., *Subclinical Atherosclerosis Burden by 3D Ultrasound in Mid-Life: The PESA Study.* J Am Coll Cardiol, 2017. **70**(3): p. 301-313.
237. Laurel, M., *Standard Methods for Calibration of 2-Dimensional and 3-Dimensional Spatial Measurement Capabilities of Pulse Echo Ultrasound Imaging Systems .* 2004: American Institute of Ultrasound in Medicine.
238. Wood, B.J., et al., *Navigation systems for ablation.* J Vasc Interv Radiol, 2010. **21**(8 Suppl): p. S257-63.
239. Sandford, R.M., et al., *Pre-discharge duplex ultrasound scans detect endoleaks not seen on completion angiography after endovascular aneurysm repair.* J Endovasc Ther, 2010. **17**(3): p. 349-53.
240. Abraha, I., et al., *Ultrasonography for endoleak detection after endoluminal abdominal aortic aneurysm repair.* Cochrane Database Syst Rev, 2017. **6**: p. Cd010296.
241. Bredahl, K.K., et al., *Contrast Enhanced Ultrasound can Replace Computed Tomography Angiography for Surveillance After Endovascular Aortic Aneurysm Repair.* Eur J Vasc Endovasc Surg, 2016. **52**(6): p. 729-734.

242. Rafailidis, V., et al., *Evolving clinical applications of contrast-enhanced ultrasound (CEUS) in the abdominal aorta.* Cardiovasc Diagn Ther, 2018. **8**(Suppl 1): p. S118-s130.
243. Erbel, R., et al., *2014 ESC Guidelines on the diagnosis and treatment of aortic diseasesDocument covering acute and chronic aortic diseases of the thoracic and abdominal aorta of the adultThe Task Force for the Diagnosis and Treatment of Aortic Diseases of the European Society of Cardiology (ESC).* Eur Heart J, 2014. **35**(41): p. 2873-2926.
244. Kopp, R., et al., *First experience using intraoperative contrast-enhanced ultrasound during endovascular aneurysm repair for infrarenal aortic aneurysms.* J Vasc Surg, 2010. **51**(5): p. 1103-10.
245. Biasi, L., et al., *Intraoperative DynaCT detection and immediate correction of a type Ia endoleak following endovascular repair of abdominal aortic aneurysm.* Cardiovasc Intervent Radiol, 2009. **32**(3): p. 535-8.
246. Schulz, C.J., et al., *Intraoperative contrast-enhanced cone beam computed tomography to assess technical success during endovascular aneurysm repair.* J Vasc Surg, 2016. **64**(3): p. 577-584.
247. Faccioli, N., et al., *CEUS versus CT Angiography in the follow-up of abdominal aortic endoprostheses: diagnostic accuracy and activity-based cost analysis.* Radiol Med, 2018. **123**(12): p. 904-909.
248. Partovi, S., et al., *Contrast-enhanced ultrasound for assessing carotid atherosclerotic plaque lesions.* AJR Am J Roentgenol, 2012. **198**(1): p. W13-9.
249. Seeger, J.M., et al., *Carbon dioxide gas as an arterial contrast agent.* Ann Surg, 1993. **217**(6): p. 688-698.
250. Huang, S.G., et al., *A prospective study of carbon dioxide digital subtraction versus standard contrast arteriography in the detection of endoleaks in endovascular abdominal aortic aneurysm repairs.* Ann Vasc Surg, 2013. **27**(1): p. 38-44.
251. Basnyat, P.S., et al., *Mortality from ruptured abdominal aortic aneurysm in Wales.* British Journal of Surgery, 1999. **86**(6): p. 765-770.
252. Sweeting, M.J., et al., *Meta-analysis of individual patient data to examine factors affecting growth and rupture of small abdominal aortic aneurysms.* BJS, 2012. **99**(5): p. 655-665.
253. Anjum, A., et al., *Explaining the decrease in mortality from abdominal aortic aneurysm rupture.* Br J Surg, 2012. **99**(5): p. 637-45.
254. Hartshorne, T.C., et al., *Ultrasound measurement of aortic diameter in a national screening programme.* Eur J Vasc Endovasc Surg, 2011. **42**(2): p. 195-9.
255. Gurtelschmid, M., M. Bjorck, and A. Wanhainen, *Comparison of three ultrasound methods of measuring the diameter of the abdominal aorta.* Br J Surg, 2014. **101**(6): p. 633-6.
256. Bonnafy, T., et al., *Reliability of the measurement of the abdominal aortic diameter by novice operators using a pocket-sized ultrasound system.* Arch Cardiovasc Dis, 2013. **106**(12): p. 644-50.
257. Sprouse, L.R., 2nd, et al., *Comparison of abdominal aortic aneurysm diameter measurements obtained with ultrasound and computed tomography: Is there a difference?* J Vasc Surg, 2003. **38**(3): p. 466-71; discussion 471-2.
258. Chiu, K.W., et al., *Ultrasound measurement for abdominal aortic aneurysm screening: a direct comparison of the three leading methods.* Eur J Vasc Endovasc Surg, 2014. **47**(4): p. 367-73.
259. Bredahl, K., et al., *Three-dimensional Ultrasound Improves the Accuracy of Diameter Measurement of the Residual Sac in EVAR Patients.* European Journal of Vascular and Endovascular Surgery, 2013. **46**(5): p. 525-532.
260. Bredahl, K., et al., *Three-Dimensional Ultrasound Evaluation of Small Asymptomatic Abdominal Aortic Aneurysms.* European Journal of Vascular and Endovascular Surgery, 2015. **49**(3): p. 289-296.
261. Leotta, D.F., et al., *Measurement of abdominal aortic aneurysms with three-dimensional ultrasound imaging: Preliminary report.* Journal of Vascular Surgery, 2001. **33**(4): p. 700-707.

262. Bredahl, K., et al., *Three-dimensional Ultrasound Improves the Accuracy of Diameter Measurement of the Residual Sac in EVAR Patients.* Euro J Vasc Endovasc Surg, 2013. **46**(5): p. 525-532.
263. Grondal, N., et al., *The cardiac cycle is a major contributor to variability in size measurements of abdominal aortic aneurysms by ultrasound.* Eur J Vasc Endovasc Surg, 2012. **43**(1): p. 30-3.
264. Klein, A., et al., *Detectability of motions in AAA with ECG-gated CTA: a quantitative study.* Med Phys, 2009. **36**(10): p. 4616-24.
265. Bredahl, K., et al., *Reproducibility of ECG-gated ultrasound diameter assessment of small abdominal aortic aneurysms.* Eur J Vasc Endovasc Surg, 2013. **45**(3): p. 235-40.
266. Landry, A., J.D. Spence, and A. Fenster, *Quantification of carotid plaque volume measurements using 3D ultrasound imaging.* Ultrasound in Medicine & Biology, 2005. **31**(6): p. 751-762.
267. Bar, M., et al., *Inter-rater reliability of carotid atherosclerotic plaque quantification by 3-dimensional sonography.* Journal of Ultrasound in Medicine, 2014. **33**(7): p. 1273-1278.
268. Delcker, A. and C. Tegeler, *Influence of ECG-Triggered Data Acquisition on Reliability for Carotid Plaque Volume Measurements with a Magnetic Sensor Three-Dimensional Ultrasound System.* Ultrasound in Medicine & Biology, 1998. **24**(4): p. 601-605.
269. AlMuhanna, K., et al., *Carotid plaque morphometric assessment with three-dimensional ultrasound imaging.* Journal of Vascular Surgery, 2015. **61**(3): p. 690-697.
270. Sandholt, B.V., et al., *Inter-Scan Reproducibility of Carotid Plaque Volume Measurements by 3-D Ultrasound.* Ultrasound Med Biol, 2018. **44**(3): p. 670-676.
271. Khan, A.A., et al., *Semiautomatic quantification of carotid plaque volume with three-dimensional ultrasound imaging.* J Vasc Surg, 2017. **65**(5): p. 1407-1417.
272. Kumar, A., et al., *Plaque Volume of Carotid Endarterectomy Specimens Measured by 3D Ultrasound Technology.* JACC Cardiovasc Imaging, 2016. **9**(9): p. 1118-1119.
273. Rozie, S., et al., *Atherosclerotic plaque volume and composition in symptomatic carotid arteries assessed with multidetector CT angiography; relationship with severity of stenosis and cardiovascular risk factors.* Eur Radiol, 2009. **19**(9): p. 2294-301.
274. Nandalur, K.R., et al., *Composition of the stable carotid plaque: insights from a multidetector computed tomography study of plaque volume.* Stroke, 2007. **38**(3): p. 935-40.
275. Zhao, H., et al., *Association of carotid atherosclerotic plaque features with acute ischemic stroke: a magnetic resonance imaging study.* Eur J Radiol, 2013. **82**(9): p. e465-70.
276. Makris, G.C., et al., *Three-dimensional ultrasound imaging for the evaluation of carotid atherosclerosis.* Atherosclerosis, 2011. **219**(2): p. 377-83.
277. Sillesen, H., et al., *Carotid Plaque Burden as a Measure of Subclinical Atherosclerosis: Comparison With Other Tests for Subclinical Arterial Disease in the High Risk Plaque BioImage Study.* JACC: Cardiovascular Imaging, 2012. **5**(7): p. 681-689.
278. Zlatanovic, P., et al., *Combined Impact of Chronic Kidney Disease and Contrast Induced Acute Kidney Injury on Long-term Outcomes in Patients with Acute Lower Limb Ischaemia.* European Journal of Vascular and Endovascular Surgery, 2018. **56**(1): p. 78-86.
279. Eiberg, J.P., et al., *Ultrasound contrast-agent improves imaging of lower limb occlusive disease.* European Journal of Vascular and Endovascular Surgery, 2003. **25**(1): p. 23-28.
280. Rutherford, R.B., et al., *Recommended standards for reports dealing with lower extremity ischemia: revised version*, in *J Vasc Surg*. 1997: United States. p. 517-38.
281. Carroll, T.J., et al., *The effect of injection rate on time-resolved contrast-enhanced peripheral MRA.* J Magn Reson Imaging, 2001. **14**(4): p. 401-10.
282. Diederichs, C.G., et al., *Blurring of vessels in spiral CT angiography: effects of collimation width, pitch, viewing plane, and windowing in maximum intensity projection.* J Comput Assist Tomogr, 1996. **20**(6): p. 965-74.
283. Huang, Q.-H. and Y.-P. Zheng, *An adaptive squared-distance-weighted interpolation for volume reconstruction in 3D freehand ultrasound.* Ultrasonics, 2006. **44**: p. e73-e77.

284. Head, H.D. and M.F. Brown, *Preoperative vein mapping for coronary artery bypass operations.* The Annals of Thoracic Surgery, 1995. **59**(1): p. 144-148.
285. Cohn, J.D. and K.F. Korver, *Optimizing saphenous vein site selection using intraoperative venous duplex ultrasound scanning.* The Annals of thoracic surgery, 2005. **79**(6): p. 2013-2017.
286. Luckraz, H., et al., *Pre-operative long saphenous vein mapping predicts vein anatomy and quality leading to improved post-operative leg morbidity.* Interactive CardioVascular and Thoracic Surgery, 2008. **7**(2): p. 188-191.
287. Temizkan, V., et al., *Comparison of conventional technique and ultrasonographic mapping in saphenous vein harvesting.* Heart Surg Forum, 2013. **16**(5): p. E248-51.
288. Choi, B.C.K. and A.W.P. Pak, *A catalog of biases in questionnaires.* Preventing chronic disease, 2004. **2**(1): p. A13-A13.
289. Head, H.D. and M.F. Brown, *Preoperative vein mapping for coronary artery bypass operations.* The Annals of Thoracic Surgery. **59**(1): p. 144-148.
290. Soo, A., D. Noel, and S. MacGowan, *Ultrasound mapping of the long saphenous vein in coronary artery bypass graft surgery.* Interact Cardiovasc Thorac Surg, 2013. **16**(6): p. 886-7.
291. Maruyama, Y., et al., *Preoperative evaluation of the saphenous vein by 3-D contrastless computed tomography.* Interact Cardiovasc Thorac Surg, 2013. **16**(4): p. 550-2.
292. Min, S.K., et al., *Role of three-dimensional computed tomography venography as a powerful navigator for varicose vein surgery.* J Vasc Surg, 2010. **51**(4): p. 893-9.
293. *NHS Improvement, National tariff payment system 2017/2018 and 2018/2019.* 27/12/2018]; Available from: https://improvement.nhs.uk/resources/national-tariff-1719/.
294. Kerr, M., et al., *Estimating the financial cost of chronic kidney disease to the NHS in England.* Nephrol Dial Transplant, 2012.
295. Itoga, N.K., et al., *Use of a proactive duplex ultrasound protocol for hemodialysis access.* J Vasc Surg, 2016. **64**(4): p. 1042-1049.e1.
296. Barril, G., et al., *Hemodialysis vascular assessment by an ultrasound dilution method (transonic) in patients older than 65 years.* Int Urol Nephrol, 2001. **32**(3): p. 459-62.
297. Lok, C.E., et al., *Endovascular Proximal Forearm Arteriovenous Fistula for Hemodialysis Access: Results of the Prospective, Multicenter Novel Endovascular Access Trial (NEAT).* Am J Kidney Dis, 2017. **70**(4): p. 486-497.
298. Yang, S., et al., *Comparison of post-creation procedures and costs between surgical and an endovascular approach to arteriovenous fistula creation.* J Vasc Access, 2017. **18**(Suppl. 2): p. 8-14.

Appendix 1

Ultra-Sound

Sound can be split into the categories of infra-sound, the audible range and ultrasound and travels in cycles of oscillating high and low pressure described as a longitudinal wave. To liken this to an object for understanding one must think of the movement of a Slinky backwards and forwards (Fig. 52). As the sound wave moves through tissue it undergoes compression (high pressure) and rarefaction (low pressure) which relates to the movement of the sound source. In understanding this principle, it is easier to consider a sound wave being pushed into the body from the transducer. This is will be explained in greater detail when explaining the piezo-electric effect.

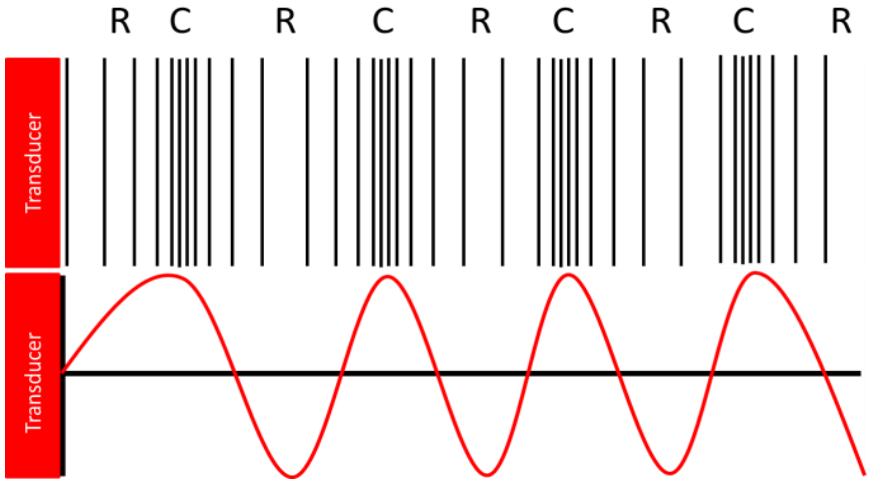

(*Figure 52. Top; A longitudinal sound wave driven from a transducer into the soft tissue with areas of compression (C) and rarefaction (R). Bottom; A sine wave driven from a transducer into the soft tissue with areas representing high and low pressure*)

A sound wave is characterised by cycles, wavelengths, amplitude and frequency (Fig 53). One cycle per second (CPS) is the change through high and low pressure of the sound wave. The number of CPS determines the frequency of that sound wave and is determined by the sound source. Amplitude is the distance above zero that the maximum or minimum pressure and can essentially be considered as the amount of power within the sound wave. This power is proportionate to the amount of electrical energy required to generate such a sound wave. The peak to peak distance between cycles is the wavelength of sound. All of these characteristics impact on the travel of sound through the human body and sounds use in diagnostic imaging.

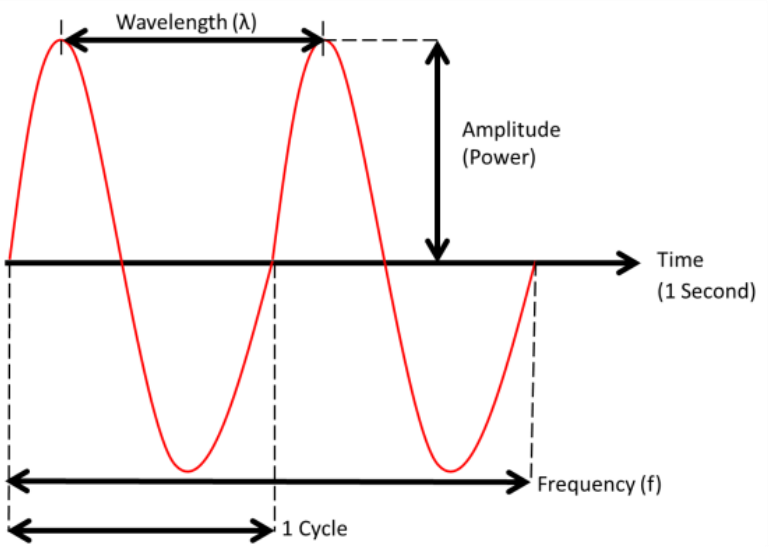

(*Figure 53. Characteristics of a sound wave represented as a Sine wave for ease of understanding*)

For sound to travel a distance it must travel through a medium. This is because sound is passed from medium particle to particle through oscillation or vibration of such a particle. It is for this reason that sound will not travel in a vacuum. This is the same principle for air or soft tissue. The higher the frequency of sound the more energy is needed for it to transmit a sound wave a distance. Due to the very high frequency and short wavelength of ultrasound, ultrasound cannot travel through air as air particles are too far apart (due to short wavelength). Hence ultrasound requires the use of coupling gel to allow transmission of sound from the transducer into the soft tissue.

Traditionally being measured in decibels, when relating to imaging it is common to measure sound in terms of frequency in the unit of Hertz (Hz). Infra-sound is classed as any sound less than 20 Hz with the audible range being between 20 Hz and 20 kilo-hertz (kHz). Ultra-sound is categorised as any sound above 20 kHz, however, for the frequency of sound to be useful for medical imaging it has to be in the range of megahertz (MHz).

Speed of Sound, Density and Stiffness

The speed of sound is crucial within vascular ultrasound imaging as it is fundamental to the use of Doppler. The speed of sound is dependent on the tissue through which it travels. Ultimately this can be broken down into the density and stiffness of the tissue and relates to particle size and proximity of the tissue.

- Dense tissues have large particles. This makes transmission of sound vibration difficult as large particles are more difficult to move. Dense tissues have slower speeds of sound.
- Stiff tissues have particles that are close together. The closer the particles mean that transmission from one to the other is easier and quicker. Stiff tissues have a faster speed of sound.

Therefore, density and stiffness have an inverse relationship on the speed of sound. The speed of sound within a tissue is therefore a trade-off of both density and stiffness. The speed of sound within bone is therefore quicker than muscle even though bone is denser than muscle as a result of stiffness. A similar principle is seen within calcified artery walls which affects the Doppler waveforms.

The speed of sound is calculated as;

$$Speed\ of\ sound\ \left(\frac{m}{s}\right) = frequency\ (Hz) \times wavelength\ (meters)$$

Or $C = f \times \lambda$

Speed of Ultrasound (1540m/s)

The human body is composed of many different tissue types, each with their own density and stiffness. Bone, muscle, fat, cartilage, ligament and nerves to name a few and each one having differing levels of water content. This poses a difficult question when performing an ultrasound scan of a particular section of anatomy as we are not scanning a single tissue type, in fact there are many differing tissue types each with different speed of sound transmissions. Table 21 outlines some different tissue types and their associated speed of sound.

Fortunately for medical imaging the majority of key tissue types have very similar speeds of sound. As a result, we can calculate an average. Assuming this average allows utilisation of ultrasound as a diagnostic tool as ultrasound scanners cannot determine different tissue types.

The assumption of an average speed of sound of 1540 m/s infers very little error as the majority of tissues that make up a single ultrasound image have a speed of sound around 1540 m/s.

	Material	m/S	
	Air	333	
	Lung	650	
*	Fat	1460	*
*	Water	1520	*
*	Amniotic fluid	1534	*
***	Average tissue	1540	***
*	Kidney	1560	*
*	Blood	1570	*
*	Liver	1578	*
*	Muscle	1580	*
	Bone	3190–3406	
	Quartz	5740	

(Table 20. Different tissue types and their associated speeds of sound. Red starred tissues make up the majority of ultrasound tissue types. Yellow star is the assumed average speed of sound within soft tissue)

Pulse Imaging

Piezo-electric effect

Ultrasound machines have the complicated job of converting ultrasound energy into ultrasound energy and vice versa. This principle relies on the piezo electric effect. When a piezoelectric crystal (such as quartz or lead zirconate titanate (PZT)) is given an electric potential, such crystal undergoes polarization and therefore changes its shape (thickness). When this electrical potential alternates so does the PZT in thickness as the particles within the PZT are effectively vibrating. This process creates a sound wave that is pushed or driven into the soft tissue. The size of the electric potential corresponds to the amplitude of the sound wave and the speed at which this potential alternates creates the frequency and therefore wavelength of the soundwave. When an echo arrives back at the PZT crystal its energy causes the PZT to change its thickness generating an electric potential which is detected by the ultrasound scanner as an echo.

Pulse Echo Principle

Continuously generating sound means that there are continuously generated echoes. This poses a problem for medical imaging as it raises the question of where two separate echoes may come from. To be able to calculate such information the scanner needs to know the time it has taken for the echo to arrive after the sound wave was transmitted to be able to calculate the depth. If the same ultrasound crystal is used for transmission and reception of an echo, then there must be a period of 'listening' for this calculation. This means that sound must be sent in pulses to be able to have this listening time. This allows calculation of echo direction, depth and amplitude. The side effect of this is higher energy is needed for pulse imaging which can mean tissue heating. This will be explained when discussing safety concerns.

The process of calculating the depth and therefore location of an echo is called range gating (fundamentally relying on pulsing) and utilises the range equation.

$$Depth\ (m) = \frac{1540\ (\frac{m}{s})\ \times t\ (s)}{2}$$

Acoustic Impedance and Dynamic Range

Acoustic impedance

The density and stiffness of a tissue create a barrier to the transmission of sound through that tissue. The resistance of that particular tissue to sound transmission is termed its acoustic impedance. When the sound travels from one tissue to another that has different acoustic impedance, an echo is generated. Acoustic impedance is calculated as;

$$Acoustic\ impedance\ (z) = density\ \left(\frac{kg}{m3}\right) \times 1540\ (\frac{m}{s})$$

The amplitude of the returning echo is determined by the ratio of reflected to transmitted sound as a result of the different acoustic impedance of each tissue type. The ratio to calculate amplitude is calculated as;

$$R = \frac{(Z2\ - Z1)}{(Z2\ + Z1)}$$

Dynamic Range and Reflection

The amplitude of an echo is dependent on two factors, the acoustic impedance ratio and the angle of transmission. The angle of reflection is always equal to transmission. This can mean that if the transmission angle is very shallow a lot of ultrasound energy will be lost as the reflected echo will not be detected by the ultrasound transducer. This is demonstrated in figure 54 and is termed oblique insonation.

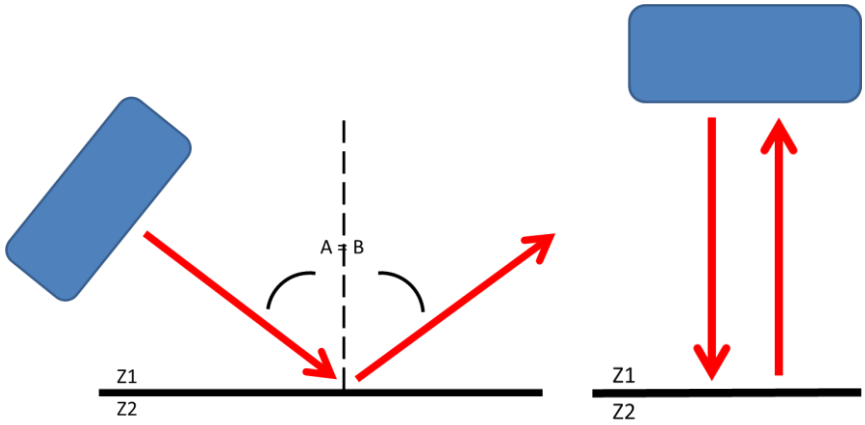

(Figure 54. Left; oblique insonation. Right; specular reflection)

For the maximum amount of reflected energy to be detected by the transducer the transmission angle must be perpendicular to the skin surface or tissue boundary. This is known as specular reflection and is depicted in figure 54.

The amplitude of any echo has an intensity as a result of the above-mentioned angles and impedance. Ultrasound scanners utilise a logarithmic scale to assign an appropriate shade of grey to a particular intensity. The ability to identify two separate structures on the scanner therefore relies on them having different acoustic impedances and therefore shades of grey. The range of grey scales is from total black (echolucent) through to bright white (echogenic) and the range of intensities that the scanner can display is termed the dynamic range. Dynamic range can be manipulated by filters so that spurious low intensity artefactual echoes can be removed from the image.

Ultrasound Image formation

Image formation is a complex process involving hundreds of ultrasound crystals. The ultrasound machine excites a single crystal driving a pulse of sound into the tissue. As the depth of the ultrasound image is set by the user the system can calculate the maximum amount of time it would take a sound pulse to travel to the maximum depth and back. The next pulse cannot be driven until after this time. In reality there are multiple reflections from the path of a single pulse transmission that from the image. Once the allotted listening time has passed the next pulse is driven.

The ultrasound image or frame is divided into slices based on the number of ultrasound crystals within the transducer. Each crystal produces a single strip of image that forms the ultrasound frame. It would take a long time (would produces images too slowly) if every crystal were to be driven in sequence. As a result, the ultrasound scanner may drive multiple crystals at the same time separated by a distance so that echoes are not detected by close by crystals. This saves time in frame formation and can increase frame rate (the time it takes to produce a single image in one second measured in Hz). Ultrasound companies can also use a frame averaging tool to help save time. In this method, alternate crystals are not driven instead that thin slice of frame is averaged from surrounding slices to generate the image. As each slice of frame is very small this does not produce significant error and allows a higher frame rate also.

The advantage of these techniques means that wires that connect the scanner to the transducer can be kept to a minimum ensuring transducer cable weight is kept light. One wire can be connected to multiple crystals and sequencing can ensure that no two crystals are sending information via the same wire at the same time. This is crucial in matrix 3D ultrasound scanning and is termed multiplexing.

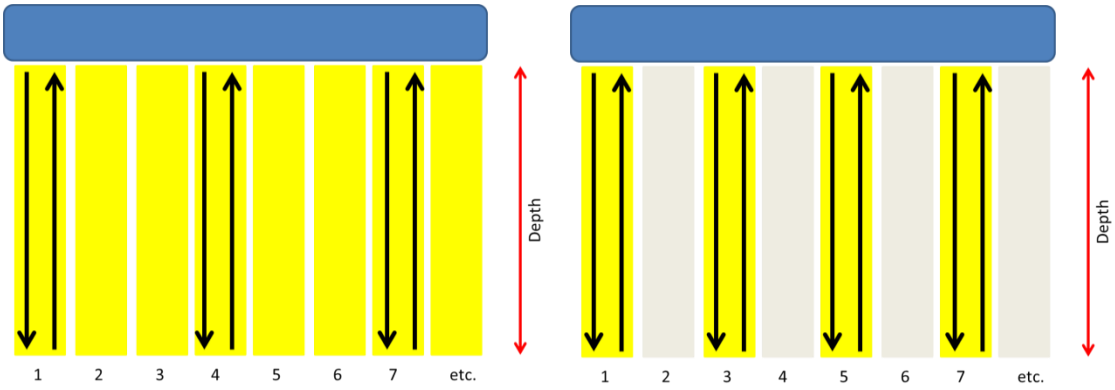

(Figure 55. Left; Shows crystal driving pulses down slices 1, 4 and 7 to form ultrasound image. Right; Frame averaging technique where pulses are driven down slices 1, 3, 5 and 7 with the information for slices 2, 4, and 6 being averaged from slices either side)

Artefact

In an ideal world, a reflector of sound would only produce one echo. Unfortunately, this is not the case. Ultrasound can bounce around the body or between the transducer and the reflector multiple times before returning to the transducer. This generates spurious echoes that are registered as true information by the ultrasound scanner as it cannot differentiate the difference. In terms of 3D ultrasound imaging some are more of a problem than others and are more of a problem to some types of 3D scanning than others.

Attenuation

As sound waves travel through soft tissue the energy within the soundwave weakens due to non-perfect transmission from one particle to the next. This means that the deeper the sound travels the weaker the echo that returns. This amount of attenuation depends on the transmission frequency. The higher the frequency, the higher the amount of attenuation and therefore the shallower the depth that can be imaged.

Reverberation

If a reflector is strong enough to generate a high energy echo the reflected sound wave can bounce off of the surface of the transducer, head back to the reflector and then back to the scanner. This can happen multiple times. Each time some energy is registered by the PZT crystal and produces an image. Reverberation will cause multiple reflections to be displayed in the image at regular depths equal to the distance from the transducer.

Acoustic Shadowing

When a structure is highly dense and a strong reflector sound will not pass through that object and instead all the energy is reflected back to the scanner. This will cause the anterior border of the reflector to appear bright white with a black streak behind it posteriorly with no other echoes. This is because there is no sound within that portion of anatomy to produce an echo. This is seen with highly calcified plaque.

Perpendicular Transmission and Posterior Enhancement

Objects that are not perpendicular to the angle of transmission will ultimately lead to oblique insonation. This is true of blood vessels. Although the anterior and posterior walls are mostly perpendicular the medial and lateral walls are not. This means that the oblique insonation will result in poor definition. This explains why medial lateral or maximal orthogonal diameters of aortic aneurysm are not accurate as defining the wall is poor.

Blood vessels also pose another type of artefact. As blood is mostly homogenous with a high content of water sound passes extremely easily through it. As a result, very little sound energy is lost when it passes through a blood vessel leading to a high energy echo. This results in a brightly represented posterior vessel wall. This is known as posterior edge enhancement.

Mirror Image and Multipath

If the transmitted sound does not return directly to the transducer but instead travels and bounces of a second reflector it is said to have taken a multipath. This can result in poor registration of the objects true depth and position. If the echo bounces of a reflector, then another dense structure and back to the reflector before returning to the transducer this can result in two structures if not every echo takes this path. This is called mirror image artefact and is seen with subclavian arteries and the pleura.

Refraction

When oblique sound reaches an interface between two tissue types where the speed of sound changes significantly one edge of the sound wave will progress into the new tissue first. This results in one edge of the sound speeding up ultimately pivoting the sound wave or bending it. This is called refraction and can lead in weak echoes but also poor representation of the true position of the reflector.

This is described by Snell's law which can be calculated as;

$$Transmission\ angle = insonation\ angle \times \left[\frac{tissue\ 2\ speed}{tissue\ 1\ speed}\right]$$

Scatter

Reflector particles are often not flat surfaces and are more closely related to spheres. When insonated with sound, this can cause sound to reflect in multiple directions, and not directly back to the scanner. This ultimately scatters the sound within the tissue and results in multiple weak echoes. This can make images look grainy. When the energy of the scattered sound is proportional to the frequency^{4th} power then it is known as a Rayleigh scatterer, a red blood cell is a good example.

Gain and Time Gain

Gain is an amplification process. Based on ambient light levels within the scan room and quality of the ultrasound monitor the overall ultrasound image may not be bright enough or could even be too bright. Gain amplifies to the dynamic range to make reflections lighter or darker. If an echo is not displayed because the returning signal is too weak it could be automatically filtered out as artefactual information by the scanner. This is called underwriting. By increasing the gain this signal will be strong enough to pass the filter and be displayed on the monitor. If the gain is set too high artefactual information that has been amplified and would usually be filtered out of the image is displayed. This is called over writing. It is important therefore to set the correct level of gain.

When considering a Carotid artery, you need to ensure that there is no plaque within the vessel lumen. If the gain is too high artefact can mimic plaque within the vessel. It is crucial to ensure that gain is set at the correct level so that the lumen of the vessel is echolucent and so that the surrounding tissues can be visualised.

As discussed above sound is attenuated at depth. It therefore makes sense to apply more gain to the reflections at depth rather than those closer to the surface. However, there is a limit, beyond that limit additional gain is ineffectual as detail becomes lost. This is called time gain compensation and is helpful for deep lying vessels where information beyond that vessel is not of clinical interest.

Resolution

Resolution can be split into temporal (Axial + lateral), elevational and monitor. Additionally, contrast resolution will not be discussed.

The number of pulses a scanner produces a second is termed as the pulse repetition frequency (PRF) and the amount of time a scanner is producing sound is termed its duty factor. The higher the PRF and therefore duty factor the higher the ultrasound frame rate (the number of times a new image is displayed per second). The higher the frame rate the higher the image resolution. The highest possible image resolution is desirable. The length of a pulse is termed spatial pulse length (SPL).

PRF is calculated as; $$PRF = \frac{number\ of\ cycles\ in\ SPL}{frequency}$$

SPL is calculated as; $$SPL\ (mm) = \frac{number\ of\ cycles\ in\ SPL \times 1540\ (\frac{cm}{s})}{frequency\ (MHz)}$$

Or; $$SPL\ (mm) = PRF\ \times 1540\ (\frac{cm}{s})$$

Axial resolution

Axial resolution is the minimum distance between two reflectors required for the scanner to represent them as two separate objects along the direction of sound travel. It is calculated as half spatial pulse length therefore it makes sense to use as short a pulse as possible. The higher the frequency of sound the shorter the SPL and hence higher axial resolution.

$Axial\ resolution\ (mm) = \frac{SPL(mm)}{2}$ or $Axial\ resolution = 0.77\ \times PRF$

Lateral resolution

Lateral resolution is the minimum distance between two reflectors required for the scanner to represent them as two separate objects perpendicular to sound travel. The distance is defined be the thickness of the ultrasound beam. Higher frequency sound has a thinner ultrasound beam hence higher resolution. Being able to focus the ultrasound beam makes it thinner and also improves lateral resolution.

Elevational resolution

It is important to remember that an ultrasound image is a 2D representation of a very thin slice of 3D anatomy. This is because an ultrasound crystal is essentially a very small cuboid with a thickness outside of its lateral thickness. This thickness is termed its elevation or slice thickness figure 56. To improve elevational resolution the ultrasound beam must be focused in the elevational plane. Focusing will be discussed below but can be by wither shaped or curved crystals, a lens or electronically.

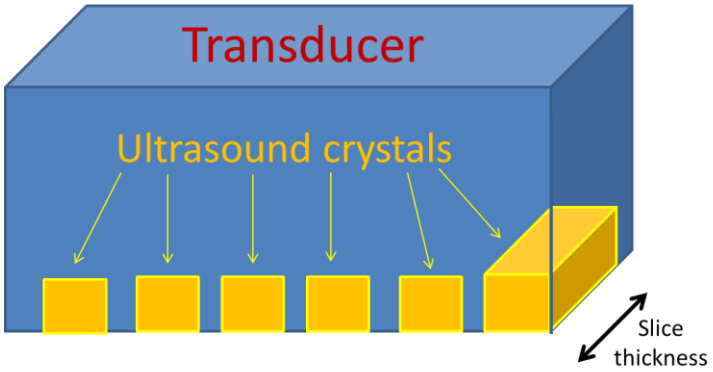

(Figure 56. Representation of ultrasound transducer with individual PZT crystals showing slice thickness)

Monitor resolution

Modern ultrasound scanners display images on a digital monitor that is divided into individual pixels. The pixel and its associated voxel are not discussed in detail here but simply the higher the resolution of the monitor the better the definition. This is defined by the number of pixels per square area. The higher the number of pixels per square area, the higher the definition and the higher the image resolution. Monitors also have a contrast resolution. This is considered beyond the scope of this review.

Transducers

Multi-element array

The majority of modern ultrasound scanners used for vascular ultrasound are not a single crystal as demonstrated in figure 56 above. Instead they are made up of an array of crystals/elements, termed multi-element array. There can be from 128 up to many hundred PZT crystals in a single array that from an image. As a result, there are multiple ultrasound beams that form the image as outlined above. Essentially there are multiple tiny ultrasounds that interact to form what is considered a single ultrasound beam. The frequency of the ultrasound is its operating frequency and is calculated as;

$$Operating\ frequency\ (Hz) = \frac{speed\ of\ sound\ of\ PZT\ \left(\frac{mm}{\mu m}\right)}{2\ \times PZT\ thickness\ (mm)}$$

In reality modern ultrasound scanners do not operate at a single frequency. Due to the electronics of modern scanners it is possible to have a small range of frequencies over which a scanner operates. This is termed its band width.

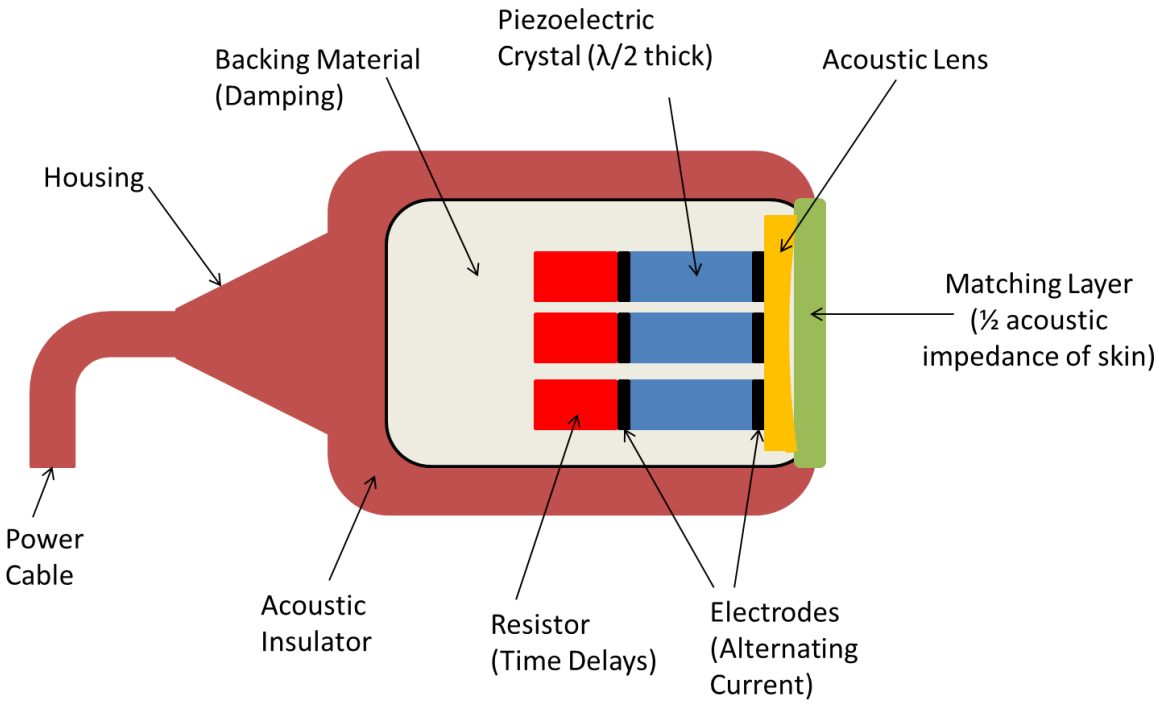

(Figure 57. The various components of a Multi-element array transducer used for vascular scanning)

Matching Layer

The matching layer is the end of the transducer in contact with the skin. It has an acoustic impedance of half that of the dermis. This is to allow efficient transmission of sound into and out of the body with an acceptable level of energy loss. The acoustic impedance of the matching layer has to be carefully calculated to ensure efficient imaging.

Acoustic Lens

The acoustic lens allows a level of initial focusing of sound before it transits into the body. This helps improve lateral resolution. Electronic focusing will be discussed below.

Electrodes

Electrodes are connected by a wire through the cable to the scanner and are used to apply an electric potential to the PZT crystal via an alternating current.

Piezoelectric Crystal

Modern crystals are made of PZT as outlined above. The thickness of the crystal is half that of the desired wavelength for the desired frequency. As described above more than one crystal is coupled to a single wire to ensure a usable size cable to save weight.

Resistor

The resistor allows the delivery of time delays to certain PZT crystals. This will be explained below. The resistor also has a second function in operating as a filter. On reception of an echo the resistor acts as a high or low pass filter. This allows the scanner to filter out low energy artefactual echoes only allowing true echoes from real structures to pass.

Backing material

The backing material ensures to isolate the PZT crystals from any other source of sound so not to corrupt the signal. Like a bell PZT will continue to ring when generating sound. This is undesirable as if a crystal continues to ring its bandwidth increases as more cycles are included within the pulse. This increases the spatial pulse length and degrades axial resolution. To ensure a high degree of axial resolution and maintain a small bandwidth and short spatial pulse length the crystal is damped. The damping material ensures this.

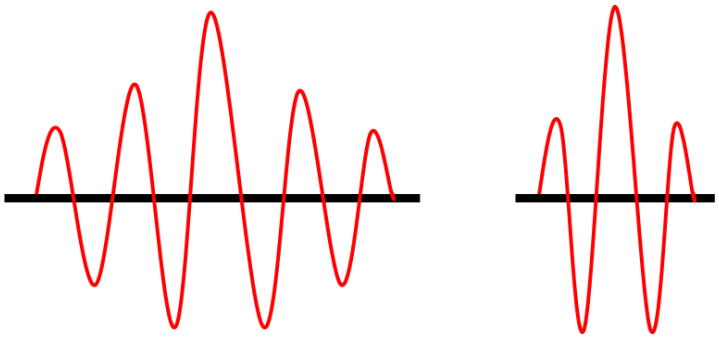

(Figure 58. Left; A sound pulse with a large bandwidth and long spatial pulse length due to poor damping, Right; A sound pulse with a small bandwidth and short spatial pulse length due to good damping)

Acoustic Insulator, Transducer Housing and Cable

The acoustic insulator and transducer housing are to protect the transducer from outside noise and damage. Its cable contains all the necessary wires to excite the PZT crystals.

Steering and Focusing

Huygens principle

As previously explained, a transducer is made of multiple PZT crystals that are considered separate sound sources. Each one emits its own pulse and generates waves of sound. Each PZT generated wave is termed Huygens wavelets which interact to form a single ultrasound wave as in figure 49.

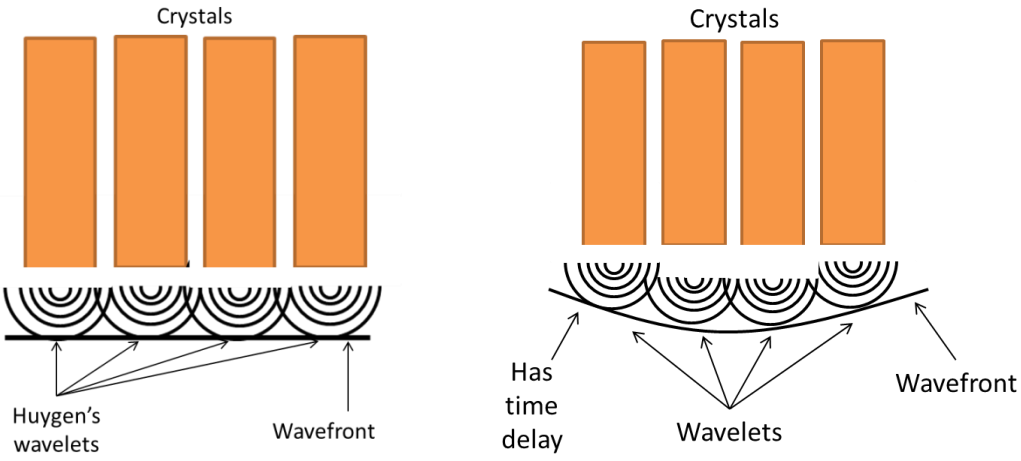

(Figure 59. Left; Emission of pulse from each PZT crystal forming Huygens wavelets that interact to form a single wave-front. Right; The PZT crystals at the edges of the transducer are given a time delay for pulse emission converging the wavelets on a specific location electronically focusing the sound)

Due to the electronic resistors, it is possible to give the PZT crystals at the edges of the transducer a time delay before emission compared to central crystals. This creates a curve in the wave-front and effectively focuses more ultrasound energy in the centre of the image (figure 59 above). This is known as electronic focusing and explains why the image is brightest in the middle of the screen. It is possible to only provide the delay to one side of the transducer, this effectively steers the beam in one direction at an angle, known as electronic beam steering (figure 60 below).

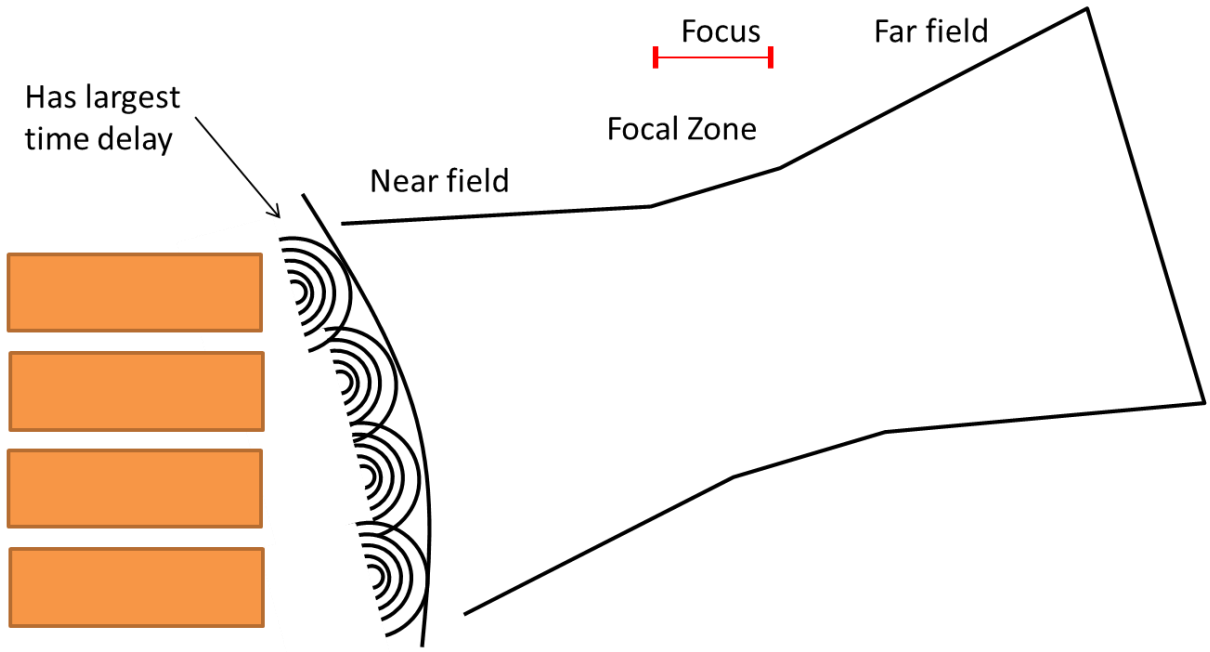

(Figure 60. Electronic beam steering as a result of individual PZT crystal time delays and wavelet interaction)

Ultrasound beam profile

As a result of focusing the sound the beam profile of an ultrasound image can be split into three areas. The near zone which offers reasonable resolution due to few reflections compared to depth. The focal zone which offers the highest resolution due to the fact this is the area which has the highest amount of ultrasound energy focused over a small area. The far field is generally considered to have the lowest resolution due to divergence of the ultrasound beam and loss of energy. As a rule of thumb, the pint of interest should be kept within the focal zone and in the centre of the image.

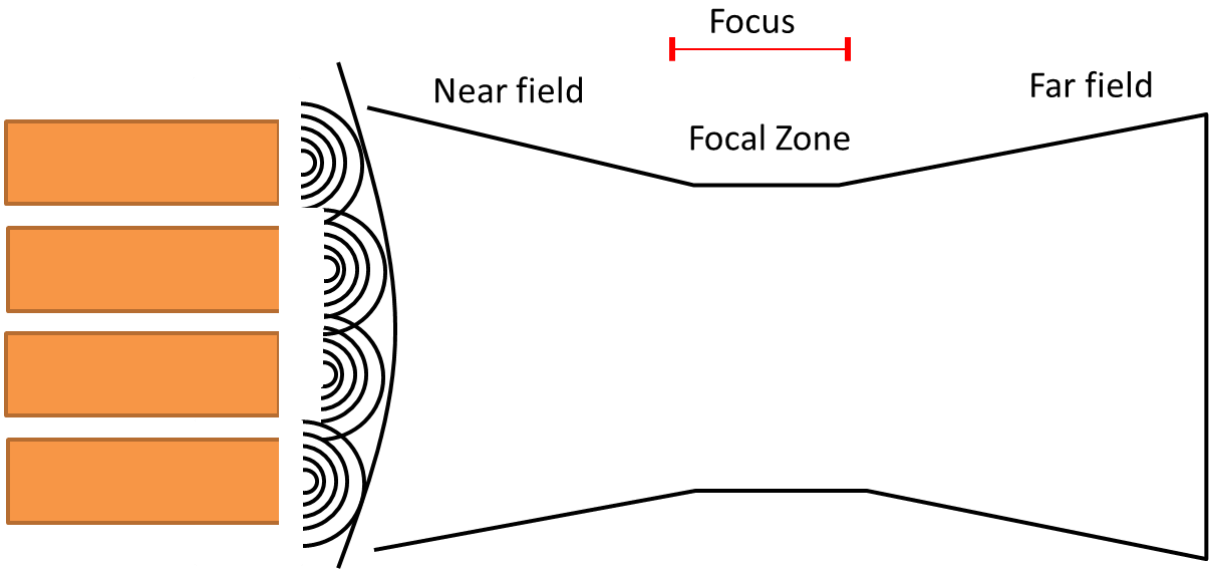

(Figure 61. Ultrasound crystals emitting Huygens wavelets interacting to form a focused wave-front with the ultrasound beam profile demonstrating the near field, focal zone and far field)

Doppler

The Doppler Effect

To be able to detect blood flow an ultrasound scanner uses the Doppler effect. The Doppler effect can be described as an observed change in frequency due to the relative motion of blood flow past the ultrasound transducer. When a sound pulse is emitted into the patient and interacts with red blood cells it undergoes a shift in frequency due to the motion of the blood. This is known as the Doppler shift. Depending on the motion of the blood flow, i.e. towards or away from the transducer, and the Doppler shift, blood will be assigned either red or blue colour or is displayed as positive or negative on the spectral baseline. The Doppler shift is calculated as;

$f_d = f_r - f_t$ Or; $f_d = \frac{2V f_t \cos\theta}{c}$

Where;

f_d	The Doppler shift
f_r	Reflected frequency
f_t	Transmitted frequency
V	Velocity of blood
$\cos\theta$	Angle of insonation
c	Speed of sound (1540 m/s)

The most important factor when considering using Doppler and understanding the Doppler equation is the angle of insonation. This is because the equation uses cosine of the angle. The importance of this can be explained by simple maths. Cosine of 90 degrees is **zero**, therefore when the angle of insonation is perpendicular to the flow of blood no flow is detected. When the angle of insonation is zero, i.e. parallel to the blood flow, the maximal Doppler shift is detected. In this scenario angle correction, would not be needed. An example of this is trans-cranial Doppler. In reality there are very few arteries where it is possible to achieve parallel flow.

When using Doppler, and taking into consideration the cosine angle there is an associated error of cosine. The larger the angle the larger the cosine error and the smaller the Doppler shift frequency that can be detected. Between 30 and 60 degrees there is acceptable error in calculated speed when using cosine. This means that any angle could be used between 30 and 60 degrees. However, being able to compare ultrasound scans done over time it is generally accepted that an ankle of 60 degrees should be used. Essentially if the angle of insonation can be calculated precisely it would not matter what angle could be used. Unfortunately, the angle of insonation when calculated with ultrasound cannot and therefore includes an error. The above discussed error is the same for spectral and colour Doppler.

Use of Doppler

In vascular ultrasound, we generally use two main types of Doppler application. Colour Doppler is utilised for demonstration of flow and provides information on vessel patency and flow turbulence. Spectral Doppler (waveforms) provides information on blood velocity, turbulence upstream and downstream patency.

Spectral Doppler

As blood flow is pulsatile there are a range of velocities across the pulse. This means that there is a range of frequencies within the Doppler shift spread over the length of time of the pulse duration. Ultrasound scanners use a process called Fast Fourier Transformation (FFT) to calculate the breakdown of the range of frequencies into the component frequencies within that Doppler shift. These are displayed on the scanner as frequency over time as a spectral trace. If the angle of insonation is known the velocity of the blood can be displayed as blood flow over time.

Colour Doppler

The drawback of using FFT is that it is a slow method of extracting information. The needs of colour Doppler mean that it must have a high temporal resolution and display information quickly. The colour box is split into hundreds of squares known as a sample volume where each sample volume requires an individual sound pulse to detect and therefore multiple pulses can be sent down a single scan line at any one time. As only one pulse can be sent at a time down a single scan line a fast method of extracting the Doppler information is needed so that the next pulse can be sent down the same scan line. This can happen on multiple scan lines at the same time. It therefore makes sense to ensure that the size of the colour box is as small as possible to ensure that there is the highest temporal resolution. Colour Doppler is also calculated by a process called autocorrelation. This will not be discussed in detail but is an average technique from the previous and the next frame. Therefore, only the mean Doppler shift will be displayed. Another major disadvantage of colour Doppler is its sensitivity. Essentially colour Doppler demonstrates motion, i.e. motion of blood through an artery. Unfortunately, transducer movement or patient movement can create colour flow falsifying results. This type of artefact can make images unreadable.

Aliasing

It is possible to set the scale or range of velocities that are displayed in colour information. This is achieved by altering the pulse repetition frequency (PRF) which is usually set to a level higher than the estimated mean velocity of flow within the artery or vein being examined. When the mean velocity of flow is higher than the PRF a type of artefact called, aliasing occurs. The reason this occurs is because the sampling limit (the number of times the flow is measured) is exceeded by the frequency of the PRF. The limit at which aliasing occurs is half the PRF and is termed the Nyquist limit. In this instance the colour scale wraps around on itself and can lead to a blue could be identified in the middle of the vessel being images mimicking reverse flow. When aliasing is present in the presence of a stenosis it is an indicator of raised velocities and turbulence indicating a haemodynamically significant lesion.

Colour bleeding

As with grey scale imaging colour imaging utilises gain. If the level of gain is set too high, i.e. the mean velocity information is amplified too great, this can cause the scanner to display colour information outside of the vessel due to the autocorrelation technique.

Non-linear propagation, Harmonics and Pulse Inversion

Non-linear propagation

As far it has been assumed that once a sound pulse is emitted it travels uniformly and generates an echo that travels uniformly through the soft tissue. Unfortunately, although this assumption aids the explanation of ultrasound physics it is incorrect to assume that this occurs. A longitudinal ultrasound wave undergoes a process known as non-linear propagation. This process occurs due to the density of sound. As described above sound travels with areas of rarefaction and compression. Compression areas travel faster through the soft tissue than areas of rarefaction and as a result an area of compression can catch up with the next area of rarefaction. At this point the sound will increase in its frequency by multiples of its transmission or fundamental frequency, i.e. 1MHz, 2MHz, 4MHz, 8MHz etc. This is known as non-linear propagation. When the distortion of the ultrasound wave occurs in this fashion harmonic echoes of the fundamental frequency are generated, i.e. the echoes at 2MHz, 4MHz, 8MHz etc. There are two ways of separating harmonic frequencies from the fundamental frequency, tissue harmonic imaging and pulse inversion technique.

Harmonic Imaging

Harmonics are ideal for ultrasound imaging. Very few harmonics are produced at shallow depth where the fundamental frequency is strong. Harmonics are generated readily through the focal zone but are attenuated almost as fast as they are generated at depth. As a result, harmonics lead too, decreased artefact through increased signal to noise ratio. This occurs because artefacts are often too weak to generate harmonics that have significant strength. Spatial resolution is also improved.

An old-fashioned method of utilising Harmonic frequencies to help improve image resolution and clarity is to use electronic filters so that the only signal that is processed by the scanner is those of the second harmonic frequency. This is an inefficient process as noise is still present in the signal and has led to development of cleaner harmonic imaging techniques.

Pulse inversion

Also, known as phase shift technique this is often a patentable method for mainstream ultrasound manufactures as a specific pulse with a specific band width is used. Each pulse would be unique to that manufacturer.

If two sound pulses are sent into a patient along the same scan line where one is a complete inversion of the other the pulses would cancel each other out (Fig. 62). However, if non-linear propagation occurs the pulse will distort unevenly with greater distortion in the positive pressure compression region than the negative rarefaction section. When these pulses are added together the signal that is left is generated by harmonics and is very clean (Fig. 62).

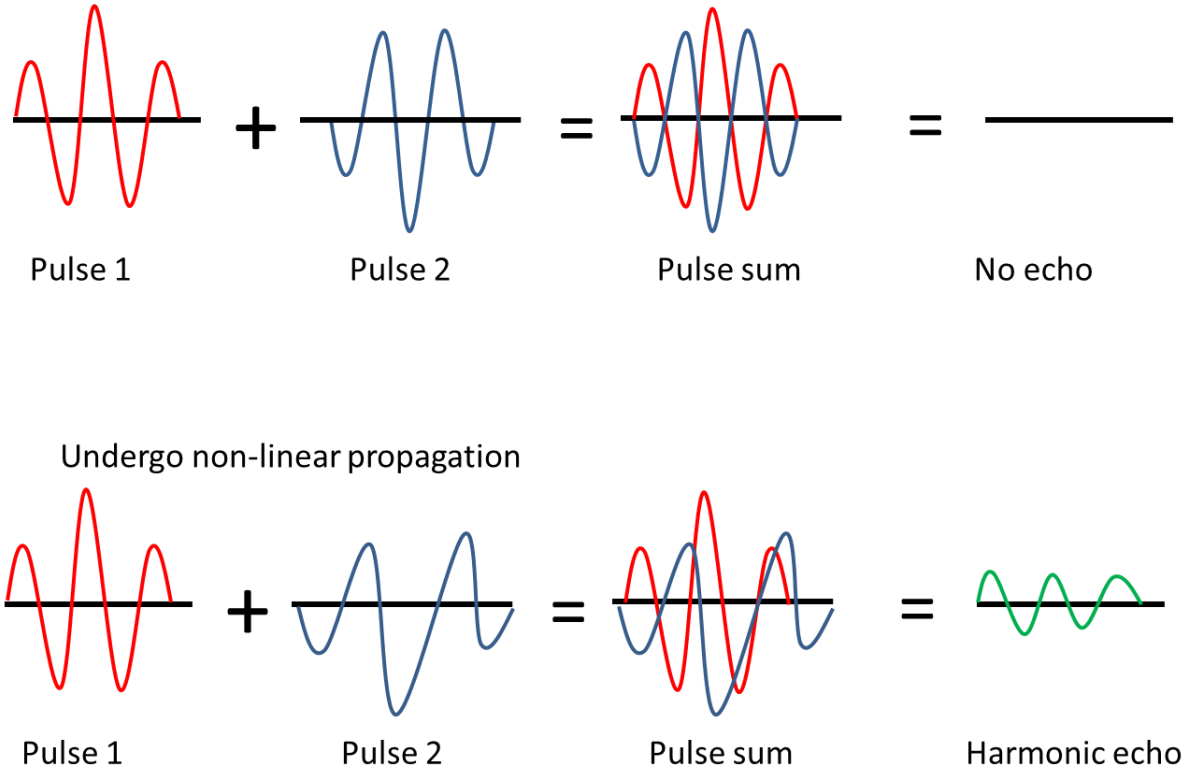

(Figure 62. Top; If both pulses are true inversions of one another the summed signal will cancel out. Bottom; Pulses undergo non-linear propagation non-uniformly and therefore generate a harmonic signal)

Safety

When considering ultrasound and the safe use of it, it must be considered in terms of energy per area per time. In simple terms, by using short ultrasound pulses we have generated a short length of time meaning a larger number of pulses per second. Short pulses are also of higher energy over a shorter time frame and as it is focused this energy is spread over a smaller area. This leads to two important safety concerns, thermal damage and mechanical damage.

Thermal concerns

As described above, ultrasound is a high amount of energy that is focused over a small area over time. As described above ultrasound is also attenuated. This is where sound energy is absorbed by the soft tissue over depth converting it to heat. Heating of tissue has been proven to effect cellular proliferation. Although heating of adult tissue is not so much of a concern hyperthermia has been proven to cause abdominal wall defects and many other potential risks. For that reason, the theoretical risk of thermal damage remains.

Mechanical concerns

Mechanical concerns of ultrasound are limited to radiation force, streaming and cavitation.

Radiation force happens when the ultrasound beam deforms the soft tissue due to its energy. The radiation force can also cause fluid objects to undergo streaming. This is where stationary fluid would benign to flow resulting in development of a shear stress that could deform or disrupt the structure. Although these risks are proven in vitro there are have been no proven effects in vivo yet the risks remain theoretical.

Cavitation has been proven within man and is the basis of contrast imaging discussed below. When the radiation force results in the generation of a micro-bubble within a liquid medium or soft tissue containing a high concentration of water stable or non-stable cavitation can occur. To understand cavitation, it is important to remember that a sound wave is an oscillation in high and low pressure.

Stable cavitation

When a sound wave passes over a micro-bubble the oscillations in high and low pressure are exerted upon the bubble. This will cause the bubble to change in size uniformly in response the pressure change. This can in turn cause streaming as described above.

Non-stable cavitation

It is possible that when as sound wave oscillates over a bubble that the bubble does not respond in a uniform way. In this instance the diameter of the bubble increases and decreases dramatically overtime in a non-stable way. This can cause the bubble to implode causing shock waves and localised high temperatures that can cause tissue damage.

ALARA

With the above safety concerns in mind it is sensible to keep ultrasound scans as short as possible using the lowest output power available. The As Low As Reasonably Achievable (ALARA) principle maintains this ethos and is promoted by the British Medical Ultrasound Society and the Society of Vascular Technology GB&I.

Mechanical and thermal indices (MI and TI)

The theoretical and mechanical risks named above must be monitored to ensure that the ALARA principle is being followed. As a stipulation by the American food and drug administration (FDA) all commercially available devices that are capable of generating ultrasound must display a mechanical and thermal index. There are three types of indices based on tissue type; vascular ultrasound is mainly concerned with MI and TI within soft tissue although a few exemptions will not be discussed here. TI indicates the theoretical effect of increasing the body tissue by one degree when displayed as 1. A temperature rise of 1.5 degrees is not thought to generate any potential theoretical risk. MI indices describe the potential theoretical risk of generating cavitation. Below an MI of 0.7 it is thought that cavitation cannot occur.

Appendix 2

Basic Physics of Contrast Enhanced Ultrasound

Mechanical Indices

Mechanical index is an indication of the peak negative pressure at the focal zone and is calculated as;

$$MI = \frac{peak\ negative\ pressure\ (Pa)}{\sqrt{Frequency\ (Hz)}}$$

In reality the peak negative pressure varies across the whole image and width of the sound wave. Therefore, the MI is an estimate of the theoretical risk as the scanner has to estimate the peak negative pressure of the frame. As a result of this estimate MI is not comparable between manufactures but also between the same models of scanner. For contrast imaging a low MI must be utilised so that microbubbles undergo stable cavitation to allow a sufficient scan length.

Microbubbles

Microbubbles are of comparable size to red blood cells and when being utilised for contrast imaging must be easily introducible via a cannula into superficial vein. The challenge of any contrast agent is that the microbubble must remain stable for a sufficient amount of time to allow a reasonable length scan to be completed. The same bubble must have negligible toxicity and needs to be detected by an ultrasound scanner constrained by the physics of sound. The advantage of contrast agents within ultrasound is the ability to detect flow at a level, below that of standard ultrasound techniques such as colour and power Doppler. Contrast agents can enhance blood to a level higher than surrounding tissue, particularly important when looking for flow within small vessels within solid organs such as the liver. Additionally, methods of supressing non-contrast bearing structures can be utilised to negate artefact.

Contrast imaging

According to the amplitude of sound used for imaging, microbubbles will scatter sound differently. When low amplitude sound is used, microbubbles produce linear echoes resulting in augmentation of the blood echo over standard B-mode imaging. If amplitude is increased microbubbles produce non-linear echoes. The advantage of this is discussed below. As amplitude increases past 1MPa the microbubble ruptures. A single millilitre of contrast enhanced blood can contain thousands of microbubbles. As a result, linear and non-linear echoes and microbubble rupture all occur simultaneously.

When a sound wave interacts with a microbubble the radius of the microbubble changes in correlation to the compressions (positive pressure) and rarefactions (negative pressure) (Fig. 63). As the microbubble oscillates in diameter this generates reflections that have a natural resonant frequency where the rate at which the microbubble absorbs and scatters sound is highly efficiently. This means small doses of contrast agents are highly effective.

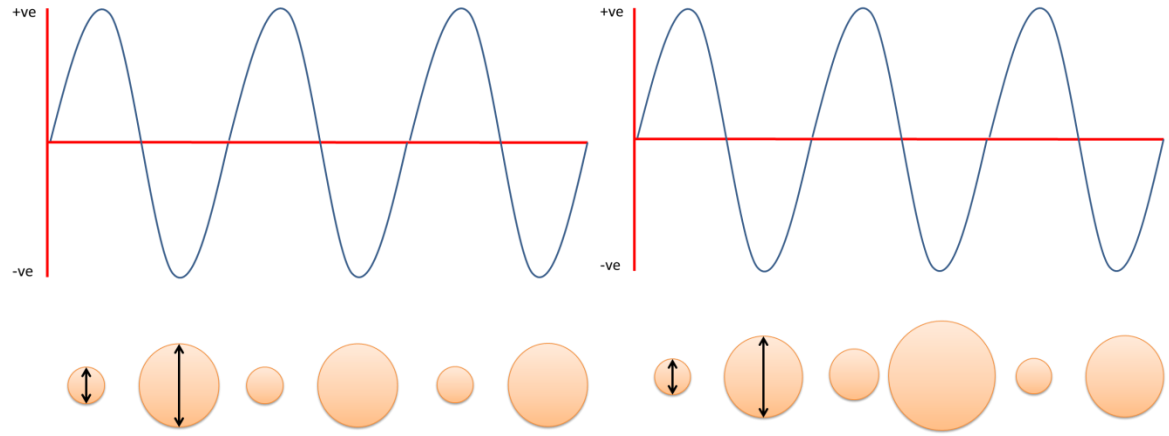

(Figure 63. Left, Microbubble undergoing equal stable cavitation. Right, Peak negative pressure is sufficient to cause harmonic cavitation)

When the amplitude of transmission is significantly higher than that utilised for stable cavitation the oscillation of the microbubble is not equal (i.e. the expansion and compression diameters are not the same) and the microbubble undergoes non-linear motion generating harmonic reflections. If the scanner is set to detect harmonic signals via either method described above, it is possible to differentiate between microbubble and soft tissue having the advantage of artefactual information not being presented on screen further improving sensitivity.